The Pennsylvania State University

The Graduate School

Department of Plant Science

MICROBIAL TRADEOFFS OF ROOT CORTICAL AERENCHYMA IN MAIZE

A Dissertation in

Horticulture

by

Tania Galindo Castañeda

Submitted in Partial Fulfillment
of the Requirements
for the Degree of

Doctor of Philosophy

August 2018

The dissertation of Tania Galindo Castañeda was reviewed and approved* by the following:

Jonathan P. Lynch
University Distinguished Professor
Dissertation Advisor
Chair of Committee

Kathleen M. Brown
Professor of Plant Stress Biology

Gretchen A. Kuldau
Associate Professor of Plant Pathology

Mary Ann Victoria Bruns
Associate Professor of Soil Microbiology and Biogeochemistry

Gregory W. Roth
Professor of Agronomy
Associate Department Head

Erin L. Connolly
Professor and Head
Department of Plant Science

*Signatures are on file in the Graduate School

ABSTRACT

The formation of air pockets in the root cortex, or root cortical aerenchyma, is a phenotype that has been associated to improved maize growth and grain yield under drought and low-nitrogen stress. A growing number of studies supports the hypothesis that roots with increased aerenchyma growing under edaphic stress have reduced demands of carbon and nutrients, or reduced metabolic burden and that aerenchyma formation may be adaptive in maize growing under nutrient and water limitations. Modeling approaches predict that maize growing under phosphorus limiting conditions would benefit by having increased aerenchyma, but the utility of aerenchyma in maize growth and productivity remains to be determined. In this research I studied the utility of increased root aerenchyma in maize growing under suboptimal phosphorus availability finding that the reduction of living cortical tissue resulting from the formation of aerenchyma was associated to better growth and grain yield.

Promising root phenotypes that may confer stress tolerance in maize, such as increased aerenchyma, should not compromise beneficial microbial associations or disease resistance. Since the root cortical tissue is the habitat of microorganisms, plants with increased aerenchyma may offer a completely different environment for microbial associations compared to plants with reduced aerenchyma. It is important to study the microbial tradeoffs of aerenchyma to inform breeding programs targeting roots with reduced metabolic burden. With this research I also explored the effects of aerenchyma on root microbial associations under optimal and suboptimal nutrient availability by evaluating mycorrhizal and *Fusarium verticilliodes* colonization, root rots, as well as the bacterial composition of the rhizosphere soil of maize plants with contrasting levels of root aerenchyma. I found that root phenotypes differentially affect mutualistic, endophytic and pathogenic root associations.

TABLE OF CONTENTS

LIST OF FIGURES

LIST OF TABLES

ACKNOWLEDGEMENTS

I am sincerely grateful to my professor Jonathan Lynch for supporting my ideas and providing the means to conduct this research. I greatly appreciate Jonathan's flexibility to integrate his work with soil microorganisms, a topic which is central to my interests as a scientist and that is related to root biology. I thank Jonathan's professional guidance, his brilliant ideas, his friendship, his interest and care for Colombia, and the opportunity to participate in fruitful collaborations at Penn State and in other institutions in the USA and in South Africa, as well as the motivation to complete my graduate work with excellent feedback throughout the writing process.

I thank the professors of my doctoral committee Kathleen Brown, Greg Roth, Gretchen Kuldau and Mary Ann Bruns for their support and feedback during my research and for facilitating spaces and facilities to conduct my experiments. My formation as a PhD was completed by learning from their expertise, perspectives and opportune suggestions to improve my work.

To my lab mates, past and present members of the Roots Lab, thanks for comradery and enjoyable moments at the office, growing plants, harvesting, phenotyping, and discussing science at lab meetings and lunch time. I would like to specially mention my friends Anica Massas, Harini Rangarajan, Molly Hanlon, Reham Abdallah, and Jennifer Yang for the support from beginning to end in this journey of the PhD.

I would have not finished my experiments without the assistance of Bob Snyder, Nancy Wenner, Andy Evensen, Michael Williams, Johan Prisloo, and Scott diLoreto. Thank you for your kindness, pragmatism and experience.

I would also like to thank a group of undergraduates who eagerly assisted me during my research: Kelly Sun, Xiangrong Guo, Pitchapa Nimwatanakul, Cella Bioni, Danielle Gibson, Noor Faralina, Lake Miller, Melda Manchidi. Thanks for your interest and curiosity.

I am thankful for the collaboration with Eoin Brodie and his team at the Lawrence Berkeley National Laboratory, for their help and guidance with the sequencing of my rhizosphere DNA samples. Also, I would like to thank Dawn Luthe and Swamjit Ray for their guidance and kind assistance with the use of PCR to detect *Fusarium verticilliodes* in maize roots.

I would like to convey my deepest appreciation for the financial support of the Colombian Government through Colciencias and the Fulbright Commission during my PhD at Penn State. In addition, the programs of Horticulture, Global Programs, and the Office of International Students of the College of Ag Sciences at Penn State have all supported me financially in various ways throughout the past years. Part of my research was also funded by the NESARE program for Graduate Students through the Grant GNE13-059.

I thank my friends during my time at Penn State, especially Claudia Rojas, Sandra del Pilar, Veronica Villena, and Flor Acevedo for being our family in State College. Also, I thank the opportunity to serve as secretary of the Latin-American Graduate Student Association at Penn State during one year of my program.

I owe much to my parents Clemencia and Luis Enrique and my sister Bibiana for their love, help and encouragement always in my life. A big thank from the bottom of my heart to my husband and colleague Hannier Pulido who joined me in this initiative to become an independent scientist and has supported me in every possible way. I would like to give special thanks to Maria Hilda Barrios who has helped me at home during the writing of my thesis and her loving cares to my daughter. Also, Marco and Jeannette, thanks for your love and cares during our time in the USA.

I dedicate this work to the kids in my family, Martín and Vivian, who have been the greatest motivation to complete this research.

INTRODUCTION

Low nutrient uptake efficiency is a major constraint for global agriculture. It has been estimated that fertilizer acquisition efficiency ranges 35 - 50% for N, and 48 - 90% of phosphorous in agricultural fields (Raun & Johnson, 1999; Cassman et al., 2002; Syers et al., 2008; Weaver & Wong, 2011). In high input systems, low nutrient uptake efficiencies cause environmental problems due to ecosystem contamination with excess of fertilizers. In low input systems, common in developing countries, high prices of fertilizers limit the amount of nutrients that can be externally applied, making the crops more dependent on residual nitrogen and phosphorous in the soil, which sometimes are not readily available for plants. The selection of plants with root phenotypes that improve soil resource acquisition is a promising and emerging approach to help improve plant growth and productivity (Gaudin et al., 2011; Lynch, 2015; Schmidt et al., 2016; Lammerts van Bueren & Struik, 2017).

The maize root system is composed by the embryonic and nodal systems which share a polyarch anatomy. The embryonic system consists of the primary root, which emerges first from the seed, and several seminal roots that emerge later. The embryonic system functions during the first days or weeks of growth. The nodal system starts developing around two weeks after emergence, and is composed by shoot-born crown roots belowground, and brace roots aboveground. Nodal roots are organized in whorls and become the most prominent and active portion of the root system two weeks after emergence. The most external whorls are the youngest. Lateral root emerge from the pericycle and endodermis of other roots, and are present throughout the embryonic and nodal system (Hochholdinger, 2009). The anatomy of maize roots consists of a central cylinder, the stele, which contains the vascular bundles and a central parenchymatous pit. The stele is surrounded by the endodermis containing the Casparian bands, a

suberized cell layer that regulates the passage of molecules to the stele. The stele and endodermis are surrounded by the cortex which is composed by several cell layers, or files, and the outermost epidermal cell layer that is usually suberized. Root anatomy is associated to different physiological and ecological processes such as nutrient and water radial conductivity (Rieger & Litvin, 1999; Hu et al., 2014), root segment respiration (Fan et al., 2007), root penetrability in hard soil layers (Chimungu et al., 2015a), abiotic stress tolerance, mycorrhizal colonization (Brundrett & Kendrick, 1988), and resistance to pests and pathogens (Hose et al., 2001; Enstone et al., 2002).

The production of air pockets in the root cortex, or root cortical aerenchyma (RCA), occurs in maize as response to drought and low nutrient stress (Evans, 2004). Recent studies support the hypothesis that aerenchyma causes a decrease in the metabolic cost of soil exploration by reducing the number of cortical cells necessary to be maintained in the root tissue, which can be adaptive under stress (Lynch, 2015). Maize genotypes with increased aerenchyma had better growth and grain yield under low nitrogen and drought (Zhu et al., 2010; Saengwilai et al., 2014; Chimungu et al., 2015b). The utility of RCA for stress adaptation to low phosphorus has been predicted in silico (Postma & Lynch, 2011a; Postma & Lynch, 2011b), but no studies have explored the RCA effect in plant growth. In the first part of this research (chapter 1) a study about the effects of aerenchyma on maize acclimation to low-phosphorus availability using greenhouse and field-grown plants is presented (Galindo-Castañeda et al., 2018). Plants with more aerenchyma had reduced root respiration and root phosphorus content, and greater leaf phosphorus content and grain yield, supporting the hypothesis that aerenchyma reduces the metabolic cost of soil exploration under low-phosphorus stress.

The microbial tradeoffs of increased aerenchyma is an important topic in the context of sustainable agriculture. Little is known about the effects of anatomical traits on the microbial interactions of plants, but this knowledge is relevant for the development of new plant varieties and cultivars with specific anatomical phenotypes. For example, beneficial associations with microorganisms or root pathogen resistance should not be compromised in plants with increased root aerenchyma. The second and third parts of this research evaluated the effect of RCA on root microbial associations in maize. In the first manuscript (chapter 2) field and greenhouse-grown plants with contrasting levels of root aerenchyma were used to evaluate colonization by mycorrhizae and fungal pathogens using a combination of plant phenotyping, laser ablation tomography, microscopy, and molecular techniques to observe and measure root anatomical phenotypes and root colonization by fungi. Axial roots with greater aerenchyma had decreased mycorrhizal colonization in the greenhouse and the field. This reduction in mycorrhizal colonization was not associated with a reduction in biomass or phosphorus uptake, likely because maize mycorrhizae occur mainly in lateral roots, while aerenchyma is significantly more extensive in the axial roots. Roots with more aerenchyma had over three times greater *Fusarium verticilliodes* (a facultative pathogen and fuminosin-producing fungi in maize) colonization in the greenhouse and no effect of aerenchyma was observed on root rots in mature field-grown maize. However, root rots were inversely correlated with mycorrhizal colonization in the field, which suggests that root traits differentially affect colonization by mycorrhizae and pathogens. The third part (chapter 3) presents a manuscript that explored rhizosphere bacterial communities in relation to root cortical aerenchyma using a metagenomics approach combined with plant phenotyping in field-grown maize in two regions of the world: Pennsylvania (US) and Limpopo (South Africa). High aerenchyma increased the rhizosphere bacterial richness under an intensively managed agricultural sandy soil in South Africa but had no effect on the rhizosphere bacterial richness in a heavier-textured soil of Pennsylvania. At both sites, rhizosphere bacterial species that were

aerenchyma-sensitive were found, with reported metabolisms that could be related to the increased oxygen in the rhizosphere of high-aerenchyma plants. These results indicate that root phenotypes may explain part of the variability in the rhizosphere bacterial composition and constitute a starting point to further study root phenotype effects on the root microbiome of agricultural species.

This work informs about the utility of RCA under low phosphorus stress in maize and contribute a new perspective of root-associated microorganisms as inhabitants of the environments provided by the diverse phenotype landscape of the root systems.

References

Brundrett MC, Kendrick B. 1988. The mycorrhizal status, root anatomy, and phenology of plants in a sugar maple forest. *Canadian Journal of Botany* 66: 1153-1173.

Cassman KG, Dobermann A, Walters DT. 2002. Agroecosystems, Nitrogen-Use Efficiency, and Nitrogen Management. *Ambio* 31: 132-140.

Chimungu JG, Loades KW, Lynch JP. 2015a. Root anatomical phenes predict root penetration ability and biomechanical properties in maize (Zea Mays). *Journal of Experimental Botany* 66: 3151-3162.

Chimungu JG, Maliro MFA, Nalivata PC, Kanyama-Phiri G, Brown KM, Lynch JP. 2015b. Utility of root cortical aerenchyma under water limited conditions in tropical maize (*Zea mays* L.). *Field Crops Research* 171: 86-98.

Enstone DE, Peterson CA, Ma F. 2002. Root Endodermis and Exodermis: Structure, Function, and Responses to the Environment. *Journal of Plant Growth Regulation* 21: 335-351.

Evans DE. 2004. Aerenchyma formation. *New Phytologist* 161: 35-49.

Fan M, Bai R, Zhao X, Zhang J. 2007. Aerenchyma formed under phosphorus deficiency contributes to the reduced root hydraulic conductivity in maize roots. *Journal of Integrative Plant Biology* 49: 598-604.

Galindo-Castañeda T, Lynch JP, Brown KM. 2018. Reduced root cortical burden improves adaptation to low phosphorus availability in maize. *Plant, Cell & Environment*.

Gaudin ACM, McClymont SA, Holmes BM, Lyons E, Raizada MN. 2011. Novel temporal, fine-scale and growth variation phenotypes in roots of adult-stage maize (*Zea mays* L.) in response to low nitrogen stress. *Plant, Cell & Environment* 34: 2122-2137.

Hochholdinger F 2009. The Maize Root System: Morphology, Anatomy, and Genetics. In: Bennetzen J, Hake S eds. *Handbook Of Maize: Its Biology*: Springer New York, 145-160.

Hose E, Clarkson DT, Steudle E, Schreiber L, Hartung W. 2001. The exodermis: a variable apoplastic barrier. *Journal of Experimental Botany* 52: 2245-2264.

Hu B, Henry A, Brown KM, Lynch JP. 2014. Root cortical aerenchyma inhibits radial nutrient transport in maize (*Zea mays*). *Annals of Botany* 113: 181-189.

Lammerts van Bueren ET, Struik PC. 2017. Diverse concepts of breeding for nitrogen use efficiency. A review. *Agronomy for Sustainable Development* 37: 50.

Lynch JP. 2015. Root phenes that reduce the metabolic costs of soil exploration: opportunities for 21st century agriculture. *Plant, Cell & Environment* 38: 1775-1784.

Postma JA, Lynch JP. 2011a. Root cortical aerenchyma enhances the growth of maize on soils with suboptimal availability of nitrogen, phosphorus, and potassium. *Plant Physiology* 156: 1190-1201.

Postma JA, Lynch JP. 2011b. Theoretical evidence for the functional benefit of root cortical aerenchyma in soils with low phosphorus availability. *Annals of Botany* 107: 829-841.

Raun WR, Johnson GV. 1999. Improving Nitrogen Use Efficiency for Cereal Production. *Agronomy Journal.* 91: 357-363.

Rieger M, Litvin P. 1999. Root system hydraulic conductivity in species with contrasting root anatomy. *Journal of Experimental Botany* 50: 201-209.

Saengwilai P, Nord EA, Chimungu JG, Brown KM, Lynch JP. 2014. Root cortical aerenchyma enhances nitrogen acquisition from low-nitrogen soils in maize. *Plant Physiology* DOI: 10.1104/pp.114.241711

Schmidt JE, Bowles TM, Gaudin AC. 2016. Using ancient traits to convert soil health into crop yield: Impact of selection on maize root and rhizosphere function. *Frontiers in Plant Science* 7.

Syers J, Johnston A, Curtin D. 2008. Efficiency of soil and fertilizer phosphorus use. *FAO Fertilizer and Plant Nutrition Bulletin* 18.

Weaver D, Wong MF. 2011. Scope to improve phosphorus (P) management and balance efficiency of crop and pasture soils with contrasting P status and buffering indices. *Plant and Soil* 349: 37-54.

Zhu J, Brown KM, Lynch JP. 2010. Root cortical aerenchyma improves the drought tolerance of maize (*Zea mays* L.). *Plant, Cell & Environment* 33: 740-749.

Chapter 1 Reduced root cortical burden improves growth and grain yield under low phosphorus availability in maize

Tania Galindo-Castañeda | Kathleen M. Brown | Jonathan P. Lynch

Department of Plant Science, The Pennsylvania State University, University Park, PA 16802, USA

Published in *Plant, Cell & Environment*

Abstract

Root phenes and phene states that reduce the metabolic cost of soil exploration may improve plant growth under low phosphorus availability. We tested the hypothesis that under low phosphorus, reduced Living Cortical Area (LCA) would increase soil exploration, phosphorus capture, biomass and grain yield. Maize genotypes contrasting in LCA were grown in the field and in greenhouse mesocosms under optimal and suboptimal phosphorus regimes. Percent LCA in nodal roots ranged from 25-67%. Plants with 0.2 mm^2 less LCA under low phosphorus had 75% less root segment respiration , 54% less root phosphorus content, rooted 20 cm deeper, allocated up to four times more roots between 60 – 120 cm depth, had between 20-150% more biomass, 35-40% greater leaf phosphorus content, and 60% greater grain yield compared to plants with high LCA. Low LCA plants had up to 55% less arbuscular mycorrhizal colonization in axial roots, but this decrease was not correlated with biomass or phosphorus content. The LCA components cortical cell file number and cortical cell size were important for biomass and phosphorus content under low phosphorus. These results are consistent with the hypothesis that root phenes that decrease the metabolic cost of soil exploration are adaptive under phosphorus stress.

Introduction

Low soil phosphorus availability is a primary constraint for global agriculture (Vance *et al.*, 2003). In high-input systems, intensive phosphorus fertilization creates significant water pollution, while in low-input systems, common in developing countries, low phosphorus availability is a primary limitation to crop production. Moreover, high-grade phosphorus ore deposits are limited and nonrenewable (Van Vuuren *et al.*, 2010). One strategy to ameliorate this problem is the development of crops that have improved phosphorus acquisition (Lynch, 2007) and utilization (Wissuwa, 2003).

Plants that capture nutrients more efficiently can be developed through breeding programs targeting root phenotypes that optimize soil exploration. Plants enhance phosphorus acquisition by several phenes (a phene is an element of a phenotype, York *et al.*, 2013) or phene aggregates such as mycorrhizal symbiosis, rhizosphere modification, root hairs, topsoil foraging, and decreased metabolic cost of soil exploration (Lynch, 2011; Lynch and Brown, 2008). Soil exploration is especially important for phosphorus capture because phosphorus is immobilized by soil constituents and therefore has very low mobility (Barber, 1995). Metabolic cost, used here to refer to the amount of carbon and nutrients invested in root growth and maintenance, is an important limitation to soil exploration and therefore soil resource acquisition under edaphic stress (Lambers *et al.*, 2002; Lynch and Ho, 2005; Nielsen *et al.*, 2001). Under low phosphorus availability, plants with root phene states that reduce respiration or phosphorus demand are likely to explore greater soil volumes than plants with phene states that demand more carbon and phosphorus (Lynch, 2015; Postma and Lynch, 2011b). For example, common bean genotypes that produce more hypocotyl-borne roots, which have 42% less linear construction cost and 29% less lateral root branching than basal roots, acquire phosphorus more efficiently than plants that produce more basal roots (Miller *et al.*, 2003).

Root phenotypes with reduced metabolic cost of soil exploration may be advantageous under edaphic stress, but may incur tradeoffs in fertile soil. These tradeoffs are poorly understood, but may include reduced capacity to engage in beneficial associations with soil microbes (including arbuscular mycorrhizas), reduced ability to tolerate biotic stress from herbivores and pathogens, reduced ability to penetrate hard soils, reduced ability to exploit localize resource patches, reduced interplant competition for soil resources, etc. However, in conditions of water and nutrient limitation, greater soil exploration should ameliorate a primary limit to plant growth and fitness. Under low nutrient stress the percent of the fixed carbon and the relative amount of nutrients used by roots is greater than in non-stress conditions (Lambers *et al.*, 2002; Nielsen *et al.*, 1998, Lynch and Ho, 2005). Thus, roots with better carbon and nutrient economy, *i.e.* equipped with phenes and phene aggregates that cause a net decrease in the carbon and nutrient demand of root tissue, have proved to be beneficial under stress conditions, but are neutral under optimal growth conditions (Chimungu *et al.*, 2014a,b; Gao and Lynch, 2016; Postma and Lynch, 2011a; Saengwilai *et al.*, 2014a,b; Zhan and Lynch, 2015; Zhu *et al.*, 2010a).

Anatomical phenes that decrease the metabolic cost of maintaining the root cortex (‘cortical burden’), are potentially important for phosphorus acquisition because of their influence on soil exploration (Lynch and Ho, 2005; Lynch, 2013; Lynch, 2015). For example, root cortical aerenchyma (RCA) is the formation of large intercellular spaces (Esau, 1960), which in maize is formed by programmed death of cortical cells, reducing the volume of living cortical tissue (Evans, 2004). Although extensively studied for its utility under hypoxia, RCA is induced by nutrient starvation as well (Bouranis *et al.*, 2003; Drew *et al.*, 1989; Evans, 2004; Fan *et al.*, 2003; Konings and Verschuren, 1980; Saengwilai *et al.*, 2014a; Siyiannis *et al.*, 2012). While RCA formation is strongly affected by the environment, it is also under genetic control (Burton *et al.*, 2015; Mano *et al.*, 2007). RCA formation decreases the respiration and nutrient content of root tissue, which is beneficial under stress conditions (Chimungu *et al.*, 2015; Fan *et al.*, 2003;

Postma and Lynch, 2011a; Saengwilai *et al.*, 2014a; Zhu *et al.*, 2010a). Under drought stress, maize lines with more RCA had a greater proportion of deep roots, and produced 30% more shoot biomass and 800% more grain yield compared to plants with low RCA (Zhu *et al.*, 2010a). The utility of RCA for grain yield in maize under drought was also demonstrated in on-farm conditions in Malawi, where accessions with greater RCA produced up to 96% more shoot biomass and 78-143% greater grain yield (Chimungu *et al.*, 2015). Two studies with the functional-structural model *SimRoot* showed that increased RCA could enhance maize grown with suboptimal nutrient availability. In these studies RCA improved the simulated growth of maize by up to 55% in low nitrogen, 54-70% in low phosphorus, and 72% in low potassium soils (Postma and Lynch, 2011a; *b*). Simulated benefits for N capture were confirmed in empirical studies conducted in the field and greenhouse which demonstrated that under N limitation, plants with increased RCA had up to 31% greater root depth, up to 81% greater leaf nitrogen content, 22% greater leaf CO_2 assimilation, 66% greater biomass and 58% greater grain yield, compared to plants with less RCA (Saengwilai *et al.*, 2014a). These results support the hypothesis that roots with reduced metabolic cost by virtue of RCA formation, can explore greater volumes of soil, resulting in greater soil resource capture (Lynch, 2015).

Living cortical area (LCA) is calculated in a root cross-section as the total cortical area minus the aerenchyma and intercellular spaces (Jaramillo *et al.*, 2013). LCA is a phene aggregate (York *et al.*, 2013) composed of cortical cell file number (CCFN), which is the number of concentric layers of parenchyma cells, cortical cell size (CCS), and inversely correlated with RCA. The relation between LCA and CCFN, and between LCA and CCS was explored by Jaramillo *et al.* (2013), and (Chimungu *et al.*, 2014a,*b*). Jaramillo *et al.* found that maize lines with reduced LCA had reduced root respiration, greater root depth, water capture, and growth under water stress, and that LCA explained these processes better than RCA. Plants with reduced CCFN (Chimungu *et al.*, 2014b), and plants with larger CCS (Chimungu *et al.*, 2014a) had

decreased root segment respiration, greater root depth, improved water acquisition and plant growth and yield under drought.

Although the influence of metabolic burden, measured as RCA or LCA, under low nitrogen and water stress is well supported by empirical data, the examination of the utility of LCA and RCA for phosphorus stress is limited to *in silico* results (Postma and Lynch, 2011a, b), and one greenhouse study (Fan *et al.*, 2007). The utility of RCA for plant growth and phosphorus acquisition in the field has not been reported. *SimRoot* predicts that under low phosphorus, RCA could increase growth of maize plants by up 70% at 40 days after germination, caused by reduced requirement for phosphorus in cortical tissue and reduced root respiration (Postma and Lynch, 2011b). Fan *et al.* (2003) found that increased RCA (caused by either ethylene manipulation or genotypic variation) led to a reduction in root respiration of 39%, and a reduction in root tissue phosphorus content of 30%. According to Postma and Lynch (2011b), plants would benefit from greater RCA formation under low phosphorus by reducing the metabolic cost of soil exploration through a reduced phosphorus requirement of the more porous tissue, and by remobilization of phosphorus from senescing cortical tissue.

The relative utility of RCA is challenging to measure mainly because other root phenotypes, such as root hair length and density, and lateral root branching, which play important roles in phosphorus acquisition, could be confounded in experiments targeting RCA. In this study, the effect of root metabolic burden in maize was investigated using maize genotypes with contrasting RCA formation, yet similar root hair and root architectural phenotypes. The objective of this study was to test the hypothesis that plants with increased RCA and decreased LCA would have reduced root respiration and root phosphorus content, and therefore greater root growth, phosphorus capture, plant growth, and yield under suboptimal phosphorus availability.

Materials and methods

Plant material

Recombinant inbred maize lines (RILs) with contrasting RCA formation were selected for field and mesocosm experiments. Data from Burton *et al.* (2010) and Zhu *et al.* (2005a) were used to select isophenic lines that minimize variation in specific root phenes such as root hair length and density, lateral root branching, number of nodal roots, and nodal root angle. The populations used by those studies were: Intermated B73×Mo17 (IBM, genotypes designated Mo#) (Kaeppler *et al.*, 2000; Senior *et al.*, 1996), and OH43×W64a (OHW, genotypes designated OHW#). The OHW population was developed by Shawn Kaeppler at The University of Wisconsin-Madison. Twenty-five selected genotypes were screened in the field under low phosphorus regimes to select genotypes with contrasting levels of RCA and LCA. Eighteen genotypes were found to produce contrasting levels of LCA and were used for one field (F-15) and two mesocosm experiments in 2014 (MC-14) and 2015 (MC-15) as described below (Table 1-4).

Mesocosm studies

Plant growth conditions and experimental design. Seeds of nine genotypes for MC-14**,** and eight for MC-15, were surface sterilized with 0.5% NaOCl and 0.02% Tween® 20 (Amresco, Inc., Solon, OH, USA) for 1 min, and then imbibed in darkness for 48 h with 0.5 mM $CaSO_4$ at 28 ± 1°C. Four germinated seeds were sown in mesocosms consisting of polyvinylchloride cylinders 15.7 cm diameter by 155 cm, lined with transparent high-density polyethylene plastic film, and filled with a mixture of sand (53% in MC-14 and 50% in MC-15), vermiculite (35%), and perlite (10%). Mesocosms were thinned to 1 plant four days after emergence. For MC-14, each column had 2% (v/v) of a phosphorus-buffered alumina (Lynch *et al.*, 1990) that buffered phosphorus at a stable concentration of 3 µM in the media solution. In MC-15, no alumina was

used, and 5% of the medium was low phosphorus soil containing 10 $mg*kg^{-1}$ available phosphorus according to Mehlich 3 (Wolf and Beegle, 1995). The soil was autoclaved (15 min. at 137.9 kPa) six months before planting. Columns with this mixture were used as the low phosphorus treatment, and columns with media mixed with an additional 10 g of triple super phosphate (20% P or 2.02 g P), were used as the high phosphorus treatment in the two experiments. Prior to planting, the columns were saturated with 4 L nutrient solution consisting of 50 µM Fe-EDTA (Ferric sodium EDTA), and 142 g of the water-soluble fertilizer Plantex® 14-0-14 (©Master Plant-Prod Inc. Brampton, ON, Canada), diluted in 100 L distilled water. The fertilizer provided the following nutrient concentration (in µM): N as NO_3 (13019), N as NH_4 (1220), K (4253), Ca (2098), Mg (1700), B (26), Cu (11), Fe (26), Mn (26), Mo (2), and Zn (11). Each mesocosm received 250 mL of this solution every day, after adjusting the pH to 5.5. A foliar micronutrient solution was applied daily early in the morning or late in the afternoon. The foliar solution consisted of (in µM): B as H_3BO_3 (46), Mn as $MnCl_2$ (9), ZnSO4 (0.77), CuSO4 (0.32), $NH_4)_6MoO_{24}$ (0.08), and Fe as Fe-DTPA (25), in 0.005% Tween® 80 (Amresco Inc., Solon, OH, USA). The experiments were conducted in August and September of 2014 (MC-14) and 2015 (MC-15), in a greenhouse located on the campus of the Pennsylvania State University, University Park (40°48'08.7"N 77°51'43.9"W). Illumination in the greenhouse ranged from 900-1200 µmol photons$*m^{-2}*s^{-1}$ at noon with additional light supplied with 400-W metal-halide lamps (GE Lighting, Multi-Vapor™, Elliptical Clear, East Cleveland, OH, USA), with a photoperiod of 14/10 h at 28°C /24°C. Humidity was 40-70%. For experiment MC-14, a liquid formulation of 400 pure aseptic spores of *Rhizophagus irregularis* (Premiere Tech Biotechnologies. Quebec, Canada) was diluted in 500 mL of sterile distilled water and thoroughly mixed with media extracted from the upper 20 cm of each column, returned to the column after inoculation and topped with a layer of 5 cm of non-inoculated media a few hours before planting. The media volume in the mesocosm (29L) approximates the soil volume for a 6 week-old maize plant in the

field at commercial planting density, based on our biomass data (Figure 1-15), growth curves by Bair (1942) and root:shoot ratios by McCullough *et al*. (1994) (APPENDIX A).

Tissue sampling. Shoots and roots were harvested 45 days after planting. Leaf tissue samples were collected from the youngest fully expanded leaf. Six 2.54 cm diameter leaf discs, and two 10 cm root segments of the second whorl per plant were collected and dried at 60°C for phosphorus analyses. The rest of the shoot was dried at 60°C for biomass determination. The roots and potting media were recovered by pulling the plastic bag out of the cylinder, carefully cutting vertically a side of the bag, and gentle washing with water. Root samples for anatomy, respiration, and mycorrhizal colonization were taken in MC-14 as described below, and the entire root system preserved in ethanol for further measurements of root length distribution with depth. Experiment MC-15 was sampled for anatomical analyses, leaf and root phosphorus content and biomass only.

Field study

Site description and experimental design. Field experiment F-15 was conducted from June – September 2015 at the Russell E. Larson Research and Education Center of The Pennsylvania State University in Rock Springs, PA, USA (40°42’37.52’’ N, 77°57’07.54’’ W, 366 m.a.s.l.). Soil at the experimental site is a Hagerstown silt loam, fine clayey, mixed, mesic Typic Hapludalf. The experiment was a randomized complete block design with four replicates, and treatments arranged in split-plots. The main plots were the phosphorus levels (high, 31 – 39 mg kg^{-1}; low, 3 – 7 mg kg^{-1}, by Mehlich 3 extraction), and the subplots were composed of 11 maize lines with contrasting levels of RCA and LCA. In order to decrease phosphorus availability, 1,560 kg *ha^{-1} DD-6 (BASF, Germany) activated alumina was disked into the soil of all plots in 2012. High-phosphorus plots received 84 kg P*ha^{-1} monoammonium phosphate (11-52-0), and the equivalent amount of ammonium was applied in the form of urea to the low phosphorus plots in order to balance the nitrogen in the two phosphorus treatments. Each block

consisted of two 0.05 ha independent fields, with the respective low and high phosphorus levels. Maize seeds were planted on June 26 of 2015, in three-row plots with 0.76 m inter-row spacing and 0.23 m in-row spacing for a final population of 57,278 plants*ha^{-1}. All the plots were managed under conventional tillage, with management of weeds and pests as needed. Plots were drip-irrigated with recommended fertilization levels applied for all the nutrients except phosphorus.

Sampling. Two representative plants per plot were excavated 80 days after planting according to the 'shovelomics' method (Trachsel *et al.*, 2011), from the central row of each replicate. The shovel was inserted 30 cm from the stem and roots carefully collected and taken to the washing station, adjacent to the experimental field. There, root crowns were excised at the soil level, soaked in water with detergent, thoroughly washed with water, and sampled. Five 2.54 cm diameter discs were collected from the youngest fully expanded leaf of each plant, pooled by plot, and dried at 60°C for analysis. Shoots of the two plants per plot were dried at 60°C and weighed. Grain yield was collected in 6 randomly selected, fully-bordered plants, 157 days after planting.

Plant measurements

Phosphorus content. Tissue samples were ashed at 495°C for 12 h, then analyzed for phosphorus concentration spectrophotometrically (Murphy and Riley, 1962).

Root anatomy. Anatomical phenotypes were analyzed in two plants per plot in the field experiment, and in each plant for the mesocosm experiments. Two root segments per plant were excised 8 – 12 cm from the base, in two representative roots of the second whorl of the nodal system. The segments were preserved in 75% ethanol in water, and stored at 4°C until processed for anatomical analysis. Root cross-sections were obtained with Laser Ablation Tomography (LAT). Briefly, the LAT system consists of a laser (Avia 7000; 355-nm, pulsed laser) that ablates samples on a stage that advances towards a camera (Canon T3i with a 5X MP-E 65 mm micro lens), which records cross-sectional images of the resulting root segment during ablation. Three

images per segment were analyzed with *RootScan* v.2.0 (Burton *et al.*, 2012) that retrieves measurements of a set of 41 anatomical characteristics, including RCA and LCA. RCA was measured as percent of the root cortical area occupied by aerenchyma lacunae (perAA) or as total aerenchyma area or the cortex (AA). LCA was measured as the total cortical area minus AA and the intercellular spaces including cell walls, expressed as area in mm^2 (LCA) or as percent of the cortical area that is LCA (perLCA).

Root depth distribution in the field. One soil core per plot was collected 100 days after planting. Coring tubes 5.1 cm diameter and 60 cm long were inserted between two plants of the same row. The extracted soil column was sectioned in 10 cm depth increments, and each 10 cm portion was washed, and roots carefully extracted by passing the sample through a 0.2 mm mesh sieve and the root length density (RLD) calculated based on total root length and the volume of the soil sample. Clean roots were dispersed in a Plexiglass tray with water, and scanned (Perfection V700 Photo; Epson America) at a resolution of 23.6 pixels*mm^{-1} (600 dots per inch). The acquired images were analyzed with WinRHIZO Pro (Regent Instruments. Quebec, Canada); the program was set up to perform the image analysis by root diameter classes at 0-0.2, 02-0.5, and >0.5. Total root length per depth increment was used to calculate D_{95} and D_{50}, i.e. the depths above which 95% or 50% of the root length is located (Schenk and Jackson, 2002).

Root depth distribution in the mesocosms. For MC-14, the entire root system of each plant was sectioned in depth increments of 20 cm. Specific root length (SRL, cm root length per g dry weight) was measured for each root class (lateral and axial) at each phosphorus level and depth increment separately and used to estimate the RLD. In order to obtain the SRL values for this experiment, lateral roots and main axis roots from three representative root segments selected from each of the 20 cm depth increments of seven randomly selected plants were scanned (Perfection V700 Photo; Epson America) at a resolution of 23.6 pixels*mm^{-1}(600 dots per inch), and images analyzed with WinRHIZO Pro (Regent Instruments, Quebec, Canada). After

scanning, lateral and axial roots were separated, dried at 60°C and weighed. The resulting data are included in Table 1-5.

Lateral root branching density (LRBD): LRBD was measured on acquired images for root depth distribution of F-15 and MC-14 (described above) from plants growing under low phosphorus, by direct counts of the lateral branches of nodal roots and calculation of the number of branches per cm root using the plugin ObjectJ (available at https://sils.fnwi.uva.nl/bcb/objectj/) for Image J (Schneider *et al.*, 2012). This analysis was performed in root fragments with diameters larger than 1 mm (considered nodal roots) recovered at 0-10, 10-20, and 20-30 cm for the soil cores of F-15, and in three 15-20 cm root segments at 0-20 cm depth for MC-14.

Root segment respiration. For MC-14, three 10 cm long root segments were collected from the second whorl of the nodal root system, 8-18 cm from the stem. Lateral roots were excised and the main axis was patted dry and used for respiration measurements. The three segments were placed in an 18 mL chamber coupled to an infrared gas analyzer (Li-Cor 6400, Li-Cor Biosciences. Lincoln, NE, USA) in closed-system mode. CO_2 accumulation in the chamber was measured at 27°C ±1°C. The samples used for root respiration were preserved for anatomical analysis as described above.

Arbuscular mycorrhizal colonization (AMC). Two root fragments per whorl were collected for MC-14 at 10-20 cm depth, from the second, third, and fourth whorls of the nodal system, for a total of six fragments per plant, then stored in 75% v/v ethanol. The roots were cleared by autoclaving 15 min at 144,79 kPa in 10% w/v KOH, and stained in blue ink (Parker® Super Quink Washable Ink), as described by Phillips and Hayman (1970) and Vierheilig *et al.* (1998). The prepared root fragments were observed under a dissecting microscope (Nikon, SMZ-U. Japan) and AMC measured in the main axes with the grid-intersect method (Giovannetti and Mosse, 1980); only arbuscules were considered for the quantifications.

Statistical analysis

Phenotype and phosphorus effects on RCA and LCA were analyzed with two-way ANOVAs separately for each experiment, since there was a significant effect of experiment on the RCA and LCA values. Simple linear regression analyses were used to study the relationship between LCA and dry biomass, phosphorus content, and AMC. ANOVA was used to identify significant differences due to phosphorus treatment and phenotypes for grain yield and D_{95} and D_{50}; *post hoc* Least Significant Difference (LSD) was used to separate individual groups. Data points that were ±3 standard deviations from the mean for a specific variable, were reviewed as possible outliers, and removed when obvious evidence of experimental error, such as data entry or poor detection with image analysis was determined. Data preparation, statistical analysis and graphs were performed using the packages *plyr* (Wickham, 2011), *dplyr* (Wickham *et al*., 2017), *nlme* (Pinheiro *et al.*, 2014), and *ggplot2* (Wickham, 2009), in *R* (R Core Team, 2014). We used linear interpolation of the total root lengths to calculate D_{95} and D_{50} for each plot by employing the function *aprox* in *R*. Subsequent *t* tests were used to find differences in RLD between high and low LCA, or between intermediate LCA and low LCA at each depth. Among the anatomical variables retrieved by *RootScan* v.2, we selected 22 that may have significance for cortical burden, and applied a Random Forest algorithm in order to identify the most important anatomical variables that predict biomass, phosphorus content, and root respiration. A complete list of variables can be found in Table 1-6. Random Forest is a non-parametric multivariate approach that uses an assembly of random classification trees to explain the variation of the explanatory variables, and in addition it returns a measure of importance for all the explanatory variables (Breiman, 2001). The *R* package *Random Forest* was employed for the data analyses, with the default options, except for the number of trees, which was set to 1001. Principal component analyses (PCA) of scaled-transformed anatomical and architectural data (when available) were performed for each experiment separately in order to assess several factors affecting plant performance (shoot dry biomass, leaf phosphorus content and grain yield).

Stepwise regression analysis of the most important anatomical variables (detected by Random Forest as described above) and the architectural variables measured in MC-14 and F-15 were performed in order to select the best multiple regression model that explained the effects of anatomy and architecture on plant performance and compare the effect of LCA and other root traits. Hierarchical regression of plant performance (shoot dry biomass, leaf phosphorus content and grain yield) were carried out with a subset of anatomical and architectural predictors in order to detect the individual contribution of each predictor to the total variation in plant performance, measured as change in R^2.

Results

Inbred lines had contrasting RCA and LCA in both mesocosm and field experiments, with RCA significantly increased by severe phosphorus stress in mesocosms (Figure 1-1). Genotypes were grouped in phenotypic classes of high, intermediate and low percent RCA and percent LCA (Table 1-4). RCA ranges of the phenotypes varied significantly among experiments, with greater RCA in the field experiment. RCA values ranged from 5-30 % in F-15, and 2-25% in MC-14 and MC-15. LCA was 25-67% in all the experiments. While no phosphorus effect on RCA was found in the field experiment, a significant induction of RCA under phosphorus stress was observed in mesocosms, where the phosphorus was very low (< 4 µM) in the low phosphorus treatment. In mesocosms, high RCA genotypes tripled their RCA under low phosphorus, whereas intermediate RCA genotypes doubled it, and low RCA genotypes were unaffected. Percent LCA had similar trends, which was unsurprising since LCA is inversely related to RCA (Figure 1-2). In the field experiment, there was no effect of phosphorus on LCA. In MC-14, low phosphorus caused LCA to decrease 10% in intermediate-LCA plants and 25% in low LCA plants, and in MC-15 the reduction in RCA due to low phosphorus was 10% for both intermediate and low LCA phenotypes.

Among the anatomical variables evaluated, LCA and RCA were among the most important explanatory variables selected by a Random Forest model for shoot phosphorus and shoot biomass (Table 1-1). Other anatomical variables that were important for biomass and phosphorus content included CCFN and CCS, as well as cortical cell number (CCN). PCA of the anatomical traits and other variables measured for each experiment under low phosphorus indicated that LCA was directly correlated with root respiration (Figure 1-10 MC-14), and perLCA was inversely correlated with total root length (Figure 1-10 MC-14) and leaf phosphorus content and plant dry biomass (Figure 1-10, all experiments). LCA was inversely correlated with grain yield in the field experiment (Figure 1-10, F-15). Other factors including anatomical phenes or phene aggregates grouped together with root respiration (cortical cell size, cortical cell file number), with plant dry biomass (axial root number and xylem vessel area), and with grain yield (cortical cell size and cortical cell file number) (Figure 1-10).

Plants with more LCA had greater root segment respiration (Figure 1-3) and greater root phosphorus content (Figure 1-4) under low phosphorus. Root diameter and RCA had no significant effect on root respiration under either low or high phosphorus (Table 1-7). An increment of 60% in LCA (from 0.3 mm^2 to 0.5 mm^2) was associated with a 75% increase in root respiration (Figure 1-3), and an increment of 40% in LCA was associated with 60% greater root phosphorus content (Figure 1-4). The linear correlation was maintained after removing the most extreme root respiration values (single plant data points,

Figure 1-11). This trend was not seen in the same genotypes growing under high phosphorus, which respired 10-50% more (Figure 1-3) and had up to twice the root phosphorus content (Figure 1-4) compared to plants growing under low phosphorus. Genotype Mo001 had significantly greater ($p < 0.05$) respiration values under low phosphorus compared to the other genotypes (Figure 1-3), had higher percent LCA ($p < 0.05$), and tended to have larger cells in the cortex in general (average of 100 μm^2), and larger cells in the epidermis and the outer cell files

(average of 142 μm^2), compared to the other genotypes, which had average cell sizes of up to 70 μm^2.

In mesocosms, phosphorus stress caused a general decrease in root length density (RLD) with variation due to the LCA phenotype (Figure 1-5, Table 1-2). Low-LCA phenotypes had deeper roots than high-LCA phenotypes, with D_{50} 10 cm deeper, and D_{95} 27 cm deeper than high LCA, allocating between 1-4 times more roots below 60 cm compared to high LCA plants, and producing roots below 120 cm, where high-LCA plants did not have roots. Vertical distribution of root biomass had a similar pattern, with low and intermediate-LCA phenotypes having greater biomass at 20 cm and below 60 cm compared to high-LCA phenotypes under low phosphorus (Figure 1-12). Plants with reduced LCA had similar LRBD compared to plants with greater LCA in the first 20 cm depth under low phosphorus conditions in MC-14, although one genotype's LRBD was significantly lower (3.5 branches cm^{-1} versus the average of 5 branches cm^{-1} for the remainder of the genotypes, Figure 1-13). In the field under low phosphorus, low-LCA plants allocated fewer roots to the shallow portions of the soil profile compared to high-LCA plants (Figure 1-14). While high-LCA and intermediate-LCA plants had a root density of 1.7 cm cm^3 in the top 10 cm, low-LCA genotypes had a root density of 1 cm cm^3, a reduction of 40% compared to high and intermediate-LCA genotypes. No significant differences in root density at any depth were found among phenotypes growing in a high phosphorus field. Intermediate-LCA phenotypes had significantly shallower roots compared to high and low LCA phenotypes (Figure 1-14, Table 1-2). An analysis of the effect of LCA phenotype on root distribution per diameter class under low phosphorus in the field (Table 1-8) revealed that plants with greater LCA had greater length of thick roots (diameters >0.5 mm) at 20 cm compared to plants with reduced or intermediate LCA. Lateral root branching density in the upper 30 cm of the soil profile in F-15 was not affected by the LCA phenotype (Table 1-9).

Plants with decreased percent LCA had greater shoot growth, leaf phosphorus content and grain yield under phosphorus stress. A decrease of 30% in percent LCA was associated with an increase in shoot biomass of 20% (Figure 1-6), and leaf phosphorus content of 35% (Figure 1-7) under low phosphorus. Grain yield under low-phosphorus stress was 60% greater for low-LCA compared to high-LCA plants (Figure 1-8). Intermediate and low-LCA plants had similar grain yield. In mesocosms, phosphorus stress reduced biomass by 90% in MC-14 and 88% in MC-15 (Figure 1-15) and leaf phosphorus content by 60% and 71% for MC-14 and MC-15 respectively (Figure 1-16). Plants with 20-40% less LCA doubled (MC-14) or tripled (MC-15) shoot dry biomass (Figure 1-6), and tripled leaf phosphorus content (Figure 1-7) under low phosphorus. In the field, phosphorus stress reduced shoot biomass by 16% (Figure 1-15), shoot phosphorus content by 35% (Figure 1-16), and grain yield by 30-40% (Figure 1-8). Percent LCA was selected through stepwise regression models as being among the best predictors for plant performance in MC-14 and F15 (shoot dry biomass, leaf phosphorus content and grain yield); in all cases, except for shoot dry biomass in MC-14, the marginal effects (which accounts for the effect of the variable given the presence of the other variables) of percent LCA were among the most significant compared to other anatomical or architectural variables (Table 1-10). However, percent aerenchyma (perAA) was associated with a significant fraction of the variation in shoot biomass and leaf phosphorus content of MC-14 and grain yield in F-15 (Table 1-11).

Mesocosm-grown plants (MC-14) formed mycorrhizae in the main axes under low phosphorus (Figure 1-9). No mycorrhizal colonization was observed in nodal root axes growing with high phosphorus, although colonization was observed in the lateral roots. Mycorrhizal colonization in axial roots in the low phosphorus plants ranged from 5-22%. Plants with 60% greater LCA had 55% more mycorrhizal colonization. No significant correlation was found between biomass or phosphorus content and mycorrhizal colonization (Table 1-3).

Discussion

Our results support the hypothesis that reduced root metabolic burden, measured as LCA, increases plant growth under mild and severe phosphorus stress. Plants with reduced LCA had less root respiration and root phosphorus content, and greater biomass, leaf phosphorus content, and grain yield under phosphorus stress. The field experiment, which included environmental factors not easily captured in mesocosms in controlled environments, allowed us to confirm results in mature plants in the field, and demonstrated the utility of decreased LCA for grain yield. Mesocosms permitted controlled phosphorus availability, controlled environmental conditions, and the ability to recover the entire root system for analysis. The agreement of results from these two contrasting environments provides robust evidence that plants with decreased cortical burden grow better under phosphorus stress.

Although previous studies have demonstrated a relationship between aerenchyma and phosphorus stress, the present research addresses for the first time the effects of aerenchyma on plant growth and grain yield under suboptimal phosphorus availability in maize. Dunn (1921) observed aerenchyma in maize and speculated that salt imbalance in the medium could be a possible explanation, but concluded that temperature could be the cause of aerenchyma formation. Later work by Konings and Verschuren (1980) indicated that among different salt solutions used for aerated hydroponic cultivation of 5-day-old maize, nitrate and phosphate would retard the formation of aerenchyma, but concluded that nitrate has the strongest effect on retarding aerenchyma formation. Subsequent studies have consistently demonstrated that low-phosphorus availability induces aerenchyma formation and have linked this response to the reduced metabolic burden hypothesis (Fan *et al*., 2003, Fernandez and Rubio, 2015), or to possible underlying cellular mechanisms such as inhibition of ethylene biosynthetic pathway (Drew *et al*., 1989) and modification in the energy status and reactive oxygen species (ROS) of the roots (Siyiannis *et al.*, 2012). Our results build on these findings by showing the value of

aerenchyma as a root phene that could be used to improve plant growth under suboptimal phosphorus availability. We used genotypes contrasting in LCA but having similar root hair length, low to intermediate production of lateral roots, as well as intermediate rooting angle, because these phene states are associated with phosphorus capture (Bates and Lynch, 2001; Ma *et al.*, 2001a,b; Postma *et al.*, 2014; Zhu *et al.*, 2005b; Zhu and Lynch, 2004). Longer root hairs are associated with improved adaptation to suboptimal phosphorus availability in maize (Zhu *et al.*, 2010b). Maize plants with shallow root systems and enhanced lateral rooting have better phosphorus acquisition (Postma *et al.*, 2014; Zhu *et al.*, 2005b; Zhu and Lynch, 2004). By avoiding plants with differences in root hair length, lateral rooting, or in root angle, we avoided confounding effects of these phenes with the anatomical phene states targeted in this study. Although we found differences in LRBD in one genotype of MC-14 (Figure 1-13), the average values per genotypes (3.5 – 6.4 cm^{-1}) fall in the low range when compared to previous studies with LRBD in nodal roots of maize (Postma *et al.*, 2014; Zhan and Lynch, 2015; Zhan *et al.*, 2015) which have reported up to 41 branches cm^{-1}. Furthermore, the effect of this difference in LRBD on plant dry biomass and phosphorus leaf content was not significant (Table 1-10). Our use of Recombinant Inbred Lines (RILs) reduces the possibility that extraneous phenotypic variation confounded our results, since RILs in the same family descend from the same two parents and thus share a common genetic background. By using two families of RILs, we reduced the possibility that genetic linkages in any one family could have confounded the results.

Living cortical area was a better predictor than RCA for biomass, phosphorus content, grain yield, and root respiration under low phosphorus. Similar results were obtained by Jaramillo *et al.* (2013) for drought tolerance in maize. LCA is a comprehensive measure of root metabolic burden, which integrates other phenes in a 'phene aggregate' (York *et al.*, 2013), combining cortical cell file number (CCFN), cortical cell size (CCS) and cortical cell number (CCN), and is directly correlated with root diameter and RCA (Jaramillo *et al.*, 2013, Figure 1-2). The utility of

the phenes that comprise LCA in maize has recently been explored under drought, with promising results. Plants with less CCFN and larger CCS have reduced metabolic burden and grow better under drought stress (Chimungu *et al.*, 2014a, b). Our observation that percent LCA is a better predictor of plant performance than LCA, RCA, and percent RCA) may be explained by the fact that LCA integrates root diameter, RCA, CCFN and CCS, and could indicate that the phenes that compose percent LCA, such as intercellular spaces, CCFN, CCS and CCN may also be related to adaptation to low phosphorus in maize. When LCA was excluded from the multiple regression analyses of plant performance as a function of anatomical phenes, there were significant effects of RCA, CCFN and CCS (Table 1-11). Closer study of the relative importance of the phenes aggregated in LCA for plant growth under edaphic stress would provide a better understanding of the utility of reduced root cortical burden. Here, we show that genotype Mo001, with significantly greater LCA and reduced RCA, had notably greater respiration although it had larger cortical cells compared to other genotypes. This may be an indication that RCA independently, or in combination with CCFN, may have greater influence on root respiration than CCS, as it has been demonstrated that larger CCS genotypes have less root respiration than genotypes with smaller CCS (Chimungu *et al.*, 2014a).

Plasticity was found in LCA and RCA across experiments. Although for some genotypes we found consistently elevated or reduced RCA or LCA expression in the different experiments, for others, the expression varied from low to intermediate, or from high to intermediate when observed in different years or experiments (Figure 1-1,Table 1-4). This can be attributed to different severities of phosphorus stress in the two greenhouse experiments and to other environmental factors in the field. In MC-14, we used phosphorus-buffered alumina, which buffered phosphorus at very low concentrations (2-3 µM), while for MC-15 we used 5% field soil having 10 mg kg^{-1} of available phosphate, producing slightly greater availability of phosphorus in the leachate (4-5 µM) than the phosphorus-buffered alumina. The alumina treatment produced

RCA values of 0 – 30% RCA, while the low phosphorus field soil produced roots ranging from 0-15% RCA. In addition to the fact that field plants were older than the mesocosm plants at sampling, other environmental factors probably affected the production of RCA, including temperature, soil impedance, varying water content, and hypoxia (Evans, 2004).

Plants with reduced LCA had deeper roots under low phosphorus, as shown in the mesocosm experiment MC-14 (Figure 1-5). Reduced phosphorus and carbon demand from the decreased volume of living tissue per unit root length in reduced LCA plants may be especially beneficial for maize, which has relatively large root diameter, and is therefore more sensitive to phosphorus stress, compared to plants with thinner roots such as common bean (Postma and Lynch, 2011b). The increased availability of phosphorus and carbon for root elongation in reduced LCA plants is a reasonable explanation for the greater root depth of the low LCA genotypes observed in the mesocosm experiment MC-14. In contrast with the mesocosms, field-grown plants under low phosphorus with reduced LCA had fewer roots in shallow soil strata and had no differences in rooting depth compared to plants with greater LCA (

Figure 1-14). The discrepancy in rooting depth between the mesocosm and field results can be attributed to methodological constraints of sampling root length distribution in the field using soil cores. Cores were taken at maximum 11.5 cm distance (midpoint of in-row plant distance) from the stem, where differences in root vertical distribution between phenotypes may not have been entirely captured, as previously observed by Miguel *et al.* (2015) in common bean. The distance for effective sampling in field-grown maize with soil cores may be even larger than common bean (15 cm) given the larger root system of maize. Furthermore, the total root length in a given horizon does not inform either the anatomical state or architectural deployment of roots in that horizon, which are both important for P capture (Lynch, 2011; Lynch and Brown, 2008). In this context, root length data from mesocosms are more robust than field data by providing precise information about the entire root system. Other factors that could have affected the root

depth distribution data in the field are soil compaction and root herbivory, both of which may have restricted root growth. Despite the contrasting results observed in terms of root growth between the field and mesocosms, the positive effect of reduced LCA phenotypes on plant growth and grain yield in the field is clear, supporting our hypothesis. A field study of the effect of LCA on architecture and total root distribution using multiple cores per plot would be needed to resolve this issue. The experimental approach of studying plant performance in mesocosms and field experiments as employed here is suitable and effective to study the effects of anatomy on maize performance as demonstrated previously (Chimungu *et al*., 2014a,b; Saengwilai *et al*., 2014a). However, the combined effects of reduced metabolic burden and increased topsoil foraging for phosphorus acquisition merit further attention. Since the volume of a mesocosm (29 L) is comparable to the soil volume available for a plant at 6 weeks in the field (APPENDIX A), the mesocosms are an appropriate experimental system for maize plants of up to 6 weeks (10-12 leaf-stage).

Our results provide experimental support for the *in silico* results by Postma and Lynch (2011a, b) with the functional-structural plant model *SimRoot,* in which the utility of RCA for the growth of maize plants was simulated under suboptimal levels of phosphorus. In the first study (Postma and Lynch, 2011b), RCA increased maize growth from 10-70%, depending on the severity of phosphorus stress. Neither phosphorus stratification nor mycorrhizal symbiosis was considered, and RCA was assumed to be equal for all root classes. In the second simulation study (Postma and Lynch, 2011a), which used actual data for RCA distribution by Burton (2010) and phosphorus stratification, plants with more RCA had up to 54% more biomass than low-RCA plants under phosphorus deficiency. We found that the benefit of greater RCA, which results in reduced LCA, in the mesocosm studies was between three to four times that predicted by the simulations. The greater benefits found in the mesocosm experiments compared to the simulation results may be explained by several factors. First, phene synergism between RCA and other root

phenes such as root hair length, root hair density, rooting angle and number of axial roots could have caused the observed increments of the RCA benefit observed in this study. Second, RCA values used in the RCA module of the simulation studies were either left constant among root classes (Postma and Lynch, 2011b), or assigned values obtained by Burton (2010) (Postma and Lynch, 2011a). Since Burton's studies with maize plants were conducted under optimum phosphorus conditions at which RCA expression is reduced compared to low phosphorus conditions, the RCA values of the simulation study may be conservative compared to real RCA values under phosphorus stress. Third, *SimRoot* simulated growth to 40 d after germination, while the present study mesocosm plants were 45 d old. Older plants may have greater benefits as RCA continues being produced in the newly formed root cortical tissue after 40 d (Deacon *et al.*, 1986). Fourth, mycorrhiza in MC-14 may have increased the benefits of reduced LCA. Fifth, lack of stratification of phosphorus distribution may have given greater phosphorus supply to our mesocosm experiments. The field experiment showed RCA benefits similar to the simulation results, with 20% biomass increments due to low-LCA in the present study compared to 15% increase in biomass at 10 µM *in silico* (Postma and Lynch, 2011b), which is a moderate degree of phosphorus stress, comparable to the stress obtained in our field study. This degree of agreement between the simulation and empirical results is remarkable considering that *SimRoot* is a heuristic model that has never been manipulated to fit empirical data. *SimRoot* primarily considers resource allocation and does not consider biotic relationships and other possible effects of root anatomy in the field. Therefore, the agreement of *in silico* and empirical results indicates that the hypothesis that LCA benefits plant growth under phosphorus stress *via* effects on the carbon and nutrient economy of roots is reasonable.

Although we are proposing that decreased root cortical burden is advantageous for phosphorus acquisition under phosphorus stress, exploring the tradeoffs of the associated root phenes will assist the selection of better maize varieties useful for specific environmental

conditions. Reduced radial nutrient and water transport Fan *et al.*, 2007; Hu *et al.*, 2014), and decreased mechanical strength (Striker *et al.*, 2007) have been proposed as possible tradeoffs of increased RCA. The effect of reduced LCA on mycorrhizae under phosphorus stress was addressed in this study as a possible microbial tradeoff of decreased LCA. We observed reduced mycorrhizal colonization in axial roots with reduced LCA (Figure 1-9). Sharda and Koide (2010) found no effect of intercellular air space of maize on mycorrhizal colonization under low phosphorus when evaluating one genotype of maize among other plant species, concluding that the control of mycorrhizal colonization may be species-specific. The present research, in contrast, addresses for the first time the effect of the variation in cortical root phenotypes of maize on mycorrhizae by using several genotypes with contrasting aerenchyma under low-phosphorus stress, suggesting that anatomy has an effect on mycorrhizal colonization of axial roots under low phosphorus. Although the interaction of mycorrhiza and RCA has been reported in rice (Gutjahr *et al.*, 2009), sedges (Muthukumar *et al.*, 2004), salt aster (Scheloske *et al.*, 2004), and palms (Dreyer *et al.*, 2010), phosphorus availability or quantitative analysis of root anatomy were not considered in those studies. The reduction of cortical habitat for mycorrhizal symbionts under suboptimal phosphorus availability could account for the observed reduction of mycorrhizal colonization with reduced LCA in axial roots, because the fungal and plant symbionts exchange resources in the cortex (Smith and Read, 2008). This decrease in mycorrhizal colonization did not affect the benefit of reduced LCA under low phosphorus (Table 1-3), possibly because the reduction in LCA mainly affects axial roots due to the presence of RCA (Burton *et al.*, 2013), while the symbiosis occurs more predominantly in lateral roots where RCA is less abundant, as observed in preliminary experiments (Figure 1-17, Figure 1-18). Therefore, the two strategies for coping with low phosphorus, reduced cortical burden and mycorrhizal colonization, seem to coexist in the same root system but in separate compartments; the reduction in LCA in the axial root, and the symbiosis in the lateral roots.

Our results indicate potential benefits of decreased root cortical burden for phosphorus acquisition under suboptimal phosphorus availability in maize, in controlled environments and in the field. Although the presence of living tissue in axial roots may have physiological and ecological functions that are important under optimal phosphorus availability, these results support the rationale that a decrease of this tissue may result in a better cost/benefit ratio under resource scarcity. The identification of phenes, phene states, phene aggregates, and ideotypes for improved phosphorus capture and use is needed to guide targeted breeding for more phosphorus-efficient crops (Lynch, 2011; 2015). Reduced root metabolic burden in maize, expressed as low LCA, appears to be one such phene aggregate. Studies of the phenes that are integrated in LCA, such as CCFN and CCS, and the combination of these phenes with root system architecture may further explain the mechanisms by which LCA is associated with better plant performance, and assist the selection of phosphorus efficient-plants.

References

Bair R.A. (1942) Growth rates of maize under field conditions. *Plant Physiology*, **17**, 619-631.

Barber S.A. (1995) *Soil nutrient bioavailability: a mechanistic approach*. (2nd ed.). John Wiley & Sons, New York, NY.

Bates T.R. & Lynch J.P. (2001) Root hairs confer a competitive advantage under low phosphorus availability. *Plant and Soil*, **236**, 243-250.

Bouranis D., Chorianopoulou S., Siyiannis V., Protonotarios V. & Hawkesford M. (2003) Aerenchyma formation in roots of maize during sulphate starvation. *Planta*, **217**, 382-391.

Breiman L. (2001) Random forests. *Machine Learning*, **45**, 5-32.

Burton A., Lynch J. & Brown K. (2013) Spatial distribution and phenotypic variation in root cortical aerenchyma of maize (*Zea mays* L.). *Plant and Soil*, **367**, 263–274.

Burton A.L. (2010) Phenotypic evaluation and genetic basis of anatomical and architectural root traits in the genus Zea. PhD Thesis, The Pennsylvania State University.

Burton A.L., Johnson J., Foerster J., Hanlon M.T., Kaeppler S.M., Lynch J.P. & Brown K.M. (2015) QTL mapping and phenotypic variation of root anatomical traits in maize (*Zea mays* L.). *Theoretical and Applied Genetics*, **128**, 93-106.

Burton A.L., Williams M., Lynch J.P. & Brown K.M. (2012) RootScan: Software for high-throughput analysis of root anatomical traits. *Plant and Soil*, doi:10.1007/s11104-012-1138-2.

Chimungu J.G., Brown K.M. & Lynch J.P. (2014a) Large root cortical cell size improves drought tolerance in maize. *Plant Physiology*, **166**, 2166-2178.

Chimungu J.G., Brown K.M. & Lynch J.P. (2014b) Reduced root cortical cell file number improves drought tolerance in maize. *Plant Physiology*, **166**, 1943-1955.

Chimungu J.G., Maliro M.F.A., Nalivata P.C., Kanyama-Phiri G., Brown K.M. & Lynch J.P. (2015) Utility of root cortical aerenchyma under water limited conditions in tropical maize (*Zea mays* L.). *Field Crops Research*, **171**, 86-98.

Deacon J.W., Drew M.C. & Darling A. (1986) Progressive cortical senescence and formation of lysigenous gas space (Aerenchyma) distinguished by nuclear staining in adventitious roots of *Zea mays*. *Annals of Botany*, **58**, 719-727.

Drew M.C., He C.J. & Morgan P.W. (1989) Decreased ethylene biosynthesis, and induction of aerenchyma, by nitrogen- or phosphate-starvation in adventitious roots of *Zea mays* L. *Plant Physiology*, **91**, 266-271.

Dreyer B., Morte A., López J.Á. & Honrubia M. (2010) Comparative study of mycorrhizal susceptibility and anatomy of four palm species. *Mycorrhiza*, **20**, 103-115.

Dunn G.A. (1921) Note on the histology of grain roots. *American Journal of Botany*, **8**, 207-211.

Esau K. (1960) *Plant Anatomy*. John Wiley & Sons, Inc., New York.

Evans D.E. (2004) Aerenchyma formation. *New Phytologist*, **161**, 35-49.

Fan M., Bai R., Zhao X. & Zhang J. (2007) Aerenchyma formed under phosphorus deficiency contributes to the reduced root hydraulic conductivity in maize roots. *Journal of Integrative Plant Biology*, **49**, 598-604.

Fan M., Zhu J., Richards C., Brown K.M. & Lynch J.P. (2003) Physiological roles for aerenchyma in phosphorus-stressed roots. *Functional Plant Biology*, **30**, 493-506.

Fernandez M.C. & Rubio G. (2015) Root morphological traits related to phosphorus-uptake efficiency of soybean, sunflower, and maize. *Journal of Plant Nutrition and Soil Science*, **178**, 807-815.Gao Y. & Lynch J.P. (2016) Reduced crown root number improves water acquisition under water deficit stress in maize (*Zea mays* L.). *Journal of Experimental Botany*, **67**, 4545-4557.

Giovannetti M. & Mosse B. (1980) An evaluation of techniques for measuring vesicular arbuscular mycorrhizal infection in roots. *New Phytologist*, **84**, 489-500.

Gutjahr C., Casieri L. & Paszkowski U. (2009) *Glomus intraradices* induces changes in root system architecture of rice independently of common symbiosis signaling. *New Phytologist*, **182**, 829-837.

Hu B., Henry A., Brown K.M. & Lynch J.P. (2014) Root cortical aerenchyma inhibits radial nutrient transport in maize (*Zea mays*). *Annals of Botany*, **113**, 181-189.

Jaramillo R.E., Nord E.A., Chimungu J.G., Brown K.M. & Lynch J.P. (2013) Root cortical burden influences drought tolerance in maize. *Annals of Botany*, **112**, 429-437.

Kaeppler S.M., Parke J.L., Mueller S.M., Senior L., Stuber C. & Tracy W.F. (2000) Variation among maize inbred lines and detection of quantitative trait loci for growth at low phosphorus and responsiveness to arbuscular mycorrhizal fungi. *Crop Science*, **40**, 358-364.

Konings H. & Verschuren G.E.R. (1980) Formation of aerenchyma in roots of *Zea mays* in aerated solutions, and its relation to nutrient supply. *Physiologia Plantarum*, **49**, 265-270.

Lambers H., Atkin O.K. & Millenaar F.F. (2002) Respiratory patterns in roots in relation to their functioning. In: *Plant Roots. The Hidden Half* (eds Y. Waisel, A. Eshel, & K. Kafkaki), pp. 782-838. Marcel Dekker, Inc., New York, NY.

Lynch J., Epstein E., Läuchli A. & Weight G. (1990) An automated greenhouse sand culture system suitable for studies of P nutrition. *Plant, Cell & Environment*, **13**, 547-554.

Lynch J. & Ho M. (2005) Rhizoeconomics: Carbon costs of phosphorus acquisition. *Plant And Soil*, **269**, 45-56.

Lynch J.P. (2007) Turner review no. 14. Roots of the second green revolution. *Australian Journal of Botany*, **55**, 493-512.

Lynch J.P. (2011) Root phenes for enhanced soil exploration and phosphorus acquisition: tools for future crops. *Plant Physiology*, **156**, 1041-1049.

Lynch J.P. (2013) Steep, cheap and deep: an ideotype to optimize water and N acquisition by maize root systems. *Annals of Botany*, **112**, 347-357.

Lynch J.P. (2015) Root phenes that reduce the metabolic costs of soil exploration: opportunities for 21st century agriculture. *Plant, Cell & Environment*, **38**, 1775-1784.

Lynch J.P. & Brown K.M. (2008) Root strategies for phosphorus acquisition. In: *The Ecophysiology of Plant-Phosphorus Interactions* (eds P.J. White & J.P. Hammond), pp. 83-116. Springer Netherlands, Dordrecht.

Ma Z., Bielenberg D., Brown K. & Lynch J. (2001a) Regulation of root hair density by phosphorus availability in *Arabidopsis thaliana*. *Plant, Cell & Environment*, **24**, 459-467.

Ma Z., Walk T.C., Marcus A. & Lynch J.P. (2001b) Morphological synergism in root hair length, density, initiation and geometry for phosphorus acquisition in *Arabidopsis thaliana*: a modeling approach. *Plant and Soil*, **236**, 221-235.

Mano Y., Omori F., Takamizo T., Kindiger B., Bird R.M., Loaisiga C.H. & Takahashi H. (2007) QTL mapping of root aerenchyma formation in seedlings of a maize × rare teosinte "*Zea nicaraguensis*" cross. *Plant and Soil*, **295**, 103-113.

McCullough D.E., Mihajlovic M., Aguilera A., Tollenaar M. & Girardin P. (1994) Influence of N supply on development and dry matter accumulation of an old and a new maize hybrid. *Canadian Journal of Plant Science*, **74**, 471-477.

Miguel M.A., Postma J.A. & Lynch J.P. (2015) Phene synergism between root hair length and basal root growth angle for phosphorus acquisition. *Plant Physiology*, **167**, 1430-1439.

Miller C.R., Ochoa I., Nielsen K.L., Beck D. & Lynch J.P. (2003) Genetic variation for adventitious rooting in response to low phosphorus availability: potential utility for phosphorus acquisition from stratified soils. *Functional Plant Biology*, **30**, 973-985.

Murphy J. & Riley J.P. (1962) A modified single solution method for the determination of phosphate in natural waters. *Analytica Chimica Acta*, **27**, 31-36.

Muthukumar T., Udaiyan K. & Shanmughavel P. (2004) Mycorrhiza in sedges—an overview. *Mycorrhiza*, **14**, 65-77.

Nielsen K.L., Bouma T.J., Lynch J.P. & Eissenstat D.M. (1998) Effects of phosphorus availability and vesicular–arbuscular mycorrhizas on the carbon budget of common bean (*Phaseolus vulgaris*). *New Phytologist*, **139**, 647-656.

Nielsen K.L., Eshel A. & Lynch J.P. (2001) The effect of phosphorus availability on the carbon economy of contrasting common bean (*Phaseolus vulgaris* L.) genotypes. *Journal of Experimental Botany*, **52**, 329-339.

Phillips J. & Hayman D. (1970) Improved procedures for clearing roots and staining parasitic and vesicular-arbuscular mycorrhizal fungi for rapid assessment of infection. *Transactions of the British Mycological Society*, **55**, 158-161.

Pinheiro J., Bates D., DebRoy S. & Sarkar D. (2014) nlme: linear and nonlinear mixed effects models.

Postma J.A., Dathe A. & Lynch J.P. (2014) The optimal lateral root branching density for maize depends on nitrogen and phosphorus availability. *Plant Physiology*, **166**, 590-602.

Postma J.A. & Lynch J.P. (2011a) Root cortical aerenchyma enhances the growth of maize on soils with suboptimal availability of nitrogen, phosphorus, and potassium. *Plant Physiology*, **156**, 1190-1201.

Postma J.A. & Lynch J.P. (2011b) Theoretical evidence for the functional benefit of root cortical aaerenchyma in soils with low phosphorus availability. *Annals of Botany*, **107**, 829-841.

R Core Team (2014) R: A language and environment for statistical computing. R Foundation for Statistical Computing, Vienna, Austria.

Saengwilai P., Nord E.A., Chimungu J.G., Brown K.M. & Lynch J.P. (2014a) Root cortical aerenchyma enhances nitrogen acquisition from low-nitrogen soils in maize. *Plant Physiology*, doi:10.1104/pp.114.241711.

Saengwilai P., Tian X. & Lynch J.P. (2014b) Low crown root number enhances nitrogen acquisition from low nitrogen soils in maize (*Zea mays* L.). *Plant Physiology*, doi:10.1104/pp.113.232603.

Sharda J.N. & Koide R.T. (2010) Exploring the role of root anatomy in P-mediated control of colonization by arbuscular mycorrhizal fungi. *Botany* **88**, 165-173.

Scheloske S., Maetz M., Schneider T., Hildebrandt U., Bothe H. & Povh B. (2004) Element distribution in mycorrhizal and nonmycorrhizal roots of the halophyte *Aster tripolium* determined by proton induced X-ray emission. *Protoplasma*, **223**, 183-189.

Schenk H.J. & Jackson R.B. (2002) The global biogeography of roots. *Ecological Monographs*, **72**, 311-328.

Schneider C.A., Rasband W.S. & Eliceiri K.W. (2012) NIH Image to ImageJ: 25 years of image analysis. *Nature Methods*, **9**, 671-675.

Senior M., Chin E., Lee M., Smith J. & Stuber C. (1996) Simple sequence repeat markers developed from maize sequences found in the GENBANK database: map construction. *Crop Science*, **36**, 1676-1683.

Siyiannis V.F., Protonotarios V.E., Zechmann B., Chorianopoulou S.N., Müller M., Hawkesford M.J. & Bouranis D.L. (2012) Comparative spatiotemporal analysis of root aerenchyma formation processes in maize due to sulphate, nitrate or phosphate deprivation. *Protoplasma*, **249**, 671-686.

Smith S.E. & Read D.J. (2008) *Mycorrhizal symbiosis*. Academic press, New York, NY.

Striker G., Insausti P., Grimoldi A. & Vega A. (2007) Trade-off between root porosity and mechanical strength in species with different types of aerenchyma. *Plant, Cell & Environment*, **30**, 580-589.

Trachsel S., Kaeppler S.M., Brown K.M. & Lynch J.P. (2011) Shovelomics: high throughput phenotyping of maize (*Zea mays* L.) root architecture in the field. *Plant And Soil*, **341**, 75-87.

Van Vuuren D.P., Bouwman A.F. & Beusen A.H.W. (2010) Phosphorus demand for the 1970–2100 period: A scenario analysis of resource depletion. *Global Environmental Change*, **20**, 428-439.

Vance C.P., Uhde-Stone C. & Allan D.L. (2003) Phosphorus acquisition and use: critical adaptations by plants for securing a nonrenewable resource. *New Phytologist*, **157**, 423-447.

Vierheilig H., Coughlan A.P., Wyss U. & Piché Y. (1998) Ink and vinegar, a simple staining technique for arbuscular-mycorrhizal fungi. *Applied and Environmental Microbiology*, **64**, 5004-5007.

Wickham H. (2009) *ggplot2: elegant graphics for data analysis*. Springer-Verlag, New York.

Wickham H. (2011) The split-apply-combine strategy for data analysis. *Journal of Statistical Software*, **40**, 1-29.

Wickham H., Francois R., Henry L. & Müller K. (2017) dplyr: A grammar of data manipulation.

Wissuwa M. (2003) How do plants achieve tolerance to phosphorus deficiency? Small causes with big effects. *Plant Physiology*, **133**, 1947-1958.

Wolf A. & Beegle D. (1995) Recommended soil tests for macronutrients: Phosphorus, potassium, calcium, and magnesium. In: *Recommended Soil Testing Procedures For The Northeastern United States. Northeast Regional Bull*, pp. 25-34, Agric. Exp. Stn., Univ. of Delaware, Newark, DE.

York L.M., Galindo-Castañeda T., Schussler J.R. & Lynch J.P. (2015) Evolution of US maize (*Zea mays* L.) root architectural and anatomical phenes over the past 100 years corresponds to increased tolerance of nitrogen stress. *Journal of Experimental Botany*, **66**, 2347-2358.

York L.M., Nord E.A. & Lynch J.P. (2013) Integration of root phenes for soil resource acquisition. *Frontiers in Plant Science*, **4**, 355.

Zhan A. & Lynch J.P. (2015) Reduced frequency of lateral root branching improves N capture from low-N soils in maize. *Journal of Experimental Botany*, **66**, 2055-2065.

Zhan A., Schneider H. & Lynch J. (2015) Reduced lateral root branching density improves drought tolerance in maize. *Plant Physiology*, **168**, 1603-1615.

Zhu J., Brown K.M. & Lynch J.P. (2010a) Root cortical aerenchyma improves the drought tolerance of maize (*Zea mays* L.). *Plant, Cell & Environment*, **33**, 740-749.

Zhu J., Kaeppler S.M. & Lynch J.P. (2005a) Mapping of QTL controlling root hair length in maize (*Zea mays* L.) under phosphorus deficiency. *Plant And Soil*, **270**, 299-310.

Zhu J., Kaeppler S.M. & Lynch J.P. (2005b) Topsoil foraging and phosphorus acquisition efficiency in maize (*Zea mays*). *Functional Plant Biology*, **32**, 749-762.

Zhu J. & Lynch J.P. (2004) The contribution of lateral rooting to phosphorus acquisition efficiency in maize (*Zea mays*) seedlings. *Functional Plant Biology*, **31**, 949-958.

Zhu J., Zhang C. & Lynch J.P. (2010b) The utility of phenotypic plasticity of root hair length for phosphorus acquisition. *Functional Plant Biology*, **37**, 313-322.

Figures and Tables

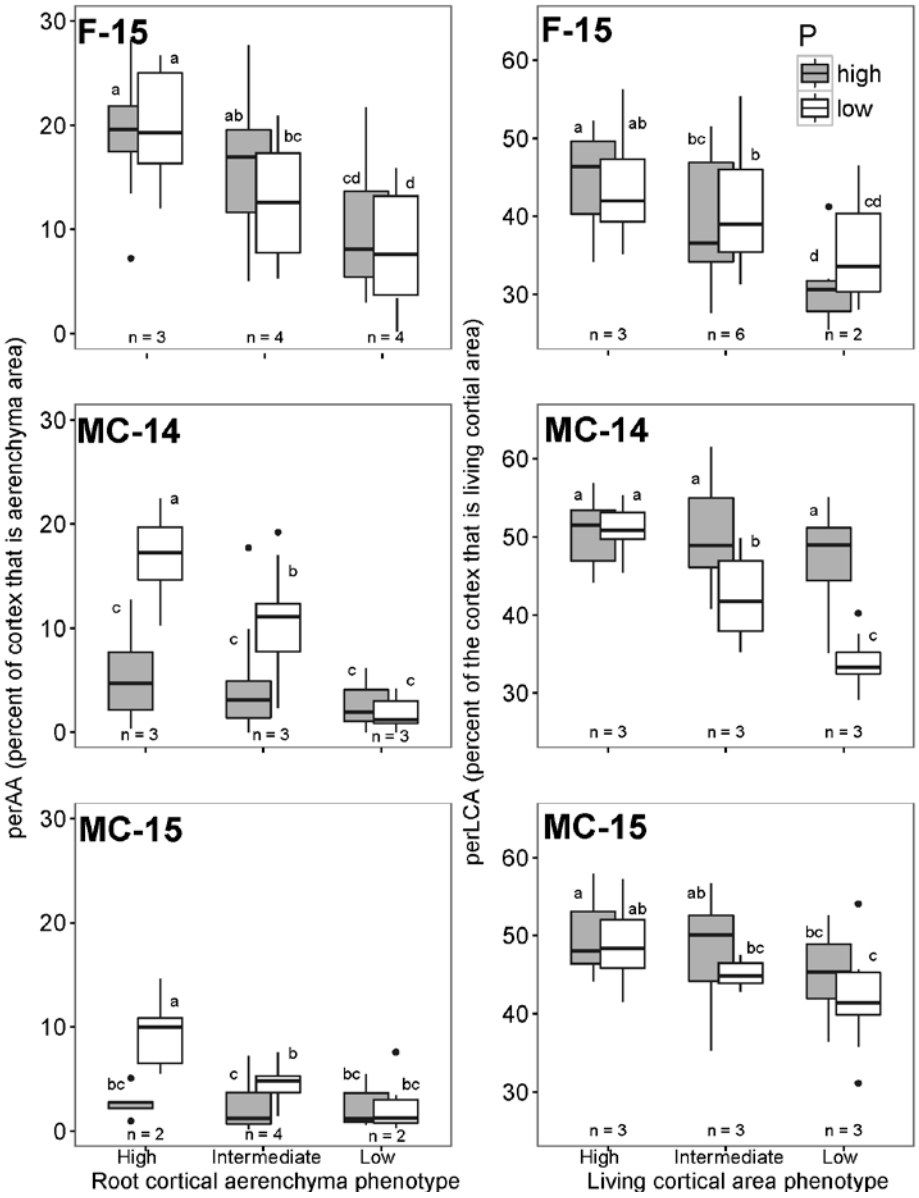

Figure 1-1. Box plots showing the phenotypic variation in root cortical aerenchyma (RCA) and living cortical area (LCA) expressed as percent of the cortical area in maize inbred lines in the two mesocosm (MC-14 and MC-15) and the field (F-15) experiment with two phosphorus treatments each. States of each phene were grouped into phenotype classes. Boxplots show means, 25th and 75th percentiles and ±1.5 IQR on the whiskers, of RCA and LCA of the specified number of genotypes (n). Means with the same letter are not significantly different ($p > 0.05$).

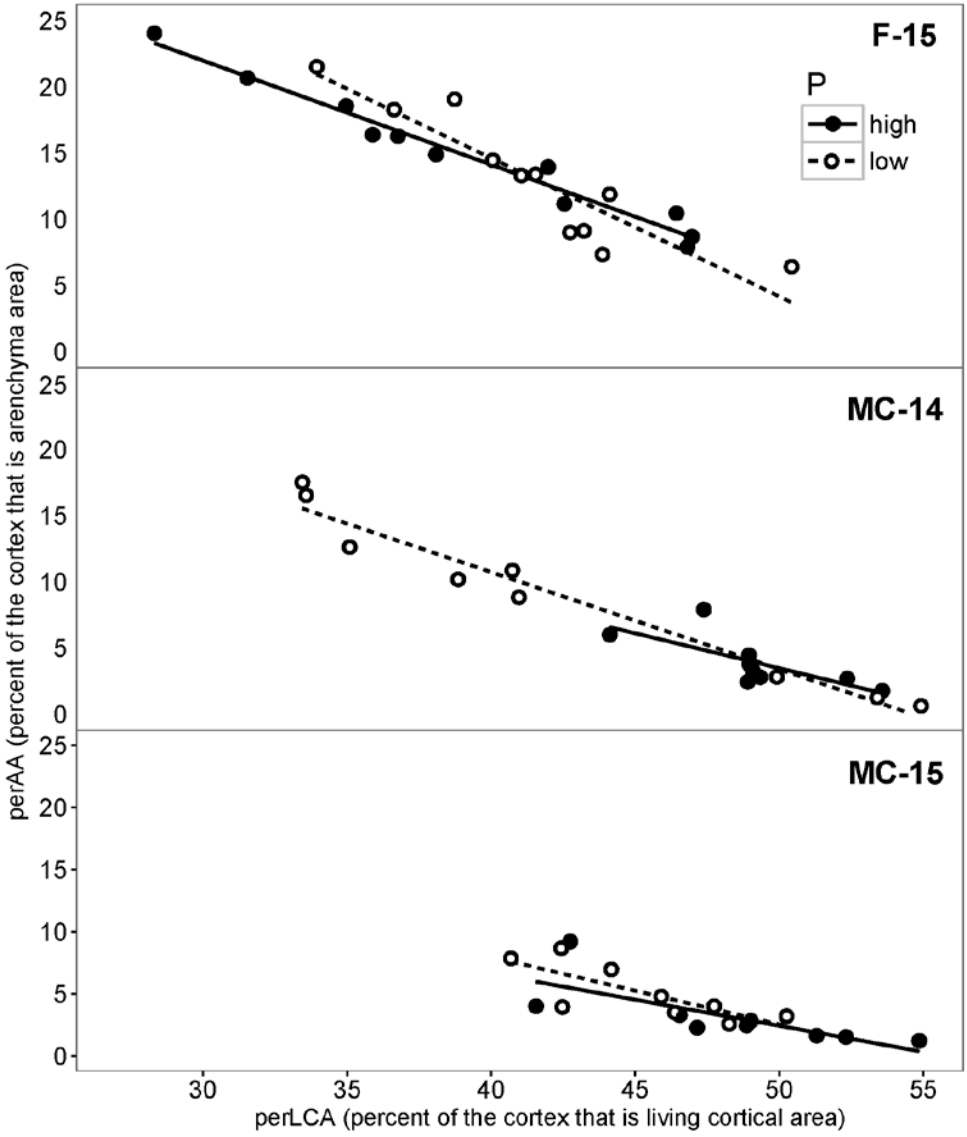

Figure 1-2**.** Linear correlations between percent living cortical area and percent root cortical aerenchyma of maize plants in the two mesocosm experiments (MC-14, MC-5), and the field experiment (F-15). High P: F-15 ($p < 0.001$, $R^2 = 0.81$); MC-14 ($p < 0.03$, $R^2 = 0.47$); MC-15 ($p < 0.03$, $R^2 = 0.49$). Low P: F-15 ($p < 0.0001$, $R^2 = 0.97$); MC-14 ($p < 0.0001$, $R^2 = 0.95$); MC-15 ($p < 0.02$, $R^2 = 0.55$). Points are means of four replicates of each genotype for each experiment.

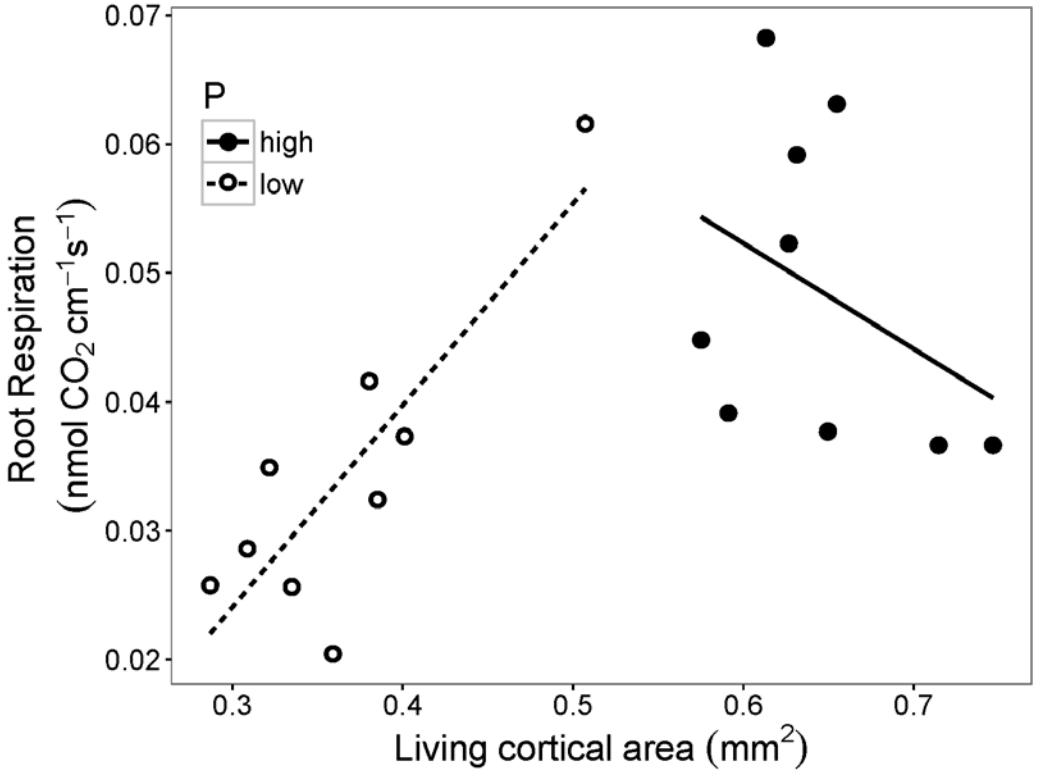

Figure 1-3. Linear correlations between living cortical area and root segment respiration of maize roots under low ($p < 0.005$, $R^2 = 0.69$) and high ($p > 0.3$, $R^2 = 0.01$) phosphorus. Points are means of four replicates per genotype of the mesocosm experiment MC-14.

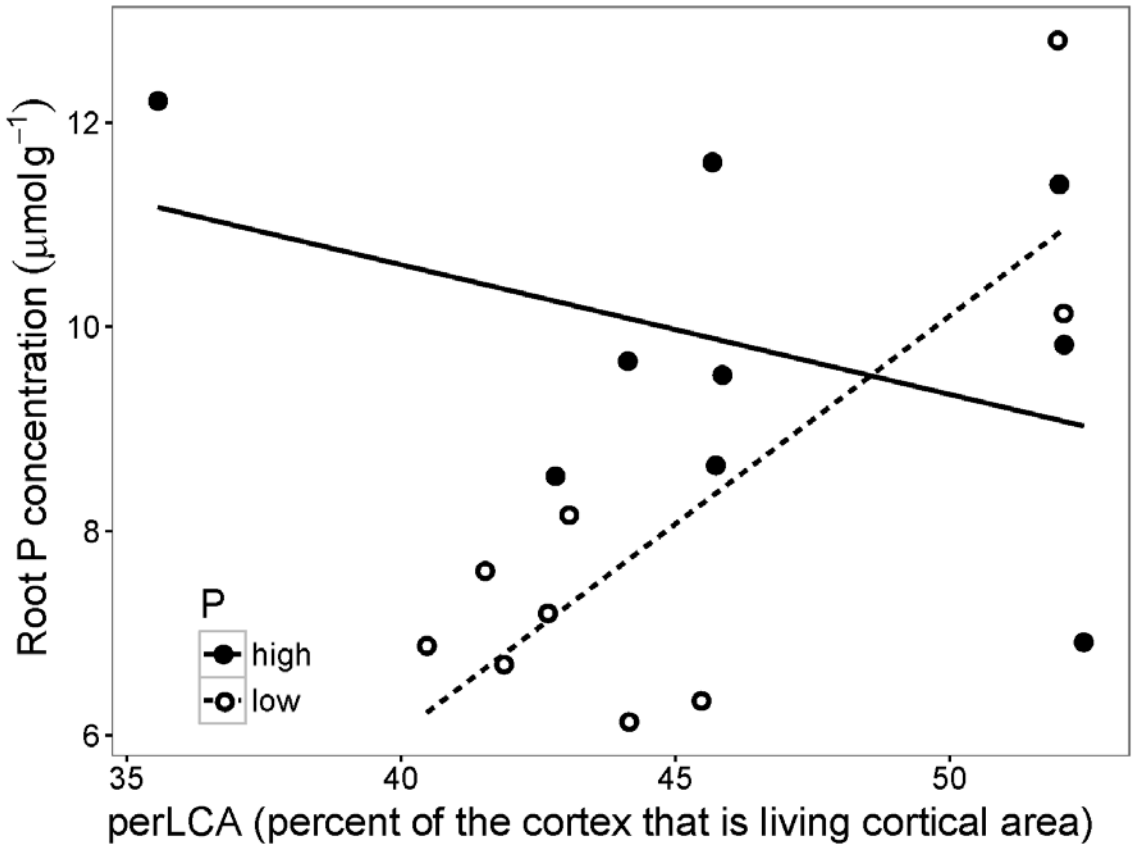

Figure 1-4. Linear correlations between percent living cortical area and phosphorus concentration under low ($p < 0.05$, R^2=0.62) and high ($p > 0.1$, R^2=0.05) phosphorus. Points are values of individual plants from the mesocosm experiment MC-15, taken in one block.

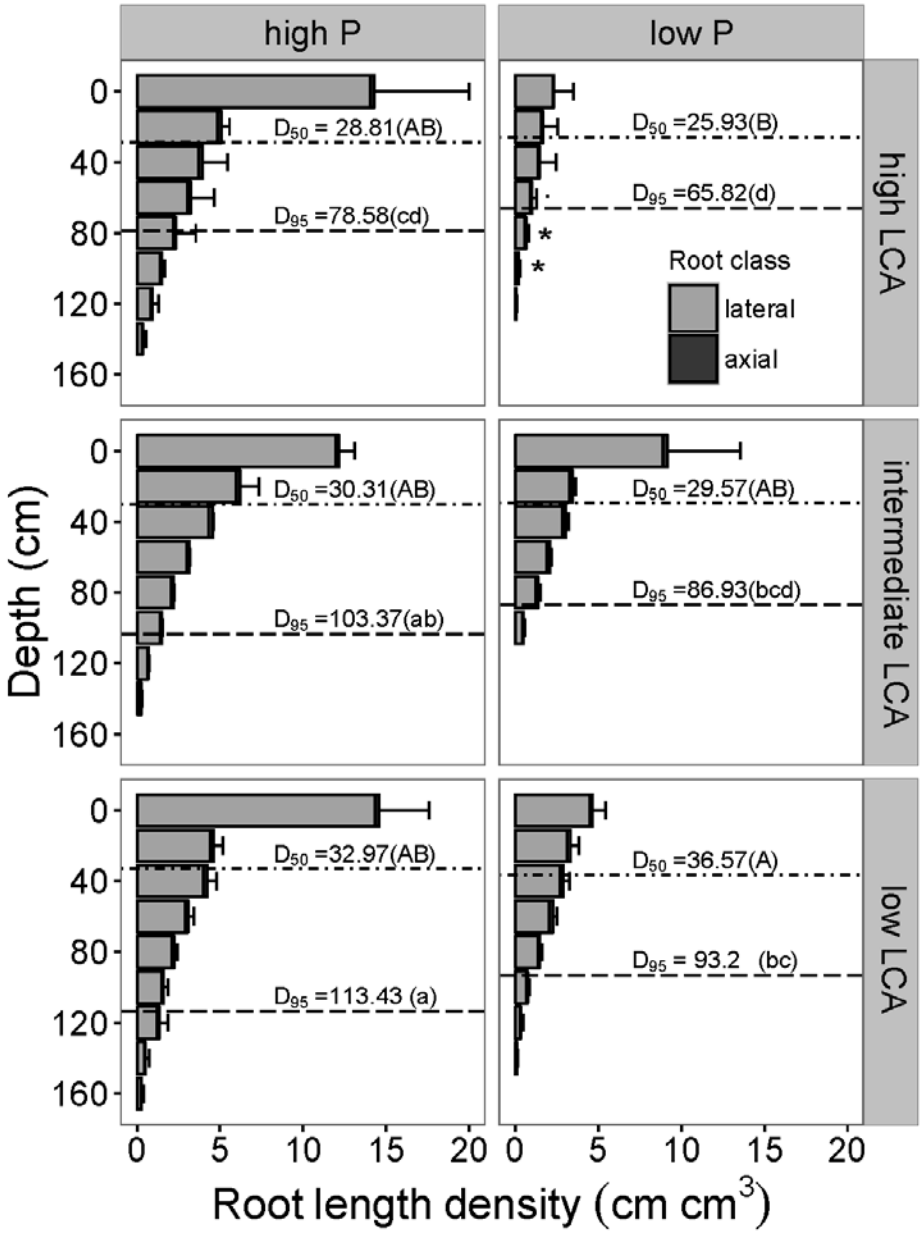

Figure 1-5. Root depth distribution in the mesocosms experiment MC-14. Bars are means of root length density (RLD) of four replicates of three genotypes for each LCA class (mean ± SE). Each bar shows the mean of lateral and axial roots at each depth. Rooting depths (D_{95} and D_{50}) with the same letter (uppercase for D_{50}, lowercase for D_{95}) were not significantly different ($p > 0.05$). LCA: Living cortical area.

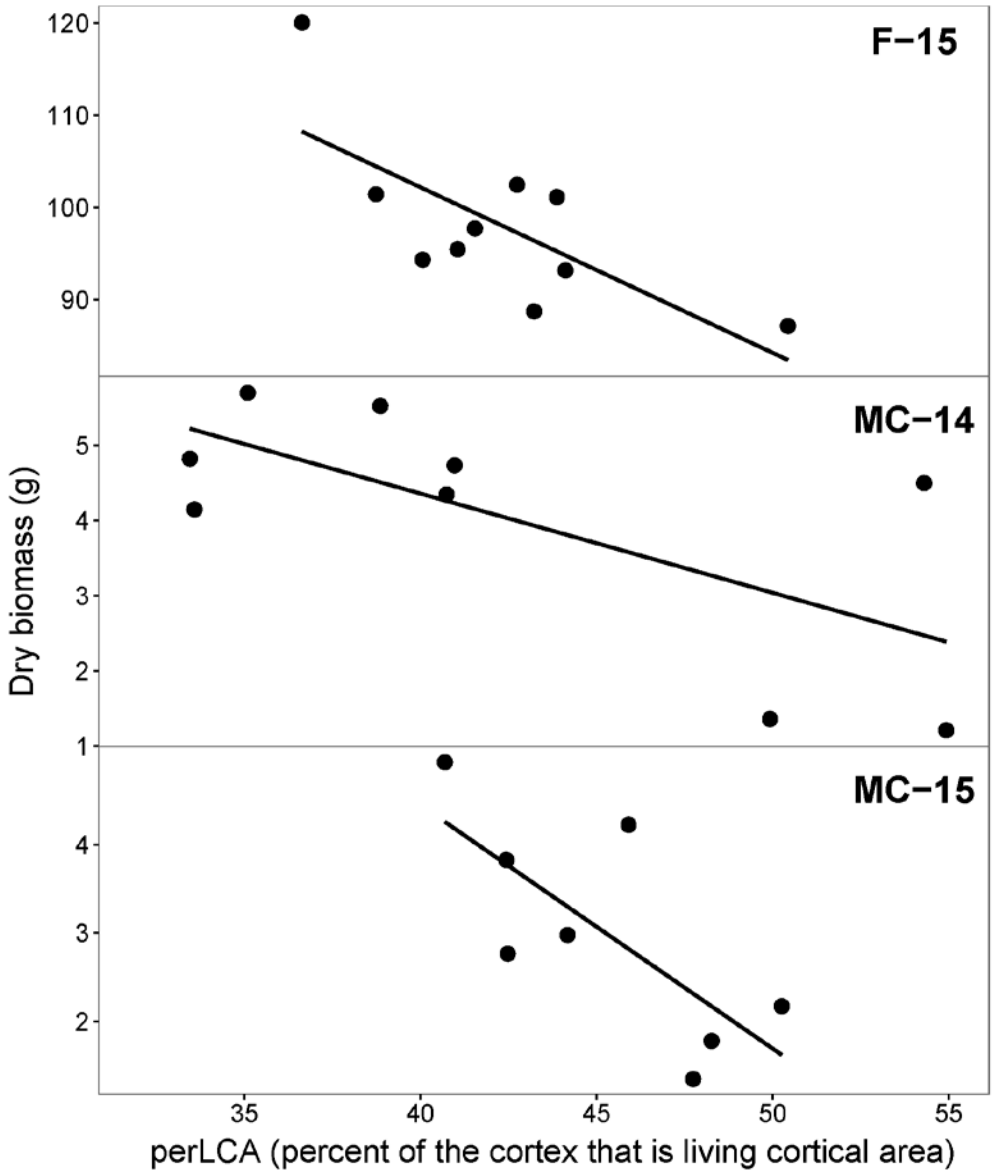

Figure 1-6. Linear correlations between percent living cortical area and dry shoot biomass under low phosphorus in the field experiment (F-15) and the two mesocosm experiments (MC-14 and MC-15). F-15 ($p < 0.03$, $R^2 = 0.39$); MC-14 ($p < 0.05$, $R^2 = 0.47$); MC-15 ($p < 0.05$, $R^2 = 0.47$). Points are means of four replicates of each genotype. Linear models under high phosphorus were not significant ($p > 0.05$, not shown).

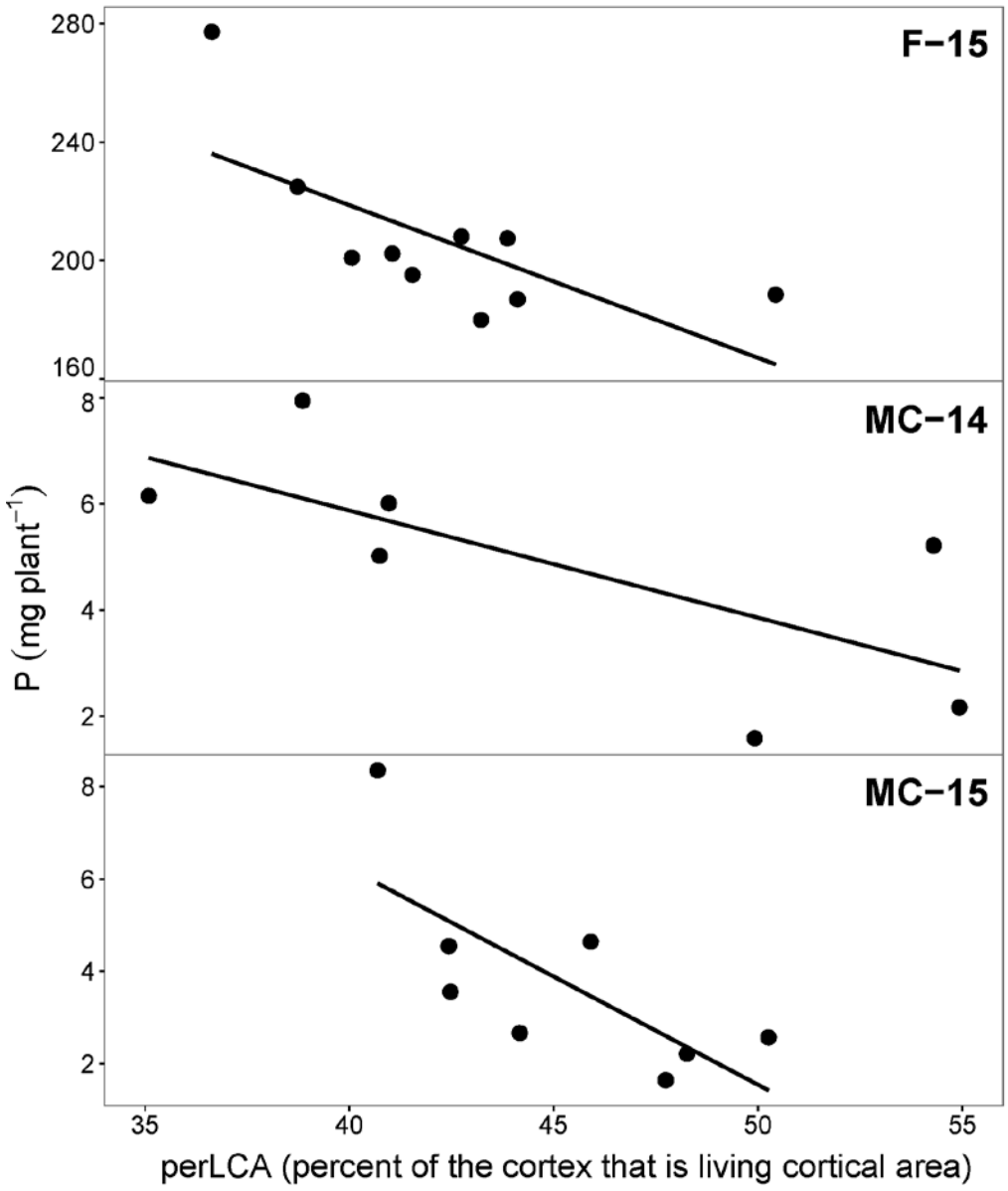

Figure 1-7. Linear correlations between percent living cortical area and leaf phosphorus content under low phosphorus in the field experiment (F-15) and the two mesocosm experiments (MC-14 and MC-15). F-15 ($p < 0.03$, $R^2 = 0.41$); MC-14 ($p < 0.05$, $R^2 = 0.38$); MC-15 ($p < 0.05$, $R^2 = 0.46$). Points are means of four replicates of each genotype. Linear models under high phosphorus were not significant ($p > 0.05$, not shown).

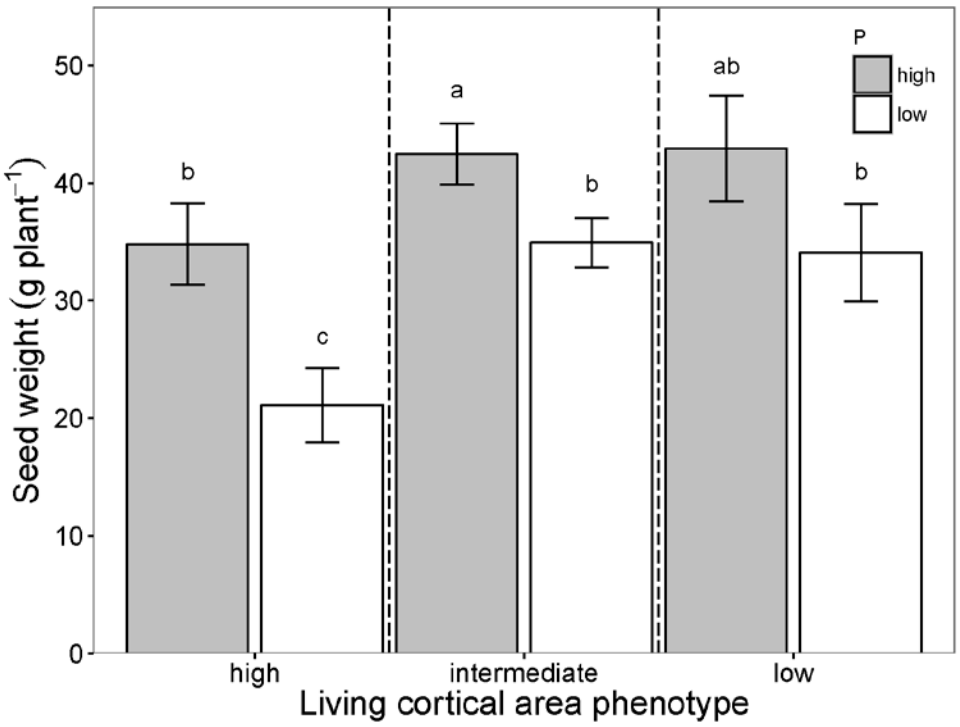

Figure 1-8 Grain yield of field-grown maize plants with low and intermediate living cortical area phenotypes under high and low phosphorus. Data are means (± SE) of four replicates of three high-LCA, six intermediate-LCA, and two low-LCA genotypes. Means with the same letter are not significantly different ($p > 0.05$).

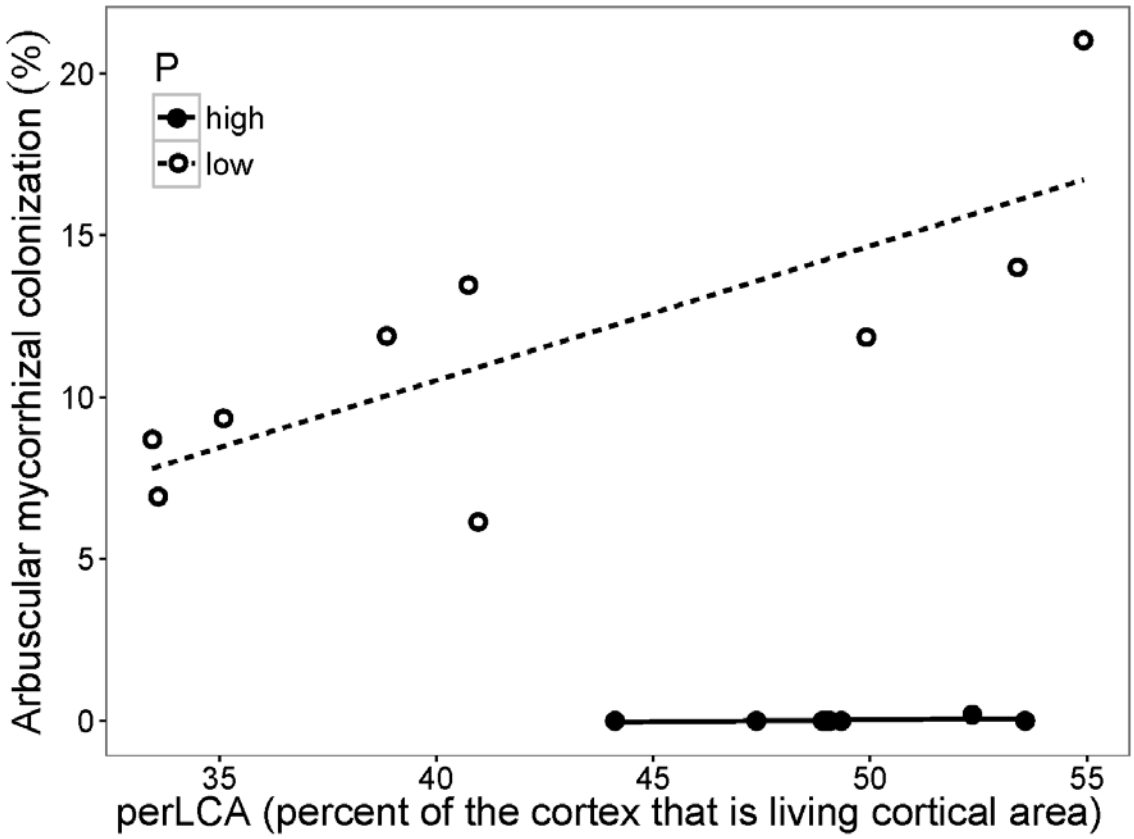

Figure 1-9. Linear correlation between percent arbuscular mycorrhizal colonization and percent living cortical area in axial nodal roots of inoculated plants under low phosphorus ($p < 0.02$, $R^2 = 0.54$). Inoculated roots showed no colonization in the axial nodal roots under high phosphorus. Points are means of four plants per genotype of a mesocosm experiment (MC-14).

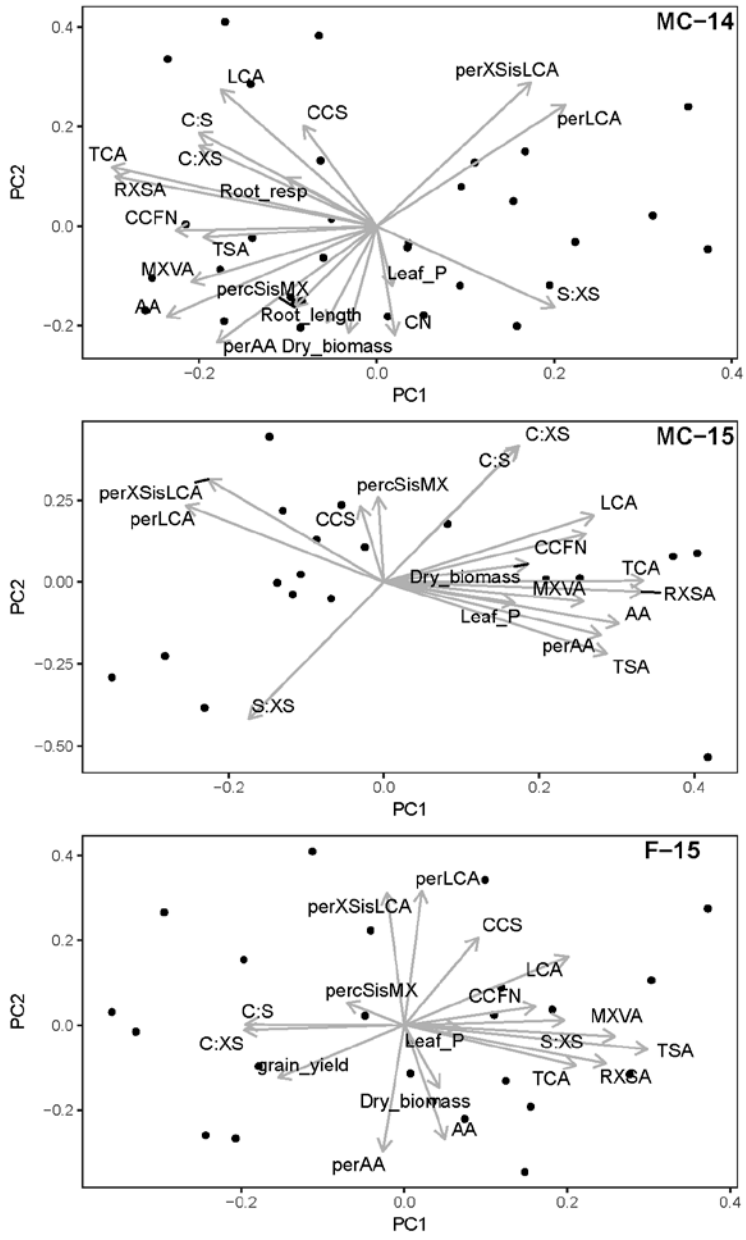

Figure 1-10. Principal component analysis (PCA) of different anatomical traits and plant biomass (Dry_biomass) and leaf phosphorus content (Leaf_P) for the mesocosm experiments (MC-14 and MC-15), and the field experiment (F-15) under low phosphorus. Additionally, root respiration (Root_resp), crown root number (CN), and total root length (Root_length) are included only in MC-14; grain yield is included only in F-15. 90° angles between two arrows indicates no linear dependence of the respective variables. RXSA: root cross-section area, TCA: total cortical area, TSA: total stele area, C:S: ratio cortex to stele, C:XS: ratio cortex to cross-section, AA: aerenchyma area, perAA: percent of the cortex that is aerenchyma area, CCFN: cortical cell file number, LCA: living cortical area, perLCA: percent of cortex that is living cortical area, perXSisLCA: percent of cross section that is living cortical area, CCS: cortical cell size, MXVA: metaxylem vessel area.

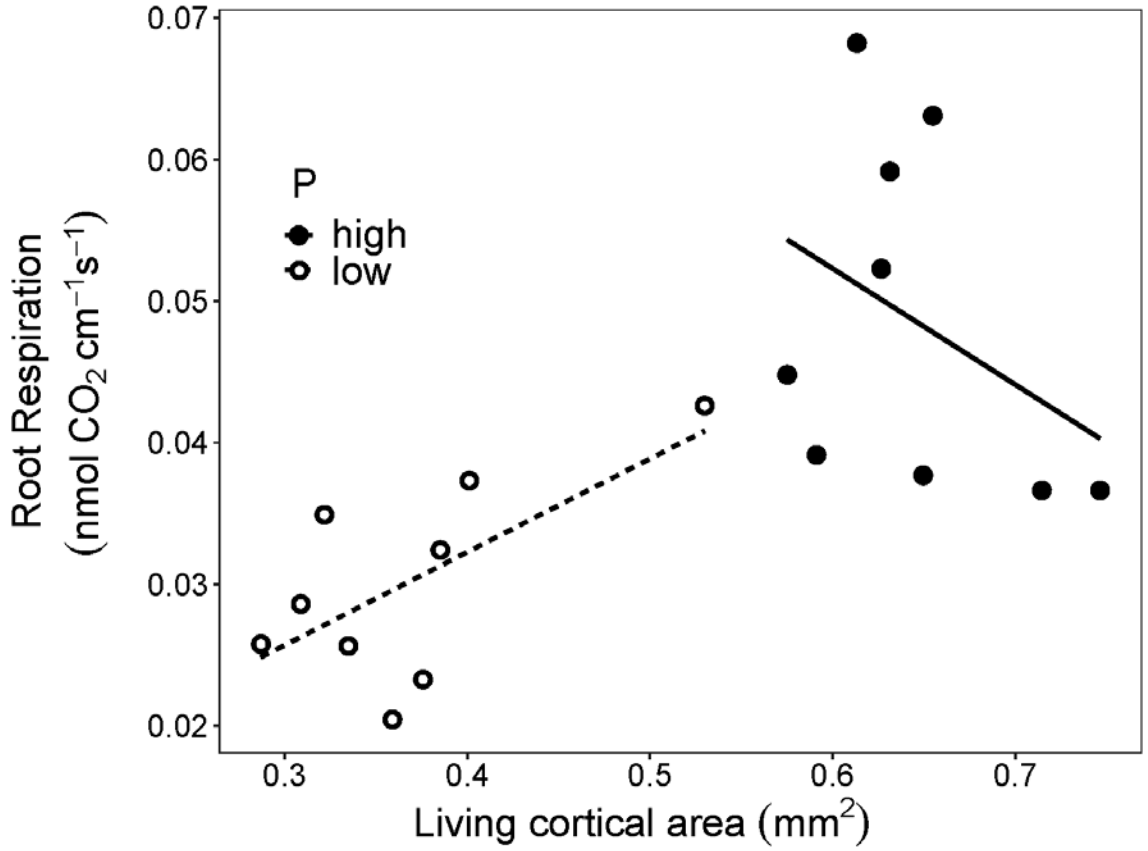

Figure 1-11. Replication of Figure 1-3 without extreme values of single plant data points. Linear correlations between living cortical area and root segment respiration under low ($p < 0.057$, $R^2 = 0.344$) and high ($p > 0.3$, $R^2 = 0.01$) phosphorus. Points are means of up to four replicates per genotype of the mesocosm experiment MC-14.

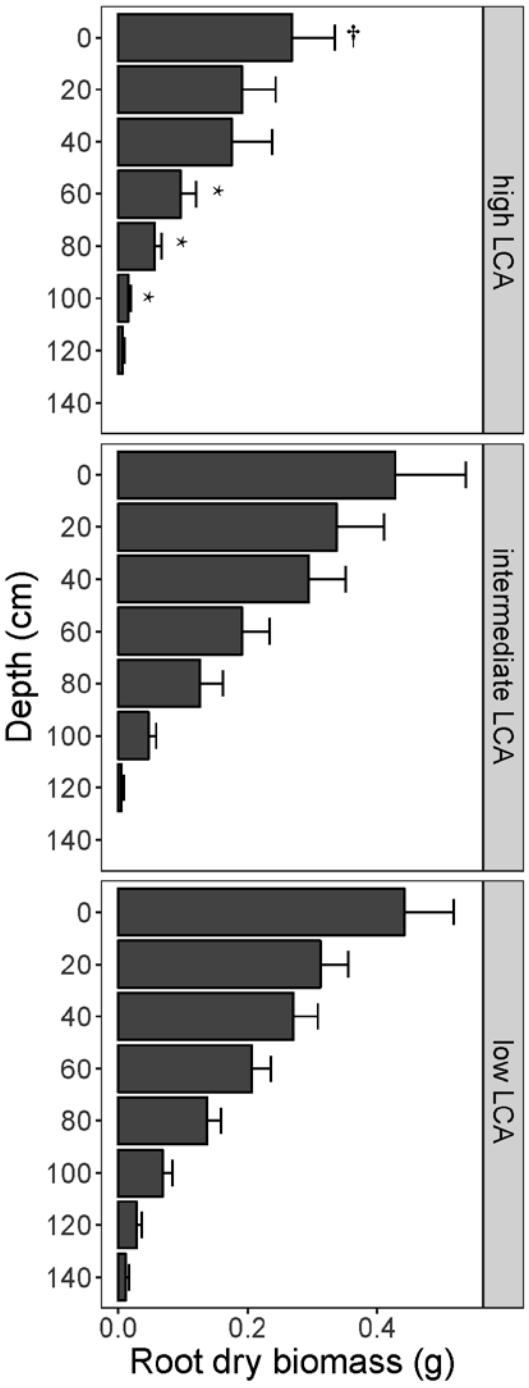

Figure 1-12. Root dry biomass of mesocosm-grown maize (50 d.a.p.) of contrasting living cortical area (LCA) phenotypes under low phosphorus in MC-14. Bars are means of three genotypes per LCA class (mean ± SE). Differences in root dry biomass between the high LCA phenotype and each of the other two LCA phenotypes per depth are shown (* $p \leq 0.05$; † $p \leq 0.1$).

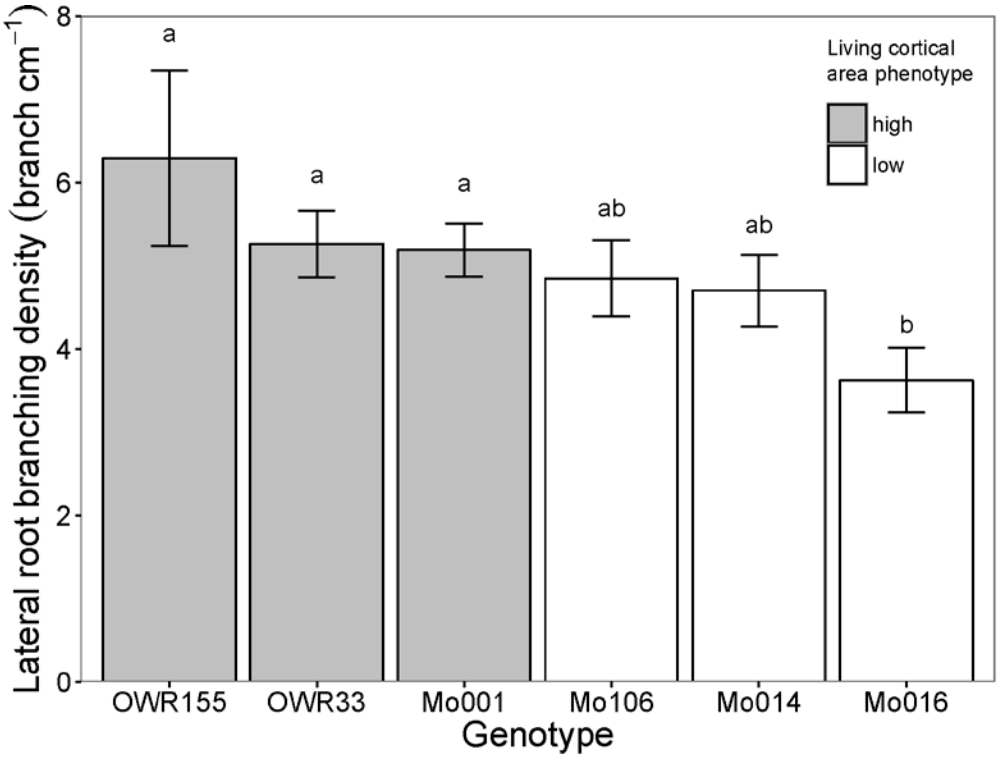

Figure 1-13. Lateral root branching density (LRBD) in mesocosm-grown plants (MC-14). Bars are average values of four replicates (± SE) per genotype under low phosphorus. Means with the same letter are not significantly different ($p > 0.05$).

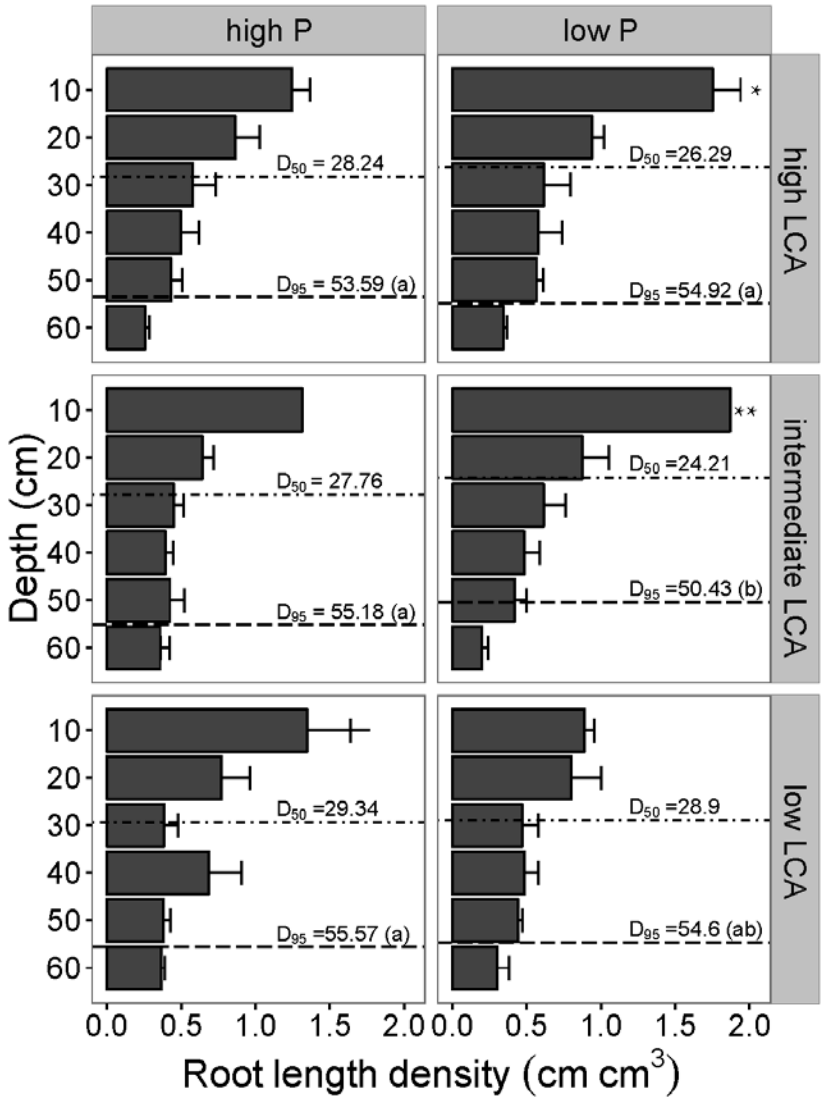

Figure 1-14. Root length distribution (RLD) of field-grown maize (100 d.a.p.) of contrasting living cortical area (LCA) phenotypes under high and low phosphorus in F-15. Bars are means of four plots of three genotypes for high-LCA, six genotypes for intermediate-LCA, and two genotypes for low-LCA (mean ± SE). Differences at 20 cm depth in RLD between the low LCA phenotype and each of the other two LCA phenotypes are shown (*$p \leq 0.05$, ** $p \leq 0.01$). No differences in RLD where found at other depths or in high phosphorus treatments. Rooting depths (D95) with the same letter or without letters (D50) are not significantly different ($p > 0.05$).

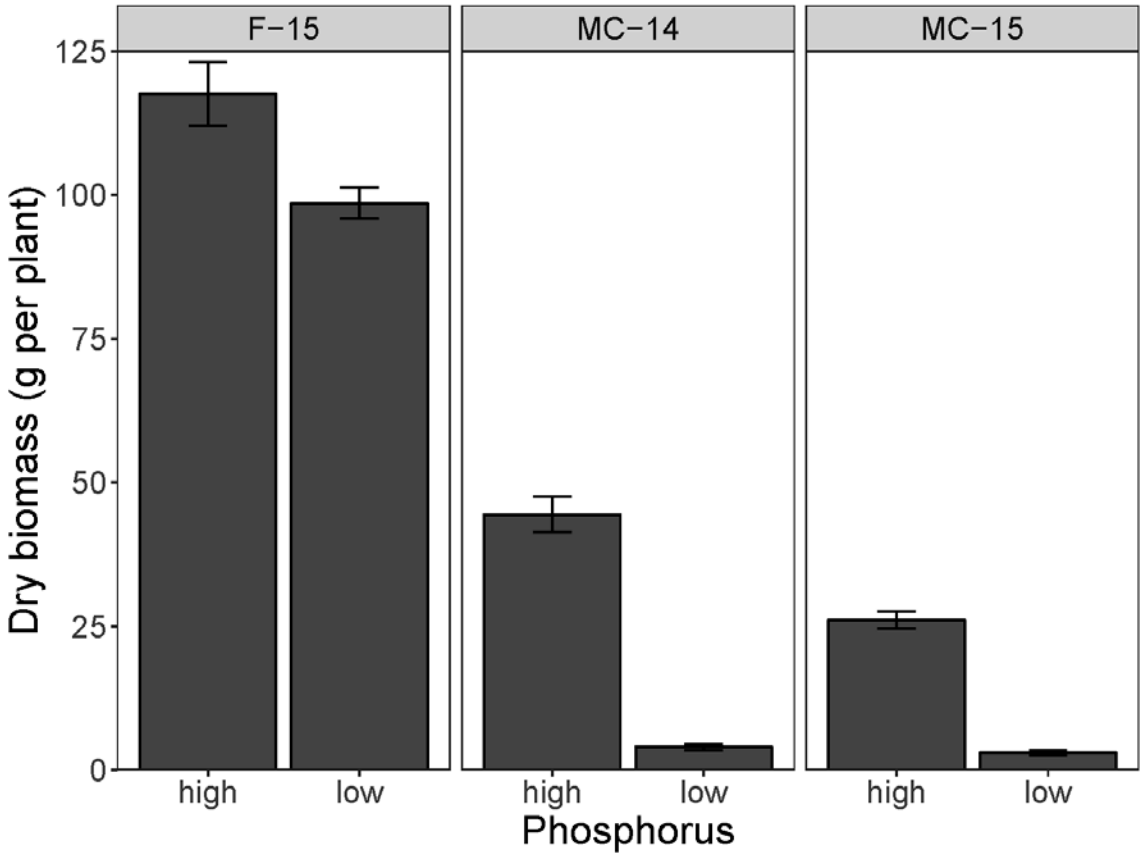

Figure 1-15. Low-phosphorus stress effect on shoot dry biomass of the mesocosm experiments (MC-14 and MC-15), and the field experiment (F-15). Data are means (± SE) of genotype means. Phosphorus treatment had significant effect on the values in all the experiments ($p \leq 0.05$). The percent reductions due to the low-phosphorus treatment were 90% (MC14), 88% (MC-15), and 16% (F-15).

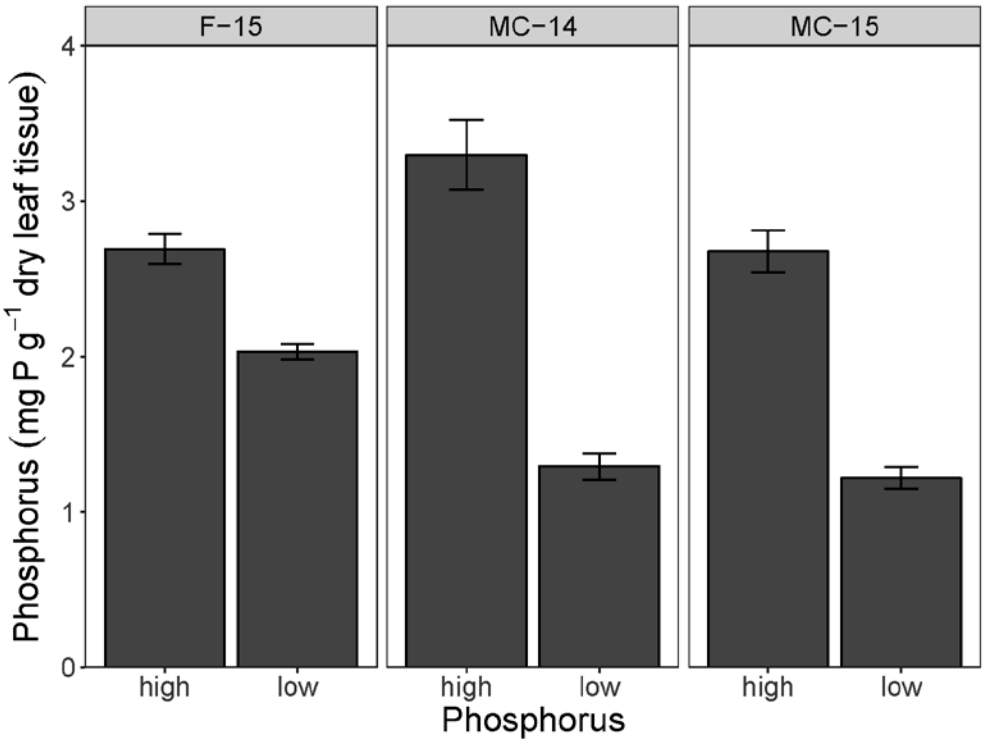

Figure 1-16. Low-phosphorus stress effect on leaf phosphorus content of the mesocosm experiments (MC-14 and MC-15), and the field experiment (F-15). Data are means (± SE) of genotype means. Phosphorus treatment had significant effect on the values in all the experiments ($p \leq 0.05$). The percent reductions due to the low-phosphorus treatment were 60% (MC14), 71% (MC-15), and 51% (F-15).

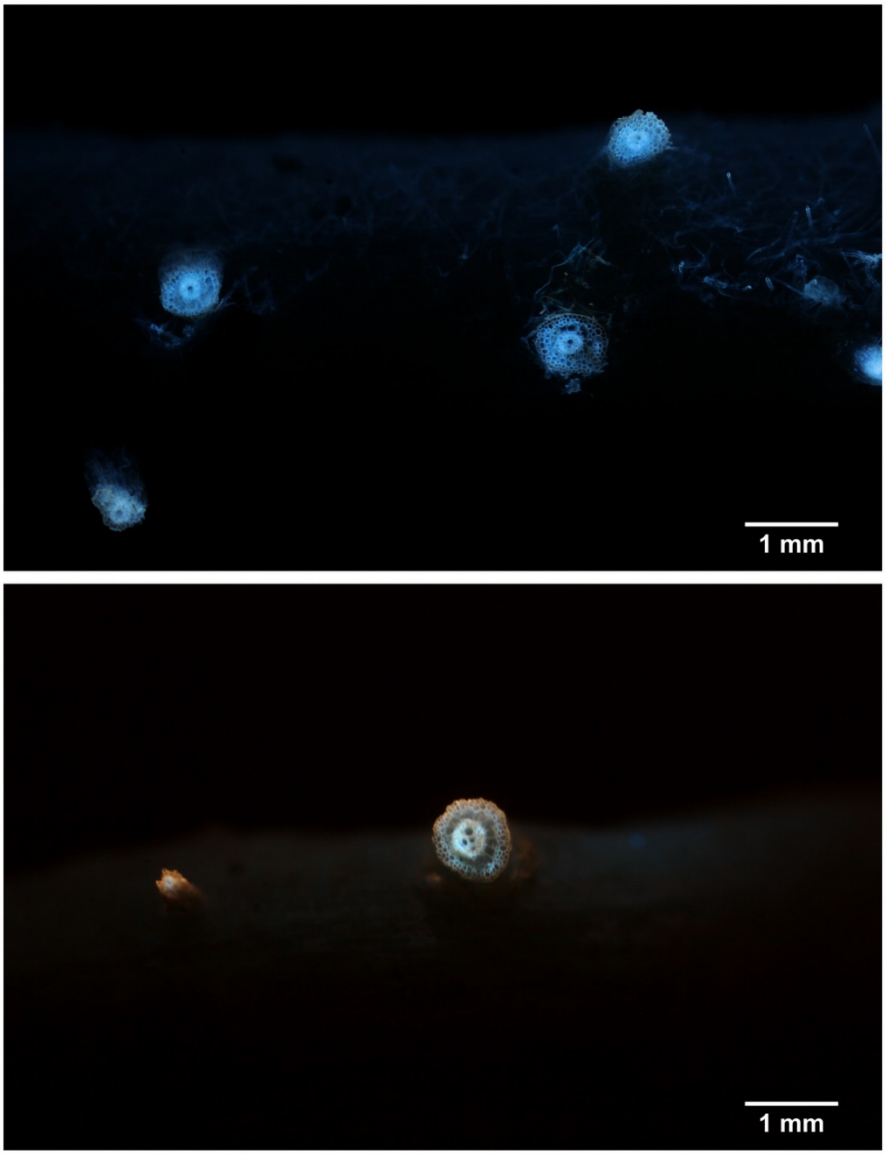

Figure 1-17. Root cortical aerenchyma (RCA) formation in lateral roots was observed in both, mesocosm-grown (top), and field-grown (bottom) plants. Images were taken within 1 cm from the main axis. No RCA formation was observed in lateral roots 1 cm beyond the point of attachment to the axial root.

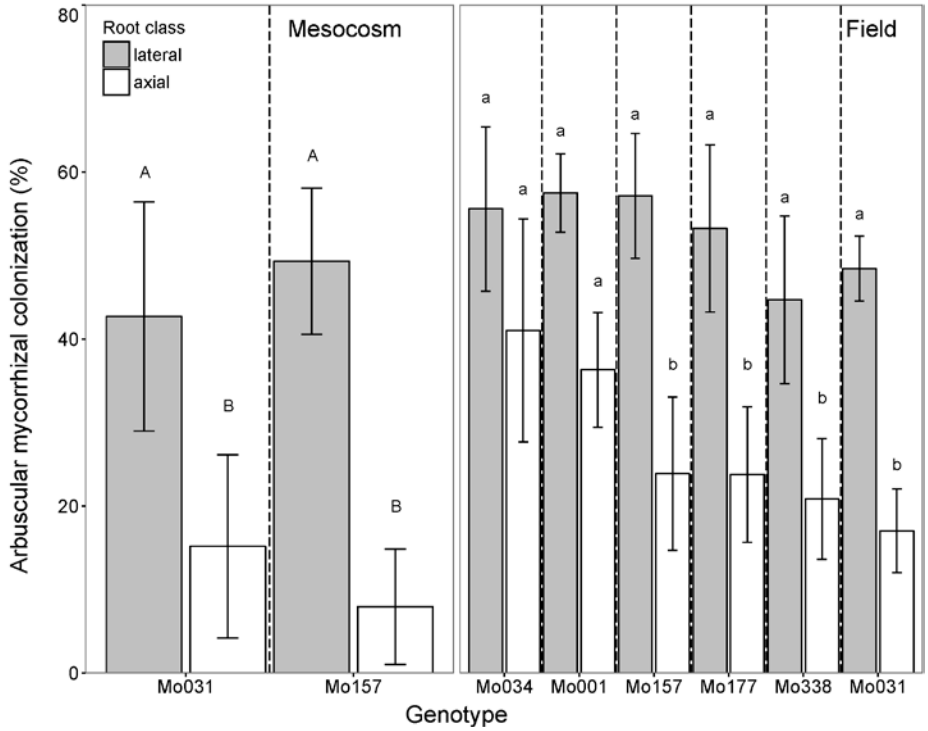

Figure 1-18. Observations of AMC of axial and lateral roots of maize plants growing under field and mesocosm conditions in 2012. Measurements done in the second and third whorls of the nodal system 0-20 cm depth. Bars are averages of three replicates per genotype in the field, and four replicates in the mesocosm experiment. Means with the same letter were not significantly different ($p > 0.05$). Fertilization was provided for the field experiment as recommended for maize, and low phosphorus was imposed in the mesocosm experiment. Growth conditions of the field plants were previously described by Saengwilai *et al.* (2014a) for the Pennsylvania site, and for the mesocosm study we used similar conditions of the experiment MC-14 of the present study.

Table 1-1**.** Importance of root cortical aerenchyma (RCA) and living cortical area (LCA) for biomass, phosphorus leaf content, root respiration, and grain yield as determined by Random Forest in the mesocosm experiments (MC-14 and MC-15), and the field experiment (F-15). The values are scores of each variable among a group of 22, where 1 is the most important and 22 is the least important variable. See Supporting Table 1-6. for the complete list of variables. Other anatomical phenes ranked among the first five most important variables are shown. RXSA: root cross-section area, TCA: total cortical area, TSA: total stele area, C:S: ratio cortex to stele areas, C:XS: ratio cortex to cross-section areas, AA: aerenchyma area, perAA: percent of the cortex that is aerenchyma area, CCFN: cortical cell file number, LCA: living cortical area, perLCA: percent of cortex that is living cortical area, perXSisLCA: percent of cross section that is living cortical area, CCS: cortical cell size.

Response variable	**Anatomical phene**				**Other important anatomical phenes**
	LCA	**perLCA**	**AA**	**perAA**	
	Importance score of the phene as predictor of the response variable				
MC-15					
Biomass	2	3	16	14	CCFN; TSA
Leaf phosphorus content	2	6	13	18	CCFN; TSA; RXSA
MC-14					
Biomass	9	1	4	3	perXSisLCA; CCS
Leaf phosphorus content	8	1	5	4	perXSisLCA; C:XS
Root respiration	8	17	12	18	CCS; RXSA; TCA
F-15					
Biomass	5	1	21	24	perXSisLCA
Leaf phosphorus content	8	7	23	24	CCFN; CCS; RXSA
Grain yield	14	15	2	6	C:S

Table 1-2. Summary of ANOVAs for D_{95} and D_{50} (which indicates the depths above which 95% or 50% of the root length are located, respectively) in field (F-15) and greenhouse-grown (MC-14) maize plants as affected by phosphorus and living cortical area (LCA) phenotype. The associated *F* values and probabilities (ns, not significant; † $p < 0.1$; * $p < 0.05$; ** $p < 0.01$; *** $p < 0.0001$) are presented.

Source of variation	**F-15**		**MC-14**	
	D_{50}	D_{95}	D_{50}	D_{95}
P	1.21^{ns}	$3.84^{\cdot}$	0.05^{ns}	11.17^{**}
LCA	1.06^{ns}	3.78^{*}	3.15†	15.33^{***}
P x LCA	0.28^{ns}	7.83^{**}	0.66^{ns}	0.21^{ns}

Table 1-3. Summary of linear models of biomass and phosphorus content as predicted by arbuscular mycorrhizal colonization (AMC) of maize plants in the mesocosm experiment MC-14. *F* values are followed by the numerator and denominator degrees of freedom in parenthesis.

Variable	R^2	*p*-value	*F*-value
Phosphorus	0.099	0.084	2.695 (2,29)
Biomass	0.049	0.183	1.803 (2,29)

Table 1-4. Maize genotypes with their respective living cortical area phenotypes used for each mesocosm (MC-14, MC-15) and in the field experiment (F-15) and root angle of nodal roots by Burton *et al.* (2010) and root hair length by Zhu *et al.* (2005a). *qualitative scale: 1 is shallow and 9 is steep.

Genotype	Living cortical area phenotype			root angle*	root hair length (mm)
	High	Intermediate	Low		
Mo001	MC-14	F-15, MC-15		6	-
Mo008	F-15	MC-15		7	2.253
Mo014			MC-14	6	2.234
Mo016			MC-14	6	-
Mo031	MC-15	F-15		5	2.125
Mo034		F-15		7	2.116
Mo048	F-15, MC-15			6	2.938
Mo058		MC-14		6	1.781
Mo060		MC-14		5	2.394
Mo067	F-15	MC-15, MC-14		6	1.925
Mo106			MC-14	6	1.438
Mo157	MC-15	F-15		6	1.296
Mo165		F-15		7	3.048
Mo196			F-15, MC-15	6	2.673
Mo199		F-15	MC-15	5	1.382
Mo337			F-15	5	-
OHW155	MC-14			6	-
OHW33	MC-14			5	-
range				3 to 9	0.616-3.467

Table 1-5. Specific root length (SRL) values used to calculate total root length for the mesocosm experiment MC-14.

Root class	Depth (cm)	P	SRL ($m*g^{-1}$ dry weight)
Lateral roots	0-160	high	189.00
Lateral roots	0-140	low	379.00
Axial roots	0-20	high	3.07
	20-40		8.85
	40-60		12.16
	60-80		9.95
	80-100		13.24
	100-120		14.84
	120-140		17.85
	140-160		17.47
	>160		27.04
Axial roots	0-20	low	12.83
	20-40		23.69
	40-60		27.60
	60-80		39.61
	80-100		33.96
	100-120		44.73
	120-140		68.97

Table 1-6. List of anatomical variables included in the multivariate analyses to identify important predictors of biomass, leaf phosphorus content, root respiration and grain yield.

Anatomical phene or phene aggregate	Abbreviation	Units
Root cross section area	RXSA	mm^2
Cortex area	TCA	mm^2
Stele area	TSA	mm^2
Cortex:Stele ratio	C:S	-
Cortex:Cross section ratio	C:XS	-
Stele:Cross section ratio	S:XS	-
Aerenchyma area (sum of all the individual aerenchyma lacunae area of each cross-section)	AA	mm^2
Percentage of cortex that is aerenchyma	perAA	%
Cortical cell file number	CCFN	Count
Living cortical area (LCA)	LCA	mm^2
Percentage of cortex that is LCA	perLCA	%
Percentage of cross section that is LCA	perXSisLCA	%
Median cortical cell size	CCS	μm^2
Cortical cell number	CCN	Count
Median of size of cells in hypodermis and the epidermis	CS_Hypo_Epi	μm^2
Median of size of cells in hypodermis	CS_Hypo	μm^2
Median of size of cells in middle layers of cortex	CS_Mid	μm^2
Median of size of cells in inner cortical area close to endodermis	CS_closetoEndo	μm^2
Number of cells in hypodermis and the epidermis	CN_Hypo_Epi	Count
Number of cells in hypodermis	CN_Hypo	Count
Number of cells in middle layers of cortex	CN_Mid	Count
Number of cells in inner cortical area close to endodermis	CN_closetoEndo	Count

Table 1-7. Summary of ANOVAS of the effects of root diameter, aerenchyma area (AA) and living cortical area (LCA) on root respiration in the mesocosm experiment MC-14 under high and low phosphorus.

	Root diameter (mm)		AA (mm^2)		LCA (mm^2)	
phosphorus level	low	high	low	high	low	high
F value	3.765	0.052	0.003	2.175	17.217	1.085
R^2	0.257	-0.134	-0.142	0.128	0.670	0.010
p	0.094	0.826	0.955	0.184	0.004	0.332

Table 1-8. Effects of living cortical area (LCA) phenotype on average root lengths per depth increment and root diameters in the soil cores of the field experiment (F-15) under low phosphorus. Means with the same letter within depth increments are not significantly different ($p > 0.05$). Significance of p values are shown as † for $p \leq 0.1$, * for $p \leq 0.05$, ** for $p \leq 0.01$; values without a symbol are not significantly different

.

Depth (cm)	>0.5 mm				0.2-0.5 mm				0-0.2 mm			
	F and *p* values	Root length mean (cm)			*F* and *p* values	Root length mean (cm)			*F* and *p* values	Root length mean (cm)		
		High LCA	Intermediate LCA	Low LCA		High LCA	Intermediate LCA	Low LCA		High LCA	Intermediate LCA	Low LCA
10	2.42	98.5	78.9	40.3	1.59	129.4	148.2	82.4	2.51†	125.4 ab	154.8 a	60.8 b
20	6.59 *	58.5 a	36.1 b	35.2 b	0.29	65.5	60.1	70.8	1.04	70.5	82.8	63.5
30	0.85	32.3	27.6	19.7	0.11	43.9	45.4	38.8	0.24	32.3	27.6	19.7
40	0.29	51.7	44.6	47.0	0.27	44.1	32.3	31.1	0.42	26.7	23.2	21.1
50	1.51	50.9	41.3	46.8	6.45**	37.6 a	19.9 b	24.8 ab	4.76*	25.8 a	21.1 ab	17.7 b
60	4.32*	16.8 a	8.1 b	15.9 ab	3.21†	23.2 a	11.4 b	21.3 ab	0.59	30.5	23.0	27.9
Total root length (cm)	7.08*	257.5 a	190.6 ab	137.6 b	2.23	345	316.2	250.6	1.44	386.9	388.9	268.7

Table 1-9. Summary of ANOVAs of the effect of living cortical area (LCA) phenotype on the lateral root branching density (LRBD) in the first 30 cm of nodal roots collected with soil cores in the field experiment (F-15). Values are means of the means of three genotypes for high LCA, four genotypes for intermediate LCA, and four genotypes for low LCA.

Depth (cm)	***F* value**	**Lateral root branching density (branch*cm^{-1})**		
		High LCA	Intermediate LCA	Low LCA
10	0.7217	4.5	4.7	3.5
20	0.982	4.383	3.854	4.749
30	0.041	4.194	4.012	3.792

Table 1-10. Summary of multiple regression models of shoot dry biomass, leaf phosphorus content and grain yield as predicted by anatomical and architectural phenes and phene aggregates. The models were selected through stepwise regression analysis and the best linear model for each variable/experiment are shown. The variables included in the stepwise regression analyses were: Root architecture: RLD: root length density in the first 20 cm, LRBD: lateral root branching density in the first 20 cm, CN: number of axial roots (only for MC-14). Root anatomy: Root diameter, RXSA: root cross-section area, TCA: total cortical area, TSA: total stele area, C:S: ratio cortex to stele, C:XS: ratio cortex to cross-section, AA: aerenchyma area, perAA: percent of the cortex that is aerenchyma area, CCFN: cortical cell file number, LCA: living cortical area, perLCA: percent of cortex that is living cortical area, perXSisLCA: percent of cross section that is living cortical area, CCS: cortical cell size. Block: experimental block effect. Significance of *p* values are shown as † for $p \leq 0.1$, * for $p \leq 0.05$, ** for $p \leq 0.01$, *** for $p \leq 0.001$.

Experiment	Response variable	Effect	Coefficient	Std. Error	Pr(>|t|)		R^2 of the model	*p* of the model
Mesocosm	Shoot dry biomass	(Intercept)	-0.02555	0.05722	0.65727		0.957	2.20E-16
MC-14		RLD	0.92717	0.03116	< 2e-16	***		
		LRBD	-0.02634	0.02917	0.371157			
		Root diameter	0.09554	0.04414	0.035527	*		
		perLCA	0.07422	0.08293	0.375371			
		perAA	0.24487	0.06679	0.000625	***		
		Block	0.19305	0.09529	0.048475	*		
Mesocosm	Leaf phosphorus content	(Intercept)	0.30131	0.19802	0.13481		0.519	5.17E-07
MC-14		RLD	-0.16359	0.10502	0.126031			
		LRBD	0.13668	0.09793	0.169365			
		perAA	1.32433	0.22296	3.32E-07	***		
		perLCA	1.25233	0.25244	9.60E-06	***		
		TSA	0.79763	0.13147	2.13E-07	***		
		Block	-1.26017	0.3467	0.000688	***		
Field	Shoot dry biomass	(Intercept)	1.84E-16	0	1		0.152	0.062
F-15		perXSisLCA	-3.59E-01	-1.905	0.0699	†		
		CCFN	-2.87E-01	-1.527	0.1411			
Field	Leaf phosphorus content	(Intercept)	-0.08948	0.26108	0.7358		0.519	0.003

F-15		perLCA	0.39473	0.15539	0.0205	*		
		RLD	0.18975	0.17128	0.2825			
		C:S	-0.24501	0.14598	0.1105			
		Block	1.24411	0.45945	0.0144	*		
Field	Grain yield	(Intercept)	-7.49E-16	1.40E-01	1		0.627	0.004
F-15		TSA	-4.94E-01	2.25E-01	0.04858	*		
		CCS	8.43E-01	2.20E-01	0.00237	**		
		perLCA	-8.65E-01	2.15E-01	0.00167	**		
		CCFN	-7.24E-01	2.48E-01	0.01271	*		
		LRBD	4.40E-01	2.01E-01	0.04926	*		
		TCA	3.75E-01	2.72E-01	0.19323			

Table 1-11. Summary of regression models of shoot dry biomass, leaf phosphorus content and grain yield as predicted by anatomical and architectural phenes and phene aggregates in mesocosm study MC-14 and field study F-15. The predictors were sequentially included step by step from regression 1 to regression 6 or 7. The variables included were: RLD (root length density in the first 20 cm), LRBD (lateral root branching density in the first 20 cm), RD (Root diameter), perAA (percent of the cortical cross sectional area that is aerenchyma), CCFN (cortical cell file number), LCA (living cortical area), perLCA (percent of cortex that is living cortical area), perXSisLCA (percent of cross section that is living cortical area), CCS (cortical cell size). perLCA was included in the model when it improved the R^2 or *p* value. Significance of *p* values are shown as † for $p \leq 0.1$, * for $p \leq 0.05$, ** for $p \leq 0.01$, *** for $p \leq 0.001$.

MC14														
Shoot biomass														
Predictor	**Regression 1**		**Regression 2**		**Regression 3**		**Regression 4**		**Regression 5**		**Regression 6**		**Regression 7**	
RD	0.38	**	0.25	†	0.49	**	0.50	**	0.16	***	0.16	***		
perAA			0.31	*	0.24	†	0.24	†	0.18	***	0.17	***		
CCFN					-0.36	*	-0.36	†	-0.12	**	-0.12	**		
CCS							-0.03		-0.02		-0.02			
RLD									0.91	***	0.91	***		
LRBD											-0.01			
R^2	0.13		0.20		0.25		0.23		0.96		0.96			
R^2 change	0.13		0.07		0.05		-0.02		0.73		0.00			
Pr(>F)			0.000	***	0.000	***	0.415		< 2.2e-16	***	0.826			
Leaf P concentration														
RD	0.30	*	0.25		0.56	**	0.53	**	0.66	**	0.70	***	0.71	***
perLCA			-0.08		1.11	**	1.16	**	1.32	***	1.31	***	1.25	***
perAA					1.08	***	1.13	***	1.17	***	1.18	***	1.17	***
CCFN							0.08		0.15		0.12		0.06	
CCS									-0.36	**	-0.37	**	-0.37	**
RLD											-0.12		-0.12	
LRBD													0.16	
R^2	0.09		0.08		0.29		0.28		0.37		0.37		0.38	
R^2 change	0.09		-0.01		0.21		-0.01		0.09		0.00		0.01	
Pr(>F)			0.602		0.000	***	0.658		0.006	**	0.333		0.178	

F15													
Shoot biomass													
Predictor	**Regression 1**		**Regression 2**		**Regression 3**		**Regression 4**		**Regression 5**		**Regression 6**		**Regression 7**
RD	0.10		0.05		0.06		0.33		0.24		0.23		0.31
perXSisLCA			-0.30		-0.35		-0.43		-0.63		-0.61		-0.63
perAA					-0.06		-0.22		-0.23		-0.23		-0.25
CCFN							-0.52	†	-0.51	†	-0.51	†	-0.66
CCS									0.26		0.25		0.31
RLD											-0.07		-0.10
LRBD													0.20
R^2	-0.02		0.03		-0.03		0.13		0.11		0.06		0.03
R^2 change	0.00		0.05		-0.05		0.16		-0.02		-0.05		-0.03
*P*r(>F)			0.183		0.866		0.070	†	0.452		0.772		0.456
Leaf P concentration													
RD	-0.11		-0.06		-0.08		-0.06		-0.04		-0.02		-0.11
perLCA			0.44	*	0.59	†	0.58	†	0.65		0.61		0.62
perAA					0.17		0.16		0.18		0.18		0.19
CCFN							-0.03		-0.03		-0.03		0.14
CCS									-0.07		-0.05		-0.11
RLD											0.17		0.20
LRBD													-0.22
R^2	0.28		0.45		0.43		0.40		0.36		0.35		0.36
R^2 change	0.28		0.17		-0.02		-0.03		-0.04		-0.01		0.00
*P*r(>F)			0.027	*	0.554		0.895		0.824		0.420		0.316
Grain yield													
RD	-0.27	*	-0.36	.	-0.36		-0.57	*	-0.57	*	-0.29		
perAA			0.55	*	0.55	*	0.66	**	0.66	**	0.62	**	
CCFN					0.00		0.09		0.11		-0.30		

CCS					0.53	*	0.54	*	0.68	**	
RLD							0.08		0.12		
LRBD									0.44	†	
R^2	0.10		0.40		0.35		0.56		0.52		0.65	
R^2 change	0.00		0.31		-0.05		0.21		-0.04		0.13	
*P*r(>F)			0.005	**	0.998		0.018	*	0.646		0.058	†

Chapter 2 Root cortical anatomy differentially affects pathogenic and symbiotic fungal colonization in maize

Tania Galindo-Castañeda[1], Kathleen M. Brown[1], Gretchen A. Kuldau[2], Gregory W. Roth[1], Nancy G. Wenner[2], Swayamjit Ray[1], Jonathan P. Lynch[1].

[1]Department of Plant Science and [2]Department of Plant Pathology and Environmental Microbiology, The Pennsylvania State University, University Park, PA. 16802, USA

Prepared to be submitted to *New Phytologist*

Summary

Rationale.

Root anatomical phenotypes vary among maize (*Zea mays*) cultivars and may have adaptive value by modifying the metabolic cost of soil exploration. However, the microbial tradeoffs of these phenotypes are unknown. We hypothesized that axial roots of maize with contrasting cortical anatomy have different patterns of mutualistic and pathogenic fungal colonization.

Methods.

Increased aerenchyma and decreased living cortical area were associated with decreased mycorrhizal colonization in mesocosm and field experiments with inbred genotypes. In contrast, mycorrhizal colonization of hybrids increased with larger aerenchyma lacunae; this increase coincided with larger root diameters of hybrid roots. *F. verticillioides* colonization was inversely correlated with living cortical area in mesocosm-grown inbreds, and no relation was found between root rots and living cortical area or aerenchyma in field-grown hybrids. Root rots were positively correlated with cortical cell file number, and inversely correlated with cortical cell size. Mycorrhizae and root rots were inversely correlated in field-grown hybrids.Arbuscular

mycorrhizal colonization in the field and mesocosms, root rots in the field, and *Fusarium verticillioides* colonization in mesocosms were evaluated in maize genotypes with contrasting root cortical anatomy.

Key results.

Increased aerenchyma and decreased living cortical area were associated with decreased mycorrhizal colonization in mesocosm and field experiments with inbred genotypes. In contrast, mycorrhizal colonization of hybrids increased with larger aerenchyma lacunae; this increase coincided with larger root diameters of hybrid roots. *F. verticillioides* colonization was inversely correlated with living cortical area in mesocosm-grown inbreds, and no relation was found between root rots and living cortical area or aerenchyma in field-grown hybrids. Root rots were positively correlated with cortical cell file number, and inversely correlated with cortical cell size. Mycorrhizae and root rots were inversely correlated in field-grown hybrids.

Conclusion.

We conclude that anatomical phenotypes differentially affect pathogens and mycorrhizal colonization of nodal roots in maize.

Introduction

Root phenotypes that improve soil exploration and resource acquisition can improve crop production under suboptimal soil nutrient availability and drought, two primary constraints to global agriculture (Bishopp & Lynch, 2015; Lynch, 2015). Since such improved cultivars with better roots should not be compromised for disease resistance or associations with beneficial organisms, the study of the interaction of root-associated microbes with root phenotypes is an important but poorly understood topic.

Root phenotypes that reduce the metabolic cost of soil exploration are those that have relatively less carbon and nutrient demands for construction and maintenance of root tissue (Lynch, 2015). Phenotypes are composed of phenes and phene aggregates, distinct measurable characteristics at a given level of organization (York *et al.*, 2013). Root cortical aerenchyma (RCA) reduces the carbon and nutrient cost of root tissue, and maize (*Zea mays*) lines with more RCA have reduced respiration, greater soil exploration, better capture of soil resources, and therefore better growth and yield under suboptimal availability of N, P, K, and water compared with lines that had less RCA (Zhu *et al.*, 2010; Postma & Lynch, 2010, Postma & Lynch, 2011; Saengwilai *et al.*, 2014; Chimungu *et al.*, 2015). Other root phenes related to the metabolic cost of soil exploration are living cortical area (LCA), cortical cell file number (CCFN) and cortical cell size (CCS) (Figure 2-1). Plants with reduced LCA had reduced root respiration and root phosphorus content, deeper roots and consequently better phosphorus uptake, plant growth and grain yield under low-phosphorus stress (Galindo-Castañeda *et al*., 2018). Under water stress, maize lines with larger CCS or smaller CCFN had less root respiration, deeper roots, and therefore better water capture, plant water status, photosynthesis, growth, and yield than lines with smaller CCS and greater CCFN (Chimungu *et al.*, 2014a,b).

Arbuscular mycorrhizae (AM) are beneficial symbioses that help ameliorate phosphorus and drought stress in maize, but they are also present under optimum nutrient and water supply (Kabir & Koide, 2000; Oehl *et al.*, 2005; Koide & Peoples, 2012; Tian *et al.*, 2013; Willmann *et al.*, 2013). In controlled experiments, maize inoculated with AM under drought and low-phosphorus stress conditions grew better than control plants (Kaeppler *et al.*, 2000; Chu *et al.*, 2013; Bárzana *et al.*, 2014; Gerlach *et al.*, 2015). AM also contribute to soil aggregate stability (Rillig & Mummey, 2006), and provide protection against pathogens and herbivores (Pozo & Azcon-Aguilar, 2007). Maize has substantial natural variation in mycorrhizal responsiveness under low phosphorus (Kaeppler *et al.*, 2000; Sawers *et al.*, 2017). Studies of the interaction of

AM with root phenotypes such as root hair length and density, root diameter, and with lateral root branching in trees, grasses and crops have not shown consistent results across species (Manjunath & Habte, 1991; Schweiger *et al.*, 1995; Yano *et al.*, 1996; Gutjahr *et al.*, 2009; Zangaro *et al.*, 2012; Brown *et al.*, 2013; Maherali, 2014). Although previous studies revealed details of the spatial distribution of AM at the cellular level in maize (Toth & Miller, 1984) and other species (Smith & Smith, 1997; Dickson, 2004; Smith & Read, 2008) the effect of root anatomy on AM has been generally ignored.

Root-rot causing fungi cause yield reduction and economic losses in maize (Sumner *et al.*, 1990; Hillocks & Waller, 1997; Govaerts *et al.*, 2007; Mueller *et al.*, 2016). Four important classes of root rots are *Pythium* root rot, *Rhizoctonia* crown and brace root rot, *Fusarium* root rot, and red root rot which is a complex of soil fungi in which *Phoma terrestris* is the primary pathogen (White, 1999). *Fusarium verticillioides* (synonym. *Fusarium moniliforme* Sheldon) is commonly found in different maize tissues as an endophyte, but it can also become pathogenic under certain circumstances that are not well understood (Nelson, 1992; Bacon & Hinton, 1996). An important concern with *F. verticillioides* infection is the production of fumonisins, mycotoxins that harm animal health and have been classified as ‘possibly carcinogenic to humans’ (Scott, 2012). While *F. verticillioides* can cause root pathology, in some maize lines the infection occurs slowly and usually the plant limits the fungal advance; for this reason, *F. verticillioides* is a suitable model for this study, as the interaction is not lethal for the plant for a period of seven weeks after planting, which is the time needed for mesocosm experiments. In maize roots, *F. verticillioides* colonization starts in the lateral roots and mesocotyl as early as 72 h after seeds have been planted in infected soil. Hyphal spread in the root cortex occurs in the following two weeks with limited fungal growth along the root axis. Three-four weeks after penetration, incipient root rots may appear (McKeen, 1977; Oren *et al.*, 2003) or the infection may remain symptomless (Bacon & Hinton, 1996).

The selection of maize genotypes with promising anatomical phenes that decrease the metabolic cost of soil exploration such as greater RCA, larger cells and fewer CCFN, may have effects on the way soil fungi colonize root tissue, thereby affecting disease resistance or mycorrhizal associations. Previous studies have tangentially examined the effect of root anatomy on fungal interactions (Muthukumar *et al.*, 2004; Gutjahr *et al.*, 2009) and there are few studies that systematically address the effect of root anatomy on AM colonization (AMC). Mycorrhizal spread along the root axis may be either facilitated or reduced by RCA. For example, mycorrhizal spread was facilitated by the formation of recently-formed RCA through which intercellular hyphae could find a low-resistance path to grow through young roots of several plant species, *Zea mays* included (Brundrett *et al.*, 1985; Brundrett & Kendrick, 1988; Smith & Smith, 1997). Conversely, mycorrhiza has been reduced in mature roots with greater RCA and a continuous sclerenchymatic ring in the outer cortex due to habitat reduction and a stronger barrier for initial penetration in palms (Dreyer *et al.*, 2010). In addition, AM spore pseudomantles were localized in parts of palm roots containing pneumatodermis, a tissue in which the cells of the outer cortex have multiple intercellular spaces (Dreyer *et al.*, 2010). Sharda and Koide (2010) explored the correlation between three root anatomical traits and AMC under low phosphorus in 15 angiosperm species including *Zea mays*, finding that no single anatomical phene consistently explained the variation of AMC in all the species and concluding that this interaction may be species-specific. Previous findings with other species suggest that RCA may affect plant susceptibility to root pathogens as well. Studies performed with spring wheat and the pathogen *Cochliobolus sativum* and with Kentucky bluegrass and the pathogen *Phialophora oraminicola* (Deacon & Lewis, 1982; Smiley & Giblin, 1986) resulted in increased pathogen spread and incidence with higher levels of RCA. However, in another study, susceptibility to the pathogen *Phytophthora cryptogea* decreased with high RCA in safflower (*Carthamus tinctorius* L. cv. Gila) (Atwell & Heritage, 1994).

We hypothesize that cortical anatomy influences fungal colonization of axial roots in maize. To test this hypothesis, we used two models. First, AM in mesocosms and field-grown maize for which we predicted a decrease in colonization with roots having greater RCA and reduced LCA. Secondly, we used root rots in field-grown maize and *F. verticillioides* colonization in mesocosm-grown maize to study the effect of root anatomy on pathogen colonization. We hypothesized that contrasting RCA and LCA levels affect pathogen colonization. We also studied other cortical phenes or phene aggregates that may be associated with fungal colonization such as root diameter, cell size, cortical cell file number, and size of aerenchyma lacunae.

Materials and Methods

Plant material

Maize (*Zea mays* L.) recombinant inbred lines (RILs) of the IBM, Intermated B73×Mo17 (Senior *et al.*, 1996; Kaeppler *et al.*, 2000), and OHW (OH43×W64a) populations were provided by Dr. Shawn Kaeppler at The University of Wisconsin-Madison (Table 2-3). Six to eleven RILs per site contrasting in anatomical phenotypes were selected through preliminary field evaluations and used in the field and mesocosm experiments. In addition, we phenotyped 32 lines of commercial maize hybrids used by Pennsylvania farmers in 2013 and 30 and 40 lines in 2014 (Table 2-4 and Table 2-5), and selected 10 lines per site that showed contrasting aerenchyma area percent (perAA) for fungal colonization studies.

Field experiments

AMC was studied in inbred lines under optimal soil fertility in 2012 (FI-12, FI as in field and inbreds) and under optimal and suboptimal phosphorus availability in 2015 (FI-15), at the Russell E. Larson Research and Education Center of The Pennsylvania State University in Rock Springs, PA, USA (40°42’37.52’’ N, 77°57’07.54’’ W, 366 m.a.s.l.). The soil at the site is a Hagerstown silt loam (fine clayey, mixed, mesic Typic Hapludalf). FI-12 was a randomized complete block design with three replicates. Each block consisted of an independent 0.2 ha field that was amended with 915 g m^{-2} sawdust the two previous years, managed with conventional tillage and fertilized in order to meet the requirements for maize production according to soil tests. FI-15 consisted of a randomized complete block design with treatments arranged in a split-plots where the main plot was the phosphorus level (high, 31 – 39 mg kg^{-1}; low, 3 – 7 mg kg^{-1}) and the subplot was the genotype. In 2012, 1,560 kg ha^{-1} DD-6 (BASF, Ludwigshafen, Germany) activated alumina was applied and disked into the soil of all plots in order to reduce soil phosphorus availability. Each block was a 0.05 ha field divided in high and low phosphorus levels in which 11 three-row plots with the genotypes were randomly distributed. Optimal soil

fertility was maintained except phosphorus, which was applied at a rate of 84 kg P ha^{-1} monoammonium phosphate (11-52-0) in high phosphorus plots. Equivalent amounts of nitrogen were applied to the low phosphorus plots as urea. No cover crops were planted the season previous to the experiment. Plants were manually seeded for a final population of 57,278 plants ha^{-1} on June 15 of 2012 (FI-12) and on June 26 of 2015 (FI-15), and roots harvested 68 and 80 d after planting (DAP) for FI-12 and FI-15 respectively. Irrigation and insect control were provided as needed.

AM and pathogen colonization were studied in hybrid maize lines under optimum soil fertility in one field in 2013 and three fields in 2014, located in commercial farms: Kulp (40° 37’ 12.7416” N,-78° 13’ 44.2662” W), England (40° 30’ 41.82” N,-78° 11’ 55.89” W) and Rock Springs (40°42’37.52’’ N, 77°57’07.54’’ W, 366 m.a.s.l.) (Roth *et al.*, 2013; Roth *et al.*, 2014). Specific field histories per site are presented in Table 2-6. These experiments are herein named as FH-13 (FH as in field and hybrids, includes Rock Springs in 2013) and FH-14 (includes Kulp, England and Rock Springs in 2014). Briefly, hybrids were planted in four-row plots for a population of 79,000 and 84,012 plants ha^{-1} in 2013 and 2014 respectively. Each hybrid was planted in triplicate at each site and roots harvested as indicated in Table 2-4 and Table 2-5.

At sampling, two plants were excavated from the central row of each plot, cutting the root system with a shovel in a circle at a radial distance of 30 cm from the stem and 40 cm depth. The excavated plant was excised ~10 cm above the brace roots and the root crowns washed with a hose. Three root segments per whorl were taken 5-15 cm from the stem in the second, third and fourth whorls and preserved in 75% ethanol for AMC colonization studies. One root segment was taken 8-12 cm from the stem in the second or third whorl (third if the second was rotten), lateral roots clipped and root fragments preserved in 2 mL plastic vials with 75% (v/v) ethanol in water for anatomical phenotyping. Root rots were evaluated in three 15 cm root segments per whorl taken acropetally from the stem in the second whorl. Root rots percentage was measured

according to a visual scale (Figure 2-2). When nematode or insect damage was present, the root segment was discarded.

Mesocosm experiments

Two mesocosm experiments were conducted under controlled conditions in a glasshouse located on the campus of the Pennsylvania State University, at University Park, PA, USA (40°48'08.7"N 77°51'43.9"W) between August and September of 2014 (MC-14) and during June to August in 2015 (MC-15). MC-14 was used to study AMC by *Rhizophagus irregularis*, and MC-15 was used to study the root colonization by *F. verticillioides*. Low phosphorus conditions were provided to half of the columns of each experiment in order to induce changes in root anatomy mainly through the production of aerenchyma lacunae (Fan *et al.*, 2003). Treatments were arranged in randomized complete blocks with four blocks as replicates and the combination of two factors (genotype and phosphorus level) randomly assigned to each plant. The mesocosms are polyvinylchloride columns 1.5 m high x 15.7 cm diameter in which a transparent plastic lining of high-density polyethylene is filled with growing media and that allows for the complete recovery of the root system at harvest. Potting media consisted of sand (50% for MC-15 and 53% for MC-14), vermiculite (35%), and perlite (10%) and either 2% v/v phosphorus-buffered alumina (Lynch *et al.*, 1990) for MC-14, or 5% v/v low phosphorus soil (10 mg kg^{-1}available phosphorus) for MC-15. Half of the columns had low phosphorus availability, and the other half were supplied with 10 g of triple super phosphate (0-46-0, with 2.02 g P). For MC-14, all the columns were inoculated at planting with a liquid formulation of 400 pure aseptic spores of *R. irregularis* (Premiere Tech Biotechnologies. Quebec, Canada) by diluting aliquots of the spores in 500 mL of sterile distilled water and thoroughly mixing with potting media extracted from 5 – 20 cm depth (2 l). After mixing the media with the spores, the inoculated media was returned to the column and topped with 5 cm depth of non-inoculated media. 1-2 h after inoculation, four germinated seeds per column. For MC-15 a similar procedure was followed with 10 g of fresh

mycelia of *F. verticillioides* per mesocosm, with the addition of a complete set of four replicates of genotype Mo157 in low and high phosphorus that received autoclaved fungal inoculant and was treated as control of the inoculation. Seed sterilization procedures and nutrient management of the plants are described in APPENDIX B. Planting and harvest were staggered in two consecutive days for MC-14 (40 DAP), and in two weeks apart for MC-15 (36 DAP).

Production of F. verticillioides *fresh mycelia*. *F. verticillioides* isolate M-1331 (Fusarium Research Center, The Pennsylvania State University) was selected for this study. Mycelia was grown in batches of 400 mL yeast extract peptone dextrose broth (see details of initial inoculation procedures in APPENDIX B), recovered by filtration, packed in doses of 10 g in 50 mL sterile plastic tubes, stored at 4 °C for at most 16 h and used for inoculation. Details of inoculation are in APPENDIX B.

Plant sampling and measurements in mesocosm experiments. At harvest, shoots and roots were separated and the media gently washed off with water. Two root segments 8-12 cm from the stem were excised from the second or third whorl (third when the second was rotten) and preserved in 75% (v/v) ethanol in water for anatomical phenotyping. Two root segments per whorl were taken 10-20 cm from the stem in the second, third and fourth (when present) whorls and preserved in 75% (v/v) ethanol in water for AMC studies in MC-14. Additionally, one 20 cm root segment (excised from the attachment point to the stem) was taken from all the whorls in two genotypes of MC-14 and used for AMC quantification. Two root segments per whorl were taken 0-18 cm from the stem in the first, second and third whorls, placed in ice, and taken to the lab for *F. verticillioides* colonization studies with real-time polymerase chain reaction (qPCR) in MC-15. For all the plants of genotype Mo157 of MC-15, growing under low and high phosphorus, and inoculated and non-inoculated with *F. verticillioides*, two 10 cm segments from 8-18 cm from the stem of the third whorl were used to study *F. verticillioides* by re-isolation in Nash and Snyder agar plates (Nash & Snyder, 1962).

Plant measurements

Root anatomy. Root segments were ablated with a pulsed UV laser as previously described (York *et al.*, 2015); further details in the "APPENDIX B". Three cross-section images per root segment were analyzed with the software *RootScan* v.2.0. (Burton *et al.*, 2012, The Pennsylvania State University, 2018) which retrieves 24 cortical phenotypes per cross-section, of which we selected those listed in Table 2-1.

Mycorrhizal colonization. AMC was measured on cleared and stained axial root segments (Phillips & Hayman, 1970; Vierheilig *et al.*, 1998) with the grid intersect method (Giovannetti & Mosse, 1980) in mesocosm-grown plants, and with the field intersect method (McGonigle *et al.*, 1990) in field-grown maize. Only arbuscules were counted. Three-dimensional reconstructions were made on 8 mm AM colonized root segments with contrasting anatomical phenotypes in order to observe the distribution of arbuscules in reference to the aerenchyma lacunae and the location in the cortex in samples from the experiment MC-14 using laser ablation tomography (LAT) (APPENDIX B) (Figure 2-3).

F. verticillioides *colonization.* Immediately after sampling, root segments of MC-15 were taken to the laboratory and processed for quantification of *F. verticillioides* colonization with real time PCR. Sample preparation and fungal colonization measurements, plant DNA extraction and primer validation are described in APPENDIX B. Real-time PCR was performed in 10 µL total volume reaction containing 5 µL 2xSYBR Green Master Mix (Roche Applied Science, USA), 0.1 µM of each primer (Fver356 fwd (CGTTTCTGCCCTCTCCCA) and Fver412 rev (TGCTTGACACGTGACGATGA) (Nicolaisen *et al.*, 2009)), and 2 µL template DNA. A 7500 Fast Real-Time PCR System (Applied Biosystems) was used for the reaction with a cycle protocol as follows: 94°C for 10 min (1 cycle), 94°C for 15 s and 60°C for 1 min (40 cycles). A standard curve with Ct values corresponding to the amount of fungal DNA was generated. The DNA template for the standard curve consisted of three replicates of standards ranging from 0.2 –

200 pg fungal DNA dissolved in a 30 ng μL^{-1} root DNA matrix. The standard curve was then used to quantitate the amount of *F. verticillioides* present in each unknown sample from its Ct value.

Statistical analyses

Root anatomy. Root segments were ablated with a pulsed UV laser as previously described (York *et al.*, 2015); further details in the APPENDIX B. Three cross-section images per root segment were analyzed with the software *RootScan* v.2.0. (Burton *et al.*, 2012, The Pennsylvania State University, 2018) which retrieves 24 cortical phenotypes per cross-section, of which we selected those listed in Table 2-1.

Mycorrhizal colonization. AMC was measured on cleared and stained axial root segments (Phillips & Hayman, 1970; Vierheilig *et al.*, 1998) with the grid intersect method (Giovannetti & Mosse, 1980) in mesocosm-grown plants, and with the field intersect method (McGonigle *et al.*, 1990) in field-grown maize. Only arbuscules were counted. Three-dimensional reconstructions were made on 8 mm AM colonized root segments with contrasting anatomical phenotypes in order to observe the distribution of arbuscules in reference to the aerenchyma lacunae and the location in the cortex in samples from the experiment MC-14 using laser ablation tomography (LAT) (APPENDIX B) (Figure 2-3).

F. verticillioides *colonization.* Immediately after sampling, root segments of MC-15 were taken to the laboratory and processed for quantification of *F. verticillioides* colonization with real time PCR. Sample preparation and fungal colonization measurements, plant DNA extraction and primer validation are described in APPENDIX B. Real-time PCR was performed in 10 µL total volume reaction containing 5 µL 2xSYBR Green Master Mix (Roche Applied Science, USA), 0.1 µM of each primer (Fver356 fwd (CGTTTCTGCCCTCTCCCA) and Fver412 rev (TGCTTGACACGTGACGATGA) (Nicolaisen *et al.*, 2009)), and 2 µL template DNA. A 7500 Fast Real-Time PCR System (Applied Biosystems) was used for the reaction with a cycle

protocol as follows: 94°C for 10 min (1 cycle), 94°C for 15 s and 60°C for 1 min (40 cycles). A standard curve with Ct values corresponding to the amount of fungal DNA was generated. The DNA template for the standard curve consisted of three replicates of standards ranging from 0.2 – 200 pg fungal DNA dissolved in a 30 ng μL^{-1} root DNA matrix. The standard curve was then used to quantitate the amount of *F. verticillioides* present in each unknown sample from its Ct value.

Results

Hybrid and inbred populations differed for almost all anatomical phenes observed (Figure 2-12). Hybrids had 2x larger root cross-section areas (RXSA) and cortical areas (TCA), and steles 1.5x thicker than inbred genotypes. Hybrids had 25% larger aerenchyma area (AA) and larger living cortical area (LCA), and 30% more cell files (which is 3 more cell files on average) and cortical cells 20% smaller than inbreds. However, percent aerenchyma (perAA) and percent living cortical area were not significantly different between hybrids and inbreds. Hybrids had less variability in anatomical root phenes among lines (Table 2-7) than inbreds (Table 2-8), and phosphorus availability had no effect on the anatomy of inbreds in FI-15. PCA showed that anatomical phenes are interrelated and grouped similarly regardless of the experiment, environment or maize material (Figure 2-13). In general, anatomical phenes in the mesocosm experiment MC-14 corresponded to larger roots compared to MC-15 (Figure 2-14). The phosphorus effect on root anatomy was stronger in MC-14 than in MC-15 and greater variability among root phenes of different genotypes was found in MC-15 than in MC-14 (Table 2-9 and Table 2-10).

We calculated the intercellular area (calculated as total cortical area – living cortical area – aerenchyma area) and its relationship with living cortical area (LCA) and living cortical area percent (perLCA). Plants with 3x larger LCA had 3x increased intercellular areas compared to plants with reduced living cortical area. However, plants in which the living cortical area comprised a larger percent of the cortex, had smaller intercellular space compared to plants in which the living cortical area was a smaller percent of the cortex (Figure 2-15).

AMC in axial roots of inbred genotypes ranged from 0-100% (average 41%) in FI-12, from 0-60% (average 15%) in FI-15 (Figure 2-16a, d), and from 0-88% (average 29%) in hybrids of FH-13 and FH-14 (Figure 2-16b, c). Specifically, AMC of hybrid plants was 19% in FH-13 and 41%, 30% and 24% AMC at England, Kulp, and Rock Springs, respectively in FH-14 (Figure

2-16). In FI-12 AMC was 0-100% and 0-80% in lateral and axial roots respectively with axial and lateral AMC significantly correlated (Figure 2-17). For all the other field experiments, AMC was measured exclusively in axial roots. AMC of inbred genotypes in FI-15 had significant effect of genotype (P = 0.006) and no significant phosphorus effect (P = 0.943).

In mesocosms, plants had less AMC compared to field-grown plants. Axial AMC under low phosphorus ranged from 0 – 55% with a distribution skewed to values below 15% (Figure 2-18). Lateral root AMC was not quantified but it was present in all plants regardless of the phosphorus treatment. Low-phosphorus plants had 10-fold greater axial root colonization compared to high-phosphorus (P = 0.001) and AMC was not significantly different among whorls (P = 0.638, Figure 2-19). Arbuscules located in the middle layers of the cortex, coexisting with aerenchyma lacunae, the latter formed mostly the inner layers, were observed in the cortical volume of axial roots (Figure 2-4 and Supporting video S1).

Significant inverse correlations between percent aerenchyma (perAA) and AMC were observed in field-grown inbred plants. In FI-12 plants under optimum phosphorus with maximum levels of aerenchyma (30% perAA) had 75% less AMC than plants with low aerenchyma (2% perRCA) (Figure 2-5). In FI-15 plants with 5x greater percent aerenchyma (perAA) had 3x less AMC under low phosphorus (Figure 2-6). No significant effect of aerenchyma (perAA or AA) on axial AMC was found under high phosphorus in FI-15. Hybrid maize roots with 2.5x larger cells and 8x larger lacunae area (LA) had 1.5x more AMC (Figure 2-7); however, no significant correlation was found between AMC and aerenchyma (AA or perAA) in hybrids. It is noteworthy that aerenchyma lacunae area (LA) was directly correlated with AMC in hybrids, as opposed to inbreds. The relation of lacunae area (LA) with AMC seems to depend on the size of the lacunae itself. In the field experiments with hybrids there was an increase in AMC with lacunae areas of 0-0.008 mm^2 (Figure 2-7), while in mesocosms with inbreds we observed a reduction of AMC with larger lacunae area when the range was 0-0.0025 mm^2 (Figure 2-8). AMC of mesocosm-

grown plants (MC-14) under low phosphorus was 70% decreased (from 21 to 6%) in plants with 15x larger percent aerenchyma (perAA), 2.5x larger lacunae area (LA), and 90% larger root cross-section area (RXSA) (Figure 2-8).

Root rots in field-grown maize ranged from 0-100% with distributions differing according to the site and year (Figure 2-20) and significant effect of genotype ($P = 0.005$). Root rots at Rock Springs had distributions skewed toward greater values, and averages of 63% in FH-13 and 78% in FH-14, while the root rots at Kulp and England (FH-14) had a distribution close to normal and means of 52% and 59% respectively (Figure 2-20). *F. verticillioides* colonization in mesocosm-grown plants varied from 0–10.4 pg fungal DNA ng^{-1} plant DNA g^{-1} root tissue (equivalent to -1.4-1.01 Log_{10} pg fungal DNA ng^{-1} plant DNA g^{-1} root tissue) with significant genotype effect ($P < 0.001$), no significant phosphorus effect ($P = 0.343$), and prevalence of smaller values (Figure 2-21). Roots collected in control non-inoculated plants produced no significant signal of *F. verticillioides* after colonization amplification with qPCR (Figure 2-22), or in Nash and Snyder agar plates. *F. verticillioides* colonization had no significant effect on shoot biomass (Figure 2-23).

Roots with 2.5x larger cells (CS_Hypo_Epi) and fewer cell files had 40% less rot (Figure 2-9). Field plants with 5 times more AMC had 40% less root rot (Figure 2-10). In MC-15, stepwise regression of anatomical phenes as predictors of *F. verticillioides* colonization gave slightly different models at high and low phosphorus (Table 2-2) and no significant model when high and low phosphorus data were combined. The best model to explain *F. verticillioides* colonization was obtained under low phosphorus; roots with 40% smaller living cortical areas that comprised smaller proportions of the cross-sections had 3.5 times greater *F. verticillioides* colonization than plants with more LCA in which the LCA comprised larger proportions of the cross-section (Figure 2-11).

Discussion

Our results support the hypothesis that root cortical anatomy influences fungal colonization of axial roots in maize. Inbred plants with increased aerenchyma and decreased living cortical area (LCA) had less mycorrhizal colonization whereas plants with greater living cortical area had less *F. verticillioides* colonization. Greater cell file number and smaller cortical cells were associated with increased root rot in hybrids. Field-grown hybrids with greater mycorrhizal colonization also had less root rot. These results indicate that root anatomy affects pathogens and mycorrhiza differently, which implies that the selection of root anatomical phenes that favor mutualistic relationships may have detrimental effects on pathogens.

We employed mesocosms and field environments, which have complementary qualities. In mesocosms we were able to control environmental factors including other pathogens and mutualists, temperature, chemical and physical properties of the growth media, and inoculum concentration of the fungus at planting. By measuring root rots and AMC in field-grown mature maize we captured root colonization by complex fungal communities, and in the case of root rots we also captured further interactions with other organisms that follow or that are associated with fungal colonization in field soils such as bacteria, nematodes, and insect larvae. In mesocosms we observed effects of anatomy on fungal colonization 5-6 weeks after planting while in the field we measured the effect of anatomy at flowering, 10 – 11 weeks after planting, widening the scope of our findings.

In general, the anatomical variation we observed was similar to other studies with maize grown in the field (York *et al.*, 2015; Yang, 2017) and in mesocosms (Chimungu *et al.*, 2014a,b; Burton *et al.*, 2015). The larger root diameters in MC-14 and stronger phosphorus effect found in MC-15 compared to MC-14 may be attributable to the differences in phosphorus buffering of the two experiments, or to a possible positive effect of mycorrhiza on root growth in MC-14. Hormone action triggered by inoculation with mycorrhizal fungi, especially gibberellin reduction

(Danneberg *et al.*, 1993) has been associated with increased root diameter in tomato (Fusconi *et al.*, 1999). The negative effect of aerenchyma on mycorrhizal colonization was supported by field and mesocosm experiments in inbreds (Figure 2-5, Figure 2-6 and Figure 2-8). However, mycorrhizal colonization in hybrids was positively affected by cell size and lacunae area (Figure 2-7) which could be related to the larger root diameters of the hybrids. Possibly, aerenchyma area has a negative effect on mycorrhizal colonization in thinner roots where the lacunae occupy a larger proportion of the cortical volume, but this effect may be attenuated in thicker roots like those found in the hybrids. The narrow AMC range of FI-15 (0-50%, Figure 2-6) could explain the lack of significant effects of anatomical phenes under high phosphorus that contrast with the observed AMC under high phosphorus in FI-12 (Figure 2-5). A factor that could have accounted for the low colonization values in FI-15 is small initial concentration of natural inoculum product or the lack of organic amendments before to the maize planting in the winter of 2014, when the entire field was fallow. The field used for FI-12, by contrast, was amended with sawdust two years previous to the experiment. Soils amended with organic matter sustain more AMC once hosts are planted (Hepper & Warner, 1983). The greater incidence of root rots at Rock Springs compared to Kulp and England (FH-14) might be a consequence of periodic inundation due to the topography at Rock Springs. *F. verticillioides* colonization was in a similar range to those reported by Kurtz *et al.* (2010) using qPCR to quantify root colonization in maize roots with the same species. In general, results of field root rot and *F. verticillioides* colonization in mesocosms support each other as both were correlated with phenes associated with living cortical area, as discussed below.

Differences in the spatial pattern of fungal colonization in the root cortex may explain the contrasting effects of aerenchyma and living cortical area on mycorrhiza and pathogens observed in this study. Plants with decreased aerenchyma (i.e. perAA and AA) and greater living tissue (e.g. increased perLCA) could have more cells to host more arbuscules, resulting in greater

mycorrhizal colonization (Figure 2-5, Figure 2-6, Figure 2-8). However, this correlation may be affected by root diameter: thicker roots (i.e. larger RXSA) had less AMC (Figure 2-8) which could be associated with either a stronger lignified epidermis of thicker roots, or with a longer pathway for the fungus to establish arbuscules in the inner cell files in the cortex that could have decreased the overall AMC. In addition, in thicker roots, where the aerenchyma effect may be even positive as in field-grown hybrids (Figure 2-7), larger aerenchyma lacunae may coexist with cortical tissue that has space to host arbuscules and pathways for the hyphae to colonize the adjacent tissue. Contrary to the effect on mycorrhiza, reduced living tissue (perLCA) and its associated reduced cell size (Figure 2-13) may have facilitated the passage and establishment of *F.verticillioides* hyphae (Figure 2-11) and root rot spread (Figure 2-9) in the apoplastic space by offering relatively more intercellular space compared to plants with greater percent living cortical area (perLCA Figure 2-15). Also, decreased percent living cortical area (perLCA) is in part caused by greater aerenchyma (perRCA; Figure 2-13 and Jaramillo *et al.* (2013)), therefore increased aerenchyma would be expected to increase *F. verticillioides* colonization in MC-15. However, the fact that *F. verticillioides* colonization was poorly correlated with aerenchyma indicates that aerenchyma had only a partial effect, possibly by facilitating hyphal spread. In this case the volumes and location of channels formed by aerenchyma could have influenced root rots and *F.verticillioides* colonization. The study of the effect of the spatial arrangement of aerenchyma on fungal colonization deserves further attention, and laser ablation tomography is a promising technique for this purpose. Smaller epidermal cells may have offered comparatively more entry points of fungal colonization than larger epidermal cells causing the increased root rots in hybrids with smaller cells (Figure 2-9). Another anatomical phene significantly associated with root rots was cortical cell file number (CCFN) (Figure 2-9b). A root cortex with more cell files (e.g. 16) and smaller cell size has more apoplastic space, compared to a cortex with fewer

cell files (e.g. 11) and larger cells. With greater apoplastic space, fungal pathogens might encounter more opportunity to colonize the root cortex.

An inverse correlation between mycorrhizal colonization and root rots was observed in hybrids in the field (FH-14, Figure 2-10). Although the antagonist effect of mycorrhizae on root pathogens has been extensively studied and discussed (Whipps, 2004; Jung *et al.*, 2012), no studies have approached this topic in field experiments with maize to our knowledge. We propose that the inverse correlation between AMC and root rots observed in the present study is caused in part by contrasting anatomical phenotypes that have divergent effects on pathogenic and mutualistic fungi. Although there may be other overlapping mechanisms of the antagonism of pathogens and mycorrhiza such as competition for space and nutrients, induced resistance to pathogens, enhanced plant nutrition, and selective microbiota in the mycorrhizosphere (Whipps, 2004; Pozo & Azcon-Aguilar, 2007; Gerlach *et al.*, 2015), our results suggest that root anatomy partially controls fungal colonization in maize by offering contrasting phenotypes preferable by one or another group of fungal colonizing organisms. Specifically, axial roots with decreased aerenchyma, larger epidermal and hypodermal cell size, and smaller diameters would favor mycorrhizal associations. On the contrary, plants with decreased living cortical area, smaller epidermal and hypodermal cell size, and increased cell files would favor pathogen colonization.

The results presented here build on previous findings regarding the utility of anatomical phenes and phene aggregates and their association with reductions in metabolic costs of soil exploration under nutrient and drought stress in maize. Greater RCA, reduced LCA, decreased CCFN and larger CCS have all been independently associated with improved resource acquisition, growth and grain yield of plants growing in drought under controlled and field conditions (Zhu *et al.*, 2010; Chimungu *et al.*, 2014a,b; Chimungu *et al.*, 2015). Similarly, plants with greater RCA grew better under nitrogen (Saengwilai *et al.*, 2014) and phosphorus stress compared to plants with reduced RCA (Postma & Lynch, 2010, Postma & Lynch, 2011, Galindo-

Castañeda *et al*., 2018). Our results suggest that selecting plants with greater RCA could have the tradeoff of decreasing AMC in axial roots. However, selecting for fewer CCFN and larger cells would be advantageous for AMC, and deleterious for root rots or *F. verticillioides* colonization. It is noteworthy that the variables retrieved by the stepwise regression model were significant for *F. verticillioides* colonization only under low phosphorus in MC-15 (Table 2-2), and that RCA had a significant effect on AMC exclusively under low phosphorus in FI-15 (Figure 2-6). Although significant effects of anatomical phenes under optimal nutrient availability in the other experiments was found, we anticipate a stronger effect of anatomy on fungal colonization under stress conditions, because stress has significant effects on root anatomy under drought (Zhu *et al.*, 2010) and low nutrient stress (Drew *et al.*, 1989; Bouranis *et al.*, 2003; Evans, 2004; Fan *et al.*, 2007; Saengwilai *et al.*, 2014; Galindo-Castañeda *et al*., 2018). Moreover, plants with root anatomical phenotypes that optimize soil resource acquisition such as increased aerenchyma and reduced living cortical area grow better under stress than plants with other phenotypes (Postma & Lynch, 2010, Postma & Lynch, 2011,, Galindo-Castañeda *et al.*, 2018), therefore may enhance pathogen resistance (reviewed by Walters & Bingham, 2007) which accords with the present results.

Several aspects of the effect of root anatomical phenes on fungal colonization remain unexplored and can be addressed in future studies. Specifically, the relation of root anatomy with root architecture and how the specific sites of colonization may be modified by anatomy are unknown for maize. For example, the effect of whorl position of the nodal root system and the effects of whorl-specific anatomy on fungal colonization are interesting topics as fungal colonization may change during the season. Recent research has shown that anatomy across whorls significantly changes in younger roots (Yang, 2017). In the present study, we found that AMC did not differ among whorls under low phosphorus availability (Figure 2-19), but further studies of the axial colonization and root anatomy by whorl with more genotypes may reveal new

patterns. In addition, the relationship of lateral root anatomy with axial root anatomy could modify fungal colonization. Surprisingly, most studies of fungal colonization lack details regarding the exact location within the root system used for sampling, and most studies are performed in small pots where the entire root system might be colonized. In contrast, fungal colonization in field-grown plants might be heterogeneously distributed along root axes and restricted to locations where natural inoculant is present. Adequate consideration of root architecture, root anatomy, and the spatiotemporal distribution of roots and fungal propagules would be useful.

In conclusion, root cortical anatomy was related to fungal colonization by mutualists and pathogens in inbred and hybrid maize lines, supporting the hypothesis that anatomy has partial control of fungal colonization. Selecting plants for decreased living cortical tissue and greater aerenchyma could decrease AMC and favor root rot-causing pathogens, whereas selecting plants with fewer cortical cell files and larger cells may be advantageous for mycorrhizae while also reducing pathogen infection. Further studies may reveal a wider spectrum of anatomical effects on fungal colonization, especially those related to the variation in anatomy among root classes and whorls. The selection of plant cultivars with improved root systems with better capabilities to use resources under stress conditions must also integrate favorable phenotypes for beneficial soil microorganisms for a more sustainable and resilient agriculture.

References

Atwell B, Heritage A. 1994. Reduced susceptibility of roots of safflower to *Phytophthora cryptogea* after prior adaptation of roots to hypoxic conditions. *Australian Journal of Botany* 42: 29-36.

Bacon CW, Hinton DM. 1996. Symptomless endophytic colonization of maize by *Fusarium moniliforme*. *Canadian Journal of Botany* 74: 1195-1202.

Bárzana G, Aroca R, Bienert GP, Chaumont F, Ruiz-Lozano JM. 2014. New insights into the regulation of aquaporins by the arbuscular mycorrhizal symbiosis in maize plants under drought stress and possible implications for plant performance. *Molecular Plant-Microbe Interactions* 27: 349-363.

Bishopp A, Lynch JP. 2015. The hidden half of crop yields. *Nature Plants* 1: 1-2.

Bouranis D, Chorianopoulou S, Siyiannis V, Protonotarios V, Hawkesford M. 2003.Aerenchyma formation in roots of maize during sulphate starvation. *Planta* 217: 382-391

Brown LK, George TS, Barrett GE, Hubbard SF, White PJ. 2013. Interactions between root hair length and arbuscular mycorrhizal colonisation in phosphorus deficient barley (*Hordeum vulgare*). *Plant and Soil* 372: 195-205.

Brundrett MC, Kendrick B. 1988. The mycorrhizal status, root anatomy, and phenology of plants in a sugar maple forest. *Canadian Journal of Botany* 66: 1153-1173.

Brundrett MC, Piché Y, Peterson RL. 1985. A developmental study of the early stages in vesicular–arbuscular mycorrhiza formation. *Canadian Journal of Botany* 63: 184-194.

Burton AL, Johnson J, Foerster J, Hanlon MT, Kaeppler SM, Lynch JP, Brown KM. 2015. QTL mapping and phenotypic variation of root anatomical traits in maize (*Zea mays* L.). *Theoretical and Applied Genetics* 128: 93-106

Burton AL, Williams M, Lynch JP, Brown KM. 2012. *RootScan*: Software for high-throughput analysis of root anatomical traits. *Plant and Soil.* doi: https://doi.org/10.1007/s11104-012-1138-2

Chimungu JG, Brown KM, Lynch JP. 2014a. Large root cortical cell size improves drought tolerance in maize. *Plant Physiology* 166: 2166-2178.

Chimungu JG, Brown KM, Lynch JP. 2014b. Reduced root cortical cell file number improves drought tolerance in maize. *Plant Physiology* 166: 1943-1955.

Chimungu JG, Maliro MFA, Nalivata PC, Kanyama-Phiri G, Brown KM, Lynch JP. 2015. Utility of root cortical aerenchyma under water limited conditions in tropical maize (*Zea mays* L.). *Field Crops Research* 171: 86-98.

Chu Q, Wang X, Yang Y, Chen F, Zhang F, Feng G. 2013. Mycorrhizal responsiveness of maize (*Zea mays L.*) genotypes as related to releasing date and available P content in soil. *Mycorrhiza* 23: 497-505.

Danneberg G, Latus C, Zimmer W, Hundeshagen B, Schneider-Poetsch H, Bothe H. 1993. Influence of vesicular-arbuscular mycorrhiza on phytohormone balances in maize (*Zea mays* L.). *Journal of Plant Physiology* 141: 33-39.

Deacon JW, Lewis SJ. 1982. Natural senescence of the root cortex of spring wheat in relation to susceptibility to common root rot (*Cochliobolus sativus*) and growth of a free-living nitrogen-fixing bacterium. *Plant and Soil* 66: 13-20.

Dickson S. 2004. The Arum-Paris continuum of mycorrhizal symbioses. *New Phytologist* 163: 187-200.

Drew MC, He C-J, Morgan PW. 1989. Decreased ethylene biosynthesis, and induction of aerenchyma, by nitrogen- or phosphate-starvation in adventitious roots of *Zea mays* L. *Plant Physiology* 91: 266-271.

Dreyer B, Morte A, López JÁ, Honrubia M. 2010. Comparative study of mycorrhizal susceptibility and anatomy of four palm species. *Mycorrhiza* 20: 103-115.

Evans DE. 2004. Aerenchyma formation. *New Phytologist* 161: 35-49.

Fan M, Bai R, Zhao X, Zhang J. 2007. Aerenchyma formed under phosphorus deficiency contributes to the reduced root hydraulic conductivity in maize roots. *Journal of Integrative Plant Biology* 49: 598-604.

Fan M, Zhu J, Richards C, Brown KM, Lynch JP. 2003. Physiological roles for aerenchyma in phosphorus-stressed roots. *Functional Plant Biology* 30: 493-506.

Fusconi A, Gnavi E, Trotta A, Berta G. 1999. Apical meristems of tomato roots and their modifications induced by arbuscular mycorrhizal and soilborne pathogenic fungi. *New Phytologist* 142: 505-516.

Galindo-Castañeda T, Brown KM, Lynch JP. 2018. Reduced root cortical burden improves growth and grain yield under low phosphorus availability in maize. *Plant, Cell & Environment.* doi: https://doi.org/10.1111/pce.13197.

Gerlach N, Schmitz J, *Polatajko* A, SchlÜTer U, Fahnenstich H, Witt S, Fernie AR, Uroic K, Scholz UWE, Sonnewald UWE, et al. 2015. An integrated functional approach to dissect systemic responses in maize to arbuscular mycorrhizal symbiosis. *Plant, Cell & Environment* 38: 1591-1612.

Giovannetti M, Mosse B. 1980. An evaluation of techniques for measuring vesicular arbuscular mycorrhizal infection in roots. *New Phytologist* 84: 489-500.

Govaerts B, Fuentes M, Mezzalama M, Nicol JM, Deckers J, Etchevers JD, Figueroa-Sandoval B, Sayre KD. 2007. Infiltration, soil moisture, root rot and nematode populations after 12 years of different tillage, residue and crop rotation managements. *Soil and Tillage Research* 94: 209-219.

Gutjahr C, Casieri L, Paszkowski U. 2009. *Glomus intraradices* induces changes in root system architecture of rice independently of common symbiosis signaling. *New Phytologist* 182: 829-837.

Hepper CM, Warner A. 1983. Role of organic matter in growth of a vesicular-arbuscular mycorrhizal fungus in soil. *Transactions of the British Mycological Society* 81: 155-156.

Hillocks RJ, Waller J. 1997. *Soilborne diseases of tropical crops*. Wallingford, Oxon, UK, New York, NY, USA: CAB International.

Jaramillo RE, Nord EA, Chimungu JG, Brown KM, Lynch JP. 2013. Root cortical burden influences drought tolerance in maize. *Annals of Botany* 112: 429-437.

Jung SC, Martinez-Medina A, Lopez-Raez JA, Pozo MJ. 2012. Mycorrhiza-induced resistance and priming of plant defenses. *Journal of Chemical Ecology* 38: 651-664.

Kabir Z, Koide RT. 2000. The effect of dandelion or a cover crop on mycorrhiza inoculum potential, soil aggregation and yield of maize. *Agriculture, Ecosystems & Environment* 78: 167-174.

Kaeppler SM, Parke JL, Mueller SM, Senior L, Stuber C, Tracy WF. 2000. Variation among maize inbred lines and detection of quantitative trait loci for growth at low phosphorus and responsiveness to arbuscular mycorrhizal fungi. *Crop Science* 40: 358-364.

Koide RT, Peoples MS. 2012. On the nature of temporary yield loss in maize following canola. *Plant and Soil* 360: 259-269.

Kurtz B, Karlovsky P, Vidal S. 2010. Interaction between western corn rootworm (Coleoptera: Chrysomelidae) larvae and root-infecting *Fusarium verticillioides*. *Environmental Entomology* 39: 1532-1538.

Lynch JP. 2015. Root phenes that reduce the metabolic costs of soil exploration: opportunities for 21st century agriculture. *Plant, Cell & Environment* 38: 1775-1784.

Maherali H. 2014. Is there an association between root architecture and mycorrhizal growth response? *New Phytologist* 204: 192-200.

Manjunath A, Habte M. 1991. Root morphological characteristics of host species having distinct mycorrhizal dependency. *Canadian Journal of Botany* 69: 671-676.

McGonigle TP, Miller MH, Evans DG, Fairchild GL, Swan JA. 1990. A new method which gives an objective measure of colonization of roots by vesicular—arbuscular mycorrhizal fungi. *New Phytologist* 115: 495-501.

McKeen W. 1977. *Fusarium* in barley and corn roots. *Canadian Journal of Botany* 55: 12-16.

Mueller D, Wise K, Sisson A. 2016. *Corn disease loss estimates from the United States and Ontario, Canada — 2016*. [WWW document] URL: http://cropprotectionnetwork.org/wp-content/uploads/2017/04/CPN-2007-16-W.pdf. [accessed July 27 2017].

Muthukumar T, Udaiyan K, Shanmughavel P. 2004. Mycorrhiza in sedges—an overview. *Mycorrhiza* 14: 65-77.

Nash SM, Snyder WC. 1962. Quantitative estimations by plate counts of propagules of the bean root rot *Fusarium* in field soils. *Phytopathology* 52: 567-572.

Nelson P. 1992. Taxonomy and biology of *Fusarium moniliforme*. *Mycopathologia* 117: 29-36.

Nicolaisen M, Supronienė S, Nielsen LK, Lazzaro I, Spliid NH, Justesen AF. 2009. Real-time PCR for quantification of eleven individual *Fusarium* species in cereals. *Journal of Microbiological Methods* 76: 234-240.

Oehl F, Sieverding E, Ineichen K, Ris E-A, Boller T, Wiemken A. 2005. Community structure of arbuscular mycorrhizal fungi at different soil depths in extensively and intensively managed agroecosystems. *New Phytologist* 165: 273-283.

Oren L, Ezrati S, Cohen D, Sharon A. 2003. Early events in the *Fusarium verticillioides*-maize interaction characterized by using a green fluorescent protein-expressing transgenic isolate. *Applied and Environmental Microbiology* 69: 1695-1701.

Phillips J, Hayman D. 1970. Improved procedures for clearing roots and staining parasitic and vesicular-arbuscular mycorrhizal fungi for rapid assessment of infection. *Transactions of the British Mycological Society* 55: 158-161.

Postma JA, Lynch JP. 2011. Root cortical aerenchyma enhances the growth of maize on soils with suboptimal availability of nitrogen, phosphorus, and potassium. *Plant Physiology* 156: 1190-1201.

Postma JA, Lynch JP. 2010. Theoretical evidence for the functional benefit of root cortical aerenchyma in soils with low phosphorus availability. *Annals of Botany* 107: 829-841.

Pozo MJ, Azcon-Aguilar C. 2007. Unraveling mycorrhiza-induced resistance. *Current Opion in Plant Biology* 10: 393-398.

R Core Team. 2014. *R: A language and environment for statistical computing*. Vienna, Austria: R Foundation for Statistical Computing. http://www.R-project.org/.

Rillig MC, Mummey DL. 2006. Mycorrhizas and soil structure. *New Phytologist* 171: 41-53.

Roth GW, Breining JA, Shaffer JA, Harkcom WS, Wells HL. 2013. *Results 2013: Pennsylvania commercial grain and silage hybrid corn tests report.* University Park, PA: The Pennsylvania State University.

Roth GW, Breining JA, Shaffer JA, Harkcom WS, Wells HL. 2014. *Results 2014: Pennsylvania commercial grain and silage hybrid corn tests report.* University Park, PA: The Pennsylvania State University.

Saengwilai P, Nord EA, Chimungu JG, Brown KM, Lynch JP. 2014. Root cortical aerenchyma enhances nitrogen acquisition from low-nitrogen soils in maize. *Plant Physiology.* doi: 10.1104/pp.114.241711

Sawers RJH, Svane SF, Quan C, Grønlund M, Wozniak B, Gebreselassie M-N, González-Muñoz E, Chávez Montes RA, Baxter I, Goudet J, et al. 2017. Phosphorus acquisition efficiency in arbuscular mycorrhizal maize is correlated with the abundance of root-external hyphae and the accumulation of transcripts encoding PHT1 phosphate transporters. *New Phytologist* 214: 632-643.

Schweiger PF, Robson AD, Barrow NJ. 1995. Root hair length determines beneficial effect of a *Glomus* species on shoot growth of some pasture species. *New Phytologist* 131: 247-254.

Scott PM. 2012. Recent research on fumonisins: a review. *Food Additives & Contaminants. Part A: Chemistry, Analysis, Control, Exposure & Risk Assessment* 29: 242-248.

Senior M, Chin E, Lee M, Smith J, Stuber C. 1996. Simple sequence repeat markers developed from maize sequences found in the GENBANK database: map construction. *Crop Science* 36: 1676-1683.

Sharda JN, Koide RT. 2010. Exploring the role of root anatomy in P-mediated control of colonization by arbuscular mycorrhizal fungi. *Botany* 88: 165-173.

Smiley R, Giblin D. 1986. Root cortical death in relation to infection of Kentucky bluegrass by *Phialophora graminicola*. *Phytopathology* 76: 917-922.

Smith FA, Smith SE. 1997. Tansley Review No. 96. Structural diversity in (vesicular)-arbuscular mycorrhizal symbioses. *New Phytologist* 137: 373-388.

Smith SE, Read DJ. 2008. *Mycorrhizal symbiosis*. New York, NY: Academic Press.

Sumner D, Gascho G, Johnson A, Hook J, Threadgill E. 1990. Root diseases, populations of soil fungi, and yield decline in continuous double-crop corn. *Plant Disease* 74: 704-710.

The Pennsylvania State University. 2018. *RootScan* - Anatomical Traits Analysis Software. [www document] URL: https://plantscience.psu.edu/research/labs/roots/methods/computer/rootscan. [accessed: January 30, 2016]

Tian H, Drijber RA, Li X, Miller DN, Wienhold BJ. 2013. Arbuscular mycorrhizal fungi differ in their ability to regulate the expression of phosphate transporters in maize (*Zea mays* L.). *Mycorrhiza* 23: 507-514.

Toth R, Miller RM. 1984. Dynamics of arbuscule development and degeneration in a *Zea mays* mycorrhiza. *American Journal of Botany* 71: 449-460.

Vierheilig H, Coughlan AP, Wyss U, Piché Y. 1998. Ink and vinegar, a simple staining technique for arbuscular-mycorrhizal fungi. *Applied and Environmental Microbiology* 64: 5004-5007.

Walters DR, Bingham IJ. 2007. Influence of nutrition on disease development caused by fungal pathogens: implications for plant disease control. *Annals of Applied Biology* 151: 307-324.

Whipps JM. 2004. Prospects and limitations for mycorrhizas in biocontrol of root pathogens. *Canadian Journal of Botany* 82: 1198-1227.

White DG. 1999. *Compendium of corn diseases*. St. Paul, MN: American Phytopathological Society (APS) Press.

Willmann M, Gerlach N, Buer B, Polatajko A, Nagy R, Koebke E, Jansa J, Flisch R, Bucher M. 2013. Mycorrhizal phosphate uptake pathway in maize: vital for growth and cob development on nutrient poor agricultural and glass house soils. *Frontiers in Plant Science.* doi: 10.3389/fpls.2013.00533

Yang J. 2017. *Integrating root and leaf phenotypes to enhance nitrogen use efficiency in maize (*Zea mays *L.).* PhD. Plant Biology PhD. Thesis, The Pennsylvania State University University Park, PA, USA.

Yano K, Yamauchi A, Kono Y. 1996. Localized alteration in lateral root development in roots colonized by an arbuscular mycorrhizal fungus. *Mycorrhiza* 6: 409-415.

York LM, Galindo-Castañeda T, Schussler JR, Lynch JP. 2015. Evolution of US maize (*Zea mays* L.) root architectural and anatomical phenes over the past 100 years corresponds to increased tolerance of nitrogen stress. *Journal of Experimental Botany* 66: 2347-2358.

York LM, Nord EA, Lynch JP. 2013. Integration of root phenes for soil resource acquisition. *Frontiers in Plant Science.* doi:10.3389/fpls.2013.00355.

Zangaro W, Alves RA, Lescano LE, Ansanelo AP, Nogueira MA. 2012. Investment in fine roots and arbuscular mycorrhizal fungi decrease during succession in three Brazilian ecosystems. *Biotropica* 44: 141-150.

Zhu J, Brown KM, Lynch JP. 2010. Root cortical aerenchyma improves the drought tolerance of maize (*Zea mays* L.). *Plant, Cell & Environment* 33: 740-749.

Figures and Tables

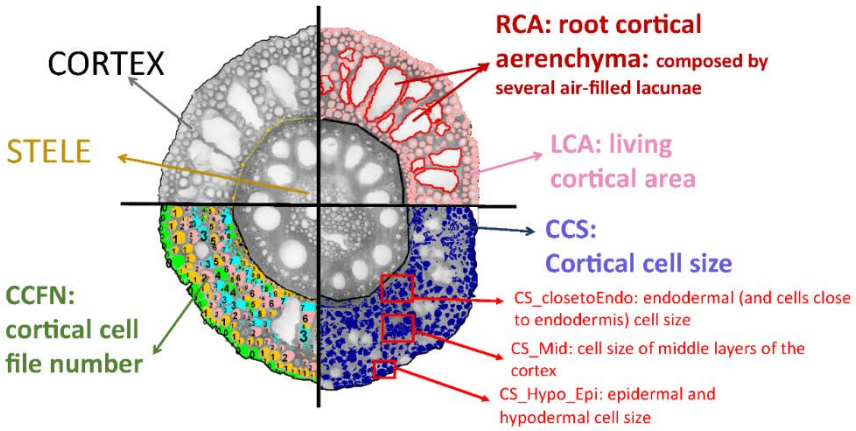

Figure 2-1. Root cross-section showing anatomical phenes in a maize (*Zea mays*) nodal root (third whorl).

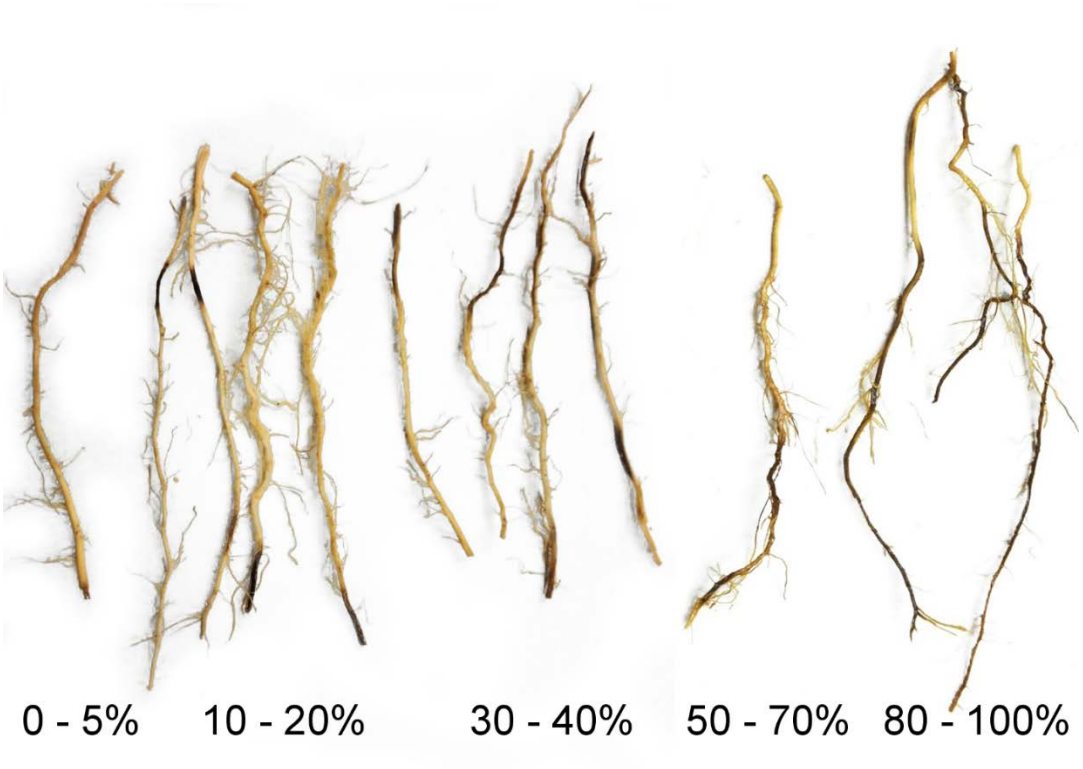

Figure 2-2. Root rot scale used for field samples. Root segments are 20 cm length.

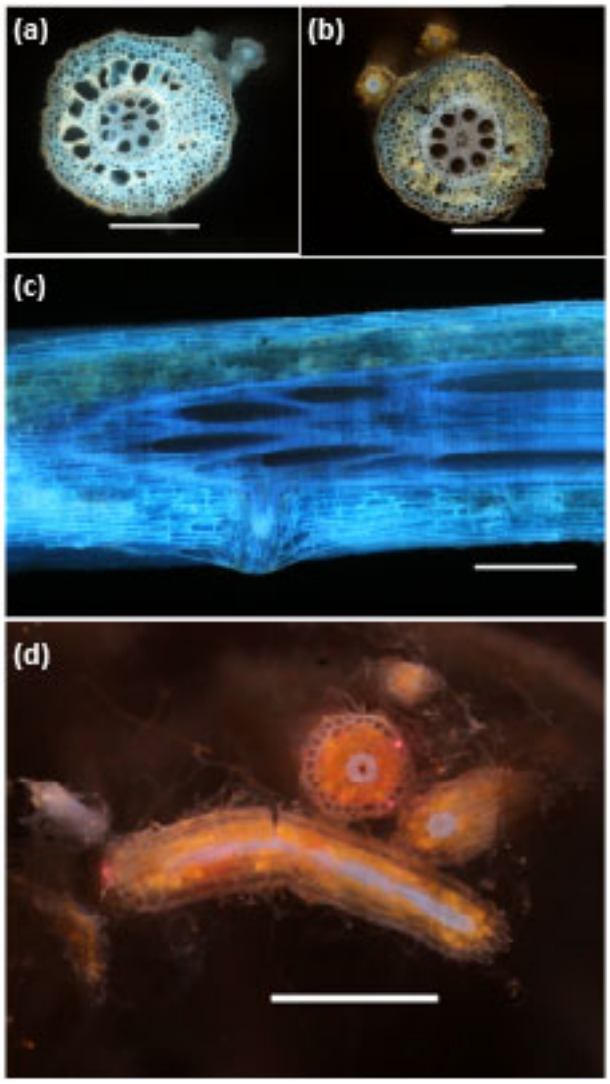

Figure 2-3. Arbuscules and root tissue emit different auto-florescence during laser-ablation of ethanol-preserved samples. Non-inoculated (a) and inoculated (b, c, d) roots taken from mesocosm-grown samples in 2014 (from MC-14) in the second whorl. Arbuscules are evident in orange or yellow. Axial roots are shown in a, b and c; lateral roots are shown next to the axial root in a and b, and separated from the axial root in d. Bars = 0.5 mm.

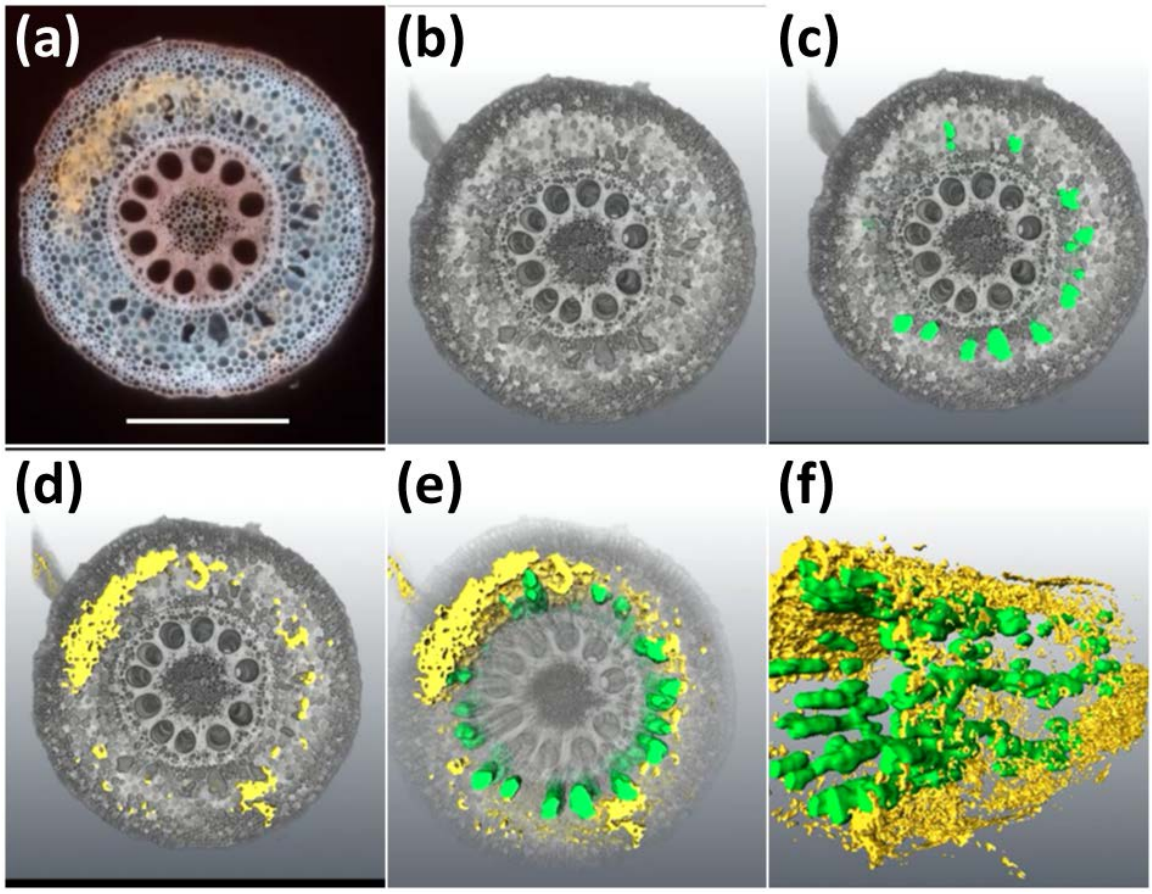

Figure 2-4. Distribution of arbuscules in the cortex of maize (*Zea mays*) roots in the mesocosm experiment of 2014 (MC-14) in three-dimensional reconstructions of colonized root segments taken in the third whorl of an arbuscular mycorrhizal-inoculated plant grown under low phosphorus. Series of cross-sections with arbuscular mycorrhiza color-differentiated were obtained with laser ablation (a), processed (b) and aerenchyma lacunae (c) and mycorrhiza (d) differentiated in green and yellow respectively and reconstructed in a 3D model (e), a side view shows how arbuscular networks colocalize with aerenchyma channels (f). Bar = 0.5 mm..

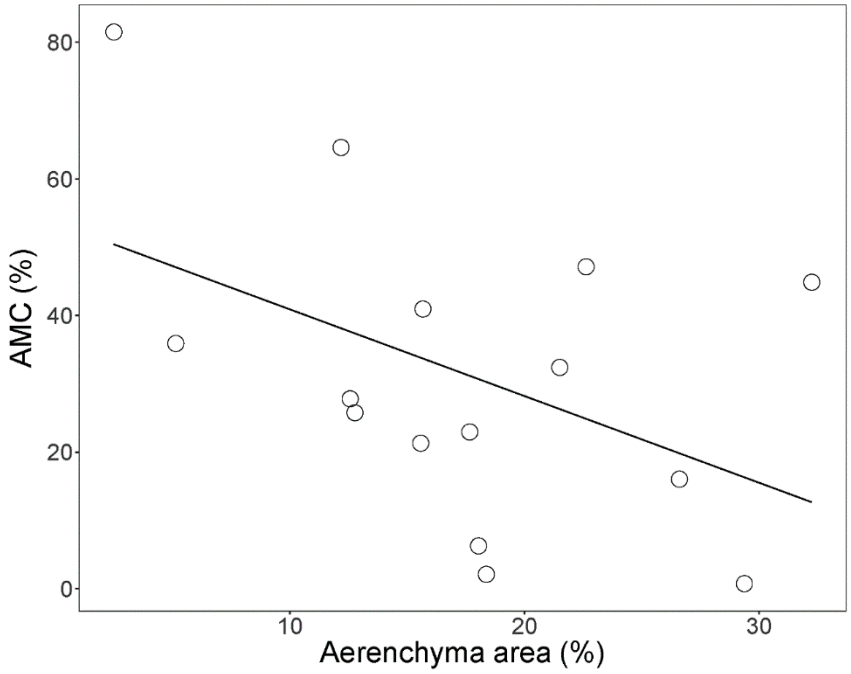

Figure 2-5. Relationship of arbuscular mycorrhizal colonization and percent aerenchyma area in axial roots of plants grown under optimal fertility in the field experiment with inbred in 2012 (FI-12) (P = 0.081, R^2=0.156). Points are averages of three replicates.

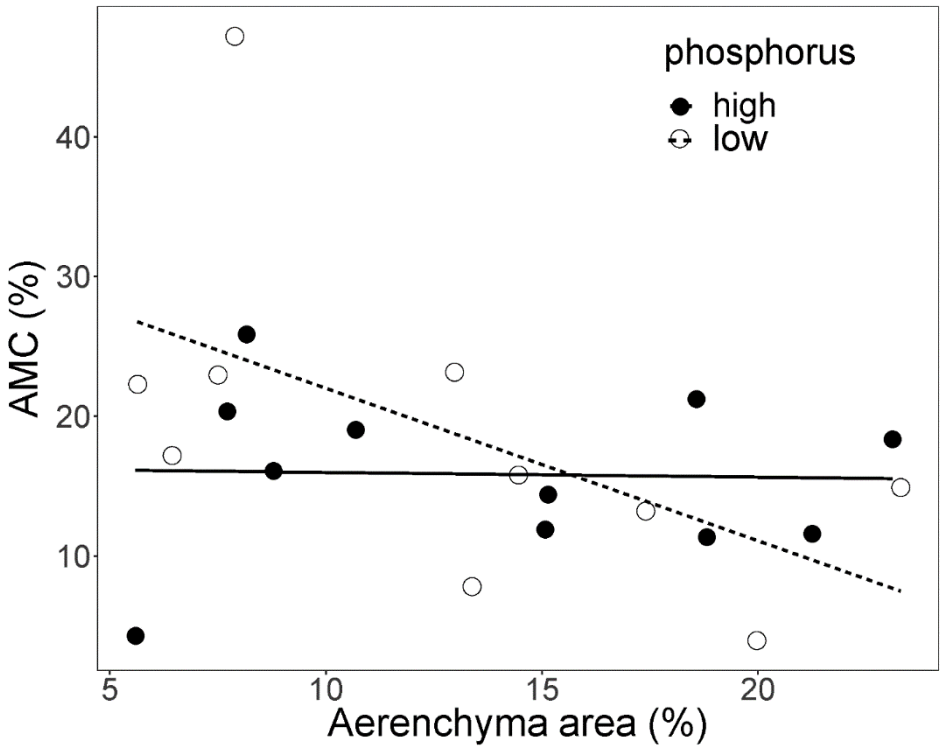

Figure 2-6. Relationship of arbuscular mycorrhizal colonization and percent aerenchyma area in inbred maize (*Zea mays*) genotypes under low phosphorus (P = 0.09, R^2=0.228) and high phosphorus (P = 0.8287, R^2=-0.026) availability in the field experiment of 2015 FI-15. Points are averages of three or four replicates per genotype.

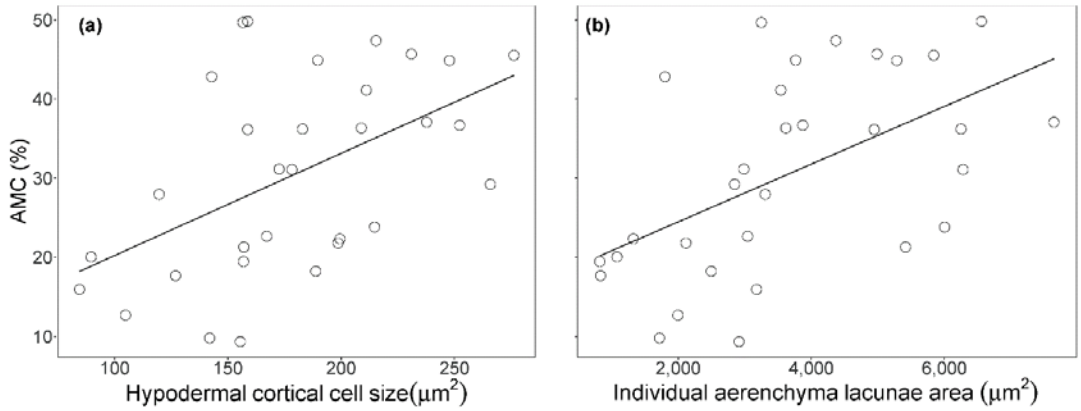

Figure 2-7. Relationship of arbuscular mycorrhizal colonization and (a) hypodermal cortical cell size (P = 0.003, R^2=0.238), and (b) aerenchyma lacunae area (P = 0.002, R^2=0.269) in axial roots of hybrid maize (*Zea mays*) lines growing under optimal fertility in the field experiment of 2014 FH-14. Points are averages of three plots per hybrid.

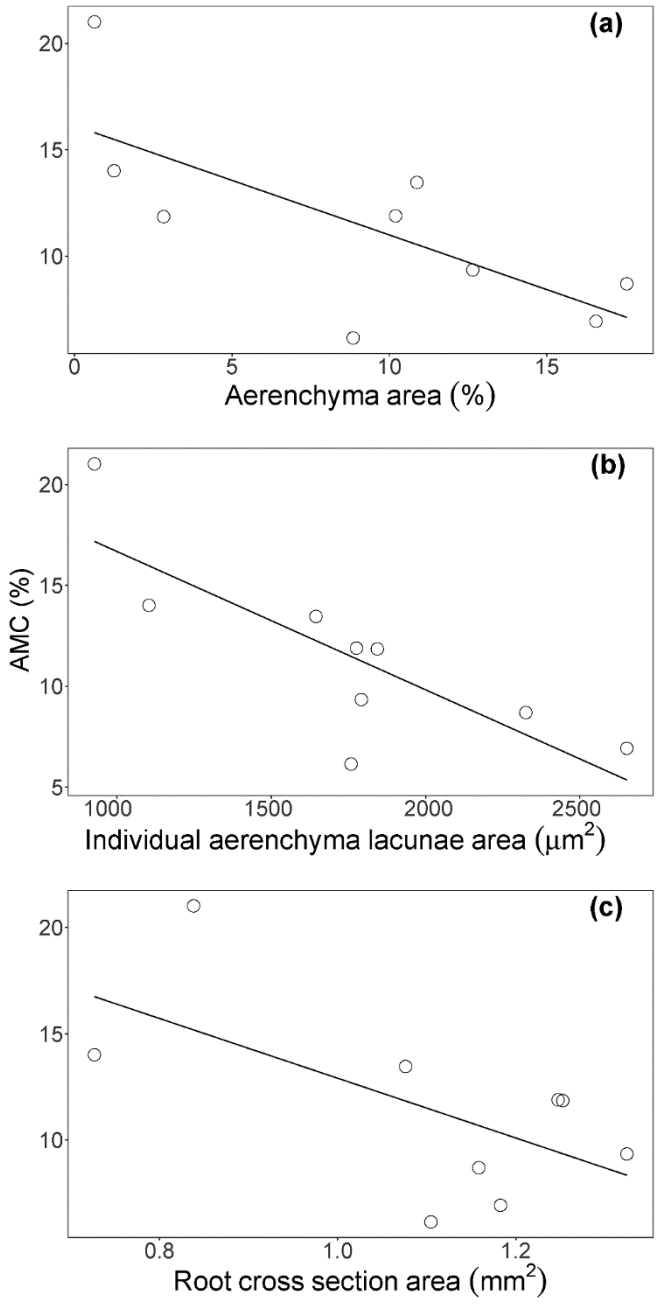

Figure 2-8. Relationship of arbuscular mycorrhizal colonization (AMC) and (a) percent aerenchyma area (P = 0.030, R^2=0.443), (b) lacunae area (P = 0.009, R^2=0.601), and (c) root cross-section area in axial roots of plants growing under low phosphorus availability in the mesocosm experiment of 2014 (MC-14) (P = 0.077, R^2=0.292). Points are averages of four plants per genotype.

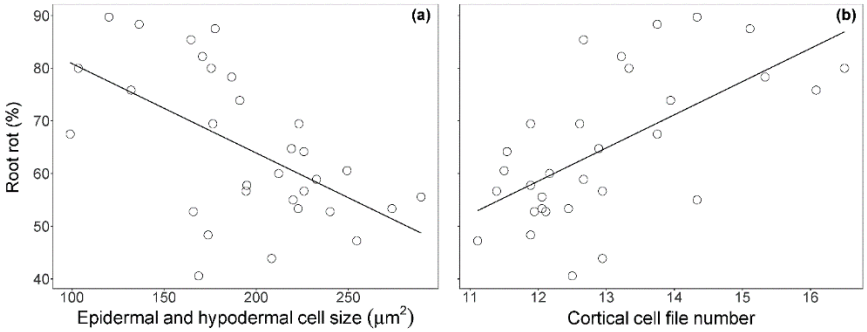

Figure 2-9. Relationship of root rot and (a) epidermal and hypodermal cell size (P = 0.001, R^2=0.295), and (b) cortical cell file number in axial roots of hybrid maize (*Zea mays*) lines growing under optimal fertility in the field (P < 0.001, R^2=0.361), experiment conducted in 2014 (FH-14). Points are averages of three plots per hybrid for each of the three sites.

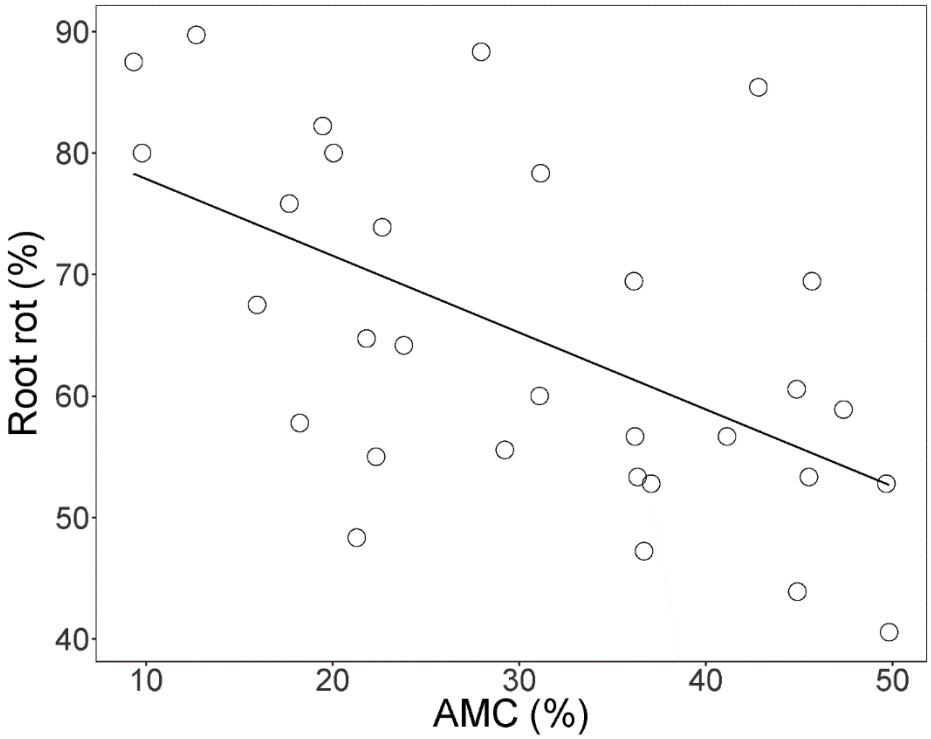

Figure 2-10. Relationship of arbuscular mycorrhizal colonization (AMC) and root rots in hybrid maize (*Zea mays*) lines growing under optimal fertility in the field (P = 0.001, R^2=0.289), FH-14. Points are averages of three plots per hybrid for each of the three sites.

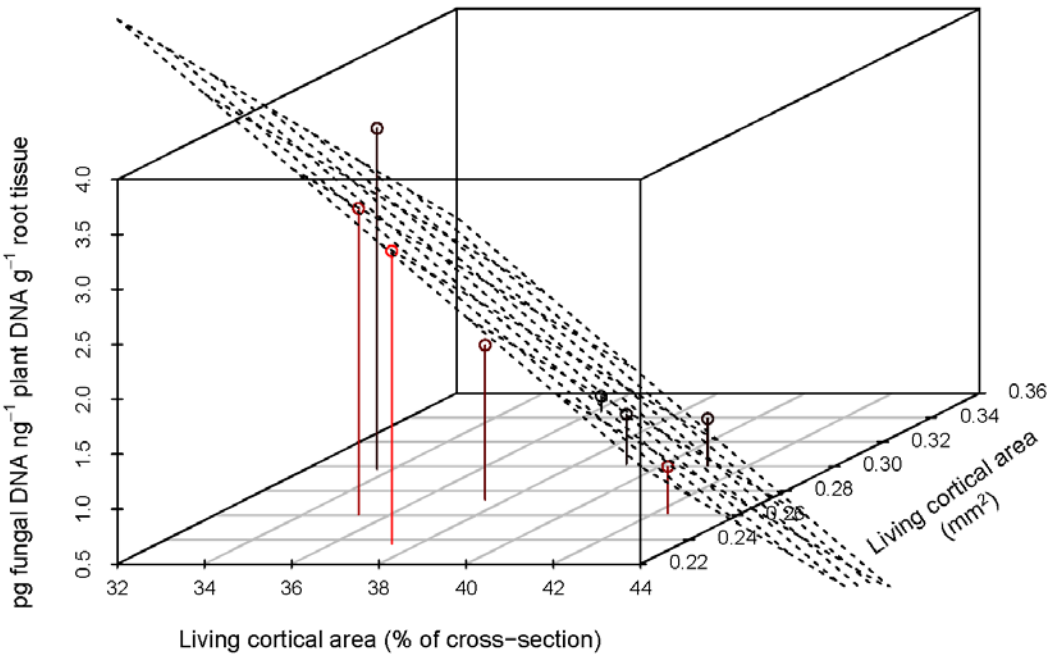

Figure 2-11. 3D scatterplot of *F. verticillioides* colonization with the root anatomical phene aggregates living cortical area (LCA) and percent of the cortex that is living cortical area (perXSisLCA) in eight recombinant inbred lines in the mesocosm experiment conducted in 2015 with inbred lines (MC-15). Points are averages of four replicates per genotype of the experiment MC-15. The plane is the linear fit of the model *F. verticillioides* concentration = LCA + perXSisLCA (P = 0.002, R^2=0.881). Red intensity relates to the 'Living cortical area' coordinates, with red in the lowest values and black in the highest values.

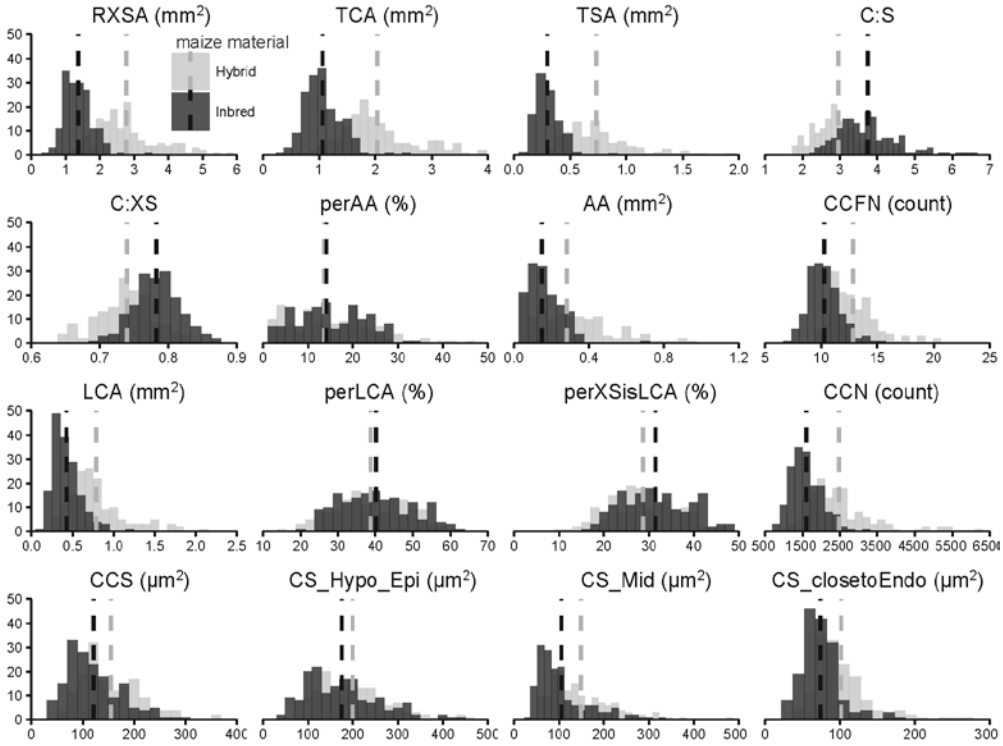

Figure 2-12. Variation in anatomical phenotypes in field-grown inbred (in 2015) and hybrid (in 2014) maize (*Zea mays*) of the experiments FI-15 and FH-14 respectively. Dash-lines represent averages. All phenotype means were significantly different between hybrids and inbred genotypes ($P < 0.010$), except perAA and perLCA ($P > 0.100$). RXSA: root cross-section area, TCA: total cortical area, TSA: total stele area, C:S: ratio cortex to stele, C:XS: ratio cortex to cross-section, perAA: percent of the cortex that is aerenchyma area, AA: aerenchyma area, CCFN: cortical cell file number, LCA: living cortical area, perLCA: percent of cortex that is living cortical area, perXSisLCA: percent of cross section that is living cortical area, CCN: cortical cell number, CCS: cortical cell size, CS_Hypo_Epi: median of size of cells in epidermis and hypodermis, CS_Mid: median of size of cells in middle layers of cortex, CS_clostoEndo: median of size of cells close to endodermis.

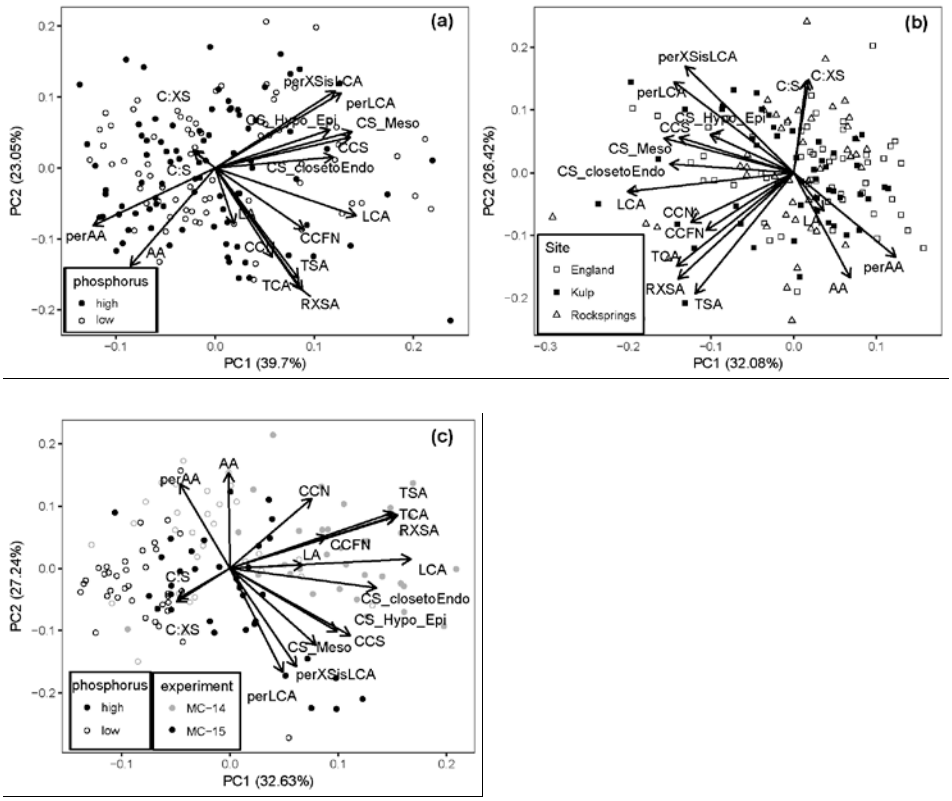

Figure 2-13. Principal component analysis (PCA) of 17 anatomical phenes and phene aggregates in the field experiments of 2015 with inbreds, FI-15 (a) and 2014 with hybrids, FH-14 (b) and the mesocosm experiments with inbreds in 2014, MC-14 and in 2015, MC-15 (c) showing the first two principal components and respective explained percentage of the total variance.. Points are the scores of each root on the two components. Arrows represent the loading of the anatomical phenes on the two components. Specific phosphorus levels, sites and experiments are indicated by grey/black and shape of the points. RXSA: root cross-section area, TCA: total cortical area, TSA: total stele area, C:S: ratio cortex to stele, C:XS: ratio cortex to cross-section, perAA: percent of the cortex that is aerenchyma area, AA: aerenchyma area, CCFN: cortical cell file number, LCA: living cortical area, perLCA: percent of cortex that is living cortical area, perXSisLCA: percent of cross section that is living cortical area, CCN: cortical cell number, CCS: cortical cell size, CS_Hypo_Epi: median of size of epidermal and hypodermal cells , CS_Mid: median of size of cells in middle layers of cortex, CS_closetoEndo: median of size of cells close to endodermal cells; LA: lacunae area.

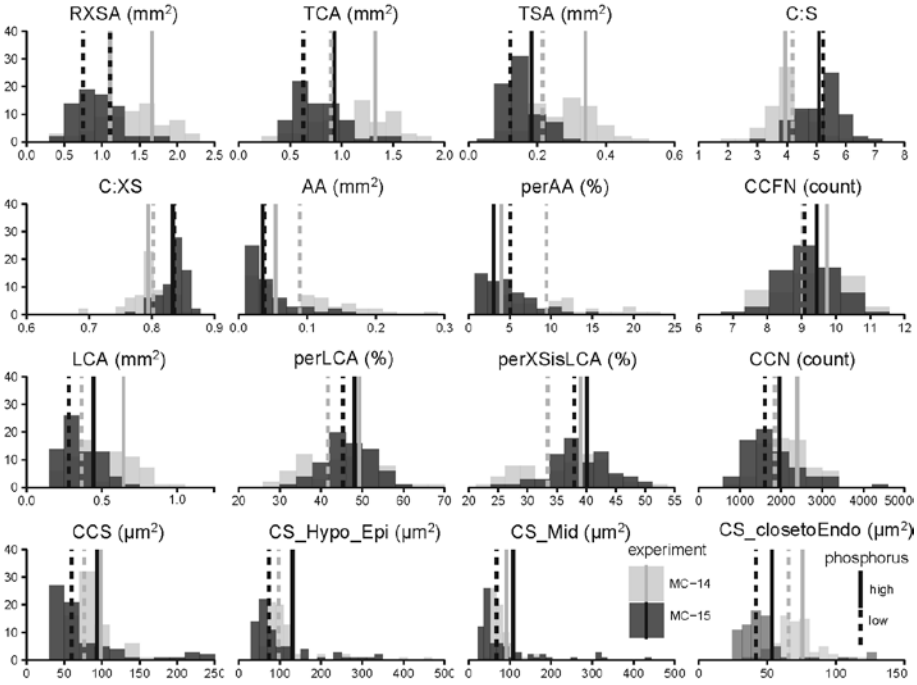

Figure 2-14. Variation in anatomical phenotypes in mesocosm-grown maize (*Zea mays*) of the mesocosm experiments with inbreds in 2015, MC-15 and in 2014, MC-14. Dash-lines represent the means of all the plants sampled per experiment and phosphorus level. All the phenes were significantly different between experiments ($P < 0.050$) except CCFN ($P = 0.297$), perLCA ($P = 0.361$), and CS_Hypo_Epi ($P = 0.224$). Phosphorus had significant effect on all the phenes or phene aggregates except C:XS ($P = 0.168$). RXSA: root cross-section area, TCA: total cortical area, TSA: total stele area, C:S: ratio cortex to stele, C:XS: ratio cortex to cross-section, perAA: percent of the cortex that is aerenchyma area, AA: aerenchyma area, CCFN: cortical cell file number, LCA: living cortical area, perLCA: percent of cortex that is living cortical area, perXSisLCA: percent of cross section that is living cortical area, CCN: cortical cell number, CCS: cortical cell size, CS_Hypo_Epi: Median of epidermal and hypodermal cells , CS_Mid: median of size of cells in middle layers of cortex, CS_closetoEndo: median of size of cells close to endodermal cells.

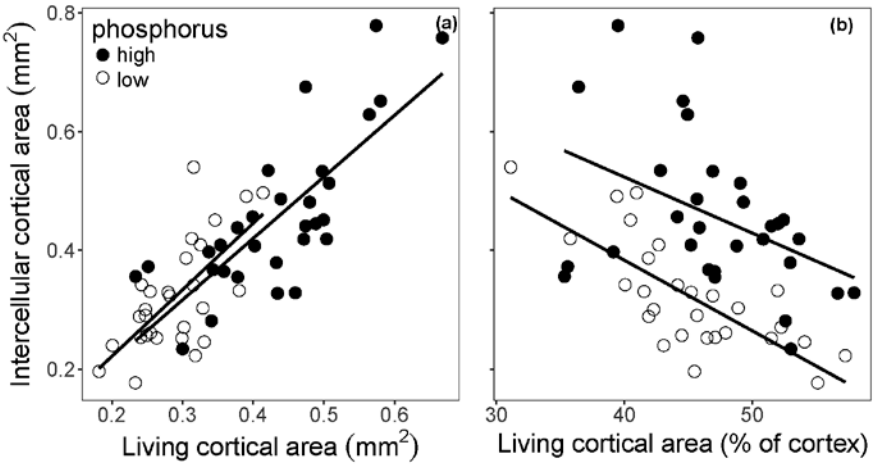

Figure 2-15. Relationship between intercellular cortical area of root cross-sections and (a) living cortical area (low phosphorus: $P < 0.001$, R^2=0.426; high phosphorus: $P < 0.001$, R^2=0.585) and (b) percent of cortex that is living cortical area (low phosphorus: $P < 0.001$, R^2=0.548; high phosphorus $P = 0.020$, R^2=0.149) in the mesocosm experiment with inbreds in 2015, MC-15.

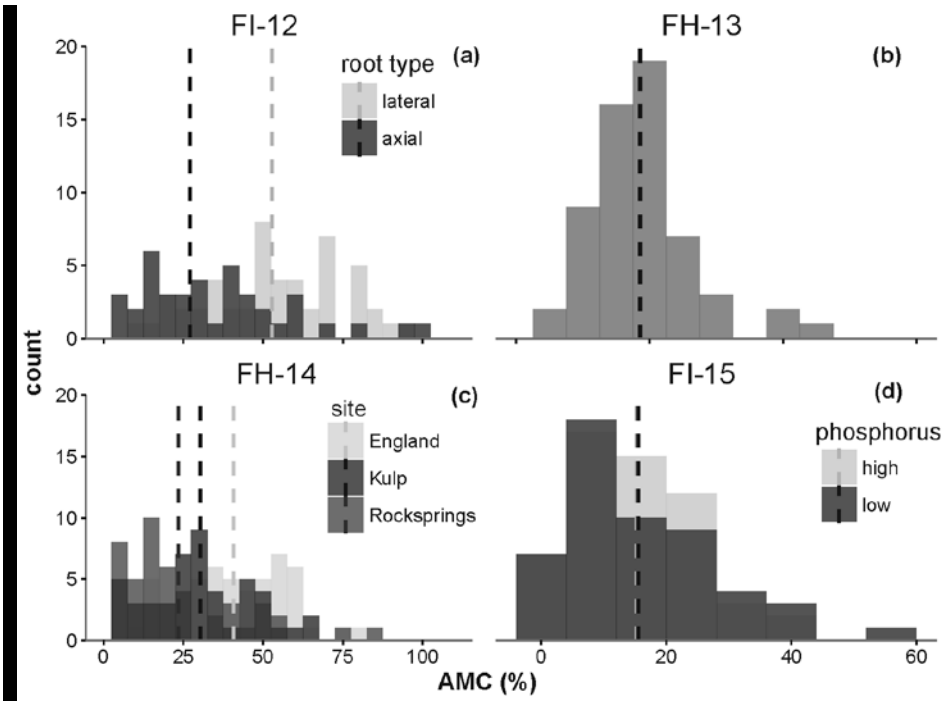

Figure 2-16. Distribution of arbuscular mycorrhizal colonization (AMC) of field-grown maize (*Zea mays*) in four experiments. Values discriminated by root class in the field experiment with inbreds in 2012, FI-12 (a), in axial root in the field experiment with hybrids in 2013, FH-13 (b), by farm in axial root in the field experiment with hybrids, FH-14 (c) and under two phosphorus levels in axial roots in the field experiment with inbreds, FI-15 (d). Dash-lines represent the average AMC of the plants sampled for each experiment and treatment. Effect of root class in a) $P < 0.001$; effect of site in c) $P < 0.001$; effect of phosphorus in d) $P = 0.943$.

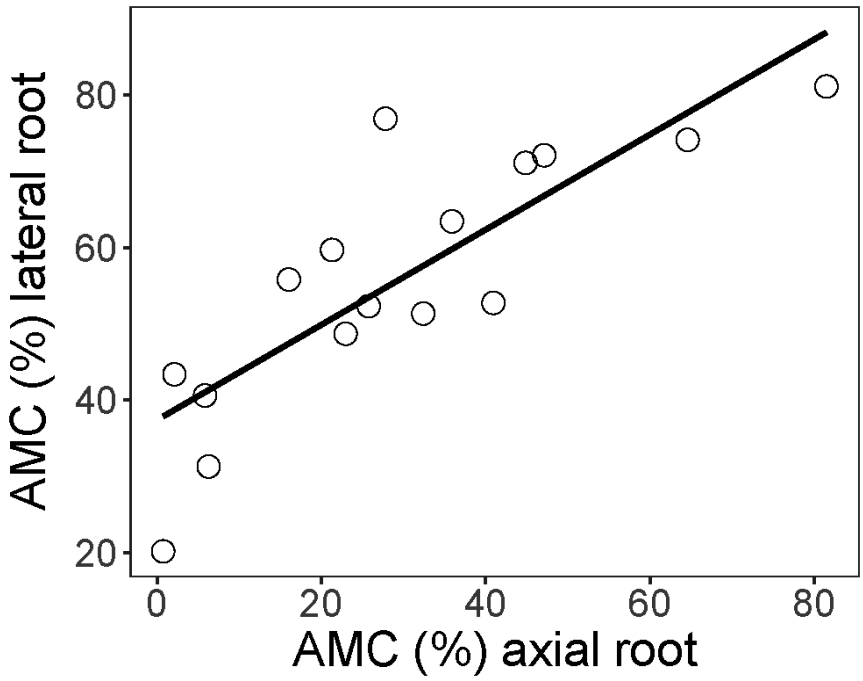

Figure 2-17. Relationship of arbuscular mycorrhizal colonization (AMC) in axial and lateral roots in plants growing under optimal fertility in the field experiment of 2012, FI-12 ($P < 0.001$, R^2=0.662).

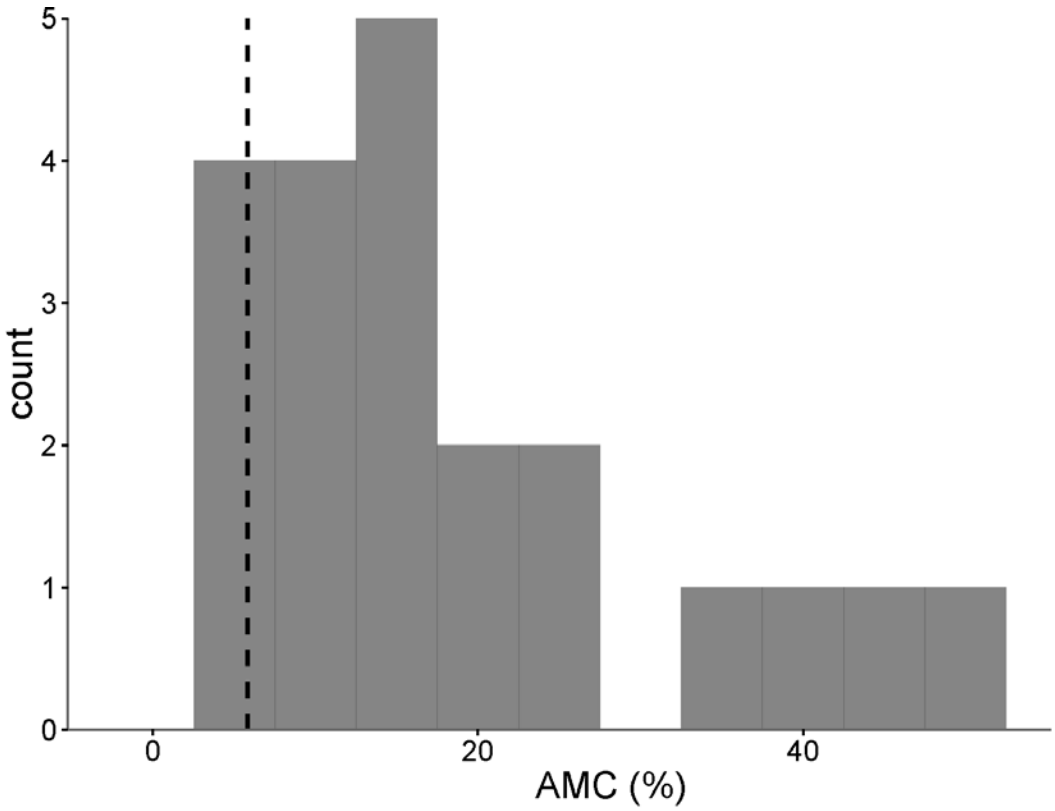

Figure 2-18. Relationship of arbuscular mycorrhizal colonization (AMC) in axial and lateral roots in plants growing under optimal fertility in the field experiment of 2012, FI-12 ($P < 0.001$, R^2=0.662). Points are AMC averages of four replicates.

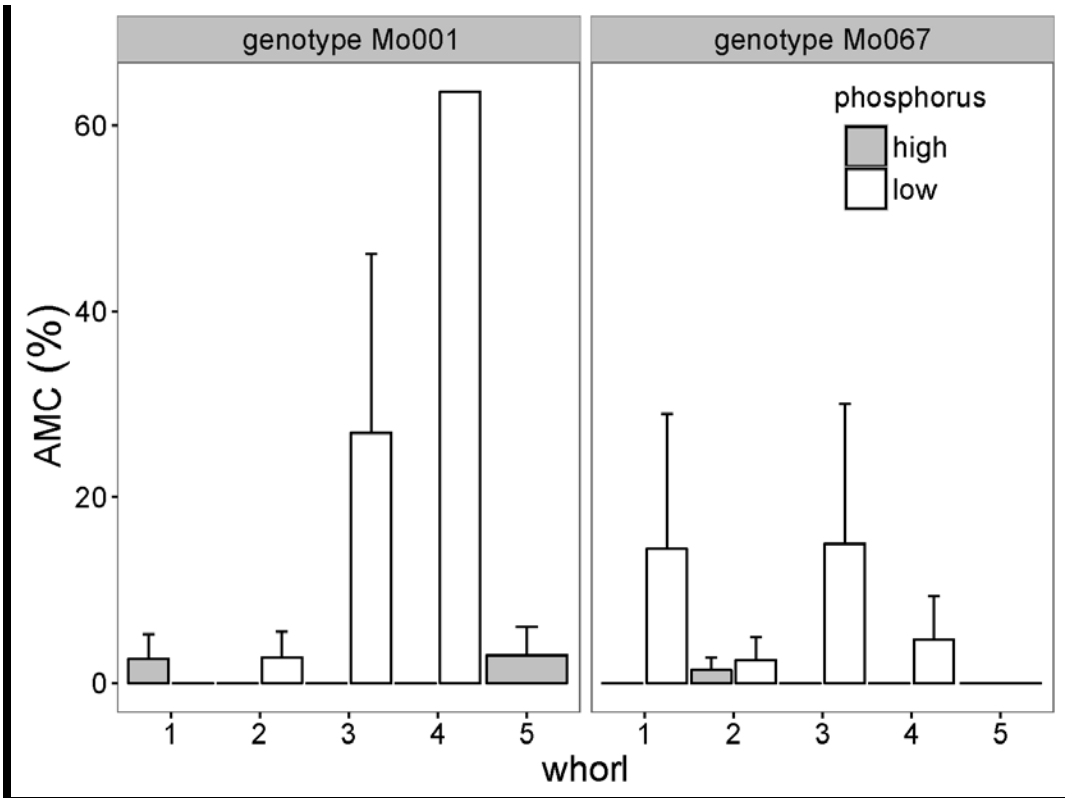

Figure 2-19. Arbuscular mycorrhizal colonization (AMC) per whorl in axial roots of two inbred genotypes growing under high and low phosphorus in the mesocosm experiment of 2014, MC-14. Plants growing under low phosphorus did not have a fifth whorl. Bars are averages of three to four plants. Error bars indicate one SE. No significant differences were found among whorls within the same phosphorus level.

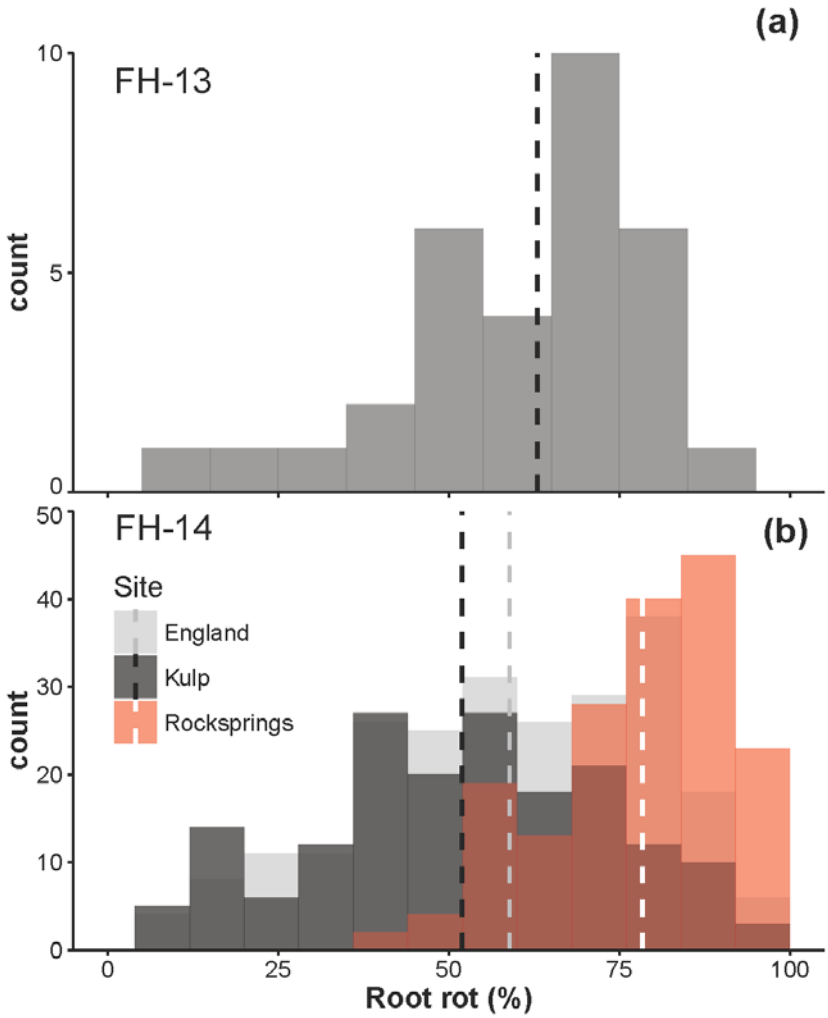

Figure 2-20. Distribution of root rot of field-grown maize (*Zea mays*) in the field experiment with hybrid maize, FH-13 (a) and by farm in the field experiment with hybrids FH-14 (b). Dash-lines represent the average root rots of the plants sampled for each site. Root rots averages significantly differed by farm in FH-14 ($P < 0.001$).

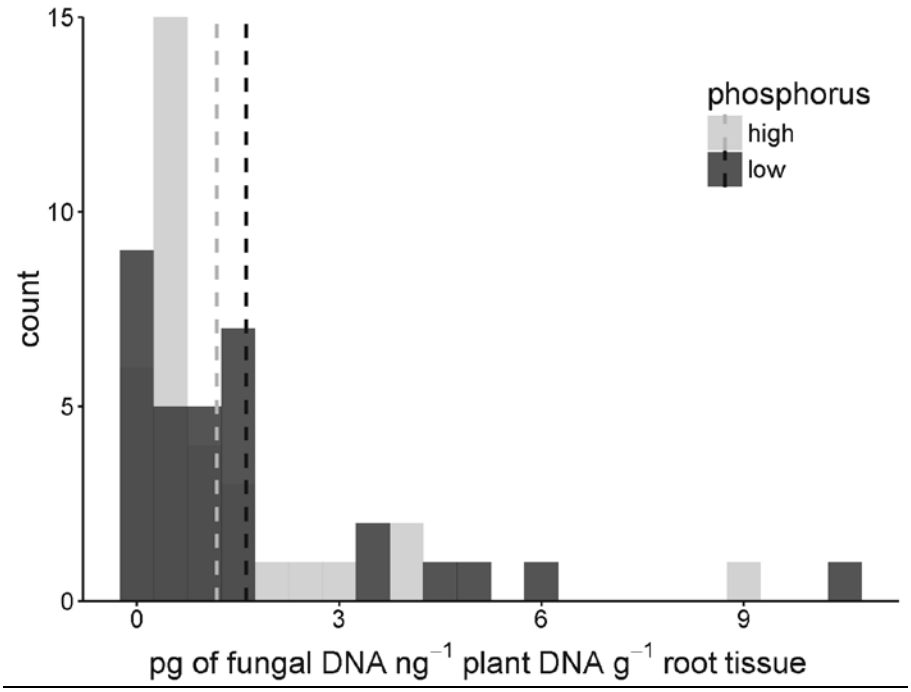

Figure 2-21. *F. verticillioides* colonization of roots in the mesocosm experiment with inbreds in 2015 MC-15 under high and low phosphorus. Dash-lines represent average of all the plants per phosphorus level.

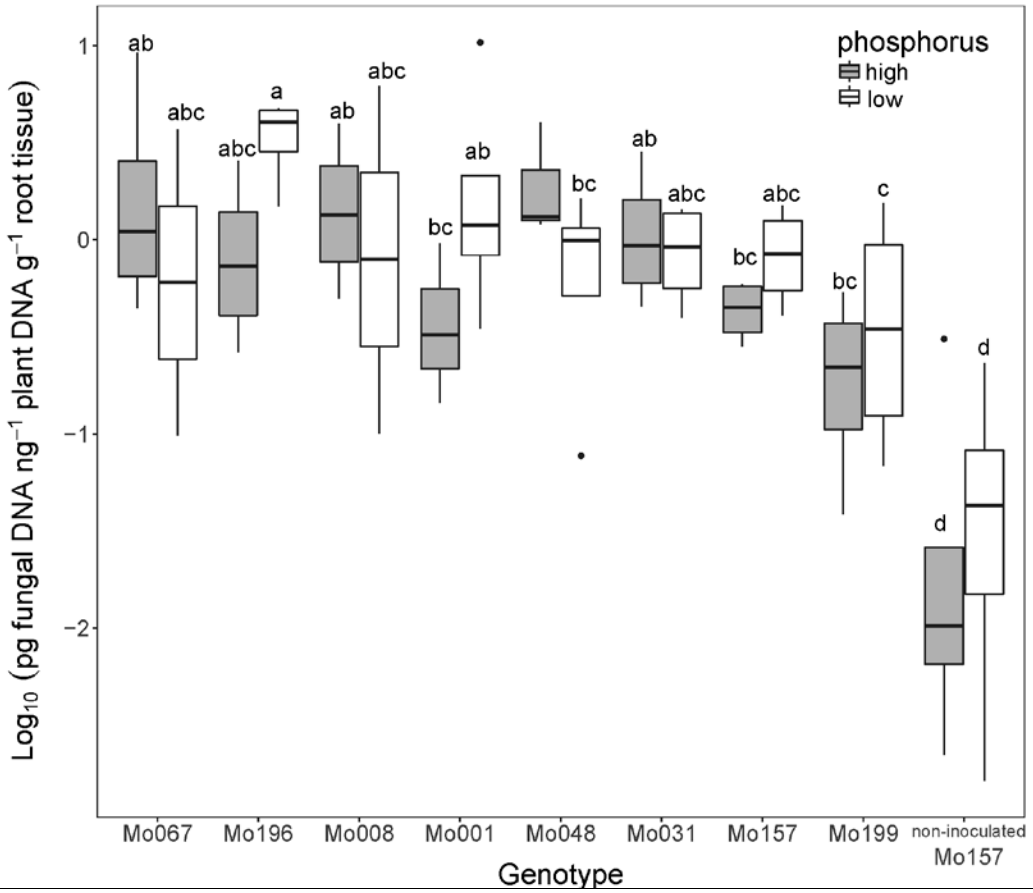

Figure 2-22. Boxplots of *F.verticillioid*es root colonization in the mesocosm experiment of 2014, MC-14 by genotype and phosphorus level, included the control non-inoculated Mo157. Horizontal box lines correspond to 25th, 50th, and 75th percentile; ranges are indicated by whiskers and points are outliers. For each boxplot n = 4. Different letters indicate significant differences at *P*=0.05.

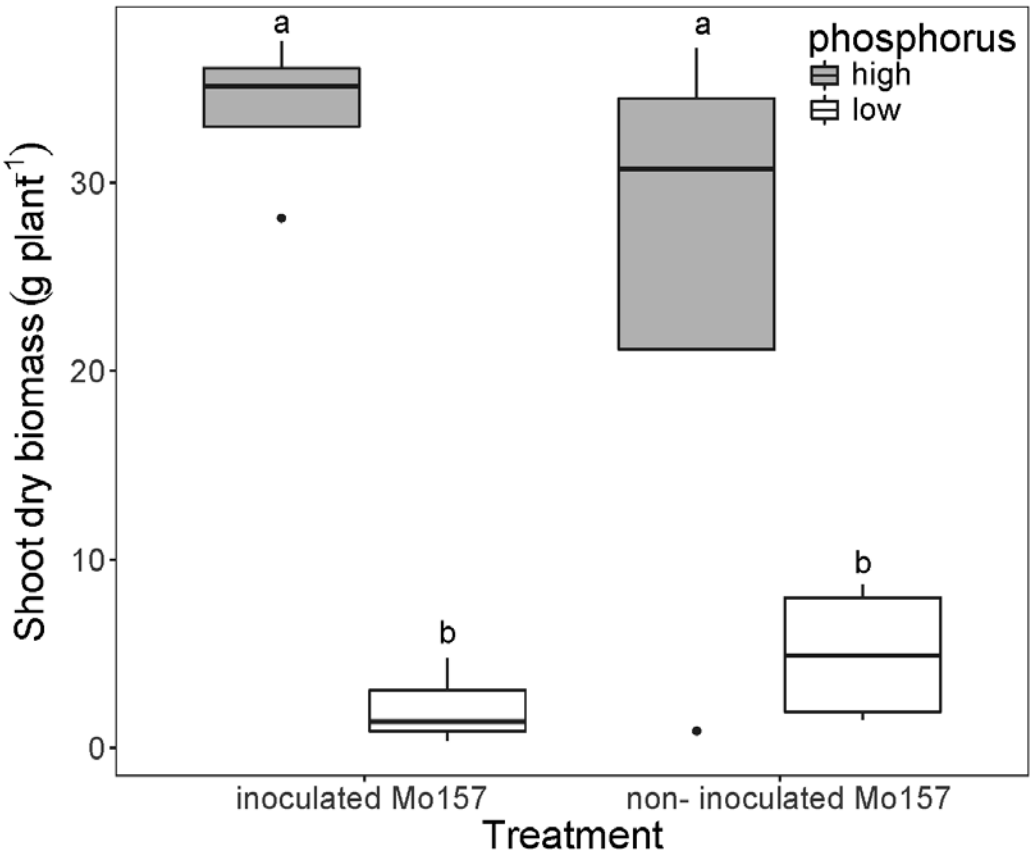

Figure 2-23. Effect of *F.verticillioides* inoculation on plant biomass in the genotype Mo157 of the mesocosm experiment with inbreds in 2015, MC-15. Horizontal box lines correspond to 25th, 50th, and 75th percentile; ranges are indicated by whiskers and points are outliers. For each boxplot n = 4. Different letters indicate significant differences at $P = 0.05$.

Table 2-1. Anatomical phenes retrieved by RootScan used for analysis in this study.

Anatomical phene or phene aggregate	Abbreviation	Units
Root cross section area	RXSA	mm^2
Cortex area	TCA	mm^2
Stele area	TSA	mm^2
Cortex:Stele ratio	C:S	-
Cortex:Cross section ratio	C:XS	-
Stele:Cross section ratio	S:XS	-
Aerenchyma area (sum of all the individual aerenchyma lacunae area of each cross-section)	AA	mm^2
Percentage of cortex that is aerenchyma	perAA	%
Cortical cell file number	CCFN	Count
Living cortical area (LCA)	LCA	mm^2
Percentage of cortex that is LCA	perLCA	%
Percentage of cross section that is LCA	perXSisLCA	%
Median cortical cell size	CCS	μm^2
Cortical cell number	CCN	Count
Median of size of cells in hypodermis and the epidermis	CS_Hypo_Epi	μm^2
Median of size of cells in middle layers of cortex	CS_Mid	μm^2
Median of size of cells in inner cortical area close to endodermis	CS_closetoEndo	μm^2
Median aerenchyma lacunae area	LA	mm^2

Table 2-2 Summary of multiple regression models of *F. verticillioides* colonization as predicted by anatomical phenotypes selected by stepwise regression in plants growing under low and high phosphorus availability in the mesocosm experiment of 2015 with inbred maize (MC-15). SE: one SE. ** $P < 0.01$. * $P < 0.05$. LCA: living cortical area, perXSisLCA: percent of cross section that is living cortical area, CS_clostoEndo: median of size of cells close to endodermis. Model at low phosphorus: F. verticillioides root concentration = LCA + perXSisLCA. Model at high phosphorus: F. verticillioides root concentration = CS_closetoEndo + perXSisLCA + LCA.

Low phosphorus				High phosphorus			
Term	Coefficient	SE		Term	Coefficient	SE	
Intercept	9.7×10^{-16}	0.12		Intercept	-1.3×10^{-15}	0.23	
LCA	-0.65	0.13	**	CS_closetoEndo	1.80	0.55	*
perXSisLCA	-0.80	0.13	**	perXSisLCA	-2.45	1.24	
				LCA	1.20	1.03	
Adjusted R^2	0.881			Adjusted R^2	0.5764		
model *P* value	0.002			model *P* value	0.1005		

Table 2-3. Inbred maize (*Zea mays*) genotypes used in the experiments.

Genotype	Experiment			
	MC-14	MC-15	FI-12	FI-15
Mo001	x	x	x	x
Mo008		x		x
Mo014	x			
Mo016	x			
Mo031		x	x	x
Mo034			x	x
Mo048		x		x
Mo058	x			
Mo060	x			
Mo067	x	x		x
Mo106	x			
Mo157		x	x	x
Mo177			x	
Mo165				x
Mo196		x		x
Mo199		x		x
Mo337				x
Mo338			x	
OWR155	x			
OWR33	x			

Table 2-4. Hybrid entries selected for sampling at the field experiment in 2013 FH-13.

Brand	Hybrid
King.s-Agriseeds-Inc.	Masters-Choice-MCT-6054
Healthy-Herd-Genetics-and-Nutrition-Inc.	43HF13
King.s-Agriseeds-Inc.	Masters-Choice-MC-535
Dupont-Pioneer	P0210AM
T.A.-Seeds	TA583-22DP
Monsanto-Corp.	DKC57-75-GENSSRIB
T.A.-Seeds	TA614-22DP
FS-InVision	InVision-FS-5667GT3
Doebler.s-PA-hybrids-Inc.	Doeblers-507SLR
Doebler.s-PA-hybrids-Inc.	RPM-604HRQ
Doebler.s-PA-hybrids-Inc.	RPM-647AM1
Monsanto-Corp.	DKC57-50-VT3
Mycogen	F2F626
Chemgro	Chemgro-6538G3N
Mycogen	TMF2H699
Mycogen	TMF2R720
Monsanto-Corp.	DKC60-63-GENVT2PRIB
T.A.-Seeds	TA657-13VP
Dupont-Pioneer	P0604YHR
FS-InVision	InVision-FS-5815GT3
Hubner-Seed	H5333RC3P
Crop-Production-Services/Dyna-Gro	CX50VP3
Hubner-Seed	H5420RC3P
Dupont-Pioneer	P0945YXR
T.A.-Seeds	TA615-16ND
T.A.-Seeds	TA545-33
Dupont-Pioneer	P1184AMX
Dupont-Pioneer	P1498AM
Chemgro	Chemgro-6638G3
Mycogen	F2F795
Monsanto-Corp.	DKC61-88-GENVT3PRIB
Dupont-Pioneer	P1449XR

Table 2-5. Hybrid entries selected for sampling at the commercial farms in 2014.

Entries per brand		Site		
Brand	Hybrid	England	Kulp	Rock Springs
Channel	Channel_203-44STXRIB	x	x	x
Channel	Channel_207-13VT3PRIB	x	x	x
Channel	Channel_210-95STXRIB	x		x
Chemgro-Seeds	Chemgro_6638G3	x	x	x
Chemgro-Seeds	Chemgro_7037RVPN	x	x	x
Doebler.s-PA-Hybrids	Doeblers_554GRQ	x	x	x
Doebler.s-PA-Hybrids	RPM_537AMX	x	x	x
Doebler.s-PA-Hybrids	RPM_604HRQ	x	x	x
Doebler.s-PA-Hybrids	RPM_647AM1	x		x
DuPont-Pioneer	P0636AMX	x	x	x
DuPont-Pioneer	P0993HR	x	x	x
DuPont-Pioneer	P1498AM	x	x	x
FS-InVISION	FS_InVISION_FS_55R25VT3P	x	x	x
FS-InVISION	FS_InVISION_FS_57R30SS	x	x	x
FS-InVISION	FS_InVISION_FS_5847VT3P	x		x
Healthy-Herd	42HFC15	x	x	x
Hubner-Seed	H5222RC3P	x	x	x
Hubner-Seed	H5333RC3P	x	x	x
Hubner-Seed	H6191RCSS	x	x	x
Hubner-Seed	H6330RCSS	x		x
King.s-AgriSeeds	Masters_Choice_MC_5250	x	x	x
King.s-AgriSeeds	Masters_Choice_MC_5660	x	x	x
King.s-AgriSeeds	Masters_Choice_MCT_5375	x	x	x
King.s-AgriSeeds	Masters_Choice_MCT_6153	x		x
Monsanto-Corp	DKC56-03RIB	x	x	x
Monsanto-Corp	DKC57-75RIB	x		x
Monsanto-Corp	DKC57-92RIB	x	x	x
Monsanto-Corp	DKC60-67RIB	x	x	x
Monsanto-Corp	DKC61-88RIB	x		x
Mycogen	TMF2H706	x	x	x
Mycogen	TMF2R720	x	x	x
Syngenta	NK_N53W-3122	x	x	x
Syngenta	NK_N59B-3111A	x	x	x
Syngenta	NK_N63R-3000GT	x		x
T.A.-Seeds	TA108-18	x	x	x
T.A.-Seeds	TA536-22DPRIB	x	x	x
T.A.-Seeds	TA566-31	x	x	x
T.A.-Seeds	TA583-28RIB	x		x
T.A.-Seeds	TA625-31	x	x	x

Table 2-6. Field history and important dates of the experiments conducted at commercial farms selected for study of anatomy and fungal colonization in hybrid maize (*Zea mays*). Modified from http://extension.psu.edu/plants/crops/grains/corn/hybrid-tests/2014-reports.

Farm, year	Kulp, 2014	England, 2014	Rock Springs, 2013 and 2014
Complete name	Kulp Family Dairy	Penn - England Farms	
Location	Skelp, PA 40° 37' 12.7416"N, -78° 13' 44.2662"W	Williamsburg, PA 40° 30' 41.817"N, -78° 11' 55.899"W	Pine Grove Mills, PA 40° 42' 50.511"N, -77° 58' 7.9212"W.
Soil	Hublersburg Cherty silt loam (HuB) Clayey, illitic, mesic Typic Hapludults	Hublersburg Cherty silt loam (HuB) Clayey, illitic, mesic Typic Hapludults	Nolin series. Fine-silty, mixed, active, mesic Dystric Fluventic Eutrudepts
Herbicides Pre-plant	not applied	946 mL Roundup, 163 mL Corvus, 710 mL Atrazine, 60 mL Lambda T, 473 mL Unison	2.0 liters.Roundup
Herbicides Post-plant	not applied	44.3 mL Option, 3.78 l Coron (25-0-0)	2.0 l ha^{-1} Roundup + 7.0 l ha^{-1} Lexar
Previous crop	Maize	Maize	Soybeans
Starter fertilizer	75 l ha^{-1} 5-8-3/ Micros (18.9 l in furrow)	75 l ha^{-1} 5-8-3/ Micros (18.9 l in furrow)	75 l ha^{-1} 5-8-3/ Micros (18.9 l in furrow)
Insecticide	Force 3G	Force 3G	Force 3G
Manure	not applied	22,713 l liquid dairy (13.9-8.7- 22.6)	not applied
Fertilizer Pre-plant	not applied	27 kg of nitrogen broadcast	not applied
Fertilizer side-dressed	not applied	not applied	180 kg N/ha applied as urea
Planting date	May 19 2014	May 19 2014	May 26 2014
Harvest date	July 28 2014	August 04 2014	August 11 2014

Table 2-7. ANOVA table of anatomical phenes and the *F* values and associated *P* values of the effect of hybrid entry and site in the field experiment conducted in 2014 FH-14. ***$P < 0.001$; ** $0.001 \leq P < 0.01$;* $0.01 \leq P \leq 0.05$; †$0.05 < P \leq 0.1$; ns not significant. RXSA: root cross-section area, TCA: total cortical area, TSA: total stele area, C:S: ratio cortex to stele, C:XS: ratio cortex to cross-section, perAA: percent of the cortex that is aerenchyma area, AA: aerenchyma area, CCFN: cortical cell file number, LCA: living cortical area, perLCA: percent of cortex that is living cortical area, perXSisLCA: percent of cross section that is living cortical area, CCN: cortical cell number, CCS: cortical cell size, CS_Hypo_Epi: median of size of cells in epidermis and hypodermis, CS_Mid: median of size of cells in middle layers of cortex, CS_closto Endo: median of size of cells close to endodermis; LA: lacunae area.

Factor	Hybrid		Site		Hybrid:Site	
RXSA	1.67	*	7.99	***	1.24	ns
TCA	1.75	**	12.20	***	1.29	ns
TSA	1.73	*	0.57	ns	1.25	ns
C:S	2.13	***	7.02	**	1.68	**
C:XS	2.25	***	7.06	**	1.77	**
AA	1.82	**	32.37	***	1.22	ns
perAA	2.35	***	34.01	***	1.10	ns
CCFN	1.79	**	19.23	***	1.57	*
LCA	1.92	**	8.61	***	0.98	ns
perLCA	2.21	***	24.57	***	1.35	ns
perXSisLCA	1.95	**	17.92	***	1.28	ns
CCS	1.35	ns	10.17	***	1.01	ns
CCN	1.38	ns	20.83	***	1.59	*
CS_Hypo_Epi	1.26	ns	4.06	**	1.11	ns
CS_Meso	1.59	*	8.73	***	0.98	ns
CS_closetoEndo	1.23	ns	0.28	ns	0.97	ns
LA	1.41	ns	39.19	***	1.00	ns

Table 2-8. ANOVA table of anatomical phenes and the *F* values and associated *P* values of the effect of genotype and phosphorus in the field experiment with inbreds FI-15. ***$P < 0.001$; ** $0.001 \leq P < 0.01$;* $0.01 \leq P \leq 0.05$; ns not significant. RXSA: root cross-section area, TCA: total cortical area, TSA: total stele area, C:S: ratio cortex to stele, C:XS: ratio cortex to cross-section, perAA: percent of the cortex that is aerenchyma area, AA: aerenchyma area, CCFN: cortical cell file number, LCA: living cortical area, perLCA: percent of cortex that is living cortical area, perXSisLCA: percent of cross section that is living cortical area, CCN: cortical cell number, CCS: cortical cell size, CS_Hypo_Epi: median of size of cells in epidermis and hypodermis, CS_Mid: median of size of cells in middle layers of cortex, CS_clostoEndo: median of size of cells close to endodermis; LA: lacunae area.

Factor	Genotype		Phosphorus		Genotype:P	
RXSA	1.43	ns	0.04	ns	0.94	ns
TCA	1.19	ns	0.06	ns	1.01	ns
TSA	2.72	**	0.19	ns	0.66	ns
C:S	6.16	***	0.46	ns	0.56	ns
C:XS	6.24	***	0.19	ns	0.61	ns
AA	5.19	***	2.01	ns	1.02	ns
perAA	4.69	***	1.85	ns	1.25	ns
CCFN	1.84	**	0.13	ns	1.29	ns
LCA	1.48	ns	0.95	ns	0.88	ns
perLCA	3.87	**	2.61	ns	1.27	ns
perXSisLCA	3.75	**	2.68	ns	1.22	ns
CCS	2.12	*	2.06	ns	0.41	ns
CCN	0.51	ns	0.18	ns	0.45	ns
CS_Hypo_Epi	1.22	ns	1.56	ns	0.37	ns
CS_Mid	2.67	*	1.72	ns	0.66	ns
CS_closetoEndo	1.08	ns	0.79	ns	0.57	ns
LA	0.82	ns	0.04	ns	0.43	ns

Table 2-9. ANOVA table of anatomical phenes and the *F* values and associated *P* values of the effect of phosphorus and genotype in mesocosm-grown maize (*Zea mays*) of the mesocosm experiment with inbreds of 2014 MC-14. ***$P < 0.001$; ** $0.001 \leq P < 0.01$;* $0.01 \leq P \leq 0.05$; †$0.05 < P \leq 0.1$; nsns not significant. RXSA: root cross-section area, TCA: total cortical area, TSA: total stele area, C:S: ratio cortex to stele, C:XS: ratio cortex to cross-section, perAA: percent of the cortex that is aerenchyma area, AA: aerenchyma area, CCFN: cortical cell file number, LCA: living cortical area, perLCA: percent of cortex that is living cortical area, perXSisLCA: percent of cross section that is living cortical area, CCN: cortical cell number, CCS: cortical cell size, CS_Hypo_Epi: median of size of cells in epidermis and hypodermis, CS_Mid: median of size of cells in middle layers of cortex, CS_clostoEndo: median of size of cells close to endodermis; LA: lacunae area.

Factor	Genotype		Phosphorus		Genotype:P	
RXSA	1.45	ns	49.65	***	0.39	ns
TCA	1.87	†	43.08	***	0.34	ns
TSA	0.29	ns	59.72	***	0.70	ns
C:S	3.29	**	2.84	†	0.93	ns
C:XS	4.49	***	2.04	ns	1.26	ns
AA	5.16	***	7.27	**	2.43	†
perAA	7.28	***	32.02	***	3.80	ns
CCFN	0.88	ns	10.02	**	0.66	ns
LCA	1.25	ns	69.17	***	0.15	ns
perLCA	4.89	***	22.85	***	2.71	*
perXSisLCA	4.24	***	20.08	***	2.54	*
CCS	2.38	*	22.03	***	1.63	ns
CCN	0.62	ns	20.56	***	0.90	ns
CS_Hypo_Epi	2.31	*	7.97	**	0.96	ns
CS_Epi	1.97	†	27.12	***	1.46	ns
CS_Mid	1.97	†	27.12	***	1.46	ns
LA	1.72	ns	21.12	***	0.81	ns

Table 2-10. ANOVA table of anatomical phenotypes and the *F* values and associated *P* values of the effect of phosphorus and genotype in mesocosm-grown maize (*Zea mays*) of the mesocosm experiment with inbreds of 2015 MC-15. ***$P < 0.001$; ** $0.001 \leq P < 0.01$;* $0.01 \leq P \leq 0.05$; †$0.05 < P \leq 0.1$; ns not significant. RXSA: root cross-section area, TCA: total cortical area, TSA: total stele area, C:S: ratio cortex to stele, C:XS: ratio cortex to cross-section, perAA: percent of the cortex that is aerenchyma area, AA: aerenchyma area, CCFN: cortical cell file number, LCA: living cortical area, perLCA: percent of cortex that is living cortical area, perXSisLCA: percent of cross section that is living cortical area, CCN: cortical cell number, CCS: cortical cell size, CS_Hypo_Epi: median of size of cells in epidermis and hypodermis, CS_Mid: median of size of cells in middle layers of cortex, CS_clostoEndo: median of size of cells close to endodermis; LA: lacunae area.

Factor	Genotype		Phosphorus		Genotype:P	
RXSA	10.35	***	118.34	***	4.17	**
TCA	10.15	***	107.92	***	4.34	**
TSA	8.97	***	114.76	***	2.09	*
C:S	5.59	***	1.02	ns	1.02	ns
C:XS	5.73	***	0.77	ns	1.00	ns
AA	5.39	***	0.16	ns	1.41	ns
perAA	3.74	**	12.14	**	3.07	*
CCFN	5.97	***	7.14	*	1.12	ns
LCA	5.13	***	132.54	***	3.80	*
perLCA	2.93	**	5.29	*	1.16	ns
perXSisLCA	2.91	*	4.10	*	0.95	ns
CCS	3.01	**	11.36	**	1.81	†
CCN	11.57	***	10.49	**	2.00	†
CS_Hypo_Epi	2.63	*	14.53	***	1.38	ns
CS_Mid	3.34	**	6.20	*	1.42	ns
CS_closetoEndo	0.94	ns	18.61	***	1.08	ns
LA	0.57	ns	0.91	ns	1.16	ns

Chapter 3 Influence of root cortical aerenchyma on the rhizosphere microbiome of field-grown maize

Abstract

Root cortical aerenchyma (RCA) decreases the metabolic cost of soil exploration and improves plant growth under drought and low soil fertility. RCA may also change the microenvironment of rhizosphere microorganisms by transporting air or possibly, by reducing carbon rhizodeposition in the rhizosphere. We tested the hypothesis that plants with contrasting levels of RCA have different rhizosphere communities. Maize inbreds were grown under low and high nitrogen regimes and their rhizosphere soil sampled at flowering in Limpopo Province ,South Africa and Pennsylvania, USA. The rhizosphere bacterial diversity of plants with contrasting levels of RCA was characterized by sequencing 16s rRNA genes. Geographic location was the most important factor determining the composition of the rhizosphere bacterial communities. In both sites root phenotype grouped the diversity of bacterial communities better than genotype. Although other root anatomical and architectural phenotypes were studied as possible cofactors affecting the variation of the bacterial diversity, RCA was among the significantly explanatory variables for the composition of the bacterial communities in the South African site and was neutral in the site in Pennsylvania. High-RCA rhizospheres harbored significantly enriched and depleted bacterial species compared to low-RCA plants at the two sites. Potential metabolisms were related to a positive effect of RCA on oxygen and a negative effect of RCA on carbon rhizodeposition in the rhizosphere. Our results are consistent with the hypothesis that root phenotypes are important drivers of rhizosphere microbial communities.

Introduction

Root-associated microbes alter plant nutrition and plant health, becoming a key aspect of root biology for the development of sustainable agriculture. Factors such as soil type, geographic location, agronomic practices and plant species and genotype are well-known modifiers of rhizosphere bacterial communities as demonstrated by metagenomic analyses (Philippot *et al.*, 2013). Despite the fact that roots create and structure the niches of rhizosphere communities, the effects of specific root phenotypes on bacterial communities are unknown. Promising root phenotypes that improve soil resource acquisition can be targeted by plant breeding programs to produce new cultivars suited for the challenges of modern agriculture (Lynch, 2015). However, selection for such phenotypes should not compromise beneficial microbial associations in the rhizosphere in order to meet the requirements of sustainable crop production. This is especially true for nitrogen, since bacterial transformations play key roles in regulating nitrogen availability in the rhizosphere by means of nitrogen fixation (Dobbelaere *et al.*, 2003), ammonification, nitrification and denitrification (Hai *et al.*, 2009; Hinsinger *et al.*, 2009; Li *et al.*, 2014; Zhao *et al.*, 2017). Therefore, understanding the effects of promising root phenotypes on the microbial communities under nitrogen limitation an important element of breeding crops with reduced requirements for N fertilizer.

Nitrogen fertilization is a primary economic, environmental, and energy cost of intensive maize production (Robertson & Vitousek, 2009; FAO, 2017). Only 33% of the nitrogen applied to cereal crops is recovered as grain, the rest, which remains as vegetative biomass or is lost to the environment, accounts for approximately $15.9 billion annual loss (Raun & Johnson, 1999). Microbial transformation in the rhizosphere may represent avenues to improve nitrogen acquisition by plant roots. For example, nitrogen fixation in the rhizosphere may account for up to 20-25% of the nitrogen assimilated by the rice plants (Kennedy *et al.*, 2004). Rhizosphere nitrification (the conversion of ammonia to nitrate), and denitrification (the reduction of nitrate to

nitrogen oxides and N_2) surpasses the bulk soil by 1.5-2.5 times (Højberg *et al.*, 1996). However, the balance of nitrification and denitrification is extremely sensitive to changes in oxygen concentration, pH, and the availability of organic carbon and water (Neumann & Römheld, 2012). A complex microbial network participates in the nitrogen cycle in the rhizosphere, with the predominant processes depending on the microhabitats created by roots, which are in large measure determined by the root morphology, architecture, anatomy and localization of exudates and carbon rhizodeposition.

One strategy to help ameliorate excessive use of nitrogen fertilizers and the loss of nitrogen in maize fields is the selection of cultivars with specific root phene states (phenes are the elements composing a phenotype (York *et al.*, 2013)) that improve nitrogen capture (Gaudin *et al.*, 2011; Lynch, 2013; Lynch, 2015; Lammerts van Bueren & Struik, 2017). Increased metaxylem vessel number in nodal roots and increased aerenchyma formation have also been reported as responses of maize to low nitrogen stress (Gao *et al.*, 2015; York *et al.*, 2015). Phene states such as steep rooting angle (Trachsel *et al.*, 2013), reduced lateral root density (Zhan & Lynch, 2015), fewer nodal roots (Saengwilai *et al.*, 2014b), and increased root cortical aerenchyma (Saengwilai *et al.*, 2014a) have been associated with increased grain yield under nitrogen stress. Maize roots with reduced cortical cell file number and increased cortical cell size have improved nitrogen capture (Yang, 2018). Under low nitrogen regimes maize has fewer nodal roots (Gaudin *et al.*, 2011; York *et al.*, 2015), decreased nodal root diameter, and increased nodal root elongation, as well as increased lateral root density and decreased root hair length and density (Gaudin *et al.*, 2011; Gao *et al.*, 2015). Together, these results are in accord with the concept that efficient maize root systems have phene states that reduce the metabolic cost of soil exploration (e.g. increased aerenchyma, fewer nodal roots, and fewer lateral roots) and improved soil foraging (e.g. deep rooting depth), especially under resource scarcity, and indicate that plant

breeding programs could deploy these phenes to develop maize cultivars better adapted to low nitrogen stress (Lynch, 2013).

Root architectural and anatomical phenotypes may change the conditions of the microsites inhabited by rhizosphere microbes. Root exudates (Zhalnina *et al.*, 2018) and oxygen availability have important effects on the composition and function of rhizosphere bacteria (Hinsinger *et al.*, 2009). Although the effect of root architecture on the production of root exudates is poorly understood (Walker *et al.*, 2003), it is logical that deep-rooting maize genotypes would allocate more exudates to deeper soil domains given that root exudates are considered to be produced in larger amounts (although not uniquely) behind the root tips (Badri & Vivanco, 2009). Root exudates produced in deep soil strata would encounter a more hypoxic rhizosphere compared to shallow-rooting genotypes, because oxygen concentration decreases with depth in the soil profile (Lynch & Wojciechowski, 2015). Roots with comparatively less lateral root density may also produce less exudates and therefore decreased capacity to sustain bacterial communities. Anatomical phenes may modify the responses of microbes to the conditions imposed by architectural root phenes. The production of aerenchyma has major impacts on the rhizosphere by changing the oxygen content of the rhizosphere and shifting facultative or anaerobic bacterial functions towards aerobic metabolisms in the vicinities of aerenchyma air pockets (Risgaard-Petersen & Jensen, 1997; Arth & Frenzel, 2000; Li *et al.*, 2008). Processes like carbon utilization, nitrogen transformation, and metal accumulation depend on soil oxygen content and redox potential (Neumann & Römheld, 2012), and may modify bacterial communities in the rhizosphere. For example, when rice shoots were clipped and O_2 and N_2 were no longer transported to the rhizosphere by means of aerenchyma channels, nitrification and denitrification were significantly decreased in planted rice soils (Arth & Frenzel, 2000). Also, a rice genotype producing greater root aerenchyma had increased nitrification activity, nitrate concentration and abundance of ammonia oxidizing bacteria in the rhizosphere compared to a

genotype with decreased aerenchyma formation (Li *et al.*, 2008). These results were in accord with the stimulatory effects of aerenchymatous roots of the aquatic plant *Lobelia dortmanna* on rhizosphere nitrification (Risgaard-Petersen & Jensen, 1997). Likewise, roots with an impermeable epidermis or reduced aerenchyma may restrict oxygen diffusion to the rhizosphere, thereby limiting aerobic bacterial metabolism and nutrient utilization.

Previous studies have analyzed the bacterial composition of the rhizosphere using high-throughput amplicon sequencing of agriculturally relevant plants such as rice (Edwards *et al.*, 2015), sugarcane (Yeoh *et al.*, 2016), wheat (Hartman *et al.*, 2018), clover (*Trifolium pretense*) (Hartman *et al.*, 2017), grape (Zarraonaindia *et al.*, 2015), *Arabidopsis thaliana* (Bulgarelli *et al.*, 2012; Lundberg *et al.*, 2012), and maize (Dohrmann *et al.*, 2013; Peiffer *et al.*, 2013; Li *et al.*, 2014; Bakker *et al.*, 2015), finding effects of planting site, soil properties, bulk soil microbial communities, root compartmentalization (bulk soil and rhizosphere vs. endosphere and rhizoplane), agronomic management, and nitrogen fertilization in the microbiome composition. To our knowledge, no high-throughput amplicon sequencing studies of the rhizosphere have considered the root phenotype as a possible source of variation. The study of phenotypic effects on the rhizosphere microbiome under low nutrient stress is important to inform plant breeding programs targeting root phenes and better root microbiomes in the context of sustainable agriculture. This study addressed the effects of root phenotypes on the composition of rhizosphere bacterial communities of maize under optimal and suboptimal nitrogen supply in field conditions. Using high throughput sequencing of 16S rRNA genes of total rhizosphere DNA, combined with root phenotyping of the same plants from two experimental maize fields, we tested the hypothesis that root anatomical and architectural phenes have significant effects on the bacterial community composition. We further looked for phenotype-specific bacterial groups for contrasting RCA expression and analyzed possible functional groups of bacteria that may be relevant for nutrient acquisition with the specific RCA phenotypes.

Methods

Field experiment and sampling

Experimental conditions and plant material. Two experiments were conducted, one at the Russell E. Larson Research and Education Center of the Pennsylvania State University in Rock Springs, PA, USA (designated herein as **RS**) (40°42′37″.52 N, 77°57′07″.54 W, 366 masl), from June – August 2012; the other at The Ukulima Root Biology Research Center (designated herein as **URBC**), Limpopo province, Republic of South Africa (24°33′00.12 S, 28°07′25.84 E, 1235 masl) from December 2013 to February 2014. Recombinant inbred maize lines (RILs) differing in aerenchyma (RCA) formation from the IBM population (B73 x Mo17) (URBC High-RCA: IBM031, IBM196; URBC Low-RCA: IBM001, IBM345; RS High-RCA: IBM031, IBM034, IBM177, RS-Low: IBM001, IBM157, IBM338) (Senior *et al.*, 1996; Kaeppler *et al.*, 2000) were planted in three row-plots with 0.76 m inter-row spacing and 0.23 m in-row spacing for a final population of 57,278 plants*ha^{-1}. The soil at the experimental sites consisted of a Hagerstown silt loam (fine, mixed, semiactive, mesic Typic Hapludalf) at RS and a clovelly loamy sand (Typic Ustipsamment) at URBC. Soil test reports from the two sites are summarized in Table 3-4. Contrasting levels of nitrogen fertilization were imposed at the two sites according to soil analyses at the beginning of the field season in order to provide low N (no application of nitrogen fertilization and residual nitrogen soil concentration of 19.5 kg ha^{-1} at RS, and 33 kg*ha^{-1} applied at URBC) treatment to half of the blocks and high N conditions (fertilized with 207 kg*ha^{-1} at URBC, and 150 kg*ha^{-1} at RS) to the other half. At RS, each block was a 0.4 ha separate field and at URBC the blocks were randomly distributed in a 20 ha irrigation pivot. In both locations, all nutrients except nitrogen were adjusted to meet the requirements for maize production as determined by soil tests. Pest control and irrigation were carried out as needed. The RS experiment was a complete randomized block design and the URBC experiment was a split-plot design with nitrogen level as the main plot with genotypes completely randomized into each

main plot. The experiment at RS had three replicates for high nitrogen and one replicate for low nitrogen, and the experiment at URBC had four replicates; all replicates were designated as blocks.

Rhizosphere soil sampling. Two plants per genotype were excavated from the central row at flowering (12 weeks after planting at RS and 13 weeks after planting at URBC) with a shovel inserted approximately 40 cm radial distance from the stem, and 30 cm depth. The root systems were processed similar to Lundberg *et al.* (2012) with some modifications in order to scale the method to maize and field studies. Briefly, the complete plants were excavated, kept in paper bags and immediately transported to the sample processing station, adjacent to the field. The root crowns were carefully shaken and ten nodal roots (two to three root segments per whorl, from the second to the fifth whorl) per plant were aseptically clipped and placed into 250 mL sterile plastic bags. A total of 20 root fragments (~40 g fresh weight) per plot were collected. The samples were kept at 4°C for maximum 24 h, and the rhizosphere soil collected in 150 mL of a 20% sterile Tween®20 solution (Amresco, Inc., Solon, OH, USA) poured into the plastic bag. Each closed plastic bag containing roots, soil and tween solution was manually and shaken for 1 min. Then, the solution with the released soil was filtered with nylon cell strainers (MACS® SmartStrainers, 100 µm), and the filtrate centrifuged at 3,000 g for 15 min. The soil pellet was immediately processed for DNA extraction for RS, and stored at -20°C for 24 h and then placed at -70°C. For the URBC samples, the soil pellet was frozen (-70°C) for 3 h prior to 48 h lyophilizing to constant weight. Three samples of bulk soil were taken per plot using a corer of 5.1 cm diameter inserted 20 cm depth in locations free of plant roots in the furrow pooled (all the samples coming from the different genotypes, collected in the same field replicate), and ~ 10 g diluted in tween solution and filtered through nylon cell strainers and the filtrate processed as described for rhizosphere soil samples. The lyophilized soil samples were aseptically stored in 2 ml vials at 4°C for 2 weeks and transported to the USA for DNA processing.

Sampling for root phenotyping. Three plants per plot were excavated and sampled for anatomical analysis as previously described (York *et al.*, 2015). These plants were different to the plants used for DNA extraction with the purpose of avoiding changes in root anatomy due to the DNA extraction processing on the roots used for rhizosphere soil collection. At URBC, two of the three plants selected for anatomical sampling were also used for architecture phenotyping with "DIRT" (Bucksch *et al.*, 2014); washed root crowns were imaged on a table with black background using a Nikon D70s digital camera with focal length ranging 22 – 29 mm, exposure time of 1/30 – 1/50 sec., maximal aperture of 3.6 – 4.1, and digital zoom only. The camera was mounted on a tripod at 50 cm above the imaging board. All the images were taken at a resolution of 3,008 x 2,000 pixels.

DNA extraction

Soil samples weighing 0.25 g of either of centrifuged rhizosphere soil (at RS) or lyophilized soil (at URBC) were processed with the PowerLyzer Power Soil DNA Kit extraction (MoBio Laboratories, Inc., Carlsbad, CA). Concentration and quality (260/280 and 230/260 absorbance ratios) were measured with a NanoDrop 1000 Spectrophotometer (Thermo Fisher Scientific Inc.). Integrity of the extracted DNA was confirmed (> 10 kb) in 0.8% agarose electrophoresis gels (110V for 1.5 h) by comparison of the extracted DNA stained with ethidium bromide with a molecular weight marker (2-Log DNA ladder, New England Biolabs® Inc.). The DNA samples were stored at -70 °C (18 months for RS and a week for URBC). Double-stranded DNA concentration was measured by fluorescence with a SPECTRAmax GEMINI-XPS microplate reader (Molecular devices, Sunnyvale, CA, USA) and with picogreen nucleic acid stain.

16S rRNA amplification and sequencing

DNA concentrations were normalized to 1 – 5 ng μl^{-1}, and used for triplicate polymerase chain reactions (PCRs) with the 515F-806R primer pair including barcodes as previously

described (Caporaso *et al.*, 2012). PCR conditions and product purification were as follows: one denaturation cycle at 94°C for 3 min followed by 30 annealing cycles (95°C for 30 sec, 52°C for 45 sec, and 72°C for 90 sec); and an extension cycle at 72°C for 12 min, and hold at 4°C in a MyCycler thermal cycler (Bio-Rad, Hercules, CA, USA). PCR products of the three reactions were pooled into a single sample, purified with 0.1% carboxyl-modified Sera-Mag Magnetic Speed-beads^{TM} (Fisher), and eluted in 1x TE for quantification. Concentrations of the purified PCR products of individual samples were determined by fluorescence with a SPECTRAmax GEMINI-XPS microplate reader (Molecular devices, Sunnyvale, CA, USA). The quality was assessed via a 2100 Bionalyzer (Agilent Technologies, Wilmington, USA). The samples were then pooled into a 25 ng*μL^{-1} (57.7 nM) library. Number of Illumina-amplifiable DNA fragments in the library were 2nM, determined by qPCR with the KAPA kit (Biosystems. Boston, MA, USA) and confirmed with a 2-point Qubit 2.0 fluorometer (Invitrogen). The library was denatured with 10 µL of 0.2N NaOH and diluted in a solution of denatured PhiX, for a final library concentration of 10 pM. Sequencing of the amplicons were performed in an Illumina MiSeq system (Illumina, San Diego, CA, USA) with 500 cycles.

Sequence analysis

The Illumina sequence data was demultiplexed, quality filters applied, dereplicated, and OTUs (Operational Taxonomic Units) assigned as previously described with the pipeline UPARSE with default options –Quality score of 16, OTU radius of 3%, and no length trimming- (Edgar, 2013). We used 97% similarity cutoff to assign biological identities to the OTUs by comparison against the database SILVA (Quast *et al.*, 2013). Non-classified OTUs at the domain levels (Bacteria or Archaea) and singleton sequences were discarded with Qiime (Caporaso *et al.*, 2010). Dataset preparation for downstream analysis including the taxonomy, OTU count table, phylogenetic tree and sample information was performed with the R package Phyloseq (McMurdie & Holmes, 2013; R Core Team, 2014).

Data analysis

OTU preprocessing. The obtained OTUs were analyzed by experiment separately. Low-count OTUs not seen more than 3 times in at least 20% of the samples were eliminated from the OTU table of each experiment. ***Species diversity.*** For diversity calculations one of the URBC samples with relatively low read-count (less than 10% of the second lowest read-count) and one sample with low OTUs (236 compared to 1115 OTUs in the second lowest OTU counts) at RS were dropped for further analyses. OTU tables were randomly subsampled without replacement (rarefied to even depth) in order to perform alpha diversity analyses with the "Shannon" diversity index. To study the beta diversity among samples, meaning the change in the number of bacterial OTUs per taxa of different samples or treatments, we used UniFrac distance metrics, which measures the relatedness of samples based on phylogenetic distance of their taxa (Lozupone *et al.*, 2010). Unweighted UniFrac distance takes into account the composition of each sample, while the weighted UniFrac accounts for the abundance of each taxa. Weighted and unweighted UniFrac distances on the rarefied OTU tables were used to perform principal coordinate analysis (PCoA), permutational multivariate analyses of variance (PERMANOVA), and constrained correspondence analyses (CCA). PCoA was used to observe patterns in sample aggregation by nitrogen levels, genotypes, rhizosphere versus bulk soil, and significant root phenotypes. PERMANOVAS revealed the effect of nitrogen and genotype on the bacterial communities, and CCA was used to measure the variation in rhizosphere bacterial communities explained by root phenes. Due to the high number of phenotypic variables resulting from *RootScan* and DIRT, we performed a selection of the most significant variables with random permutations with the function ordistep of the R package Vegan (Oksanen *et al.*, 2017). The resulting variables were then included in the model of the ordination. The significance of the model and of the phenes included in the model were calculated with permutation tests with the function anova.cca of the R package Vegan.

Phenotype-sensitive OTUs. Association of significantly enriched OTUs to contrasting root phenotypes were performed by fitting a generalized linear model with a negative binomial distribution to normalized abundance values. We used the "trimmed means of M" method for the normalization available through the BioConductor package edgeR (Robinson *et al.*, 2010; McCarthy *et al.*, 2012) and expressed the normalized counts as relative abundance counts per millions (CPM) for each OTU in each site and nitrogen level. To test for differential abundance we used a likelihood ratio tests (LRT) with the R package edgeR. OTUs with fold-change (compared to the control treatment, see results section for more details) p values < 0.01 were considered phenotype-responsive. To further explore potential functions of the phenotype-sensitive OTUs, we explored documented metabolism and ecology at the family and genus levels within available literature (File S1) and included hypothetical explanations in the discussion section of this work.

Plant phenotyping. The effect of root architectural and anatomical phene states on UniFrac distance metrics was assessed with the scale-transformed quantitative values of the measured phenotypes retrieved by *RootScan* and DIRT. The significant phenes were grouped into categorical states and assigned to each root sample for the PCoA as described above.

Results

Taxonomy and diversity

A total of 3,776,195 high quality sequences were obtained from the two experimental sites with a median read count per sample of 59,275 (range of 1,865 – 126,242). 17,693 microbial OTUs resulted from the alignment of the sequences with the SILVA dataset (Quast *et al.*, 2013). After low-count OTU removal the total sequences decreased from 1,323,562 to 1,220,568 at RS, and from 2,452,633 to 2,225,747 at URBC; and the total number of OTUs from 12,478 to 3,129 at Rocksprings and from 14,073 to 2,146 at URBC.

26 and 28 phyla were found at URBC and RS respectively. Proteobacteria, Acidobacteria, Actinobacteria, Verrucomicrobia, Bacteroidetes, and Firmicutes were among the most abundant phyla overall (Figure 3-1). Rhizosphere soil at the two sites had a greater proportion of Proteobacteria and Bacteroidetes, and smaller proportion of Acidobacteria and Nitrospirae than bulk soil. Gemmatimonadetes, Chloroflexi and Crenarchaeota were reduced in the rhizosphere at URBC but not at RS. The candidate phyla WPS-2 and TM7 were found only at URBC and Spirochaetes, and the candidate phyla FCPU426, SBR1093, and AD3 were unique to RS. Sphingomonadaceae (Phylum Proteobacteria) and Micrococcaceae (Phylum Actinobacteria) were the most abundant families at URBC, and Xanthomonadaceae and Burkholderiaceae (both from the phylum Proteobacteria) were at larger proportion in rhizosphere soil compared to bulk soil (Figure 3-8a). Xanthomonadaceae, Rhizobiaceae, Oxalobacteriaceae, and Burkholderiaceae were among the ten most abundant families at URBC but not among the ten most abundant families at RS. Hyphomicrobiaceae and Sphingomonadaceae (Phylum Proteobacteria) were the most abundant families at RS with Sphingomonadaceae slightly decreased in bulk soil samples at high nitrogen (Figure 3-8b). RS had higher OTU richness compared to URBC, and bulk soil had higher average species diversity than rhizosphere soil at URBC (Figure 3-2).

Nitrogen, genotype and rhizosphere effect on bacterial communities

Bacterial communities separated mainly by site (PCoA 1, Figure 3-3) although there was a remarkable overlap of the community structure of bulk soil at URBC with bulk and rhizosphere soil communities at RS. However, bulk soil samples aggregated apart from rhizosphere regardless of the nitrogen level at URBC and grouped by nitrogen levels at RS (Figure 3-9). Genotype was not a determinant grouping factor at either of the two locations (Figure 3-3, Figure 3-9). The results obtained with PCoA were confirmed by PERMANOVA analysis (Table 3-1) showing that neither genotype nor nitrogen were determinant grouping factors for the weighted UniFrac distances at URBC while nitrogen was a significant differentiating factor at RS. When the effect

of soil type (bulk and rhizosphere) was analyzed, there was a significant effect of soil type (rhizosphere vs. bulk soil) at the two sites (Table 3-5) but the percent of variation in beta diversity explained by soil type was over five times greater at URBC compared to RS. For the two experimental sites we found a significant block effect.

Effect of root phenes on bacterial communities

Contrasting aerenchyma phenotypes were found among the plants evaluated (Figure 3-4). Ranges and other descriptive statistics of the complete set of anatomical and architectural phenes measured are presented in Table 3-6 and Table 3-7. The effect of specific root phenes on rhizosphere bacterial communities depended on site. After controlling for nitrogen, genotype and block, we modeled the effect of quantitative phene measurements on the unweighted and weighted UniFrac distances of bacterial communities from rhizosphere samples using constrained correspondence analysis (CCA). Among the anatomical and architectural phenes measured at URBC (Table 3-2), root-cross section area (RXSA) was significant for the unweighted and the weighted UniFrac distances; aerenchyma area (AA), living cortical area (LCA), and rooting angle (BottomAngle) were among the significant phenes for the unweighted UniFrac distance, and rooting angle (D10) was significant for weighted UniFrac distance. Among the anatomical variables measured at RS (Table 3-3), root cross-section area (RXSA) was significant for the weighted UniFrac distance. No significant models (with p values < 0.1) were found for the unweighted UniFrac distance at RS. The significant phenes were converted into qualitative ranks in order to observe bacterial community separation among the different phene states (Table 3-8). The category “intermediate” was included in order to differentiate mid-points from the most contrasting phenotypes. Communities separated between contrasting (high and low) states of aerenchyma area (AA), living cortical aerenchyma (LCA) and between shallow and steep states of rooting angle at URBC (Figure 3-5) in agreement with the PERMANOVAs and CCA results. Other phenes that were significant according to the CCA at URBC (see Table 3-2) did not clearly

separate in the PCoA plots (results not shown). Nitrogen was the main factor separating the microbial communities at RS (see Figure 3-9) and no clear separation of the RS samples by phene states were found by the PCoAs ordination plots, even by exploring the phenes with significant effects according to the CCA (see Table 3-3, Figure 3-10). Aerenchyma area (AA) was selected to further study the phenotype effect on specific OTUs at the two experimental sites and is referred as **RCA** herein.

Phenotype-sensitive OTUs

High-RCA plants had specific sets of rhizosphere bacteria that were significantly enriched or depleted compared to low-RCA plants (Figure 3-6, Figure 3-11, Figure 3-12). At URBC high-RCA rhizospheres hosted a richer bacterial community than low-RCA rhizospheres as indicated by the ratio between significantly increased and decreased OTUs (nearly 3) under high and low nitrogen (Figure 3-6) and by the specific abundance values of OTUs by phylum and family (Figure 3-13 and Figure 3-14). When compared to bulk soil, rhizospheres of high-RCA plants had also a greater number of significantly enriched OTUs than low-RCA rhizospheres (Figure 3-11a), as well as a greater number of unique significantly enriched and decreased OTUs (Figure 3-11b). RCA phenotype had a weaker effect on the rhizosphere communities under high nitrogen at RS as there were fewer significantly enriched and depleted OTUs due to the RCA phenotype and the ratio between the two was almost 1 (Figure 3-6). The weaker rhizosphere effect at RS is also evident when contrasting RCA phenotypes were compared to bulk soil (Figure 3-12). Due to a lack of replicates, this analysis could not be done at RS under low nitrogen.

At URBC, RCA-sensitive OTUs from high RCA phenotypes shared some common features between high and low nitrogen. Significantly enriched bacteria at high-RCA under high nitrogen (as shown in Figure 3-6) belonged mainly to the phyla Proteobacteria (32%), Acidobacteria (27%), and Bacteroidetes (10%) and in minor proportions to the phyla Chloroflexi and Firmicutes (Figure 3-13a), similar to the distribution of the enriched OTUs in high-RCA

rhizospheres of low nitrogen plots with Proteobacteria (32% of the total enriched OTUs), Bacteroidetes (21%), and Acidobacteria (17%) and smaller proportions of Chloroflexi and Firmicutes (Figure 3-13b, File S1). At the family level, High-RCA plants of the two nitrogen levels have some families in common (although OTUs did not overlap) such as Chitinophagaceae, Cytophagaceae, Bacillaceae, Paenibacillaceae, Comamonadaceae, Gaiellaceae, Oxalobacteraceae and Xanthomonadaceae (Figure 3-14b).

There was greater diversity among the enriched OTUs of high-RCA plants at high nitrogen compared to low nitrogen at URBC. Enriched OTUs from the phyla Actinobacteria and Gemmatimonadetes in high-RCA plants were associated with high nitrogen, while an enrichment of OTUs from the phylum Armatimonadetes was associated with low nitrogen (Figure 3-13). Several families were unique to high-RCA plants at each nitrogen level (Figure 3-14). Among the OTUs with the greatest abundance at high-RCA in high nitrogen, the families Sphingomonadaceae, Moraxellaceae, and Nitrososphaeraceae, had the most abundant significantly enriched OTUs compared to low-RCA rhizospheres (Figure 3-14). The most abundant OTUs enriched at low-RCA and high nitrogen belonged to the families Comamonadaceae, Xanthomonadaceae and to the genus Caulobacter, all in the phylum Proteobacteria. With low nitrogen and high-RCA, Bradyrhizobiaceae had the most abundant OTUs. The families Chitinophagaceae, Cytophagaceae, Bacillaceae, Paenibacillaceae, Comamonadaceae, Gaiellaceae, Oxalobacteraceae and Xanthomonadaceae had OTUs that were shared between high and low nitrogen in high RCA plants, and that were among the most abundant and significantly enriched OTUs (Figure 3-14).

High-RCA rhizosphere of high-nitrogen plots at RS had 14 enriched OTUs which was 15% of the number of enriched OTUs of high-RCA plants and high nitrogen at URBC. There was one shared OTU between URBC and RS high-RCA and high-nitrogen samples (OTU 11202, an unclassified species of the family Xanthomonadaceae, Figure 3-6b). Enriched OTUs of high-

RCA in high nitrogen were distributed among Acidobacteria (28% of the total enriched OTUs), Actinobacteria (21%), and Planctomycetes (21%) and in smaller proportions among Firmicutes (14%), Bacteroidetes (7%), and Proteobacteria (7%) (Figure 3-13, File S1); whereas the enriched OTUs of low-RCA rhizospheres in high nitrogen had a contrasting distribution with Proteobacteria (38%), Bacteroidetes (22%) as dominant phyla followed by Acidobacteria (11%), Actinobacteria (11%) and Armatimonadetes (11%). The most abundant OTUs in RS at high nitrogen belonged to the family Koribacteraceae in high-RCA plants, and to the families Caulobacteraceae, Sphingomonadaceae, Chitinophagaceae, Xanthomonadaceae, and Comamonadaceae in low-RCA plants.

Discussion

In this study we tested the hypothesis that root phenotype in general and root cortical aerenchyma in particular influences the bacterial composoition of the rhizosphere in maize grown in the field in the USA and South Africa. Regardless of the nitrogen fertilization treatment, aerenchyma formation increased the rhizosphere bacterial richness under an intensively managed agricultural sandy soil in South Africa but had no significant effect on the rhizosphere bacterial richness in a finer-textured soil of Pennsylvania. We found rhizosphere bacterial OTUs that were sensitive to RCA, with reported metabolisms that could be hypothetically related to the increased oxygen and decreased carbon input in the rhizosphere of high-RCA plants. Our results indicate that root phenotypes may explain part of the variability in the rhizosphere bacterial composition and constitute a starting point to further study root phenotype effects on the root microbiome of agricultural species. A summary of our results and how they support our hypotheses is presented in Figure 3-7.

The dominant phyla Proteobacteria, Acidobacteria, Bacteroidetes and Actinobacteria found here overlap those reported among the dominant phyla in agricultural and rhizosphere soils (Lundberg *et al.*, 2012; Peiffer *et al.*, 2013; Sul *et al.*, 2013, and review by Philippot *et al.*, 2013). The stronger rhizosphere effect observed at URBC (South Africa) compared to RS (USA) could be explained by the differences in the soil properties and agricultural management of the two sites. The sandy, low organic matter soil at URBC offered a more restrictive environment for microbial growth compared to the more fertile silt-loam at RS (Table 3-4) as indicated by the smaller diversity at URBC versus RS (Figure 3-2). Additionally, crop rotations at RS in comparison with maize monoculture at URBC could have provided more diverse microbial communities at RS (Figure 3-2). Therefore, root phenotypes had a more significant impact on soil microorganisms at URBC, where soils had less organic matter content (<0.5%, Table 3-4) and were probably less structured given the loamy sand texture than at RS where the soil had greater

organic matter content (>0.9%) and a silt loam texture likely providing better structure. Better soil structure (e.g. more aggregates) creates more diverse microenvironments and greater microbial diversity (Sexstone *et al.*, 1985; Fierer, 2017). Likewise, greater organic matter content is associated with greater microbial biodiversity due to the more diverse carbon sources for microbial decomposition (Sul *et al.*, 2013). The effect of nitrogen on bacterial communities was significant only at RS (Figure 3-9), where soils retain some of the nitrogen in the epipedon compared to URBC where nitrogen is readily lost due to the leaching and limited organic. Despite the differences in rhizosphere effects between the two sites, it is noteworthy to find two enriched (Proteobacteria and Bacteroidetes) and two depleted (Acidobacteria and Nitrospirae) phyla in maize rhizospheres of the two sites and in accord with previous studies in which Proteobacteria and Bacteroidetes were enriched (Peiffer *et al.*, 2013; Bakker *et al.*, 2015) and Acidobacteria depleted in the rhizosphere soil (Fierer *et al.*, 2007; Peiffer *et al.*, 2013; Niu *et al.*, 2017). These common findings demonstrate the selectivity that maize roots exert on the soil microbial communities.

Our results support the hypothesis that root control of rhizosphere communities among plants of related genotypes is more associated with root phenotypes rather than with the genotypes themselves (Figure 3-5, Table 3-1). While the genotypic effect of related maize lines has shown modest or weak effects on rhizosphere bacterial communities in the present and in previous studies (Fang *et al.*, 2005; Dohrmann *et al.*, 2013; Peiffer *et al.*, 2013; Bakker *et al.*, 2015), no exploration of root phenotypes has been reported to our knowledge. Moreover, there appear to be root phenes or phene aggregates that are more important than others as drivers of the bacterial composition in the rhizosphere as shown by the CCA analysis - when controlling for nitrogen, genotype and block effects (Table 3-2 and Table 3-3). The root phenes shaping the rhizosphere communities varied by site, with root cross-section area (directly related to root diameter) significant for the UniFrac distance metrics at the two sites and other anatomical

phenes being important only at URBC. The link between root cross-section area, or root diameter, and microbial communities could result from the effect of root surface area, amounts of root exudates, modifications of the epidermis, or changes in the ratio cortex:stele that could affect the rhizosphere microenvironment. Thicker nodal roots could harbor more microorganisms on a larger surface area, produce more exudates per unit of root length, have thicker epidermis, or a different cortex:stele ratio compared to thinner roots. However, root diameter is a complex phene aggregate at the anatomical level of organization that has shown collinearity with other anatomical phenes (Burton *et al.*, 2015; Chimungu *et al.*, 2015). When exploring the PCoAs of the different classes of root cross-section area, we found no clear separation of the microbial communities at any site demonstrating the complex nature of the interaction between root cross-section area (or root diameter) and rhizosphere communities.

Root cortical aerenchyma separated the microbial communities at URBC, where there was a significant rhizosphere effect (Figure 3-5 and Table 3-5). Two possible mechanisms that could be further studied as factors affecting rhizosphere microbial diversity are the diffusion of oxygen from aerenchyma lacunae and the rhizodeposition of carbon as influenced by RCA. Greater oxygen concentration and possibly, differences in carbon rhizodeposition into the rhizosphere of the high-RCA plants may be associated with the three times greater number of significantly enriched OTUs observed in these phenotypes compared to low-RCA plants at URBC under high and low nitrogen (Figure 3-6 and Figure 3-7). Plants with increased RCA may have a reduced carbon rhizodeposition in axial roots as a consequence of the loss of cortical tissue; this effect may be intensified under low nitrogen given the overall low nitrogen content of the plant. However, it is also possible that under low nitrogen, plants with increased RCA have more carbon to invest in rhizodeposition compared to reduced RCA as an indirect consequence of the benefits of RCA on nitrogen acquisition under low nitrogen (Saengwilai *et al.*, 2014a).

Reduced cortical tissue of high-RCA plants reduces the metabolic burden of soil exploration and nutrient capture (Lynch, 2015).

Our results support the hypothesis that RCA formation alters the bacterial composition of the rhizosphere. We propose that the diversity associated with contrasting levels of aerenchyma may be associated with a diverse set of functions in the rhizosphere microbial community. We assigned functions reported in literature to some of the OTUs at each aerenchyma level (File S1) and build Figure 3-15 (for functions in the nitrogen cycle) and Figure 3-16 (for habitats, carbon metabolism and other relevant characteristics). Detailed descriptions of functional or ecological traits of the enriched bacterial OTUs at each aerenchyma level are presented as APPENDIX D. Aerenchyma had significant effects on the abundances of putative nitrogen transforming bacteria under high nitrogen at URBC (Figure 3-15). Ammonia oxidation, nitrate reduction and nitrogen fixation were among the reported functions of the significantly enriched taxa in high-RCA rhizospheres under high nitrogen (Figure 3-15, File S1). Noteworthy are the high abundances of the ammonia oxidizing archaean *Candidatus Nitrososphaerae* in high-RCA plants growing under high nitrogen at URBC. Enrichment of the archaean *amoA* genes (genes encoding for the ammonia monooxygenase) were previously found in a study with field-grown maize rhizosphere (Li *et al.*, 2014) in accordance with our findings. High abundances of *Nitrososphaerae* could cause a net decrease of ammonia in the rhizosphere, forcing other bacterial species or even the plant itself to invest reductive power in nitrate assimilation or could also promote nitrogen losses from the rhizosphere if the nitrate generated is ultimately converted into gaseous nitrogen (Stahl & Torre, 2012). The enrichment of *Nitrososphaerae* in high-RCA and high-N plants at URBC could indicate a low continuous supply of ammonium in accordance with previous research indicating that archaeal ammonia oxidizers prefer nitrogen-poor conditions (Hatzenpichler, 2012; Stahl & Torre, 2012; Sterngren *et al.*, 2015). However, since our analyses are merely taxonomic these hypotheses deserve further research.

Reported functions of the OTUs found in plants with contrasting aerenchyma phenotypes can be hypothetically associated with differences in carbon rhizodeposition or oxygen diffusion into these rhizospheres. Among the enriched bacterial families and genera in high-RCA plants at URBC there are several reported bacteria associated with plant growth promotion and disease suppressive soils with reported aerobic metabolism (Figure 3-16, File S1). Cellulose and macromolecules degradation, oligotrophy, disease suppression, and plant-growth promotion (Figure 3-16) were common characteristics of the enriched OTUs of high-RCA plants in the two nitrogen levels at URBC. Genera and families that were uniquely enriched at high nitrogen and high-RCA are known to participate in the degradation of macromolecules, amino acid, and organic matter (Figure 3-16). Families uniquely enriched in high-RCA under low nitrogen at URBC were cellulose and macromolecule degraders (Figure 3-16). In low-RCA plants at URBC, plant-growth-promoting bacteria were significantly enriched as in the high-RCA plants, but more significantly-enriched OTUs have, or are closely related to taxa with reported cellulolytic activity and utilization of other carbon compounds such as chitin, lignin, methylamine and pectin (File S1), which may be linked to an increased rhizosphere carbon deposition in fleshier root cortexes of the low-RCA plants. Low-RCA plants at URBC had some enriched facultative or even obligate anaerobes (e.g. Koribacteraceae) not present in high-RCA plants, which could be associated with shifts from aerobic to microaerophilic or anaerobic conditions due to the reduced oxygen diffusion to the rhizosphere or these plants compared to high-RCA plants. Although the differences in aerenchyma at RS had no significant effects on rhizosphere bacterial diversity (Table 3-3), we found a few uniquely enriched taxa with each phenotype (high and low-RCA) under high nitrogen (Figure 3-6), with the most abundant taxa being associated with disease suppressive soils or pathogen antagonists (File S1). Surprisingly, a species of the strictly anaerobe genus *Koribacteraceae* was enriched in the high-RCA rhizosphere at RS. This result corresponds to the weak phenotype effect of RCA on rhizosphere bacterial communities at RS where the

phenotype difference was decreased and where the rhizosphere effect was weaker compared to URBC. These hypotheses about the functional traits of the bacterial rhizosphere communities as they relate to root aerenchyma merit investigation.

Our results build on previous microbial surveys of maize rhizosphere by looking at the bacterial composition of the rhizosphere through the perspective of the root phenotype. Similar to our results, Proteobacteria and specifically, *Burkholderia* and *Sphingobium* were enriched, and Acidobacteria and Chloroflexi were depleted in rhizosphere of field-grown maize in the US (Peiffer *et al.*, 2013). The family Opitutaceae (phylum Verrucomicrobia) that has been regarded as oligotophs (Rodrigues & Isanapong, 2014) with preference of moderately recalcitrant carbon compounds (like xylan and pectin) provided in low concentration, was among the enriched phyla in the rhizosphere of high-RCA plants at URBC, indicating the possible delivery of such type of compounds in these rhizospheres. Also, similar to our results, Dohrmann *et al.* (2013) found that nitrifiers were slightly enriched in the rhizosphere of genetically modified Bt field-grown maize but they found bacteria (*Nitrosomonas* and *Nitrospira*) as opposed to the ammonia oxidizing archaeans *Candidatus Nitrososphaerae* found here. Dohrmann *et al.* (2013) suggested that their enrichment of nitrifying bacteria could be linked to a greater protein content in Bt maize due to the possible overexpression of Cry proteins. Since ammonia oxidizing archaeans outcompete ammonia oxidizing bacteria under lower ammonia concentration (Hatzenpichler, 2012), our results may correspond to nitrogen-poor rhizospheres of high-RCA plants.

The present study provides insights into the possible effects of root cortical aerenchyma on the rhizosphere bacterial communities of maize grown in two contrasting environments and give rise to interesting questions and hypotheses for future research (Figure 3-7). Aerenchyma-sensitive OTUs possibly reflect the microenvironment provided by the presence or lack of aerenchyma lacunae. The functional consequences of aerenchyma on microbial communities are beyond the scope of the present study but would greatly improve our understanding of the

interactions between root phenotypes and microbial nutrient transformations. Further research could be conducted to reveal more detailed effects exploring more root phenotypes and expanding to architectural phenes. Here, we found that together with aerenchyma, the phenes living cortical area and rooting angle had significant effects on the bacterial communities in the maize rhizosphere at URBC (Figure 3-5). Further exploration of these phenes by analyzing OTUs specific to phenotypes could be performed to improve the understanding of the phenotypes effects on the rhizosphere communities. The use of larger sets of genotypes as well as the study of the effects of phenotypes in combination with plant developmental stages will also add to our findings. Additionally, the inclusion of eukaryotes is crucial for the understanding of the effects of aerenchyma and other phenotypes on the fungal populations closely related to the root cortex.

The selection of plants targeting root ideotypes that improve soil exploration under low-nutrient and drought stress would be enormously benefited by a concomitant selection of beneficial microbiomes. This study is a pioneer in this endeavor by suggesting possible habitat changes provided by contrasting aerenchyma and the associated bacteria. Plant and microbiome breeding together could produce ideal combinations of roots and microbes adapted to resource scarcity to improve plant growth and productivity.

Acknowledgements

Dr. Eoin L. Brodie (Lawrence Berkeley National Lab, LBNL) provided the facility for DNA sequencing and reviewed the manuscript. Dr. Ulas Karaöz (LBNL) performed the UPARSE work of the raw sequences. Dr. Claudia Rojas Alvarado performed the work with Qiime and reviewed the manuscript. Dr. Kathleen M. Brown (Penn State University) critically reviewed the manuscript.

References

Arth I, Frenzel P. 2000. Nitrification and denitrification in the rhizosphere of rice: the detection of processes by a new multi-channel electrode. *Biology and Fertility of Soils* 31: 427-435.

Badri DV, Vivanco JM. 2009. Regulation and function of root exudates. *Plant, Cell & Environment* 32: 666-681.

Bakker MG, Chaparro JM, Manter DK, Vivanco JM. 2015. Impacts of bulk soil microbial community structure on rhizosphere microbiomes of *Zea mays*. *Plant and Soil* 392: 115-126.

Bucksch A, Burridge J, York LM, Das A, Nord E, Weitz JS, Lynch JP. 2014. Image-based high-throughput field phenotyping of crop roots. *Plant Physiology* 166: 470-486.

Bulgarelli D, Rott M, Schlaeppi K, Ver Loren van Themaat E, Ahmadinejad N, Assenza F, Rauf P, Huettel B, Reinhardt R, Schmelzer E, et al. 2012. Revealing structure and assembly cues for *Arabidopsis* root-inhabiting bacterial microbiota. *Nature* 488: 91-95.

Burton AL, Johnson J, Foerster J, Hanlon MT, Kaeppler SM, Lynch JP, Brown KM. 2015. QTL mapping and phenotypic variation of root anatomical traits in maize (*Zea mays* L.). *Theoretical and Applied Genetics* 128: 93-106.

Caporaso JG, Kuczynski J, Stombaugh J, Bittinger K, Bushman FD, Costello EK, Fierer N, Peña AG, Goodrich JK, Gordon JI, et al. 2010. QIIME allows analysis of high-throughput community sequencing data. *Nature Methods* 7: 335.

Caporaso JG, Lauber CL, Walters WA, Berg-Lyons D, Huntley J, Fierer N, Owens SM, Betley J, Fraser L, Bauer M, et al. 2012. Ultra-high-throughput microbial community analysis on the Illumina HiSeq and MiSeq platforms. *The Isme Journal* 6: 1621.

Chimungu JG, Loades KW, Lynch JP. 2015. Root anatomical phenes predict root penetration ability and biomechanical properties in maize (*Zea mays*). *Journal of Experimental Botany* 66: 3151-3162.

Dobbelaere S, Vanderleyden J, Okon Y. 2003. Plant Growth-Promoting effects of diazotrophs in the rhizosphere. *Critical Reviews in Plant Sciences* 22: 107-149.

Dohrmann AB, Küting M, Jünemann S, Jaenicke S, Schlüter A, Tebbe CC. 2013. Importance of rare taxa for bacterial diversity in the rhizosphere of Bt- and conventional maize varieties. *The Isme Journal* 7: 37-49.

Edgar RC. 2013. UPARSE: highly accurate OTU sequences from microbial amplicon reads. *Nature Methods* 10: 996-998.

Edwards J, Johnson C, Santos-Medellín C, Lurie E, Podishetty NK, Bhatnagar S, Eisen JA, Sundaresan V. 2015. Structure, variation, and assembly of the root-associated microbiomes of rice. *Proceedings of the National Academy of Sciences* 112: E911-E920.

Fang M, Kremer RJ, Motavalli PP, Davis G. 2005. Bacterial diversity in rhizospheres of nontransgenic and transgenic corn. *Applied and Environmental Microbiology* 71: 4132-4136.

FAO. 2017. World fertilizer trends and outlook to 2020: Food and Agriculture Organization of the United Nations.

Fierer N. 2017. Embracing the unknown: disentangling the complexities of the soil microbiome. *Nature Reviews Microbiology* 15: 579.

Fierer N, Bradford MA, Jackson RB. 2007. Toward an ecological classification of soil bacteria. *Ecology* 88: 1354-1364.

Gao KUN, Chen F, Yuan L, Zhang F, Mi G. 2015. A comprehensive analysis of root morphological changes and nitrogen allocation in maize in response to low nitrogen stress. *Plant, Cell & Environment* 38: 740-750.

Gaudin ACM, McClymont SA, Holmes BM, Lyons E, Raizada MN. 2011. Novel temporal, fine-scale and growth variation phenotypes in roots of adult-stage maize (*Zea mays* L.) in response to low nitrogen stress. *Plant, Cell & Environment* 34: 2122-2137.

Hai B, Diallo NH, Sall S, Haesler F, Schauss K, Bonzi M, Assigbetse K, Chotte J-L, Munch JC, Schloter M. 2009. Quantification of key genes steering the microbial nitrogen cycle in the rhizosphere of sorghum cultivars in tropical agroecosystems. *Applied and Environmental Microbiology* 75: 4993-5000.

Hartman K, van der Heijden MG, Roussely-Provent V, Walser J-C, Schlaeppi K. 2017. Deciphering composition and function of the root microbiome of a legume plant. *Microbiome* 5: 2.

Hartman K, van der Heijden MGA, Wittwer RA, Banerjee S, Walser J-C, Schlaeppi K. 2018. Cropping practices manipulate abundance patterns of root and soil microbiome members paving the way to smart farming. *Microbiome* 6: 14.

Hatzenpichler R. 2012. Diversity, physiology, and niche differentiation of ammonia-oxidizing archaea. *Applied and Environmental Microbiology* 78: 7501-7510.

Hinsinger P, Bengough AG, Vetterlein D, Young IM. 2009. Rhizosphere: biophysics, biogeochemistry and ecological relevance. *Plant and Soil* 321: 117-152.

Højberg O, Binnerup SJ, Sørensen J. 1996. Potential rates of ammonium oxidation, nitrite oxidation, nitrate reduction and denitrification in the young barley rhizosphere. *Soil Biology and Biochemistry* 28: 47-54.

Kaeppler SM, Parke JL, Mueller SM, Senior L, Stuber C, Tracy WF. 2000. Variation among maize inbred lines and detection of quantitative trait loci for growth at low phosphorus and responsiveness to arbuscular mycorrhizal fungi. *Crop Science* 40: 358-364.

Kennedy IR, Choudhury ATMA, Kecskés ML. 2004. Non-symbiotic bacterial diazotrophs in crop-farming systems: can their potential for plant growth promotion be better exploited? *Soil Biology and Biochemistry* 36: 1229-1244.

Lammerts van Bueren ET, Struik PC. 2017. Diverse concepts of breeding for nitrogen use efficiency. A review. *Agronomy for Sustainable Development* 37: 50.

Li X, Rui J, Xiong J, Li J, He Z, Zhou J, Yannarell AC, Mackie RI. 2014. Functional potential of soil microbial communities in the maize rhizosphere. *PLoS ONE* 9: e112609.

Li YL, Fan XR, Shen QR. 2008. The relationship between rhizosphere nitrification and nitrogen-use efficiency in rice plants. *Plant, Cell & Environment* 31: 73-85.

Lozupone C, Lladser ME, Knights D, Stombaugh J, Knight R. 2010. UniFrac: an effective distance metric for microbial community comparison. *The Isme Journal* 5: 169.

Lundberg DS, Lebeis SL, Paredes SH, Yourstone S, Gehring J, Malfatti S, Tremblay J, Engelbrektson A, Kunin V, Rio TGd, et al. 2012. Defining the core *Arabidopsis thaliana* root microbiome. *Nature* 488: 86-90.

Lynch JP. 2013. Steep, cheap and deep: an ideotype to optimize water and N acquisition by maize root systems. *Annals of Botany* 112: 347-357.

Lynch JP. 2015. Root phenes that reduce the metabolic costs of soil exploration: opportunities for 21st century agriculture. *Plant, Cell & Environment* 38: 1775-1784.

Lynch JP, Wojciechowski T. 2015. Opportunities and challenges in the subsoil: pathways to deeper rooted crops. *Journal of Experimental Botany* DOI: 10.1093/jxb/eru508

McCarthy DJ, Chen Y, Smyth GK. 2012. Differential expression analysis of multifactor RNA-Seq experiments with respect to biological variation. *Nucleic Acids Research* 40: 4288-4297.

McMurdie PJ, Holmes S. 2013. phyloseq: an R package for reproducible interactive analysis and graphics of microbiome census data. *PLoS ONE* 8: e61217.

Neumann G, Römheld V 2012. Chapter 14 - Rhizosphere Chemistry in Relation to Plant Nutrition A2 - Marschner, Petra. *Marschner's Mineral Nutrition of Higher Plants (Third Edition)*. San Diego: Academic Press, 347-368.

Niu B, Paulson JN, Zheng X, Kolter R. 2017. Simplified and representative bacterial community of maize roots. *Proceedings of the National Academy of Sciences* 114: E2450-E2459.

Oksanen J, Blanchet FG, Friendly M, Kindt R, Legendre P, McGlinn D, Minchin PR, O'Hara RB, Simpson GR, Solymos P, et al. 2017. *vegan: Community Ecology Package*. https://CRAN.R-project.org/package=vegan.

Peiffer JA, Spor A, Koren O, Jin Z, Tringe SG, Dangl JL, Buckler ES, Ley RE. 2013. Diversity and heritability of the maize rhizosphere microbiome under field conditions. *Proceedings of the National Academy of Sciences* 110: 6548-6553.

Philippot L, Raaijmakers JM, Lemanceau P, van der Putten WH. 2013. Going back to the roots: the microbial ecology of the rhizosphere. *Nature Reviews Microbiology* 11: 789-799.

Quast C, Pruesse E, Yilmaz P, Gerken J, Schweer T, Yarza P, Peplies J, Glöckner FO. 2013. The SILVA ribosomal RNA gene database project: improved data processing and web-based tools. *Nucleic Acids Research* 41: D590-D596.

R Core Team. 2014. *R: A language and environment for statistical computing*. Vienna, Austria: R Foundation for Statistical Computing. http://www.R-project.org/.

Raun WR, Johnson GV. 1999. Improving nitrogen use efficiency for cereal production. *Agronomy Journal* 91: 357-363.

Risgaard-Petersen N, Jensen K. 1997. Nitrification and denitrification in the rhizosphere of the aquatic macrophyte *Lobelia dortmanna* L. *Limnology and Oceanography* 42: 529-537.

Robertson GP, Vitousek PM. 2009. Nitrogen in agriculture: balancing the cost of an essential resource. *Annual Review of Environment and Resources* 34: 97-125.

Robinson MD, McCarthy DJ, Smyth GK. 2010. edgeR: a Bioconductor package for differential expression analysis of digital gene expression data. *Bioinformatics* 26: 139-140.

Rodrigues JLM, Isanapong J. 2014. The Family Opitutaceae. In: The Prokaryotes: Other Major Lineages of Bacteria and The Archaea (eds E. Rosenberg, E.F. DeLong, S. Lory, E. Stackebrandt, & F. Thompson), pp. 751-756. Springer Berlin Heidelberg, Berlin, Heidelberg.

Saengwilai P, Nord EA, Chimungu JG, Brown KM, Lynch JP. 2014a. Root cortical aerenchyma enhances nitrogen acquisition from low-nitrogen soils in maize. *Plant Physiology* DOI: 10.1104/pp.114.241711

Saengwilai P, Tian X, Lynch JP. 2014b. Low crown root number enhances nitrogen acquisition from low nitrogen soils in maize (*Zea mays* L.). *Plant Physiology* DOI: 10.1104/pp.113.232603

Senior M, Chin E, Lee M, Smith J, Stuber C. 1996. Simple sequence repeat markers developed from maize sequences found in the GENBANK database: map construction. *Crop Science* 36: 1676-1683.

Sexstone AJ, Revsbech NP, Parkin TB, Tiedje JM. 1985. Direct measurement of oxygen profiles and denitrification rates in soil aggregates1. *Soil Science Society of America Journal* 49: 645-651.

Stahl DA, Torre JRdl. 2012. Physiology and diversity of ammonia-oxidizing archaea. *Annual Review of Microbiology* 66: 83-101.

Sterngren AE, Hallin S, Bengtson P. 2015. Archaeal ammonia oxidizers dominate in numbers, but bacteria drive gross nitrification in n-amended grassland soil. *Frontiers in Microbiology* 6: 1350.

Sul WJ, Asuming-Brempong S, Wang Q, Tourlousse DM, Penton CR, Deng Y, Rodrigues JLM, Adiku SGK, Jones JW, Zhou J, et al. 2013. Tropical agricultural land

management influences on soil microbial communities through its effect on soil organic carbon. *Soil Biology and Biochemistry* 65: 33-38.

Trachsel S, Kaeppler SM, Brown KM, Lynch JP. 2013. Maize root growth angles become steeper under low N conditions. *Field Crops Research* 140: 18-31.

Walker TS, Bais HP, Grotewold E, Vivanco JM. 2003. Root exudation and rhizosphere biology. *Plant Physiology* 132: 44-51.

Yang X. 2018. *Enlarged cortical cells and reduced cortical cell file number improve maize growth under suboptimal nitrogen, phosphorus and potassium availability*. MSc thesis, The Pennsylvania State University, University Park, PA, USA.

Yeoh YK, Paungfoo-Lonhienne C, Dennis PG, Robinson N, Ragan MA, Schmidt S, Hugenholtz P. 2016. The core root microbiome of sugarcanes cultivated under varying nitrogen fertilizer application. *Environmental Microbiology* 18: 1338-1351.

York LM, Galindo-Castañeda T, Schussler JR, Lynch JP. 2015. Evolution of US maize (*Zea mays* L.) root architectural and anatomical phenes over the past 100 years corresponds to increased tolerance of nitrogen stress. *Journal of Experimental Botany* 66: 2347-2358.

York LM, Nord EA, Lynch JP. 2013. Integration of root phenes for soil resource acquisition. *Frontiers in Plant Science* 4: 355.

Zarraonaindia I, Owens SM, Weisenhorn P, West K, Hampton-Marcell J, Lax S, Bokulich NA, Mills DA, Martin G, Taghavi S. 2015. The soil microbiome influences grapevine-associated microbiota. *MBio* 6: e02527-02514. DOI:10.1128/mBio.02527-14.

Zhalnina K, Louie KB, Hao Z, Mansoori N, da Rocha UN, Shi S, Cho H, Karaoz U, Loqué D, Bowen BP, *et al*. 2018. Dynamic root exudate chemistry and microbial substrate preferences drive patterns in rhizosphere microbial community assembly. *Nature Microbiology* 3: 470-480.

Zhan A, Lynch JP. 2015. Reduced frequency of lateral root branching improves N capture from low-N soils in maize. *Journal of Experimental Botany* 66: 2055-2065.

Zhao M, Jones CM, Meijer J, Lundquist P-O, Fransson P, Carlsson G, Hallin S. 2017. Intercropping affects genetic potential for inorganic nitrogen cycling by root-associated microorganisms in *Medicago sativa* and *Dactylis glomerata*. *Applied Soil Ecology* 119: 260-266.

Figures and Tables

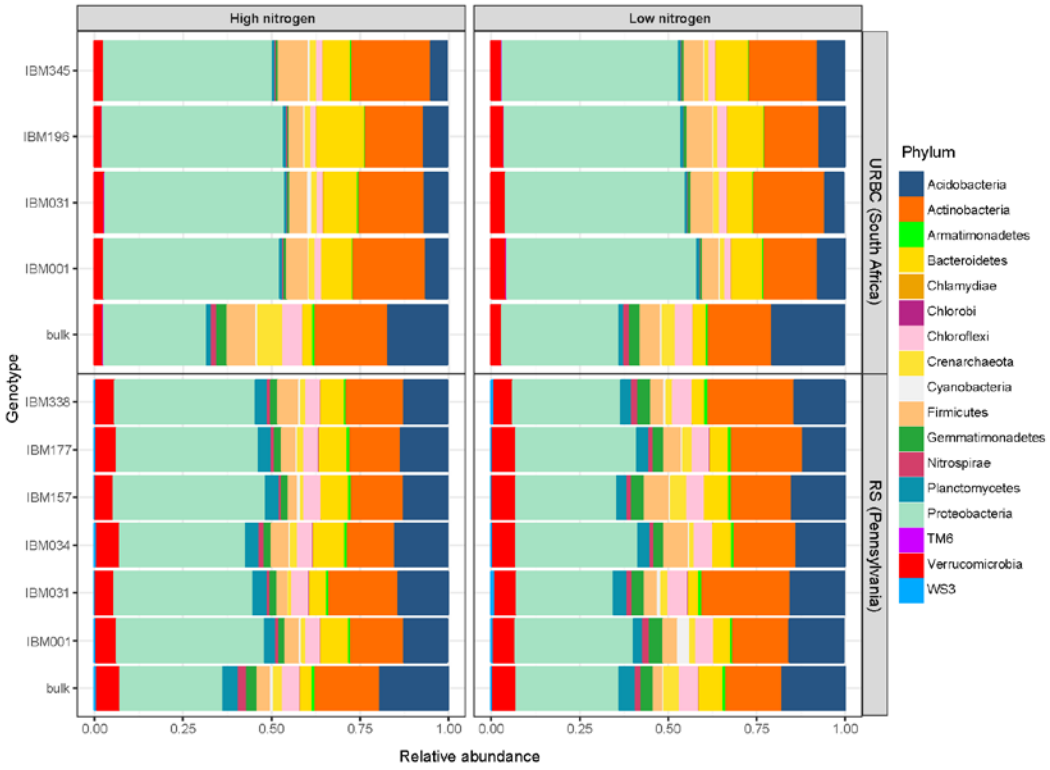

Figure 3-1. Bar plots of the relative abundances of the 15 most abundant phyla in each rhizosphere sample and bulk soil by experimental site (URBC and RS) under the respective nitrogen fertilization regimes. Values are means of four replicates at URBC, three replicates at RS, high nitrogen, and one replicate at RS, low nitrogen.

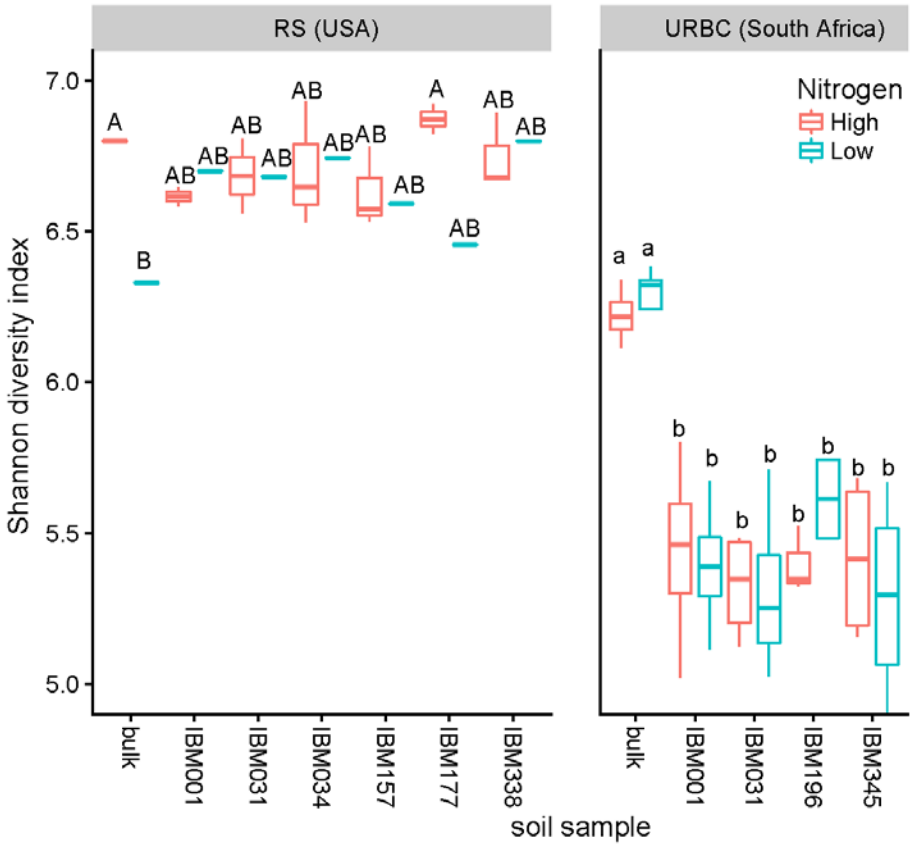

Figure 3-2. Alpha diversity of rhizosphere soil collected from all genotypes and bulk soil at the two sites under low nitrogen regimes. Horizontal box lines correspond to 25th, 50th, and 75th percentile; ranges are indicated by whiskers and points are outliers. For each boxplot n = 1-4. Boxes with the same letters indicate no significant differences in Shannon diversity indexes according to a LSD test with $p<0.05$.

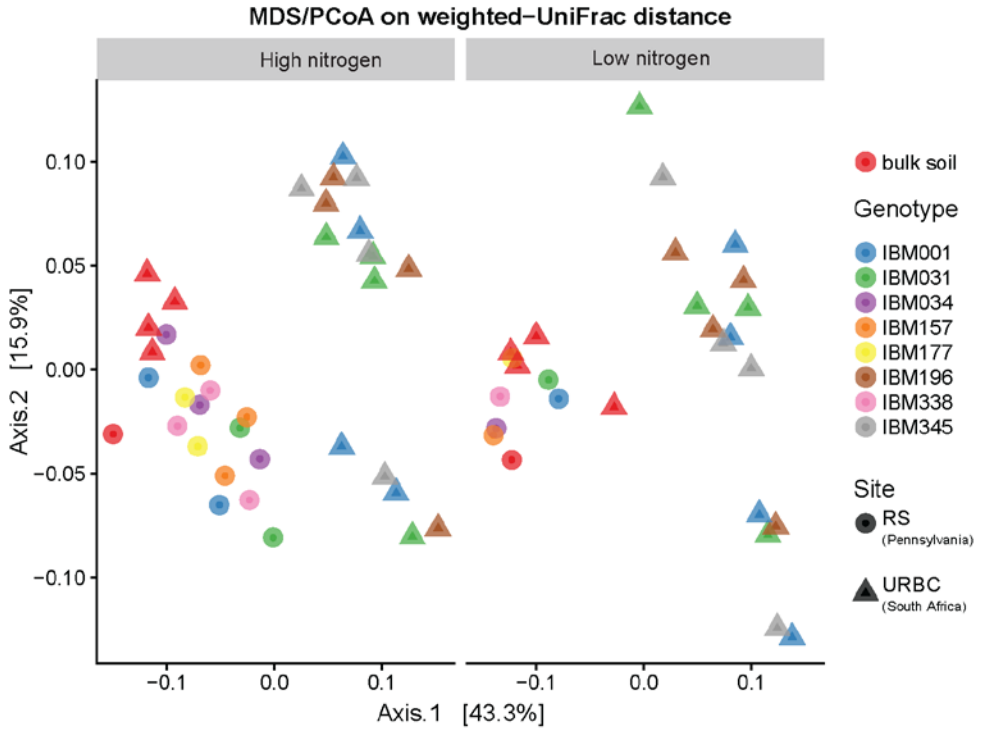

Figure 3-3. PCoAs using weighted UniFrac distances under low and high nitrogen.

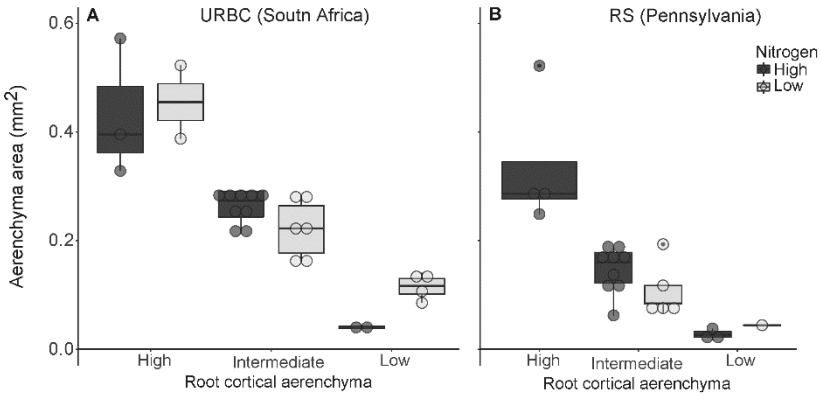

Figure 3-4. Phenotypic variation of the plants evaluated at A) URBC and B) RS and boxplots of measured aerenchyma area by phenotypic class under low and high nitrogen. Horizontal box lines correspond to 25th, 50th, and 75th percentile; ranges are indicated by whiskers and points out of the boxes are outliers. For each boxplot the data points are indicated in open circles.

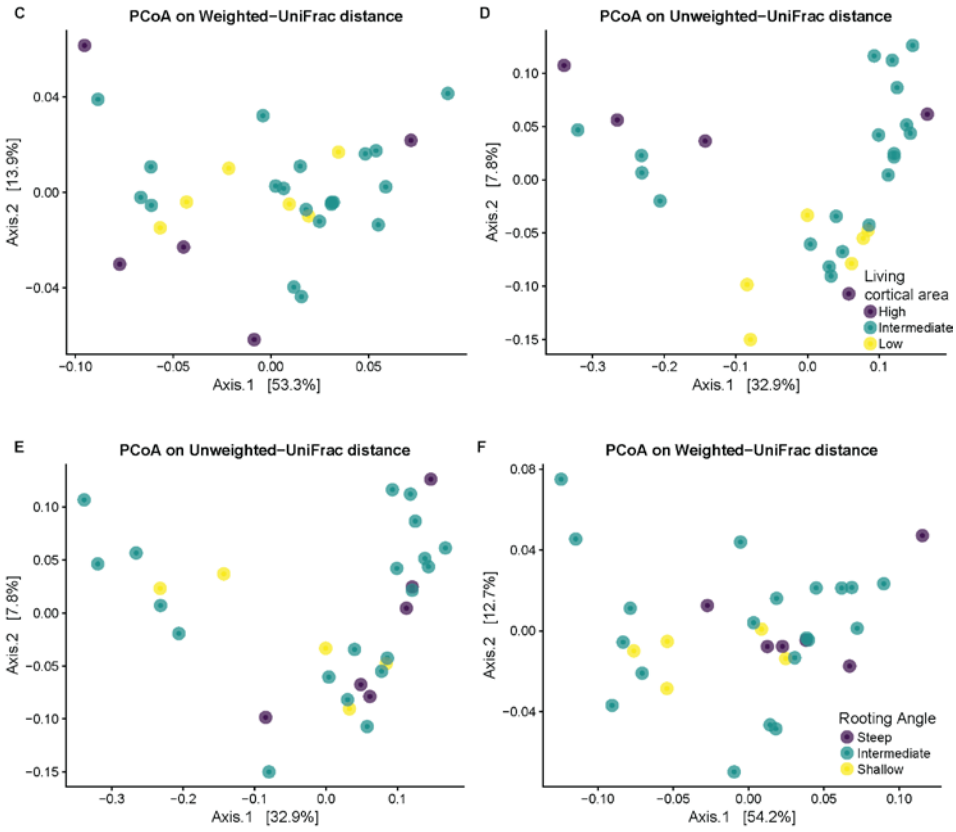

Figure 3-5. PCoAs using weighted and unweighted UniFrac distances indicate that bacterial rhizosphere communities at URBC (South Africa) separate by root phenotypes (A, B) aerenchyma area, (C, D) living cortical area and (E, D) rooting angle.

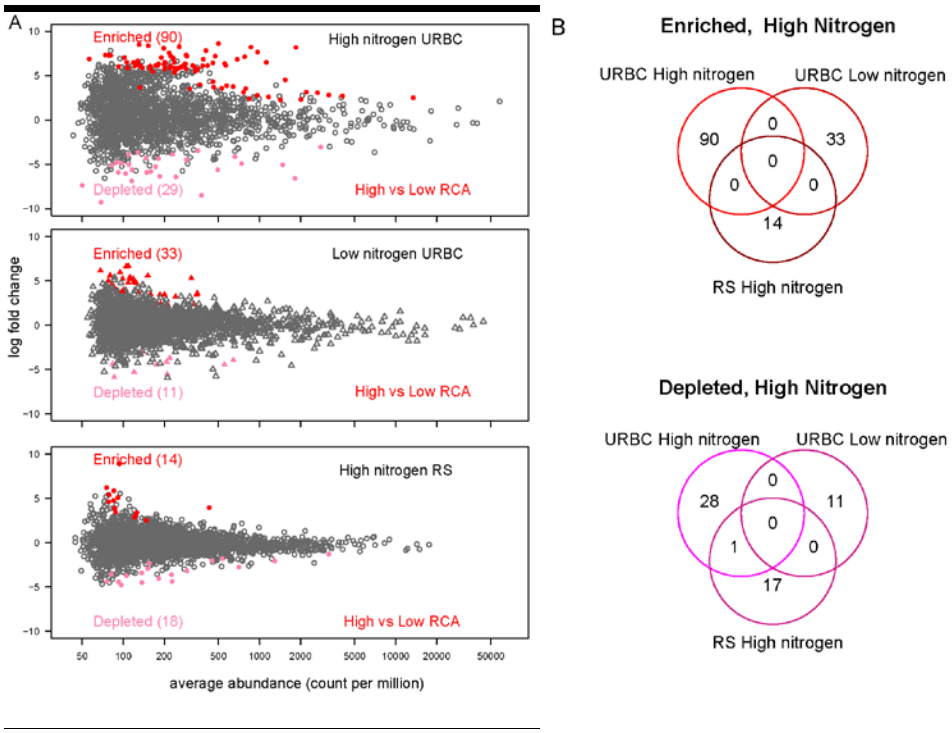

Figure 3-6. (A)Rhizosphere soil of high RCA plants was enriched or depleted for specific OTUs compared to rhizosphere soil of low RCA plants under high and low nitrogen at URBC and under high nitrogen at RS. Plots showing the abundance log change (y axis) of all the OTUs when rhizosphere and bulk soil were compared. Colored points indicate differentially enriched (red) and depleted (pink) OTUs according to a likelihood ratio test with $p<0.01$, and grey points were non-differentially abundant between the two types of samples, Number of OTUs significantly enriched or decreased at each condition are in parenthesis. (B) Number of the differentially enriched and depleted OTUs between each phenotype and nitrogen level at the two sites.

Nitrogen species sources

Fertilizers are sources of nitrate and ammonia when applied

Ammonia originated from root exudation, soil organic matter decomposition and nitrogen fixation

Nitrate from nitrification

Plant and microbe nitrogen uptake of ammonia preferable over nitrate

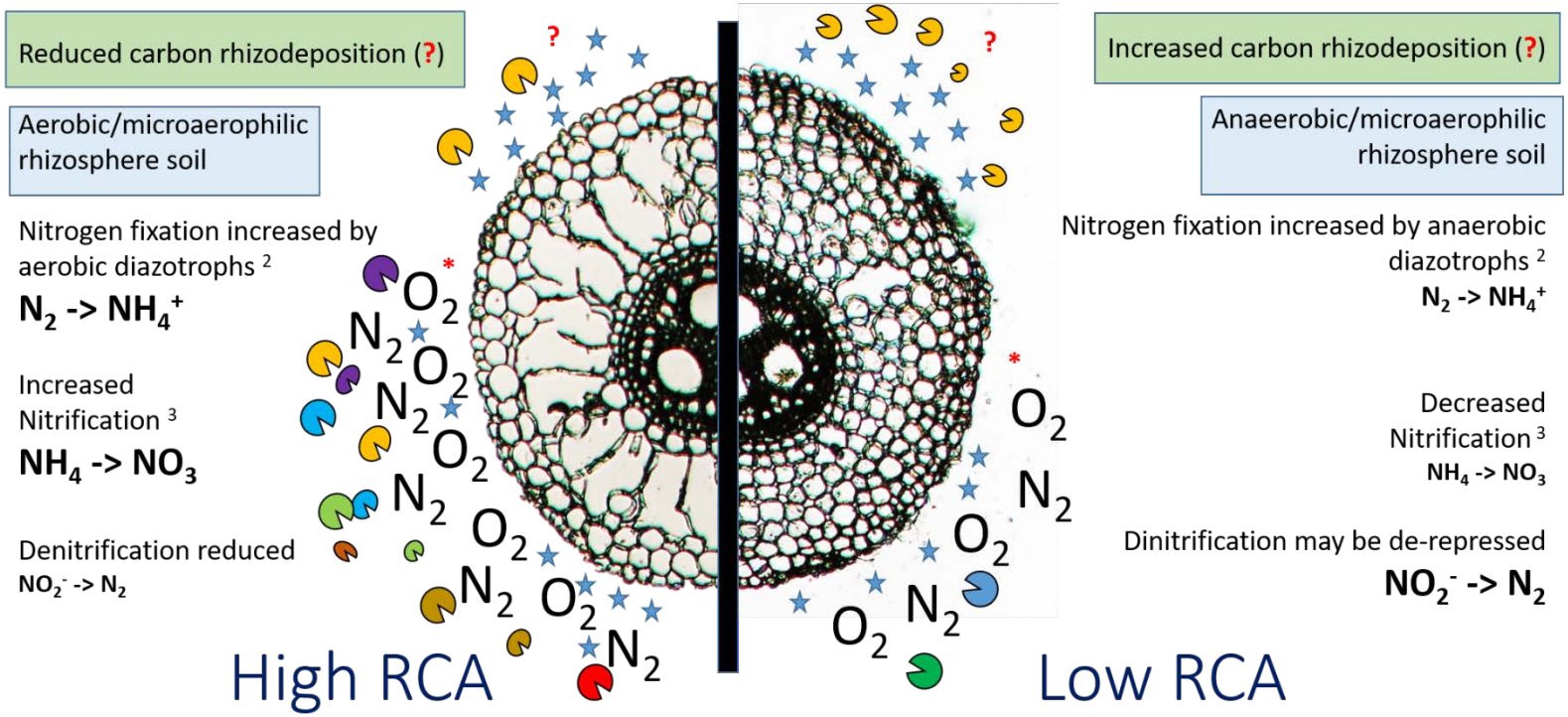

Figure 3-7. Hypotheses about changes in bacterial community diversity and abundance and nitrogen transformations in the rhizosphere of maize due to changes in root cortical aerenchyma (RCA). The green and blue squares represent central hypothesis of our work and may determine diversity and resource utilization in the rhizosphere. Carbon rhizodeposition is represented by stars; the number of stars is related to the hypothesized amount at each aerenchyma phenotype. Air is represented by the gaseous oxygen and nitrogen chemical formulas. The little pies represent bacterial communities and the colors represent the diversity, more colors, greater diversity, and the size and number represent the expected microbial biomass. * Hypothesis for which the present study is providing support. (?) Hypothetical statement, needs experimental support. [1](Arth and Frenzel, 2000; Li et al., 2008; Risgaard-Petersen and Jensen, 1997). [2](Kennedy et al., 2004). [3] (Arth and Frenzel, 2000; Risgaard-Petersen and Jensen, 1997).

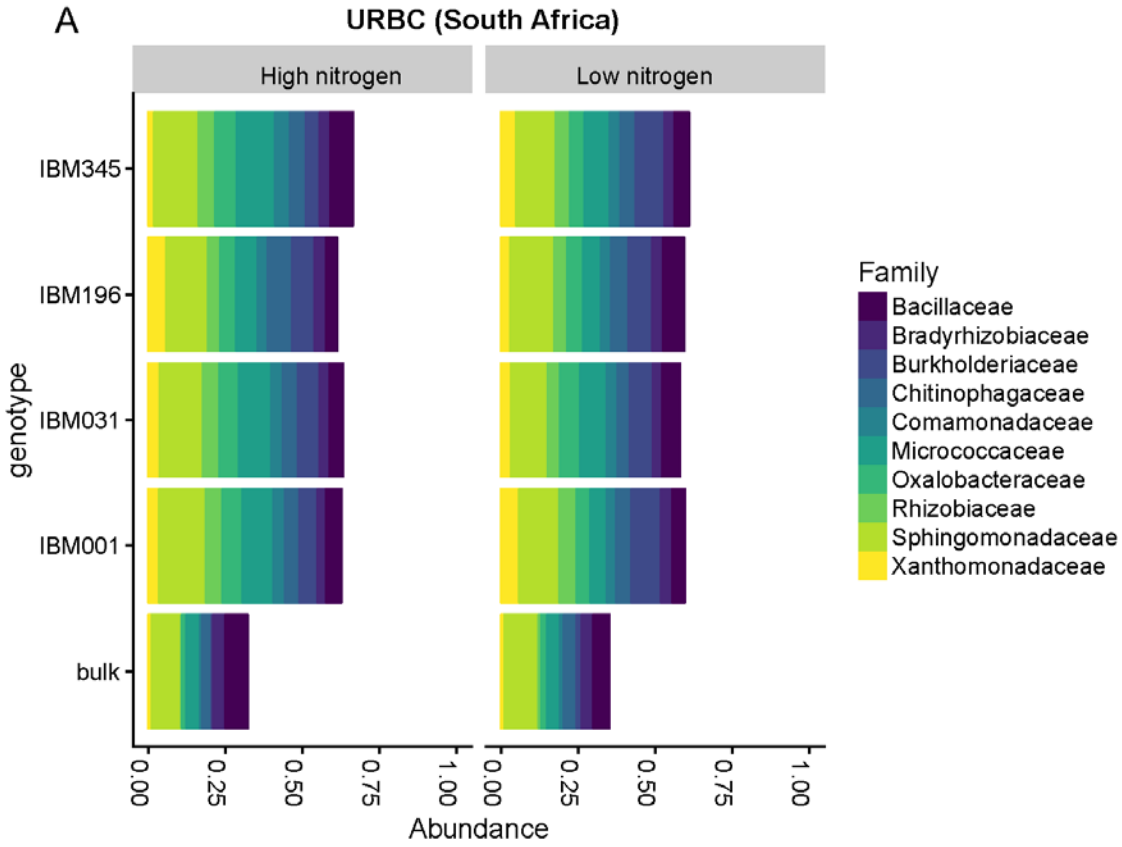
A
URBC (South Africa)
High nitrogen
Low nitrogen
genotype
IBM345
IBM196
IBM031
IBM001
bulk
0.00
0.25
0.50
0.75
1.00
Abundance
Family
Bacillaceae
Bradyrhizobiaceae
Burkholderiaceae
Chitinophagaceae
Comamonadaceae
Micrococcaceae
Oxalobacteraceae
Rhizobiaceae
Sphingomonadaceae
Xanthomonadaceae

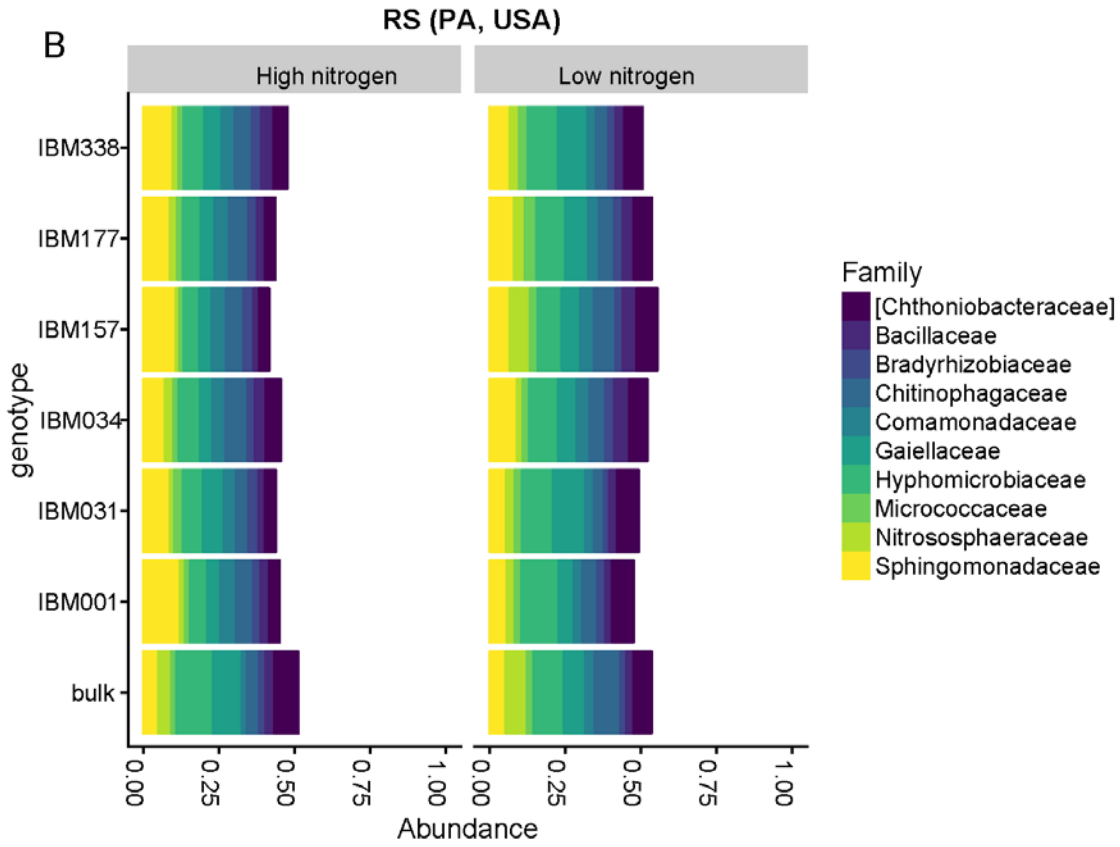

Figure 3-8. Bar plots of the relative abundances of the 10 most abundant families in each rhizosphere bulk soil sample by experimental site under contrasting nitrogen fertilization regimes.

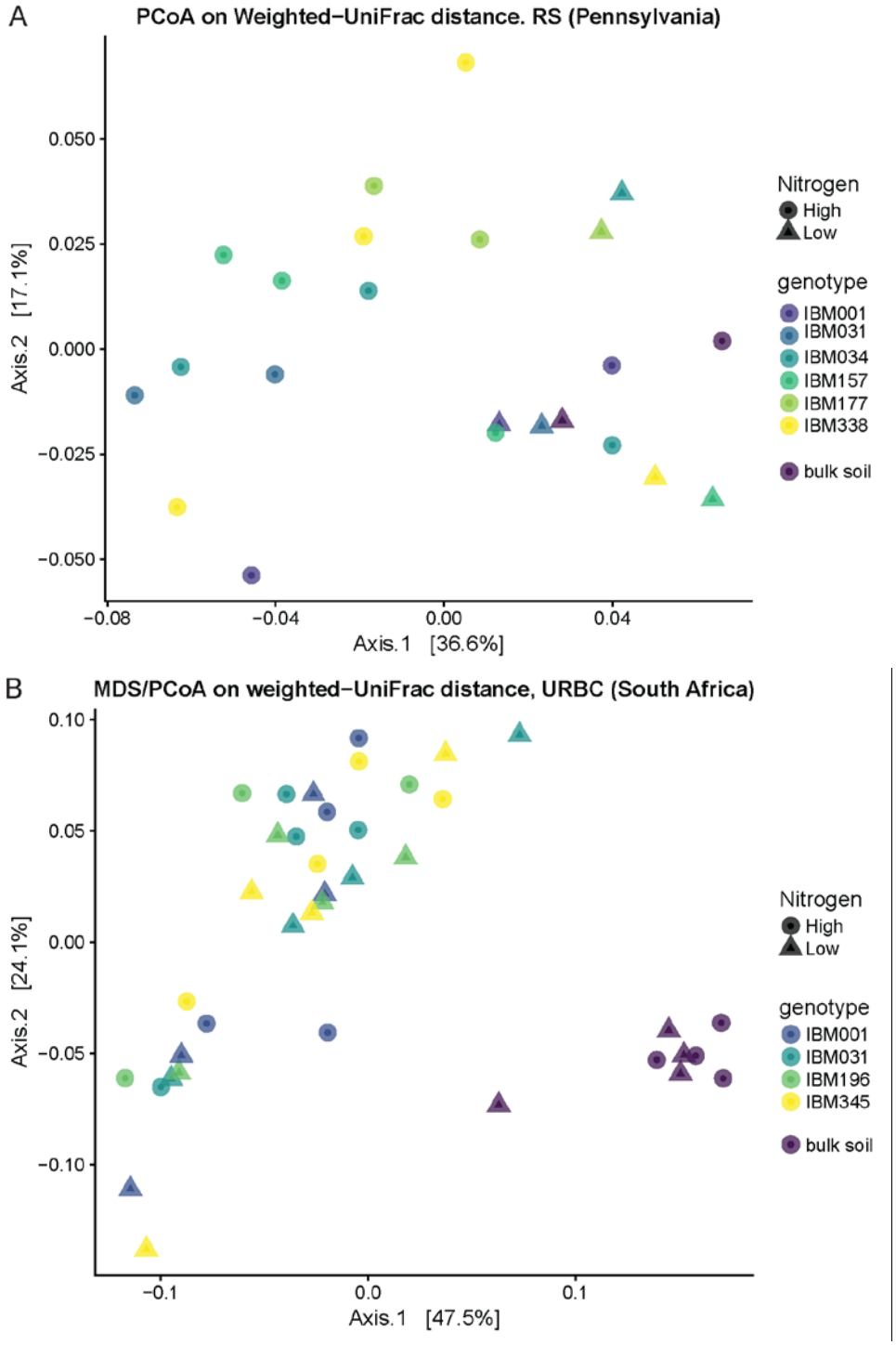

Figure 3-9. PCoAs using weighted UniFrac distances of each experimental site indicate that bacterial communities separate by nitrogen level at RS (A) and by type of soil sample (rhizosphere vs bulk soil) at URBC (B).

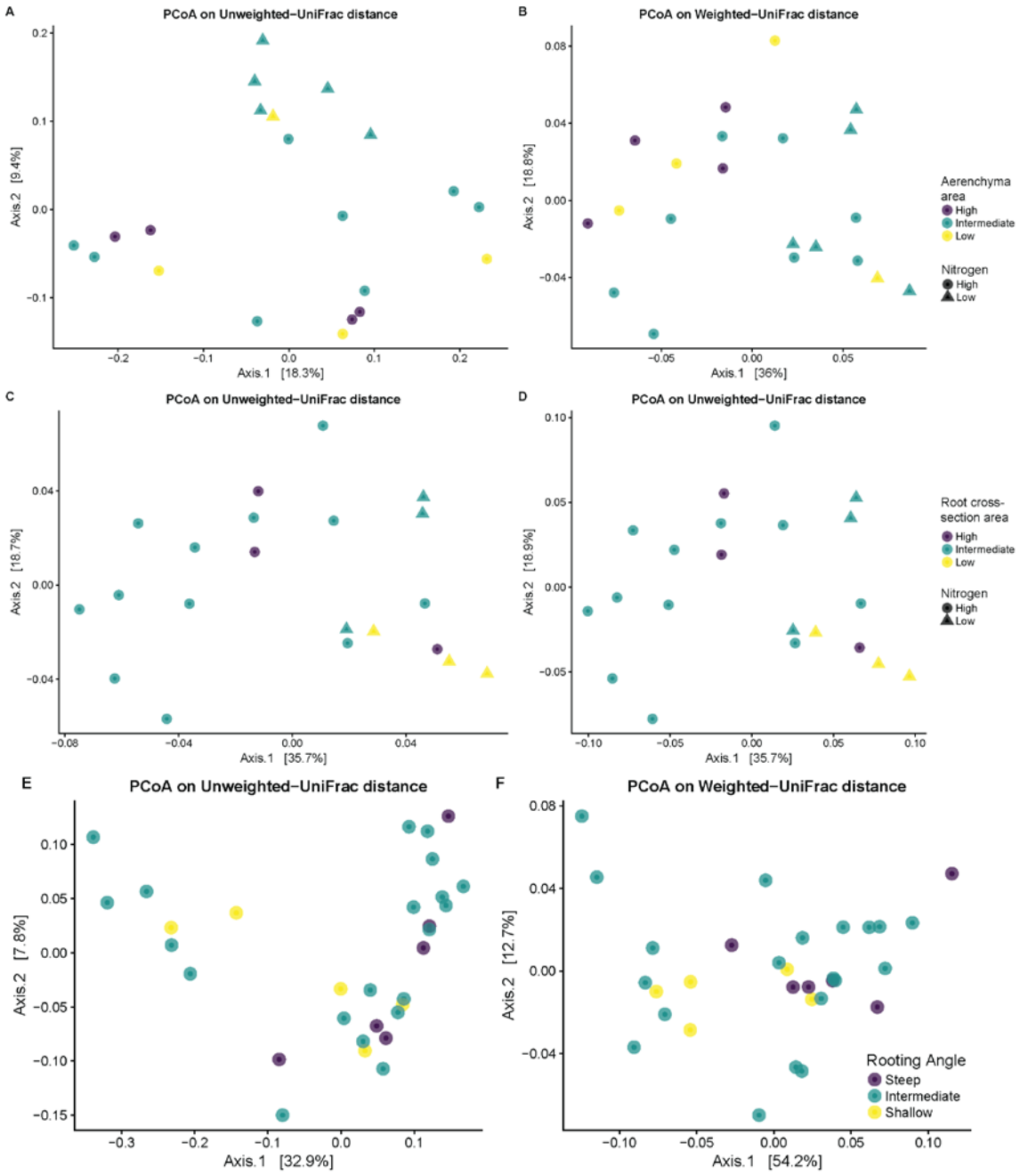

Figure 3-10. PCoAs using weighted and unweighted UniFrac distances indicate that bacterial rhizosphere communities at RS separate by nitrogen root phenotypes aerenchyma area (A, B), living cortical area (C, D) and rooting angle (E, D).

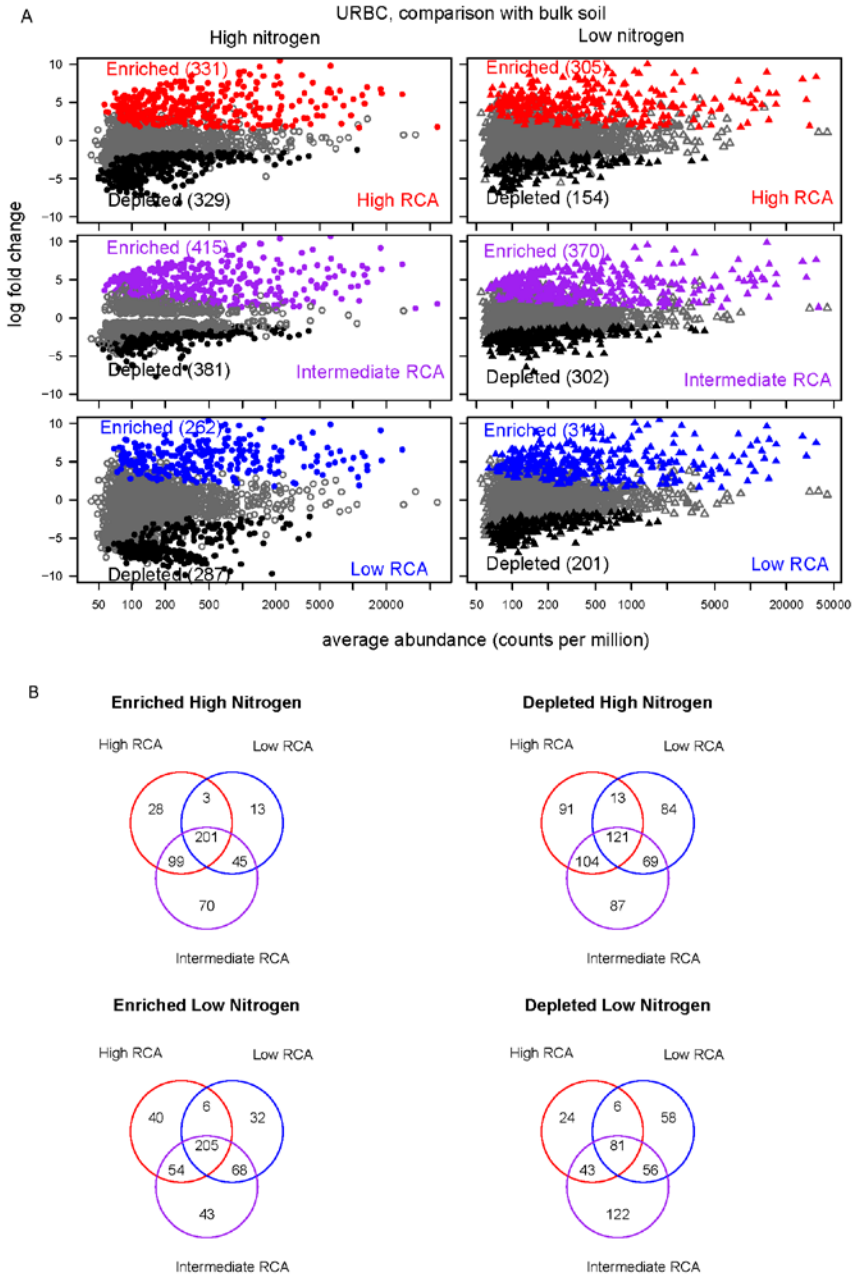

Figure 3-11. Rhizosphere soil of contrasting RCA plants was enriched or depleted for specific OTUs compared to bulk soil under high and low nitrogen at URBC. Abundance log change (y axis) of all the OTUs when rhizosphere of each of the RCA levels and bulk soil were compared (A). Colored points indicate differentially enriched (red, purple or blue) and depleted (black) OTUs according to a likelihood ratio test with $p<0.01$, and grey points were non-differentially abundant between the respective rhizosphere and bulk soil samples, number of OTUs significantly enriched or decreased at each condition are in parenthesis. Number of the differentially enriched and depleted OTUs between each phenotype and bulk soil under the respective nitrogen level (B).

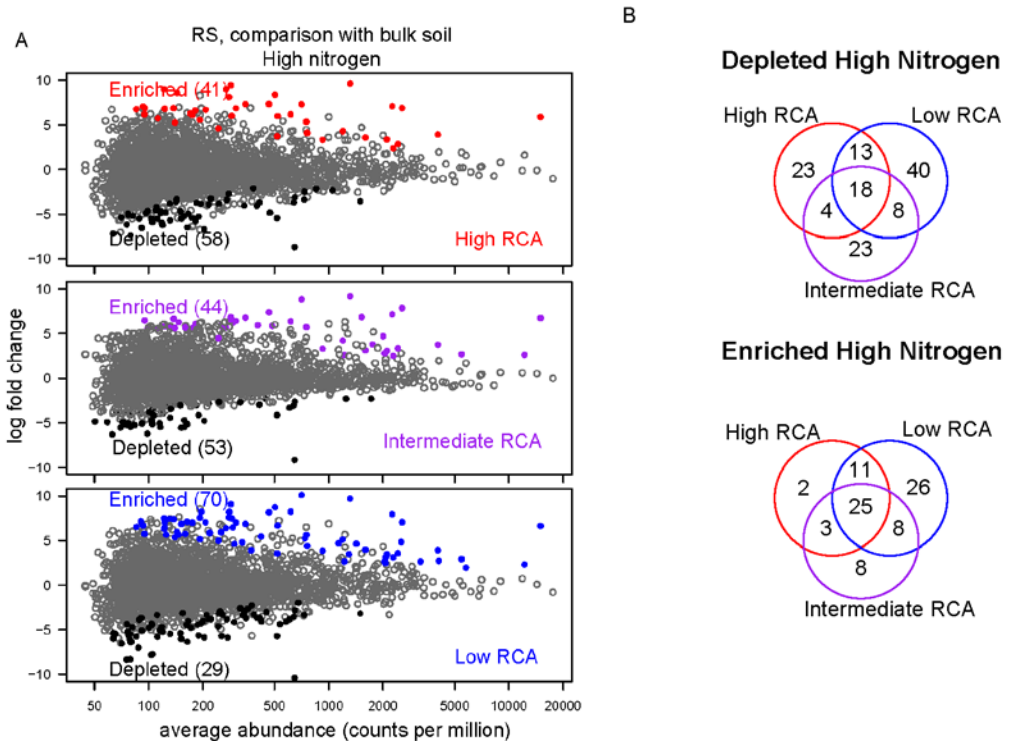

Figure 3-12. Rhizosphere soil of contrasting RCA plants was enriched or depleted for specific OTUs compared to bulk soil under high nitrogen at RS. Abundance log change (y axis) of all the OTUs when rhizosphere of each of the RCA levels and bulk soil were compared (A). Colored points indicate differentially enriched (red, purple or blue) and depleted (black) OTUs according to a likelihood ratio test with $p<0.01$, and grey points were non-differentially abundant between the two types of samples; number of OTUs significantly enriched or decreased at each condition are in parenthesis. Number of the differentially enriched and depleted OTUs between each phenotype and bulk soil (B).

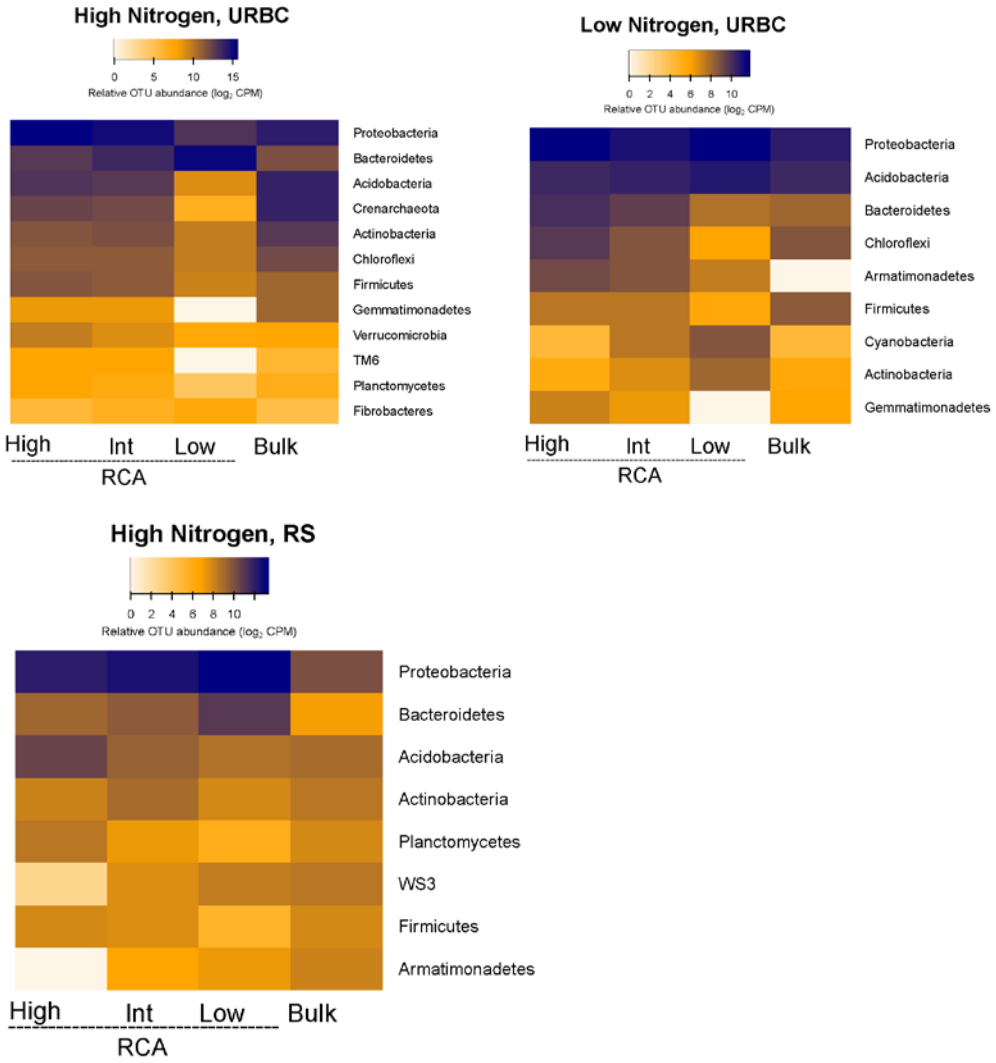

Figure 3-13. Mean relative abundances (counts per million, CPM; log2 scale) of root cortical aerenchyma (RCA)-sensitive OTUs (found as described in Figure 3-6), summarized at phylum level under high and low nitrogen at URBC and under high nitrogen at RS and in comparison with the abundance values of bulk soil.

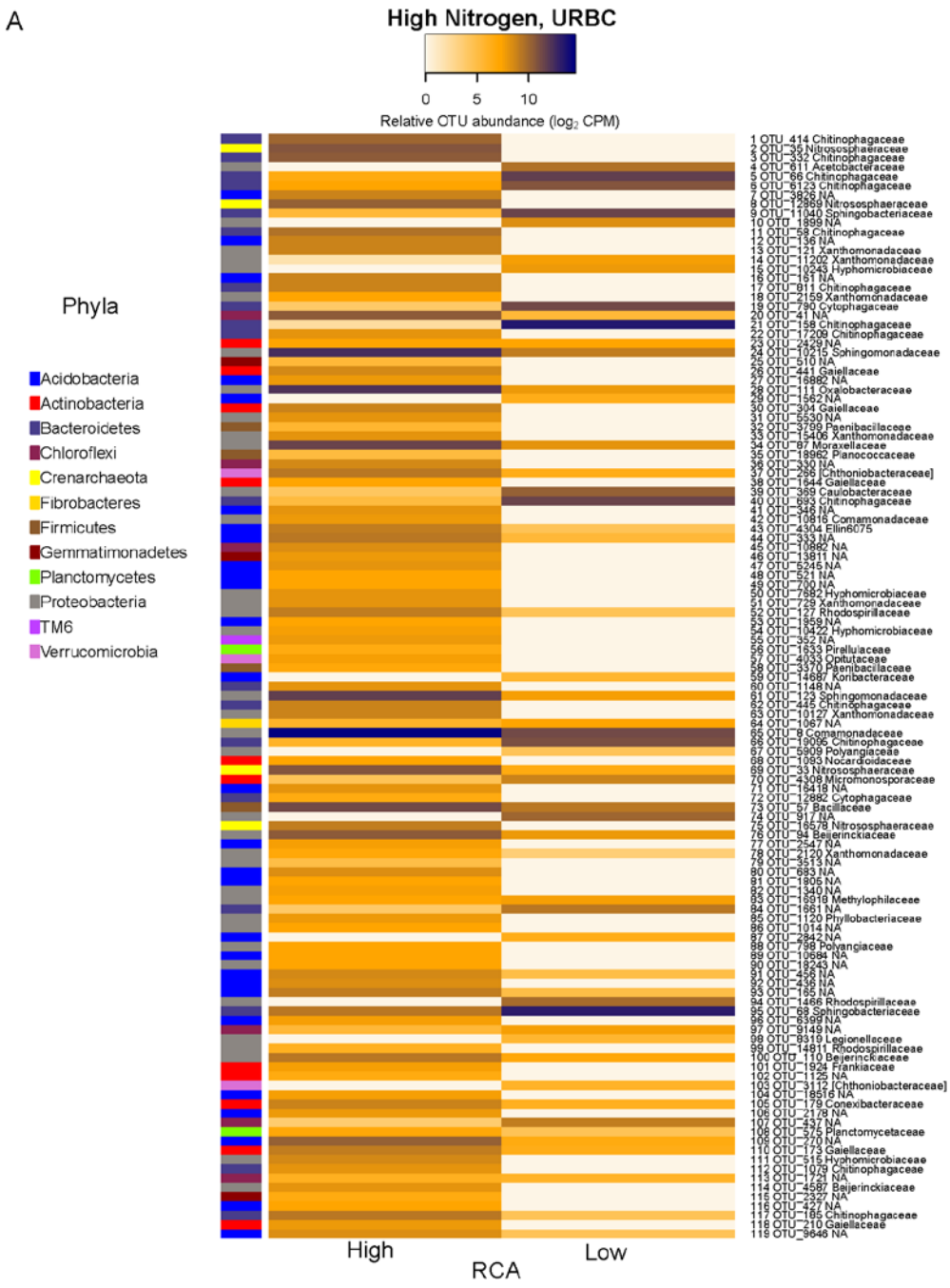
A
High Nitrogen, URBC
0
5
10
Relative OTU abundance (log2 CPM)
Phyla
Acidobacteria
Actinobacteria
Bacteroidetes
Chloroflexi
Crenarchaeota
Fibrobacteres
Firmicutes
Gemmatimonadetes
Planctomycetes
Proteobacteria
TM6
Verrucomicrobia
1 OTU_414 Chitinophagaceae
2 OTU_35 Nitrososphaeraceae
3 OTU_332 Chitinophagaceae
4 OTU_611 Acetobacteraceae
5 OTU_66 Chitinophagaceae
6 OTU_6123 Chitinophagaceae
7 OTU_3826 NA
8 OTU_12889 Nitrososphaeraceae
9 OTU_11040 Spingobacteriaceae
10 OTU_1898 NA
11 OTU_59 Chitinophagaceae
12 OTU_136 NA
13 OTU_121 Xanthomonadaceae
14 OTU_11202 Xanthomonadaceae
15 OTU_10243 Hyphomicrobiaceae
16 OTU_161 NA
17 OTU_911 Chitinophagaceae
18 OTU_2159 Xanthomonadaceae
19 OTU_790 Cytophagaceae
20 OTU_41 NA
21 OTU_158 Chitinophagaceae
22 OTU_17209 Chitinophagaceae
23 OTU_4429 NA
24 OTU_10215 Sphingomonadaceae
25 OTU_510 NA
26 OTU_441 Gaiellaceae
27 OTU_16882 NA
28 OTU_111 Oxalobacteraceae
29 OTU_1562 NA
30 OTU_394 Gaiellaceae
31 OTU_5530 NA
32 OTU_3799 Paenibacillaceae
33 OTU_15406 Xanthomonadaceae
34 OTU_97 Moraxellaceae
35 OTU_18962 Planococcaceae
36 OTU_332 NA
37 OTU_256 [Chthoniobacteraceae]
38 OTU_1644 Gaiellaceae
39 OTU_359 Caulobacteraceae
40 OTU_693 Chitinophagaceae
41 OTU_346 NA
42 OTU_10818 Comamonadaceae
43 OTU_4304 Ellin6075
44 OTU_333 NA
45 OTU_10882 NA
46 OTU_13811 NA
47 OTU_5246 NA
48 OTU_521 NA
49 OTU_709 NA
50 OTU_7882 Hyphomicrobiaceae
51 OTU_729 Xanthomonadaceae
52 OTU_127 Rhodospirillaceae
53 OTU_1959 NA
54 OTU_10422 Hyphomicrobiaceae
55 OTU_352 NA
56 OTU_1633 Pirellulaceae
57 OTU_4093 Opitutaceae
58 OTU_3370 Paenibacillaceae
59 OTU_14687 Koribacteraceae
60 OTU_1148 NA
61 OTU_123 Sphingomonadaceae
62 OTU_445 Chitinophagaceae
63 OTU_10127 Xanthomonadaceae
64 OTU_1067 NA
65 OTU_9 Comamonadaceae
66 OTU_19086 Chitinophagaceae
67 OTU_5909 Polyangiaceae
68 OTU_1093 Nocardioidaceae
69 OTU_33 Nitrososphaeraceae
70 OTU_4308 Micromonosporaceae
71 OTU_18418 NA
72 OTU_12882 Cytophagaceae
73 OTU_57 Bacillaceae
74 OTU_917 NA
75 OTU_18578 Nitrososphaeraceae
76 OTU_94 Beijerinckiaceae
77 OTU_2547 NA
78 OTU_4120 Xanthomonadaceae
79 OTU_8513 NA
80 OTU_693 NA
81 OTU_1905 NA
82 OTU_1340 NA
83 OTU_18618 Methylophilaceae
84 OTU_1661 NA
85 OTU_1120 Phyllobacteriaceae
86 OTU_1014 NA
87 OTU_2842 NA
88 OTU_798 Polyangiaceae
89 OTU_10584 NA
90 OTU_18243 NA
91 OTU_458 NA
92 OTU_436 NA
93 OTU_165 NA
94 OTU_1466 Rhodospirillaceae
95 OTU_68 Sphingobacteriaceae
96 OTU_5599 NA
97 OTU_9149 NA
98 OTU_9319 Legionellaceae
99 OTU_14811 Rhodospirillaceae
100 OTU_110 Beijerinckiaceae
101 OTU_1924 Frankiaceae
102 OTU_1125 NA
103 OTU_3112 [Chthoniobacteraceae]
104 OTU_18516 NA
105 OTU_179 Conexibacteraceae
106 OTU_2178 NA
107 OTU_437 NA
108 OTU_575 Planctomycetaceae
109 OTU_770 NA
110 OTU_173 Gaiellaceae
111 OTU_515 Hyphomicrobiaceae
112 OTU_1079 Chitinophagaceae
113 OTU_1721 NA
114 OTU_4587 Beijerinckiaceae
115 OTU_2327 NA
116 OTU_427 NA
117 OTU_185 Chitinophagaceae
118 OTU_210 Gaiellaceae
119 OTU_9646 NA
High
Low
RCA

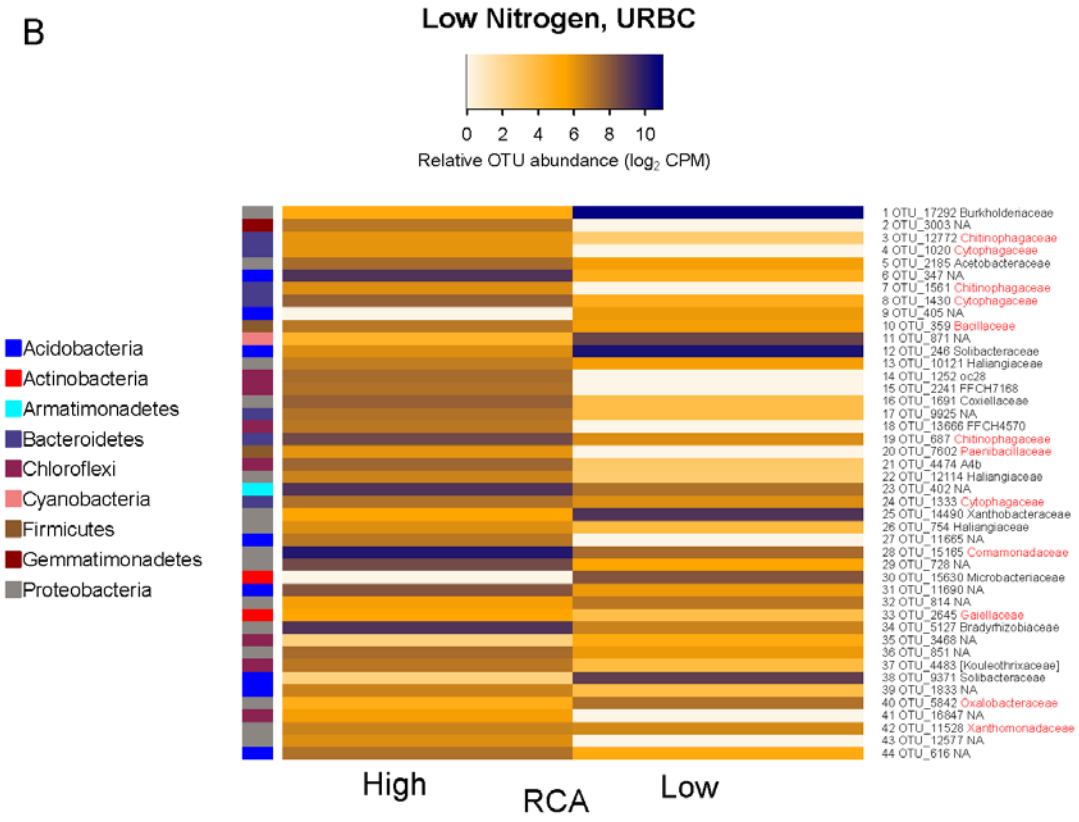
B
Low Nitrogen, URBC
0 2 4 6 8 10
Relative OTU abundance (log2 CPM)
Acidobacteria
Actinobacteria
Armatimonadetes
Bacteroidetes
Chloroflexi
Cyanobacteria
Firmicutes
Gemmatimonadetes
Proteobacteria
1 OTU_17292 Burkholderiaceae
2 OTU_3003 NA
3 OTU_12772 Chitinophagaceae
4 OTU_1020 Cytophagaceae
5 OTU_2185 Acetobacteraceae
6 OTU_347 NA
7 OTU_1561 Chitinophagaceae
8 OTU_1430 Cytophagaceae
9 OTU_405 NA
10 OTU_359 Bacillaceae
11 OTU_871 NA
12 OTU_246 Solibacteraceae
13 OTU_10121 Haliangiaceae
14 OTU_1252 oc28
15 OTU_2241 FFCH7168
16 OTU_1691 Coxiellaceae
17 OTU_9925 NA
18 OTU_13666 FFCH4570
19 OTU_687 Chitinophagaceae
20 OTU_7602 Paenibacillaceae
21 OTU_4474 A4b
22 OTU_12114 Haliangiaceae
23 OTU_402 NA
24 OTU_1333 Cytophagaceae
25 OTU_14490 Xanthobacteraceae
26 OTU_754 Haliangiaceae
27 OTU_11685 NA
28 OTU_15165 Comamonadaceae
29 OTU_728 NA
30 OTU_15630 Microbacteriaceae
31 OTU_11690 NA
32 OTU_814 NA
33 OTU_2645 Gaiellaceae
34 OTU_5127 Bradyrhizobiaceae
35 OTU_3468 NA
36 OTU_851 NA
37 OTU_4483 [Kouleothrixaceae]
38 OTU_9371 Solibacteraceae
39 OTU_1833 NA
40 OTU_5842 Oxalobacteraceae
41 OTU_16847 NA
42 OTU_11528 Xanthomonadaceae
43 OTU_12577 NA
44 OTU_616 NA
High
RCA
Low

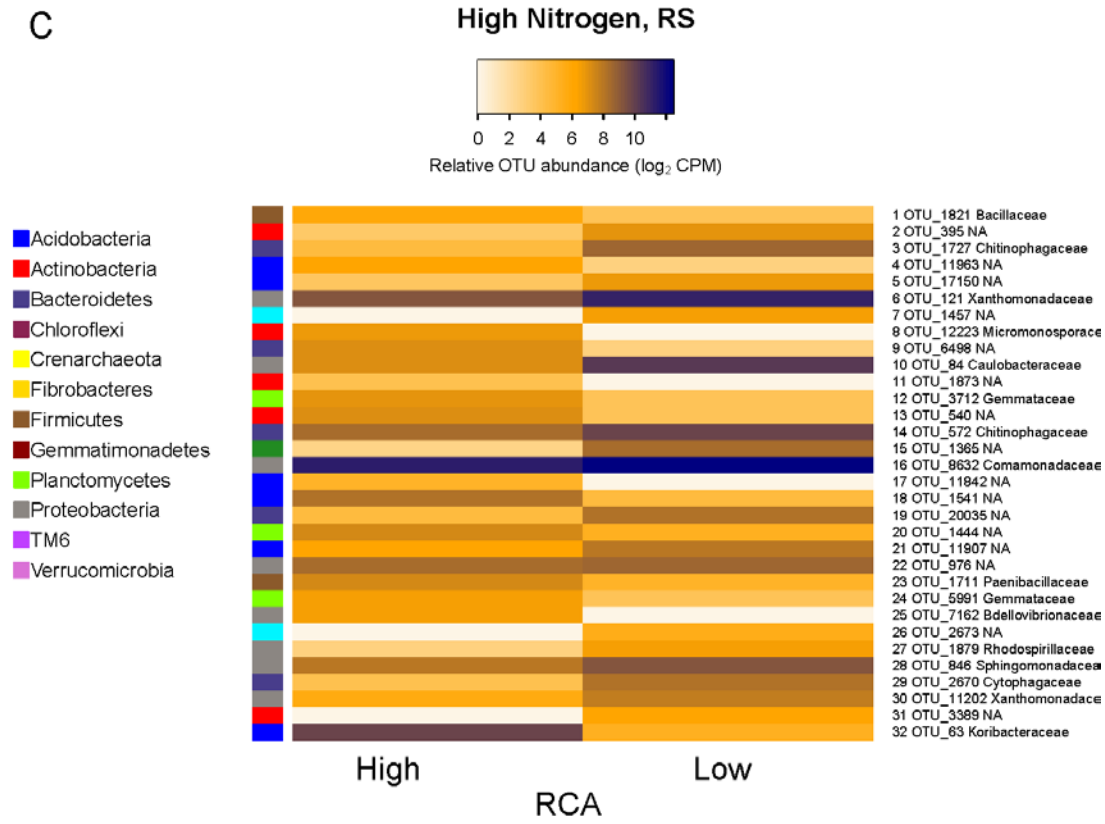

Figure 3-14. Mean relative abundances (counts per million, CPM; log2 scale) of root cortical aerenchyma (RCA)-sensitive OTUs (found as described in Figure 3-6) at URBC (A and B) and at RS (C), summarized at family level (listed on right) under high (A) and low nitrogen (B). Lists of the families and genera are also provided in File S1. The phylum level taxonomy assignment is given in the colored bar of each graph (on left). Families of high-RCA phenotypes shared between high and low nitrogen levels at URBC are highlighted in red (B).

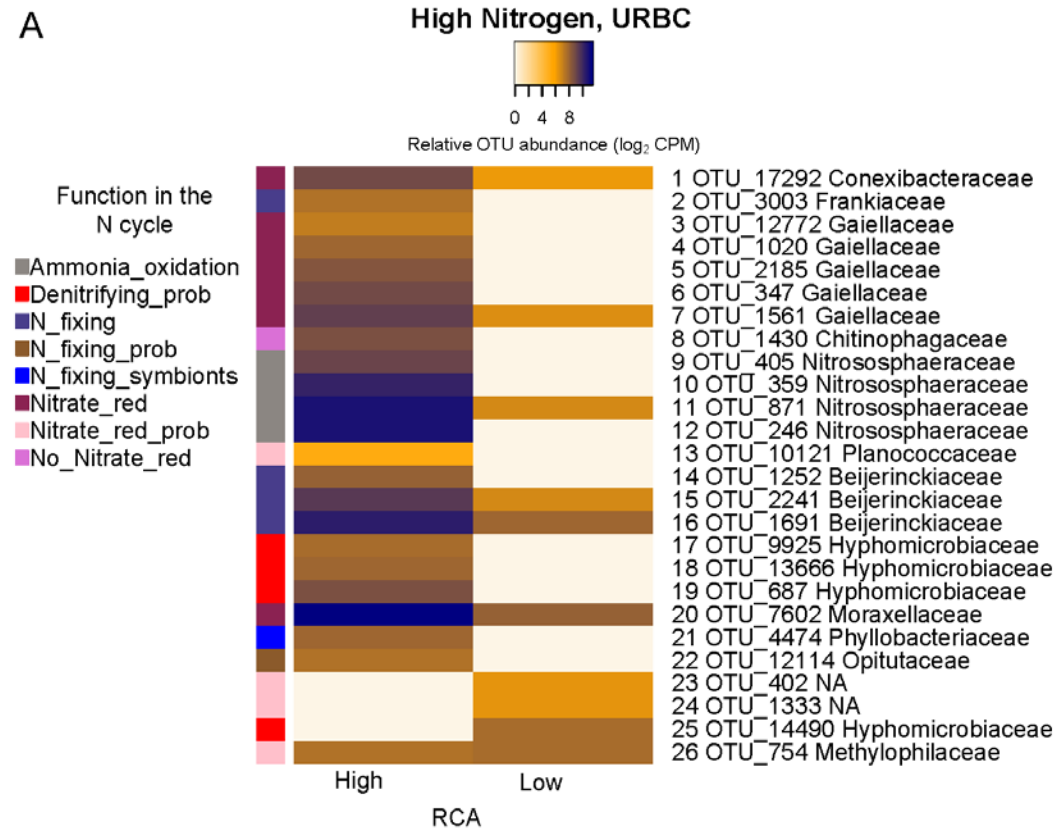
A
High Nitrogen, URBC
0 4 8
Relative OTU abundance (log2 CPM)
Function in the N cycle
Ammonia_oxidation
Denitrifying_prob
N_fixing
N_fixing_prob
N_fixing_symbionts
Nitrate_red
Nitrate_red_prob
No_Nitrate_red
1 OTU_17292 Conexibacteraceae
2 OTU_3003 Frankiaceae
3 OTU_12772 Gaiellaceae
4 OTU_1020 Gaiellaceae
5 OTU_2185 Gaiellaceae
6 OTU_347 Gaiellaceae
7 OTU_1561 Gaiellaceae
8 OTU_1430 Chitinophagaceae
9 OTU_405 Nitrososphaeraceae
10 OTU_359 Nitrososphaeraceae
11 OTU_871 Nitrososphaeraceae
12 OTU_246 Nitrososphaeraceae
13 OTU_10121 Planococcaceae
14 OTU_1252 Beijerinckiaceae
15 OTU_2241 Beijerinckiaceae
16 OTU_1691 Beijerinckiaceae
17 OTU_9925 Hyphomicrobiaceae
18 OTU_13666 Hyphomicrobiaceae
19 OTU_687 Hyphomicrobiaceae
20 OTU_7602 Moraxellaceae
21 OTU_4474 Phyllobacteriaceae
22 OTU_12114 Opitutaceae
23 OTU_402 NA
24 OTU_1333 NA
25 OTU_14490 Hyphomicrobiaceae
26 OTU_754 Methylophilaceae
High
Low
RCA

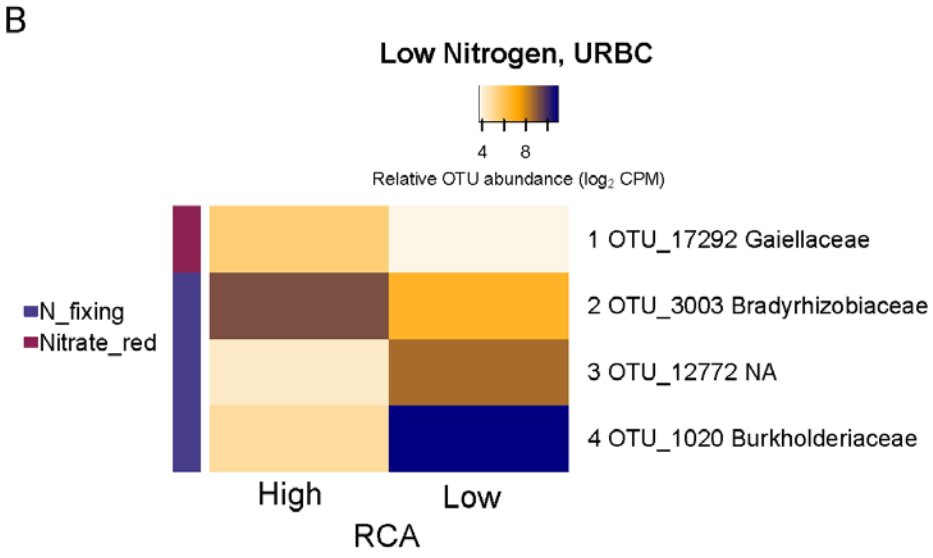
B
Low Nitrogen, URBC
4 8
Relative OTU abundance (log2 CPM)
N_fixing
Nitrate_red
1 OTU_17292 Gaiellaceae
2 OTU_3003 Bradyrhizobiaceae
3 OTU_12772 NA
4 OTU_1020 Burkholderiaceae
High
Low
RCA

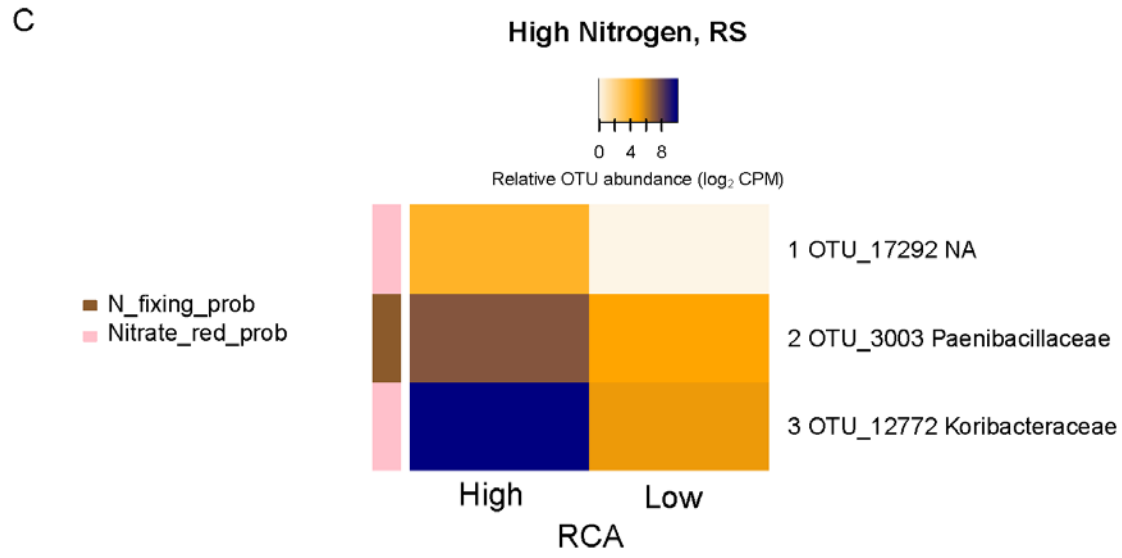

Figure 3-15. Mean relative abundances (counts per million, CPM; log2 scale) of root cortical aerenchyma (RCA)-sensitive OTUs (found as described in Figure 3-6) at URBC (A and B) and at RS (C), summarized at family level (listed on right) under high (A) and low nitrogen (B). The putative function in the nitrogen cycle is given in the colored bar of each graph (on left). prob: probable; red: reduction. Lists of the families and genera as well as references where the functions are reported are provided in File S1.

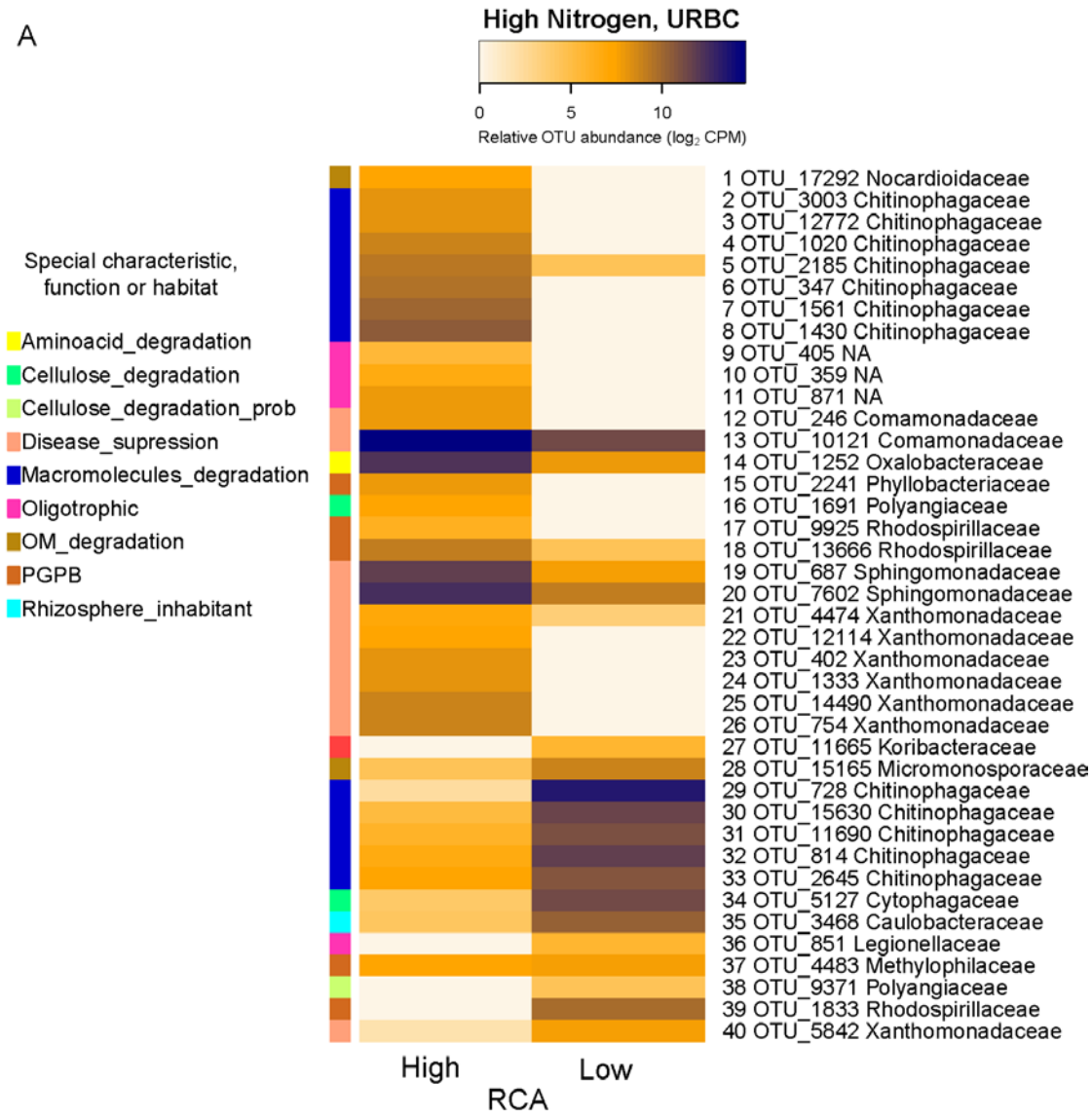
A
High Nitrogen, URBC
0
5
10
Relative OTU abundance (log2 CPM)
Special characteristic, function or habitat
Aminoacid_degradation
Cellulose_degradation
Cellulose_degradation_prob
Disease_supression
Macromolecules_degradation
Oligotrophic
OM_degradation
PGPB
Rhizosphere_inhabitant
1 OTU_17292 Nocardioidaceae
2 OTU_3003 Chitinophagaceae
3 OTU_12772 Chitinophagaceae
4 OTU_1020 Chitinophagaceae
5 OTU_2185 Chitinophagaceae
6 OTU_347 Chitinophagaceae
7 OTU_1561 Chitinophagaceae
8 OTU_1430 Chitinophagaceae
9 OTU_405 NA
10 OTU_359 NA
11 OTU_871 NA
12 OTU_246 Comamonadaceae
13 OTU_10121 Comamonadaceae
14 OTU_1252 Oxalobacteraceae
15 OTU_2241 Phyllobacteriaceae
16 OTU_1691 Polyangiaceae
17 OTU_9925 Rhodospirillaceae
18 OTU_13666 Rhodospirillaceae
19 OTU_687 Sphingomonadaceae
20 OTU_7602 Sphingomonadaceae
21 OTU_4474 Xanthomonadaceae
22 OTU_12114 Xanthomonadaceae
23 OTU_402 Xanthomonadaceae
24 OTU_1333 Xanthomonadaceae
25 OTU_14490 Xanthomonadaceae
26 OTU_754 Xanthomonadaceae
27 OTU_11665 Koribacteraceae
28 OTU_15165 Micromonosporaceae
29 OTU_728 Chitinophagaceae
30 OTU_15630 Chitinophagaceae
31 OTU_11690 Chitinophagaceae
32 OTU_814 Chitinophagaceae
33 OTU_2645 Chitinophagaceae
34 OTU_5127 Cytophagaceae
35 OTU_3468 Caulobacteraceae
36 OTU_851 Legionellaceae
37 OTU_4483 Methylophilaceae
38 OTU_9371 Polyangiaceae
39 OTU_1833 Rhodospirillaceae
40 OTU_5842 Xanthomonadaceae
High
Low
RCA

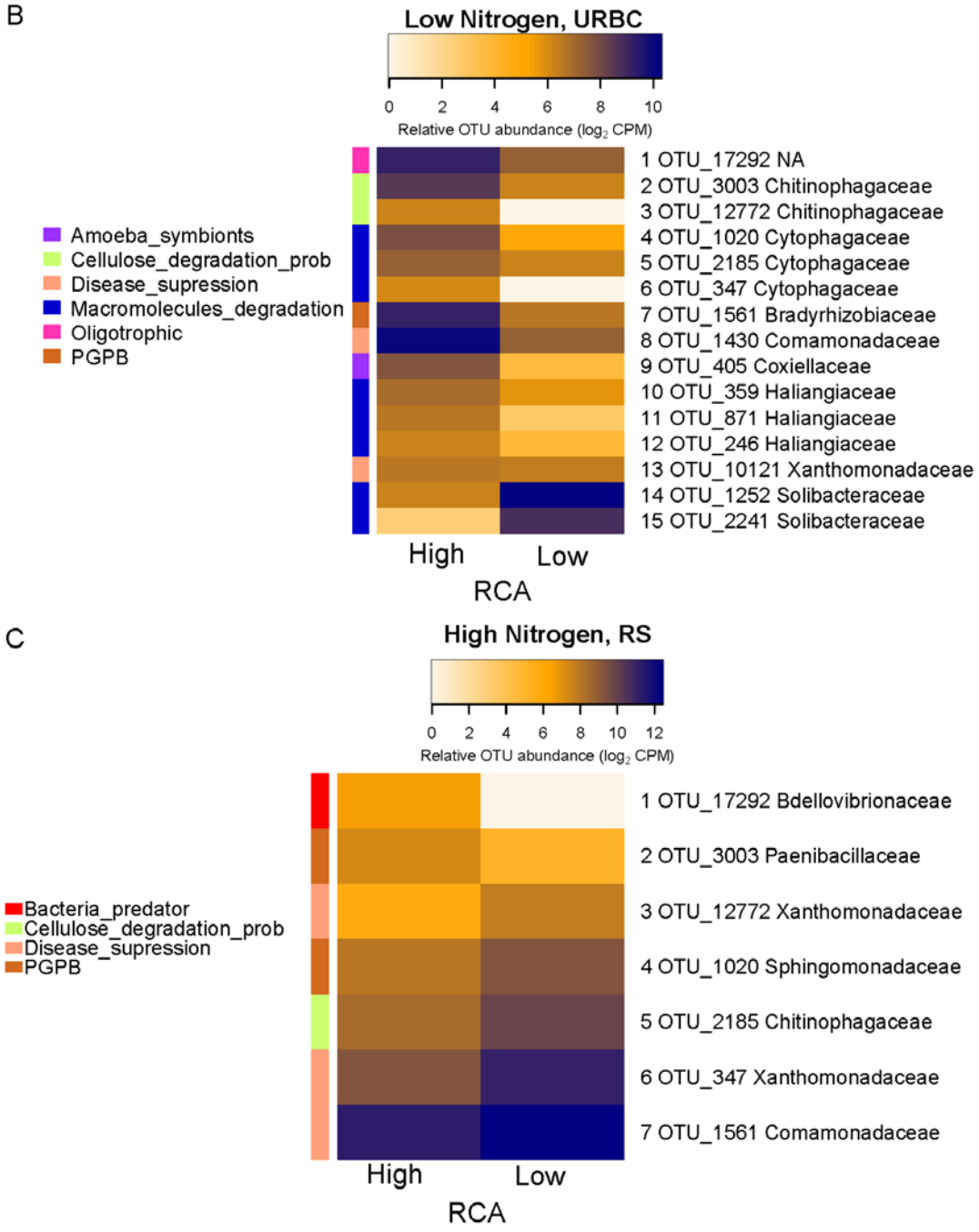

Figure 3-16. Mean relative abundances (counts per million, CPM; log2 scale) of root cortical aerenchyma (RCA)-sensitive OTUs (found as described in Figure 3-6) at URBC (A and B) and at RS (C), summarized at family level (listed on right) under high (A) and low nitrogen (B). Lists of the putative characteristic, metabolism or habitat are given in the colored bar of each graph (on left). prob: probable; PGBP:reported plant growth promoting bacteria; OM: organic matter. Lists of the families and genera as well as references where the functions are reported are provided in File S1.

Table 3-1. Permutational MANOVA results using weighted UniFrac as a distance metric for the experiments by site. The model for each experiment was weighted UniFrac distance ~ Genotype * Nitrogen + Block. Bulk soil samples were excluded from the analysis.

Site	Factor	SS	% Explained	P value
URBC (South Africa)	Genotype (no bulk soil)	0.02	5.8	0.79
	Nitrogen	0.01	4.1	0.236
	Block	0.04	16.4	0.004
	genotype:Nitrogen	0.01	5.8	0.816
	Residuals	0.17	67.9	
	Total	0.26		
RS (Pennsylvania)	Genotype (no bulk soil)	0.02	16.2	0.724
	Nitrogen	0.02	18.7	0.001
	Block	0.02	19.0	0.001
	Genotype:Nitrogen	0.02	15.2	0.776
	Residuals	0.04	30.9	
	Total	0.13		

Table 3-2. Models of unweighted and weighted UniFrac distances as functions of anatomical and architectural phenes at URBC and significances per variable, as selected by random permutations. Constrained correspondence analyses (CCA) were constrained by the factors Nitrogen, Genotype and Block. RXSA: Root cross-section area. TCA: Total cortical area. TSA: Total stele area. AA: Aerenchyma area. MXVA: Total metaxylem vessel area. MXVS: Mean metaxylem vessel size. MXVN: Metaxylem vessel number. CCFN: Cortical cell file number. CCS: Cortical cell size. C:S: Ratio cortex:stele areas. percCisA: Percentage of cortex that is aerenchyma. percCisCC: Percentage of cortex that is LCA. percXSisCC: Percentage of cross section that is LCA. LCA: Living cortical aerenchyma. TopAngle: Angle along the outline of the root at 10% width accumulation. BottomAngle: Angle along the outline of the root at 70% width accumulation. D10: Accumulated width over the depth at 10% of the central path length. Closely related to the root-top angle for maize. NodalRootDiam: Average nodal root diameter. DistFirstLat: Distance to first lateral. Significant variables ($p < 0.1$) are bolded.

URBC unweighted UniFrac ANATOMY			
Model:	distance=RXSA+TCA+TSA+AA+MXVA+MXVS+MXVN+CCFN+CCS+C:S+percCisA+percCisCC+percXSisCC+LCA+Condition (Nitrogen+Genotype+Block))		
p value of the model	0.031		
Factor	SS	F	Pr (>F)
RXSA	0.142	2.95	**0.009**
TCA	0.042	0.87	0.532
TSA	0.049	1.01	0.38
AA	0.081	1.67	**0.095**
MXVA	0.051	1.07	0.352
MXVS	0.090	1.88	**0.06**
MXVN	0.067	1.39	0.152
CCFN	0.070	1.46	0.167
CCS	0.047	0.98	0.411
C:S	0.067	1.39	0.178
percCisA	0.059	1.22	0.266
percCisCC	0.059	1.23	0.259
percXSisCC	0.050	1.05	0.356
LCA	0.137	2.84	**0.01**
Residual	0.240		
URBC weighted UniFrac ANATOMY			
Model	distance = RXSA + CCFN + LCA + Condition(Nitrogen + Genotype + Block)		
p value of the model	0.016		
Factor	SS	F	Pr (>F)
RXSA	0.024	3.89	**0.022**
CCFN	0.018	2.83	**0.039**
LCA	0.005	0.86	0.455
Residual	0.099		
URBC unweighted UniFrac ARCHITECTURE			

Model	distance = TopAngle + BottomAngle + D10 + Condition (Nitrogen + Genotype + Block)		
p value of the model	0.072		
Factor	SS	F	Pr (>F)
TopAngle	0.054	0.88	0.498
BottomAngle	0.116	1.88	**0.047**
D10	0.097	1.57	0.120
Residual	0.985		
URBC weighted UniFrac ARCHITECTURE			
Model	distance = TopAngle + BottomAngle + D10 + NodalRootDiam + DistFirstLat + Condition (Nitrogen + Genotype + Block)		
p value of the model	0.03		
Factor	SS	F	Pr(>F)
TopAngle	0.009	1.48	0.184
BottomAngle	0.011	1.79	0.147
D10	0.018	3.06	**0.044**
NodalRootDiam	0.010	1.66	0.163
DistFirstLat	0.014	2.28	**0.064**
Residual	0.084		

Table 3-3. Models of unweighted and weighted UniFrac distances as functions of anatomical and architectural phenes at RS and significances per variable, as selected by random permutations. Constrained correspondence analyses (CCA) were constrained by the factors Nitrogen, Genotype and Block. RXSA: Root cross-section area. TCA: Total cortical area. Significant variables ($p < 0.05$) are bolded.

RS unweighted UniFrac ANATOMY			
Model	distance = TCA + Condition (Nitrogen + Plot)		
pvalue of the model		0.112	
Factor	SS	F	Pr(>F)
TCA	0.006	1.57	0.112
Residual	0.069		
RS weighted UniFrac ANATOMY			
Model	distance = TCA + RXSA + Condition (Nitrogen + Plot)		
pvalue of the model		0.027	
Factor	SS	F	Pr (>F)
TCA	0.006	1.65	0.093
RXSA	0.007	1.89	**0.048**
Residual	0.062		

Table 3-4. Summary of soil analyses performed at URBC (South Africa) and RS (Pennsylvania) as an external service. Extraction methods: P - Bray I \ Olsen (pH >= 7.3), Cations – NH_4OAc, Organic C - Walkley-Black method, Fe,Mn,Zn,Cu,Ni – DTPA, Tot-N - 0.1N K_2SO_4. NA: not available information.

Measurement	**Units**	**Values**		
		URBC		**RS**
		LN	**HN**	**HN**
Bulk density	$g*cm^3$	1.250-1.511		1.400-1.600
pH	KCl	3.8-5.3		6.7-7.3
S	$mg*kg^{-1}$	7.0 - 89.0		7.6-16.4
P	$mg*kg^{-1}$	16-73		35-111
K	$mg*kg^{-1}$	46-70		87-271
Ca	$mg*kg^{-1}$	86-240		1165-2907
Mg	$mg*kg^{-1}$	26-57		98-168
ECEC	Calculated	1.1-1.9		8.3-16.7
Total N	$mg*kg^{-1}$	6.0-13	NA	NA
NO_3	$mg*kg^{-1}$	5.0-12	NA	NA
NH_4	$mg*kg^{-1}$	1.0-3	NA	NA
Organic matter content	%	0.1-0.5		0.9-2

Table 3-5 Permutational MANOVA results using weighted UniFrac as a distance metric for the experiments by site. The Adonis model for each experiment was weighted UniFrac distance ~ Soil type * Nitrogen + Block. Soil type refers to rhizosphere soil and bulk soil.

Site	Factor	SS	% Explained	P value
URBC (South Africa)	Soil type	0.185	38.6	0.001
	Nitrogen	0.010	2.1	0.224
	Block	0.040	8.4	0.002
	Soil type:Nitrogen	0.005	1.0	0.58
	Residuals	0.239	49.9	
	Total	0.479		
RS (Pennsylvania)	Soil type	0.010	7.0	0.021
	Nitrogen	0.020	14.1	0.003
	Block	0.031	21.6	0.001
	Soil type:Nitrogen	0.005	3.3	0.342
	Residuals	0.076	54.0	
	Total	0.142		

Table 3-6. Descriptive statistics of anatomical and architectural phenes measured at URBC.

Phene abbreviation	Description	Units	Median	Mean	min	max	Standard Error	Variance	Standard Deviation	Coefficient of Variation
RXSA	Root cross section area	mm^2	1.908	1.941	0.642	5.106	0.081	0.603	0.777	0.40
TCA	Total cortex area	mm^2	1.423	1.426	0.454	3.657	0.058	0.310	0.557	0.39
TSA	Total stele area	mm^2	0.495	0.537	0.172	1.644	0.027	0.066	0.257	0.48
AA	Aerenchyma area	mm^2	0.240	0.248	0.000	0.597	0.016	0.022	0.149	0.60
MXVA	Total metaxylem vessel area	mm^2	0.074	0.074	0.025	0.136	0.002	0.000	0.022	0.30
MXVS	Mean metaxylem vessel size	mm^2	0.006	0.006	0.002	0.013	0.000	0.000	0.002	0.26
MXVN	Metaxylem vessel number	count	12.000	12.391	7.000	21.000	0.319	9.364	3.060	0.25
CCFN	Cortical cell file number	count	10.333	10.733	6.000	18.000	0.231	4.966	2.229	0.21
LCA	Living cortical area	mm^2	0.221	0.263	0.107	1.093	0.022	0.028	0.168	0.64
CCS	Cortical cell size	mm^2	0.000237	0.000259	0.000139	0.000456	0.000009	0.000000	0.000082	0.315817
C:S	Cortex:Stele ratio	dimensionless	2.673	2.805	1.661	4.928	0.068	0.431	0.656	0.23
perCisA	Percentage of cortex that is aerenchyma	%	19.965	17.823	0.000	34.237	0.946	76.128	8.725	0.49
perCisCC	Percentage of cortex that is LCA	%	18.804	19.465	10.209	29.895	0.580	19.840	4.454	0.23
perXSisCC	Percentage of cross section that is LCA	%	13.977	14.538	7.429	25.025	0.476	13.362	3.655	0.25
S_Diam	Stem diameter	mm	14.852	14.376	6.988	18.771	0.304	6.020	2.454	0.17
RootArea	number of pixels that belong to the root system	number of pixels	16716.534	16598.836	7441.681	26802.388	568.519	21008886.169	4583.545	0.28

RootDensity	Ratio between root and background pixels	root pixels*background pixels^{-1}	3.696	3.879	1.262	7.287	0.164	1.747	1.322	0.34
TopAngle	Angle along the OTUline of the root at 10% width accumulation	Sexagesimal degree (°)	7.289	22.820	0.061	68.237	2.997	583.971	24.165	1.06
BottomAngle	Angle along the OTUline of the root at 70% width accumulation	Sexagesimal degree (°)	26.228	25.418	0.552	44.612	1.438	134.372	11.592	0.46
RootPaths	Number of paths detected for the root system. Correlated with number of root tips	Count	542.000	594.031	249.000	1336.000	26.431	45409.843	213.096	0.36
D10	Accumulated width over the depth at 10% of the central path length. Closely related to the root-top angle for maize.	%	0.340	0.334	0.173	0.453	0.008	0.004	0.066	0.20
LatRootLength	Average length of the detected lateral roots emerging from the central path long of the excised roots	cm	193.399	192.664	137.866	268.145	4.033	1057.415	32.518	0.17
NodalRootLenght	Length of the central path along the excised root	cm	299.660	293.717	186.522	392.363	5.547	1999.905	44.720	0.15
LatBD	Lateral branching density	lateral roots*cm^{-1}	11.985	12.436	1.293	31.368	0.936	56.974	7.548	0.61
NodalRootDiam	Average nodal root diameter	µm	174.402	170.041	13.120	294.623	7.401	3560.569	59.670	0.35

DistFirstLat	Distance to first lateral	cm		0.575	1.415	0.000	10.269	0.251	4.108	2.027	1.43

Table 3-7. Descriptive statistics of anatomical phenes measured at RS.

Phene abbreviation	Description	Units	min	max	Median	Mean	Standard Error	Variance	Standard Deviation	Coefficient of Variation
RXSA	Root cross section area	mm^2	0.576	2.750	1.229	1.261	0.096	0.222	0.472	0.37
TCA	Total cortex area	mm^2	0.400	2.149	0.956	0.959	0.077	0.142	0.377	0.39
TSA	Total stele area	mm^2	0.158	0.601	0.273	0.302	0.022	0.011	0.107	0.35
C:S	Cortex:Stele ratio	dimensionless	1.816	4.951	3.316	3.200	0.142	0.481	0.693	0.22
AA	Aerenchyma area	mm^2	0.017	0.522	0.129	0.151	0.022	0.012	0.110	0.72
perCisA	Percentage of cortex that is aerenchyma	%	1.930	29.710	16.498	15.645	1.562	58.559	7.652	0.49
MXVA	Total metaxylem vessel area	mm^2	0.034	0.136	0.059	0.066	0.005	0.001	0.025	0.37
MXVS	Mean metaxylem vessel size	mm^2	0.002	0.009	0.006	0.006	0.000	0.000	0.002	0.29
MXVN	Metaxylem vessel number	count	8	20	10.5	11.639	0.773	14.347	3.788	0.33
CCFN	Cortical cell file number	count	7	13	9.5	9.597	0.279	1.865	1.365	0.14
LCA	Living cortical area	mm^2	0.132	0.579	0.351	0.347	0.027	0.017	0.131	0.38
perCisCC	Percentage of cortex that is LCA	%	26.943	49.813	36.288	36.646	1.413	47.899	6.921	0.19
perXSisCC	Percentage of cross section that is LCA	%	19.322	39.014	26.738	27.666	1.098	28.914	5.377	0.19
CCS	Cortical cell size	mm^2	71.225	240.201	123.916	137.241	9.565	2195.808	46.859	0.34

Table 3-8. Phene states and quantitative values measured at RS and URBC. The presented phenes were selected by constrained correspondence analysis (CCA) and were significant for the unweighted UniFrac or weighted UniFrac distances of the OTUs at each site. Root cortical aerenchyma was not significant for the distance metrics at RS but it is presented for comparison purposes and because it was further studied.

Site	Phene	Phene states	Quantitative values	units
URBC	Root cortical aerenchyma	High	>0.3	m^2 m^{-1}
		Intermediate	0.15 - 0.3	
		Low	<0.15	
	Living cortical area	High	>0.6	m^2 m^{-1}
		Intermediate	0.3 - 0.6	
		Low	<0.3	
	Rooting angle	Steep	<15	°
		Intermediate	15-35	
		Shallow	>35	
RS	Root cortical aerenchyma	High	>0.2	m^2 m^{-1}
		Intermediate	0.06 - 0.2	
		Low	<0.06	
	Root cross-section area	High	>1.5	m^2 m^{-1}
		Intermediate	0.7 - 1.5	
		Low	<0.7	

Appendix A: Calculations of mesocosm media volume available for a 6 week-old maize plant

Soil available for root exploration in a maize plant at anthesis under commercial field conditions. Current planting densities for maize are > 88,880 plants/ha, or 8.8 (~9) plants per m^2 and 0.11 m^2 per plant. 0.11 m^2 multiplied by 0.5 m depth (based on observed D95 values) would be 0.056 m^3 or 55.5 L per plant. A mesocosm is 52% of this volume.

Soil volume potentially used by a field plant at week 6. A healthy maize plant with optimal fertilization and irrigation grows ~35% (dry matter) of its above-ground biomass at week 6 (~12-leaf stage) (see Fig S6 and Bair, 1942). The root:shoot ratio decreases from 0.3 to 0.2 (based on dry matter values) in this time (from week 6 to anthesis, McCullough *et al.*, 1994). Although absolute values would surely vary within varieties and cultivars, we assume the root:shoot values remain similar across cultivars and commercial lines. So, the root biomass of a plant that grows about 100 g dry biomass at anthesis (York *et al.*, 2015 and Figure 2-17-F15) will have about 35 g shoot and 9.6 g roots at week 6 and 20 g of roots at anthesis. This means that at week 6 the root system has grown approximately 50% of the maximum biomass it will reach at anthesis. If we consider that the mesocosm has about 52% of the available soil volume, it is reasonable to infer that the mesocosm is a realistic representation of the soil volume that a maize plant has in the field at week 6 and earlier since at this time the plant roots have accumulated 50% of the total biomass.

Appendix B: Detailed methods for seed, fungal hyphae production, and DNA work for Chapter 2

Seed sterilization for MC-14

Planted seedling that had been surface sterilized with 0.5% NaOCl and 0.02% Tween® 20 (Amresco, Inc., Solon, OH, USA) for 1 min, and then imbibed in darkness for 48 h with 0.5 mM $CaSO_4$ at 28 ± 1°C, were sown 5 cm depth and thinned to 1 plant four days after emergence.

Seed sterilization for MC-15

For MC-15 the seeds were sterilized as previously described (Bacon *et al*., 1994). Seeds were first soaked in 2.625% sodium hypochlorite solution for 5 minutes and washed three times with distilled sterile water, imbibed in water for 4h and then covered with new distilled sterile water and everything brought to 60 °C in a water bath with continuous swirl for 5 min. Immediately after, the water was decanted and seeds washed and stored at 4 °C for 48 h before planting.

Nutrient management in the mesocosm experiments

Nutrients were provided to the mesocosm experiments initially by saturation of the column with a 4L nutrient solution containing 50 µM Fe-EDTA and 142 g of the water-soluble fertilizer Plantex® 14-0-14 (©Master Plant-Prod Inc. Brampton, ON, Canada), diluted in 100 l distilled water and pH adjusted to 5.5, added one day before inoculation and planting. Starting at emergence, the same solution was added every day with a drip irrigation system at a rate of 250 mL d^{-1} per mesocosm.

Three-dimensional reconstruction of AMC in root segments

Each root was mounted on a motorized stage and moved at a rate of 100 µm sec^{-1} into a scanning UV nanosecond pulsed laser beam, which simultaneously vaporized and illuminated each cross-section. The root tissue and the arbuscules are visible and color-differentiated by the

fluorescence produced by the cell wall composition of each organism. Videos were recorded at a rate of 30 frames per s during ablation, and camera white balance and aperture were manually adjusted to optimize visualization of arbuscules (Canon T3i with a 5X MP-E 65 mm micro lens). About 2500 images were extracted from each video with the software 'Free Video to JPG Converter', and subsamples of ~450 images were used for the 3D reconstruction. This produced an image stack of 1.6 µm thick slices of the root sample, with a pixel resolution of 1173 pixels mm^{-1}. The resulting images were edited with ImageJ (Schneider *et al.*, 2012) and segmented (arbuscules, aerenchyma and root tissue differentiated) with the software MIPAR™ (Sosa *et al.*, 2014). The reference (original color images) and segmented (arbuscules, root tissue and lacunae) files were used to reconstruct the root volume with the software Avizo 9 Lite (VSG Inc., Burlington, MA, USA).

Preparation of *F. verticillioides* mycelia

A stock of the fungus previously stored in 15 % glycerol at -80 °C was used to produce a conidial suspension by inoculation in potato dextrose agar (PDA) Petri plates and incubation at 25-26 °C for 7 d. The conidia were harvested and a suspension in distilled water prepared. 1 mL aliquots ($3.2x10^7$ conidia) were inoculated in 1L flasks containing 400 mL yeast extract peptone dextrose broth and incubated at 25-26 °C and 100 rpm for 6 d. Mycelia was harvested by filtration

Mesocosm sample preparation, *F. verticillioides* and plant DNA extraction, and primer validation

Sample preparation. Each root sample was washed with 1% sodium hypochlorite for 2 min and rinsed five times with autoclaved ultrapure Type I water, pad-dried with towel paper under aseptic conditions, packed in 15 mL vials and flash-frozen in liquid nitrogen until processing with qPCR for detection and quantification of *F. verticillioides* colonization.

Fungal DNA extraction: Fresh *F. verticillioides* mycelia were collected from six day old potato-dextrose broth cultures (20 °C, 100 rpm) by filtration. The mycelia were lyophilized for 24 h and stored until processing for DNA extraction three weeks later. A total of ~400 mg dry mycelia were recovered and processed in batches of 40 mg with the Wizard® Genomic DNA purification kit (Promega, USA) according to the product instructions. DNA was quantified using a Nanodrop (Thermo-Fisher Scientific, USA). *Root DNA extraction*: Plant DNA extraction was performed in MC-15 samples for *F. verticillioides* quantification, and in non-inoculated rootlets in order to obtain plant DNA solutions for the calibration curves for fungal determinations as described in the subsection 'Plant measurements' (see 'Materials and Methods' section in the main text of Chapter 2). Non-inoculated rootlets were collected and flash-frozen from 1 week germinated seedlings previously sterilized as described in the paragraph 'Seed germination' (see above) (for MC-15) and grown in paper rollups and 0.5 mM $CaSO_4$ at 28 ± 1°C under aseptic conditions. Frozen root samples were homogenized with a GenoGrinder 2000 (OPS Diagnostics, USA) and ~1 g of ground tissue was used for DNA extraction with the DNeasy® Plant Maxi Kit (Qiagen, USA) according to the manufacturer's instructions. *Primer validation.* Primers Fver356 fwd (CGTTTCTGCCCTCTCCCA) and Fver412 rev (TGCTTGACACGTGACGATGA) (Nicolaisen *et al.*, 2009) which amplify a 56 pb region of the fungal gene EF1α was used to detect known amounts of *F. verticillioides* DNA as measure of the presence of the fungal pathogen. First, PCR products of the primers on *F. verticillioides* DNA were obtained (10 min at 95 °C, followed by 40 cycles with 15 sec at 95 °C, 1 min at 60 °C, and 1 min at 72 °C) using Green Go Taq polymerase (Promega, USA) and cloned with the plasmid pGEM®-T (Promega, USA) according to the manufacturer's protocol with modifications. In the transformation step, 100 µL cells were added to 10 µL of the ligation reaction and incubated in ice for 20 min; after the heat shock, the tube was incubated for 30 min on ice. Luria-Bertani liquid media was used to recover transformed cells from the heat shock for 2hrs before plating. Plasmids were extracted from the

transformed cells and sequenced in order to confirm that amplicon from Fver primers used were a part of the EF1α gene of F. *verticilloides* (Altschul *et al.*, 1990). Correct quantification was confirmed and primers validated for their use on the root samples.

References

Altschul SF, Gish W, Miller W, Myers EW, Lipman DJ. 1990. Basic local alignment search tool. *Journal of Molecular Biology* 215: 403-410.

Bacon CW, Hinton DM, Richardson MD. 1994. A corn seedling sssay for resistance to *Fusarium moniliforme*. *Plant Disease* 78: 302-305.

Schneider CA, Rasband WS, Eliceiri KW. 2012. NIH Image to ImageJ: 25 years of image analysis. *Nature Methods* 9: 671-675.

Sosa JM, Huber DE, Welk B, Fraser HL. 2014. Development and application of MIPAR™: a novel software package for two- and three-dimensional microstructural characterization. *Integrating Materials and Manufacturing Innovation* 3: 10.

Nicolaisen M, Supronienė S, Nielsen LK, Lazzaro I, Spliid NH, Justesen AF. 2009. Real-time PCR for quantification of eleven individual *Fusarium* species in cereals. *Journal of Microbiological Methods* 76: 234-240.

Appendix C: 3D reconstructions of maize root segments with arbuscular mycorrhiza

Video S1. 3D reconstruction of mycorrhiza in maize (*Zea mays*) root segments with contrasting living cortical area and aerenchyma. Available online at: https://photos.app.goo.gl/6FuLBlEX88QaJtKJ3 and attached to this thesis.

Appendix D: Taxonomy and putative functions of enriched OTUs at contrasting RCA phenotypes

Among the most abundant OTUs of high-RCA in high nitrogen conditions at URBC, the families Comamonadaceae and Xanthomonadaceae and the genus Kaistobacter (family Sphingomonadaceae) have been associated with disease-suppressive soils (Li *et al.*, 2015; Liu *et al.*, 2016). Bacteria of the nitrogen fixing families Beijerinckiaceae, Frankiaceae, and the genus Mesorhizobium (family Phyllobacteriaceae) where significantly enriched in high-RCA rhizospheres under high nitrogen, as well as ammonia oxidizing archaeans of the family Nitrososphaeraceae, and nitrate-reducers Gaiellaceae, Conexibacteraceae in addition to members of the phylum Acidobacteria and Actinobacteria that have been associated with the reduction of nitrate to nitrite by the assimilatory pathway (Albuquerque & da Costa, 2014b; Albuquerque & da Costa, 2014a; Campbell, 2014). Also, the families Chitinophagaceae and Cytophagaceae which can degrade different organic macromolecues such as chitin and cellulose (McBride *et al.*, 2014; Rosenberg, 2014), were found abundant in high-RCA plants under high nitrogen. Likewise, members of the phylum Chloroflexi of unknown but potentially very diverse metabolic capabilities (Hanada, 2014) were enriched in high-RCA rhizospheres. Low-RCA plants growing under high nitrogen conditions had three times less enriched OTUs compared to high-RCA. The most abundant phyla were Proteobacteria (37%) and Bacteroidetes (33%) with the rest of phyla distributed among Acidobacteria, Actinobacteria, Chloroflexi, Fibrobacteres, and Verrucomicrobia. The two most abundant families among the enriched OTUs were Sphingobacteriaceae and Chitinophagaceae (both from the phyla Bacteroidetes). Sphingobacteriaceae are aerobes chemoorganotrophs (Lambiase, 2014), and Chitinophagaceae are aerobes or facultative anaerobes with the potential to degrade macromolecules such as

proteins, lipids, starch, pectin, chitin, carboxymethylcellulose or cellulose (McBride *et al.*, 2014; Rosenberg, 2014).

Rhizospheres from low nitrogen plots at URBC had overall lower OTU abundances and a similar enriched-OTU distribution among the most abundant phyla compared to high nitrogen (32% Proteobacteria, 21% Bacteroidetes, and 17% Acidobacteria), with the difference that Armatimonadetes, a family generally considered aerobic of oligrotrophic metabolism (Lee *et al.*, 2014) was uniquely enriched under low nitrogen in high and intermediate RCA plants, and Cyanobacteria was enriched in low-RCA plants (Figure 3-13). Another difference in the high and low nitrogen treatments at URBC was the lack of enrichment of the family Nitrososphaeraceae of high-RCA plants. Similarly to the high nitrogen treatment, bacteria of the families Comamonadaceae and Xanthomonadaceae were enriched in high-RCA rhizospheres at low nitrogen as well as nitrogen-fixing symbionts such as Bradyrhizobiaceae (Figure 3-14b and File S1), the two families Chitinophagaceae and Cytophagaceae from the phylum Bacteroidetes, and families of the phylum Chloroflexi that had been reported in soil and rhizosphere microbial surveys (Vik *et al.*, 2013; Lebeis *et al.*, 2015; Castillo *et al.*, 2017; Schmid *et al.*, 2017).

Among the OTUs with the highest abundance at high-RCA in high nitrogen, Koribacteraceae (phyllym Acidobacteria) consists of strictly anaerobe bacteria which usually coexist with other microorganisms in complex ecosystems (Clavel *et al.*, 2014), followed by a family of the phylum Actinobacteria which may have nitrate reducing activity, may assimilate ammonia and degrade cellulose (Kielak *et al.*, 2016); and for a member of the genus Paenibacillus (Phylum Firmicutes), aerobes or facultative anaerobes very common in rhizosphere of crop species and known for the production of phytohormones, nitrogen fixing capabilities, degradation of carbon macromolecules and production of antifungal compounds (Priest, 2015). The most abundant OTUs enriched at low-RCA and high nitrogen belonged to the families

Comamonadaceae, Xanthomonadaceae and to the genus Caulobacter, all in the phylum Proteobacteria. Caulobacter is an aerobic rhizosphere inhabitant (Abraham *et al.*, 2014).

References

Abraham W-R, Rohde M, Bennasar A 2014. The Family Caulobacteraceae. In: Rosenberg E, DeLong EF, Lory S, Stackebrandt E, Thompson F eds. *The Prokaryotes: Alphaproteobacteria and Betaproteobacteria*. Berlin, Heidelberg: Springer Berlin Heidelberg, 179-205.

Albuquerque L, da Costa MS 2014a. The Families Conexibacteraceae, Patulibacteraceae and Solirubrobacteraceae. In: Rosenberg E, DeLong EF, Lory S, Stackebrandt E, Thompson F eds. *The Prokaryotes: Actinobacteria*. Berlin, Heidelberg: Springer Berlin Heidelberg, 185-200.

Albuquerque L, da Costa MS 2014b. The Family Gaiellaceae. In: Rosenberg E, DeLong EF, Lory S, Stackebrandt E, Thompson F eds. *The Prokaryotes: Actinobacteria*. Berlin, Heidelberg: Springer Berlin Heidelberg, 357-360.

Campbell BJ 2014. The Family Acidobacteriaceae. In: Rosenberg E, DeLong EF, Lory S, Stackebrandt E, Thompson F eds. *The Prokaryotes: Other Major Lineages of Bacteria and The Archaea*. Berlin, Heidelberg: Springer Berlin Heidelberg, 405-415.

Castillo JD, Vivanco JM, Manter DK. 2017. Bacterial microbiome and nematode occurrence in different potato agricultural soils. *Microbial Ecology* 74: 888-900.

Clavel T, Lepage P, Charrier C 2014. The Family Coriobacteriaceae. In: Rosenberg E, DeLong EF, Lory S, Stackebrandt E, Thompson F eds. *The Prokaryotes: Actinobacteria*. Berlin, Heidelberg: Springer Berlin Heidelberg, 201-238.

Hanada S 2014. The Phylum Chloroflexi, the Family Chloroflexaceae, and the Related Phototrophic Families Oscillochloridaceae and Roseiflexaceae. In: Rosenberg E, DeLong EF,

Lory S, Stackebrandt E, Thompson F eds. *The Prokaryotes: Other Major Lineages of Bacteria and The Archaea*. Berlin, Heidelberg: Springer Berlin Heidelberg, 515-532.

Kielak AM, Barreto CC, Kowalchuk GA, van Veen JA, Kuramae EE. 2016. The Ecology of Acidobacteria: Moving beyond Genes and Genomes. *Frontiers in Microbiology* 7: 744.

Lambiase A 2014. The Family Sphingobacteriaceae. In: Rosenberg E, DeLong EF, Lory S, Stackebrandt E, Thompson F eds. *The Prokaryotes: Other Major Lineages of Bacteria and The Archaea*. Berlin, Heidelberg: Springer Berlin Heidelberg, 907-914.

Lebeis SL, Paredes SH, Lundberg DS, Breakfield N, Gehring J, McDonald M, Malfatti S, Glavina del Rio T, Jones CD, Tringe SG, et al. 2015. Salicylic acid modulates colonization of the root microbiome by specific bacterial taxa. *Science* 349: 860-864.

Lee KCY, Dunfield PF, Stott MB 2014. The Phylum Armatimonadetes. In: Rosenberg E, DeLong EF, Lory S, Stackebrandt E, Thompson F eds. *The Prokaryotes: Other Major Lineages of Bacteria and The Archaea*. Berlin, Heidelberg: Springer Berlin Heidelberg, 447-458.

Li X, Zhang Yn, Ding C, Jia Z, He Z, Zhang T, Wang X. 2015. Declined soil suppressiveness to *Fusarium oxysporum* by rhizosphere microflora of cotton in soil sickness. *Biology and Fertility of Soils* 51: 935-946.

Liu X, Zhang S, Jiang Q, Bai Y, Shen G, Li S, Ding W. 2016. Using community analysis to explore bacterial indicators for disease suppression of tobacco bacterial wilt. *Scientific Reports* DOI: 10.1038/srep36773

McBride MJ, Liu W, Lu X, Zhu Y, Zhang W 2014. The Family Cytophagaceae. In: Rosenberg E, DeLong EF, Lory S, Stackebrandt E, Thompson F eds. *The Prokaryotes: Other Major Lineages of Bacteria and The Archaea*. Berlin, Heidelberg: Springer Berlin Heidelberg, 577-593.

Priest FG 2015. Paenibacillus. *Bergey's Manual of Systematics of Archaea and Bacteria 1-40*: John Wiley & Sons, Ltd in association with Bergey's Manual Trust.

Rosenberg E 2014. The Family Chitinophagaceae. In: Rosenberg E, DeLong EF, Lory S, Stackebrandt E, Thompson F eds. *The Prokaryotes: Other Major Lineages of Bacteria and The Archaea*. Berlin, Heidelberg: Springer Berlin Heidelberg, 493-495.

Schmid CAO, Schröder P, Armbruster M, Schloter M. 2017. Organic amendments in a long-term field trial—consequences for the bulk soil bacterial community as revealed by network analysis. *Microbial Ecology*. https://doi.org/10.1007/s00248-017-1110-z

Vik U, Logares R, Blaalid R, Halvorsen R, Carlsen T, Bakke I, Kolstø A-B, Økstad OA, Kauserud H. 2013. Different bacterial communities in ectomycorrhizae and surrounding soil. *Scientific Reports* 3: 3471.

Vita – Tania Galindo Castañeda

EDUCATION

Pennsylvania State University	PhD	Horticulture with minor in Soil Sciences	2018
Universidad Nacional de Colombia	MSc	Microbiology	2008
Universidad Nacional de Colombia	BSc	Biology	2006

PUBLICATIONS

- **Galindo-Castañeda, T**. Brown, K. M., Lynch, J.P. (2018). Reduced root cortical burden improves growth response and grain yield under low phosphorus availability in maize. *Plant, Cell & Environment* 1–14. https://doi.org/10.1111/pce.13197
- York, L. M., **Galindo-Castañeda, T.**, Schussler, J. R., and Lynch, J. P. (2015). Evolution of US maize (*Zea mays* L.) root architectural and anatomical phenes over the past 100 years corresponds to increased tolerance of nitrogen stress. *Journal of Experimental Botany* 66, 2347-2358.
- Acevedo, E., **Galindo-Castañeda, T.**, Prada, F., Navia, M., and Romero, H. M. (2014). Phosphate-solubilizing microorganisms associated with the rhizosphere of oil palm (Elaeis guineensis Jacq.) in Colombia. *Applied Soil Ecology* 80, 26-33.
- **Galindo-Castañeda, T.**, and Romero, H. M. (2013). Mycorrhization in oil palm (*Elaeis guineensis* and *E. oleifera* x *E. guineensis*) in the pre-nursery stage. *Agronomía Colombiana* 31, 95-102.
- **Galindo, T.**, Nieves, J. S., and Polanía, J. (2006). Capacidad solubilizadora de fosfatos de microorganismos rizosféricos asociados a dos manglares del Caribe colombiano. *Acta Biológica Colombiana* 11, 153-154.

GRANTS AND AWARDS

- Walter Thomas Memorial Scholarship for graduate students conducting research in the area of plant nutrition and who exhibit research or teaching potential. (2014-2017)
- North East SARE (Sustainable Agriculture, Research and Education) grant for graduate students of the northeast region of the United States. (2013-2015)
- De la Torre Endowment for Latin American Students. (2012-2013)
- Scholarship Fulbright–Becas Caldas to conduct doctoral studies in the United States. (2011-2016)
- COLCIENCIAS research grant awarded to the project "*Micorrizas arbusculares efectivas para la palma de aceite en la zona oriental y central colombianas*" (Effective arbuscular mycorrhiza for oil palm in the central and eastern zones of Colombia) (2010-2014).

APPOINTMENTS

- Research Graduate Assistant. Department of Plant Science, Penn State University. University Park, PA 2012-2018
- Research Assistant. Oil Palm Biology Program. *Centro de Investigación en Palma de Aceite*, Cenipalma. Bogotá, Colombia 2008 – 2011
- Instructor, Soil Microbiology. Departamento de Biología. Universidad Nacional de Colombia. Bogotá, Colombia 2008
- Laboratory Technician**.** *Instituto de Biotecnología*. *Universidad Nacional de Colombia*. Bogotá, Colombia. 2005 –2006